INSPECTION, ASSESSMENT, AND REPAIR OF GROUTED DUCTS IN POST-TENSIONED BRIDGE

A Dissertation

by

SEOK BEEN IM

Submitted to the Office of Graduate Studies of
Texas A&M University
in partial fulfillment of the requirements for the degree of

DOCTOR OF PHILOSOPHY

December 2009

Major Subject: Civil Engineering

INSPECTION, ASSESSMENT, AND REPAIR OF GROUTED DUCTS IN POST-TENSIONED BRIDGE

A Dissertation

by

SEOK BEEN IM

Submitted to the Office of Graduate Studies of
Texas A&M University
in partial fulfillment of the requirements for the degree of

DOCTOR OF PHILOSOPHY

Approved by:

Co-Chairs of Committee,	Stefan Hurlebaus
	David Trejo
Committee Members,	Kenneth F. Reinschmidt
	David Woodcock
Head of Department,	John Niedzwecki

December 2009

Major Subject: Civil Engineering

ABSTRACT

Inspection, Assessment, and Repair of Grouted Ducts in Post-tensioned Bridge.
(December 2009)

Seok Been Im, B.E., Korea Univerisity, Seoul, South Korea;
M.S., Korea University, Seoul, South Korea
Co-Chairs of Advisory Committee: Dr. David Trejo
Dr. Stefan Hurlebaus

Segmental post-tensioned (PT) bridges are major structures that carry significant traffic. Recent investigations of these bridges have identified voids in their ducts. and some of these exposed strands at these void locations are undergoing corrosion. The corrosion of strands may lead to the failure of tendons. As such, an effective inspection process for identifying these voids is needed. From a literature review, several non-destructive testing (NDT) methods are compared for applicability in inspecting voids in external tendons. The impact echo (IE), ultrasonic pulse velocity (UPV), and sounding inspection methods were selected and assessed for identifying voids in preliminary test setup. The sounding inspection method is further assessed for its effectiveness in identifying voids in a full-scale, external tendon system. The results indicate that the sounding inspection slightly underestimates the size of the voids. However, the inspected size and locations of voids have a close correlation with actual voids in ducts. Thus, the sounding inspection can be an effective tool for identifying voids because of its easy application in the field.

Recently, the investigated failures of segmental post-tensioned (PT) bridges called attention to the rehabilitation and mitigation methods of voided ducts in PT structures. Although controversy exists on how to best protect PT tendons from corrosion, filling these voids with grout may be one option. An optimized grouting

procedure for repairing these voids is needed how best to protect the strands from corrosive environments. This research investigates three grouting methods for efficiently repairing the voids in PT duct systems. These methods are (1) vacuum grouting (VG), (2) pressure grouting (PG), and (3) pressure-vacuum grouting (PVG). Each method is being evaluated for filling capability, filling performance, and economic feasibility. Also, three different pre-packaged grouts for repair are assessed in this research to propose the most suitable material for repairing voided PT ducts. The results indicate that the PG and PVG methods are more constructible and likely more economical than the VG method. However, the PVG and VG methods seem to be more effective than the PG method in filling the voids. As a result of these tests, the PVG method is recommended for filling voids in tendons. The results also show that C-1 and C-2 grouts have better filling capability than C-3 grout.

Although experimental tests using prototype specimens of external PT tendons are performed to propose an effective repair grouting method and material, the experimental conditions cannot cover all voids types, duct types, and other effects of repair grouting methods in the field. Thus, the grout flow in voided ducts is predicted using a commercial Computational Fluid Dynamics (CFD) program. The simulation of the flow is challenging due to the complicated geometry of voided ducts, but the simplified model in this research shows close correlations with experimental results. Thus, various parameters of repair methods and materials are assessed in this research, and the PVG method with grouts having low viscosity exhibited the best performance. If it is determined that filling voids with grout is appropriate and prevents future corrosion, it is recommended that voids in the field be filled using the PVG method with grouts exhibiting low viscosities.

DEDICATION

To my father and mother

To my father in law and mother in law

To my son

To my wife, Yoon Jung

ACKNOWLEDGMENTS

I would like to express my sincere gratitude to my co-advisors Dr. Hurlebaus and Dr. Trejo from the bottom of my heart. My first gratitude and appreciation goes to Dr. Hurlebaus for his guidance, encouragement, and support. His insight and suggestions led me to successful achievement in my research. I am also deeply grateful to Dr. Trejo whose perceptive advice and willing assistance helped bring the research to a successful conclusion. I especially wish to extend my gratitude to Dr. Reinschmidt and Dr. Woodcock for their encouragement, guidance, and invaluable comments.

Many thanks go to my friends and colleagues. Because of their willing assistance I can finish my experiments in my research.

My special thanks go to my family. I am sincerely grateful to my father, mother, father in law, and mother in law for their prayer and supports. Last but not least, I would like to acknowledge my deepest appreciation to my wife, Yoon Jung Lee for her love, sacrifice, and encouragement.

TABLE OF CONTENTS

Page

Page

Page

Page

LIST OF FIGURES

Page

Page

Page

Page

Page

Page

Page

Page

LIST OF TABLES

Page

Page

Page

Page

1. INTRODUCTION

Post-tensioned (PT) structural elements are used quite often in bridges due to their ability to span long widths economically while providing an aesthetically pleasing structure. In addition, the use of PT systems in long-span bridges is desirable since they reduce the overall cost of the substructure. This is especially significant when substructure costs increase due to complexities in span conditions such as bridges spanning seas, valleys, and developed urban areas. PT systems are also preferred in bridge construction because they greatly increase structural capacities and are fairly easy to construct effectively.

The construction of a basic PT system consists of placing steel prestressing tendons in ducts which are entirely or partially embedded in concrete structures. Once the concrete segments are assembled, the tendons are placed and then tensioned, and as a result an overall compression force is exerted on the concrete. The compressive stresses induced by the PT tendons are advantageous since they reduce or perhaps even eliminate tensile stresses, which concrete has little strength to resist. These systems make it feasible and more economical to use concrete for long-span bridge structures.

PT bridge systems can include both external and internal post-tensioned tendons. While the internal PT tendons are embedded in concrete structures with sheath ducts, the external PT tendons are installed inside the open area in box girders with PVC ducts. The external PT tendons are typically utilized to reduce the congestion between reinforcing steel and internal tendons. Along with reducing congestion external tendons are also advantageous because they are easier to inspect and replace than the internal PT tendons.

This dissertation follows the format of the *ASCE Journal of Engineering Mechanics*.

The advantages of PT structures may not be realized if they do not achieve their designed service lives, which is typically over 75 years. Exposure to harsh environments contributes to the early deterioration of PT structures. To protect PT strands from early deterioration, they are placed in ducts and cementitious materials are grouted into the areas between the steel strands and the internal surface of the duct. The combination of the duct and the cementitious material is supposed to provide a protective system for the strands against moisture and corrosion.

Although PT systems provide many advantages for designers and constructors, corrosion of the PT strands has raised many concerns about the longevity of these structural systems. Unlike conventional reinforced concrete systems, where corrosion distress can be identified by the observation of excessive staining, cracking, or spalling of the concrete cover, corroding PT systems seldom show these surface distress indicators. These indicators are not visible in PT tendons because the tendons are embedded in ducts and are away from the external surface of the structure. The difficulty in identifying tendon distress is particularly problematic since the degree of corrosion is critical to the structural performance of PT elements.

Improper grouting has been shown to be a major contributor to early PT tendon corrosion and deterioration. Recent bridge inspections conducted by various federal and state transportation agencies reported the presence of voids in grouted tendons (ASBI 2000; FDOT 1999; FDOT 2001a; FDOT 2001b; Hansen 2007; NCHRP 1998). Poor quality grout materials and poor grouting procedures have been cited as one of the causes for void formation in PT bridges (FDOT 2001a). Henrikson et al. (1998) surveyed several post-tensioned bridges and reported tendon corrosion related to improper grouting in Denmark. In 2000, an external tendon failure caused by corrosion was discovered at the Mid-Bay Bridge during a regular bridge inspection (Figure 1-1, (FDOT 2001a)). Tilly (2002) and Pielstick (2002) summarized performance issues related to defective grouting procedures found in various PT bridge performance reports. They also reported that improper grouting procedures during construction resulted in

voids throughout the ducts. Under certain environmental conditions, severe corrosion can occur in these voids. While voids in grouted ducts can cause significant, long-term problems in PT elements, limited work has been performed on how to identify and repair these voids such that they do not become a cause for corrosion.

(a) (b)

Figure 1-1. (a) Close-up View of a Tendon Failure on the Mid-Bay Bridge and (b) External Ducts (Duct on Left Contains Failed Tendon) inside PT Girders (FDOT 2001a).

1.1. Research Significance

The vacuum grouting method has been used for repairing voided ducts, but this method requires air-tight conditions throughout the entire duct, which can be extremely difficult to do in the field: significant effort is required to create the "air tight" conditions. In addition, this method was not properly compared with other repair methods. This research proposes the use of the pressure-vacuum grouting method and it is expected that this method could be easier to perform while providing similar performance as the vacuum grout methods. The process is also expected to be more economical and faster to perform. This research program will perform experimental and numerical studies to assess the applicability of an alternative grouting method that may be faster and more economical than the commonly used existing method.

This research also performs experiments using three different repair grouts and estimates the filling performance of repair grouts. Simultaneously, the simulation of grout flow will be analyzed to investigate its effectiveness for filling voids in PT ducts. Thus, this research will contribute to the state-of-the-knowledge by proposing a better material for repair grouting.

In late 2007, a PT bridge in Virginia experienced failure of a tendon which had been recently repaired. It was believed that the failure could be a result of galvanic cells formed by the different grout environments. Although the State of Virginia placed a moratorium on repairing PT tendons using grouts, in-depth research is required to assess the galvanic coupling. If the issue for the galvanic coupling is resolved, the proposed repair grouting method is effective to fill voids in external PT tendons.

1.2. Research Objectives

This study proposes three major objectives to ensure effective inspection and repair procedures for external PT system. The following objectives will be addressed:

- Objective 1: Develop and propose effective inspection procedures for external PT tendons

  A critical aspect of the overall assessment and repair of voids in grouted ducts is the determination of the existence and location of voids in ducts. To determine the existence of voids in PT ducts, a sounding inspection is typically performed in the field. This research evaluates the effectiveness of sounding inspections by using transparent acrylic ducts, which makes it possible to visually estimate sounding results. The voids located by the sounding inspection are also evaluated using a borescope. Consequently, if the locations identified by the sounding inspection do not correlate with the location of actual voids, then it will be necessary to propose an alternative inspection method for field applications.

- Objective 2: Develop and propose an effective repair grouting method and assess repair materials

Currently, the recommended grout repair method is the vacuum grouting (VG) method, which, if properly performed, is capable of adequately filling voids in ducts. However, this method is very expensive and time-consuming because of the requirement to have an air-tight duct for successful repairs. In addition, limited working areas in typical PT structures make it difficult to maintain an air-tight condition in the entire duct. Alternatively, the pressure grouting (PG) method can be used to repair voids in grouted ducts. This method overcomes the obstacles of the VG method because it can be easily performed in the field and it requires minimal preparation time. It has been found that this method traps air-pockets in the ducts. To overcome this, a combination of the PG and VG methods, the pressure-vacuum grouting (PVG) method, is considered. This method will utilize the benefits of both the PG and VG procedures.

Furthermore, various grout types will be evaluated as repair grout materials. Specifically, three different commercially available grouts and three different repair methods will be tested for (1) filling capability in ducts, (2) repair performance, and (3) economic feasibility.

- Objective 3: Validate the proposed method and materials with Computational Fluid Dynamics (CFD) analysis

From experimental tests, the prototype specimens of external PT tendons are fabricated and evaluated using different repair grouting methods and materials. However, experimental conditions cannot cover all void conditions in the field. Therefore, it is difficult to propose the most effective repair grouting method and materials based on the experimental results. Although the initial condition of the experimental test setup seems to be similar, the different void formations could affect the filling capability of repair grouting methods and materials. Therefore, the filling of voids is simulated using a CFD analysis program that uses the

Finite Volume Method (FVM). Also, three repair grouting methods will be evaluated using various void profiles.

1.3. Organization of Dissertation

This dissertation is organized as follows.

First, a literature review of PT systems is presented in Section 2. This section includes accounts of failure incidents caused by corrosion in PT tendons. Also, this section provides an overview of grouting in PT systems, and outlines the issues caused by improper grouting procedures. In regards to mitigating corrosion in ducts, previous research about nondestructive techniques for detecting voids and repair grouting methods for filling voids are also introduced in this section. Finally, research development for simulation of filling and flows in pipe is provided to perform an analysis of grout flow in ducts.

Section 3 presents the experimental program and results for void detection and damage assessment strategies. The section provides the design of experimental test specimens, and describes inspection methodologies for the sounding and visual inspection. Finally, the effectiveness of the sounding inspection is assessed, and equations for volume estimation of voids are provided.

In Section 4, the experimental program and results on mitigation or repair strategies are presented. This section provides repair grouting procedures for the developed method as well as the currently used method. Also included in this section is an analysis plan for evaluating repair grouting methods and materials. Finally, repair grouting methods and materials are assessed in regard to filling capability, filling performance, and economic feasibility.

In Section 5, a numerical program is adopted to predict grout flows in voided ducts of external PT systems. First, the analysis program and conditions are introduced and preliminary analysis is performed to verify the applicability of the analysis program. Details of numerical analysis models and plans are then described. Finally, the simulation of repair grouts in voided ducts and a parametric study are carried out.

Section 6 presents the conclusions and proposed recommendations for implementing the findings at this research. Future research needs are then provided.

2. LITERATURE REVIEW

2.1. Introduction

The corrosion of strands has been a long-standing issue in post-tensioned (PT) structures because strands corrosion can lead to the collapse of these bridges. In 1967, the sudden collapse of the Bickton Meadows Footbridge in the United Kingdom (UK) raised concerns about the durability of PT bridges, while the failure of Yns-y-Gwas Bridge in Wales, UK, further emphasized the severity of corrosion in PT systems (Pearson-Kirk 2003; Raiss 1995; Schokker et al. 2001). Recently, the investigated failures of an external tendon in the Mid-Bay Bridge and a vertical loop tendon in the Sunshine Skyway Bridge called attention to the deficiencies in the inspection and maintenance methods of grouted ducts in PT structures (FDOT 2001a; Pielstick 2002). The Virginia Department of Transportation (VDOT) reported failures in external PT tendons in the Varina-Enon Bridge in 2007. As a result, they emphasized the need for an appropriate health monitoring system based on a failure analysis (Sprinkel and Napier 2008). Therefore, research in effective mitigation as well as feasible inspection of grouted ducts is required to better ensure the bridge integrity and safety.

The following sub-sections summarize previous research conducted in the area of grouting in PT systems, inspection methods in PT structures, repair grouting in external PT systems, and simulations for filling and flows in ducts. This overview introduces major components of PT systems, adequate inspections for detection of voids in ducts, and advanced grouting procedures and materials. Also, previously developed inspection techniques and repair tests performed on existing PT ducts are introduced and evaluated. Finally, previous research for Computational Fluid Dynamics (CFD) analysis is introduced to perform a numerical approach and algorithms to predict overall behavior of fluids.

2.2. Major Components of PT Systems

The external PT bridge system consists of four main components, namely grout, strands, ducts, and anchorages. The following sub-sections present a review of these bridge components.

2.2.1. Grout materials

Most grouts are mixtures cement with water (Warner 2004). Grouts are generally used to cover strands in PT systems and rehabilitate crack or other defects in concrete structures because they have good flow and corrosion protection characteristics. In grouted PT systems, the interstitial spaces between the ducts and the steel strands are supposed to be filled with grout after strands are tensioned. The main purpose of using grout is to protect the steel strands from external environment and potential corrosion. Portland cement grout (a mixture of ASTM Type I cement and water) is called as class A grout and commonly used to fill the void spaces of PT ducts.

2.2.2. Post-tensioning strands

Post-tensioning strands that are generally used in most PT bridges are made of seven helically coiled wires (six outer wires helically coiled around one center wire) with a nominal diameter of 0.6 inches (15.24 mm). These strands meet the ASTM A416 specifications. According to PTI (1998), the minimum ultimate tensile strength (*MUTS*) of a strand is defined as the force equal to the nominal cross-sectional area of strand, or bar, times their nominal ultimate tensile stress. The *MUTS* of a 270 ksi (1860 MPa) grade, 0.6 inch (15.2 mm) diameter, seven-wire "as-received" strand meeting the ASTM A 416 specifications is 58.6 kips (261 kN).

2.2.3. Post-tensioning ducts

As discussed in Volume-1 of this report, tendons are classified as internal and external systems. The duct systems for internal and external systems are different.

2.2.3.1. Ducts for internal tendons

For internal tendons, galvanized steel or high density polyethylene (HDPE) ducts are used. To ensure proper bonding with the adjacent concrete and to avoid slippage, the surfaces of these ducts are corrugated. Because galvanizing is supposed to reduce corrosion and friction losses in tendons, galvanized metal ducts were initially used in PT bridges (FHWA 2004; Ganz 2001). However, concerns about hydrogen embrittlement in PT strands were raised while using galvanized ducts; thus, corrugated, thick-walled plastic ducts were introduced in the internal PT system (FHWA 2004; Ganz 2001). Before the thick-walled plastic ducts were introduced, thin-walled corrugated polyethylene ducts were utilized between 1968 and 1974 (Della Vedova and Elsener 2006; Elsener 2004). However, the thin-walled plastic ducts were phased out due to excessive duct profile wobbling which can cause excessive friction losses while stressing. Also, the thin-walled ducts are easily damaged during stressing; grout leakage occurred frequently during grout injection (Ganz 2001). These issues led to the use of corrugated, thick-walled HDPE ducts by the early 1990s. Since then corrugated, thick-walled HDPE ducts have been used on PT bridges.

2.2.3.2. Ducts for external tendons

For external tendons, HDPE ducts with smooth surfaces are used. This is because the ducts are in contact with the box girder only at the deviator blocks and anchorages and therefore corrugated surfaces are not needed. Thick walled HDPE pipe has been commonly used in external tendon systems. However, since HDPE ducts are not embedded in concrete they have to resist a significant pressure from the grout during injection without support from the external concrete. Thus, the European code specifies

that external HDPE ducts have to be designed to resist an internal pressure of 145 psi (1 MPa) (Ganz 2001). The HDPE ducts used in the US are black in color and are opaque. This leads to difficulties in visually inspecting the quality of grouting and the presence of voids, if any, in the external tendons. Recently, transparent ducts have been used in a PT bridge in Japan to inspect grouting quality, the presence of potential voids, and corrosion (Ganz 2001).

2.2.3.3. Cross-sectional area of ducts

The total cross-sectional area of the strands in a duct should not exceed 40 to 45 percent of the inside cross-sectional area of ducts (VSL 2002). Circular ducts with smaller cross-sectional area could lead to difficulties associated with placing the strands inside the ducts (i.e., congestion) and then filling the congested areas inside the ducts with grout (Ganz 2001).

2.2.4. Anchorage blocks and diaphrams

Anchorage systems commonly consist of a concrete diaphragm, bearing plate, anchor head, and anchor wedges. Bearing plates, anchor heads, and anchor wedges are commercially available for different numbers of strands and strand diameters. These systems are suitable for 7, 12, and 19 strands. These systems are also available for strands with a nominal diameter of 0.5 and 0.6 inches (13 and 15 mm). To ensure the quality of the anchorage system, it must pass three basic tests: the static tensile test for verifying the durability of an anchorage system by post-tensioning, the load transfer test for confirming the effectiveness of a transferred load by post-tensioning, and the fatigue test for assessing the performance of an anchorage system (Ganz 2001).

2.3. Overview of Grouting in PT System

Grouting in PT systems is necessary for structural performance. Park (1975) studied the need for grout in post-tensioned tendon ducts and compared them with unbonded post-tensioned tendons. His study showed that cement-based grout significantly reduces corrosion in PT tendons. Furthermore, tendons that are not grouted tend to weaken under repeated loading (Park 1975). Also, ungrouted tendons can induce propagating cracks around the tendon that can eventually result in brittle failure. O'Neal and Schupack (1997) tested post-tensioned I-beam specimens having different end anchorage protections. These specimens were transported to Treat Island, Maine in 1961 to evaluate the behavior of PT tendons in severe environmental conditions. While some end anchorage protections failed, these failures did not result in an overall tendon failure. However, unbonded tendons using grease or paper wrap showed severe corrosion which eventually led to tendon breaking during exposure. Therefore, grouting in PT system is desirable for ensuring structural performance.

Voids in grouted PT ducts are fairly common. According to previous studies, void areas in the grouted ducts exist in 35% of the entire duct systems in Japan (Woodward and Miller 1990). In another study, 30% of tested ducts in 1000 post-tensioned bridges in the UK contained voids while 19% of inspected bridges in the United States were found to have some voids (Pearson-Kirk 2003). Based on the investigation of Texas Department of Transportation (TxDOT), nearly 80% of investigated anchorage parts in a PT bridge included corrosion and voids, and 30% of investigated anchorage parts were assessed to be worse conditions (TxDOT 2004). Voids, in these studies, usually formed at the top surface of the investigated ducts and near the end anchorages. These voids are formed by entrapped air pockets, grout bleeding, and improper grouting (Woodward and Miller 1990; PCI 1997).

Extensive research has been done in the area of improving grout materials, grouting procedures, grout protection, and grout placement training (Pielstick 2002; Schokker et al. 2001; Pearson-Kirk 2003; Raiss 1995; Woodward and Miller 1990;

Smith and Wood 2001; ASBI 2000; Hope and Ip 1988). Woodward and Miller (1990) suggested the use of suitable admixtures for good grout properties. They emphasized effective grouting procedures such as grout materials, equipment, and venting locations. The authors also mentioned the necessity of having trained experts for initial grouting and reinjection of grouts to reduce the formation of large voids. Raiss (1995) summarized appropriate tests for each construction step for effective management of PT structures. The author explained the details of a grout protection system in order to prevent the ingress of detrimental materials inducing corrosion. He also mentioned the importance of developing high performance grout and effective grout procedures. Smith and Wood (2001) stressed the necessity for grouting trials and provided practical feedback for grouting operations to improve performance. They proposed replaceable fittings in duct systems as a way to reduce the risk of improper grouting. Pearson-Kirk (2003) studied the previous investigation of PT bridges and concluded that the local voids were not critical for strand corrosion. He noted that the main cause of strand corrosion was the ingress of water or deleterious chemicals from damaged ducts. He focused on the improvement of grout materials, grouting procedures, and grout protections. However, Pillai (2009) performed corrosion testings for strands and found that small local voids can impact performance of strands. The American Segmental Bridge Institute (ASBI 2000) provided statements about proper grouting requirements and they mentioned the need for a training program for practical grouting. In addition, a significant amount of research has been performed on improving grout materials. These studies were performed and tested to reduce grout bleeding using various admixtures (Schokker et al. 2001; Hope and Ip 1988; Qian et al. 2004).

While a significant amount of research has been carried out on the initial grouting of PT systems, significantly less research has been done on the repair of large voids. Raiss (1995) recommended the vacuum grouting method for repair. However, he mentioned that it could be ineffective when the ducts are not in an air-tight condition. Moreover, most studies recommend the vacuum grouting method for filling large voids in ducts (FDOT 2001a; Pielstick 2002; VSL 2002; FHWA 2004; Shoji et al. 2003).

Shoji et al. (2003) reported the use of the water-jet method for safe drilling and application of vacuum grouting. The authors successfully filled voided ducts using the vacuum method. The Federal Highway Administration (FHWA) recommended the application of vacuum grouting under pressure (FHWA 2004). A VSL report (2002) described the repair grouting by using the vacuum method where the vacuum pump can be used to reduce pressure in the duct by 80%. Figure 2-1 shows the VSL vacuum control and grouting equipment. The Florida Department of Transportation (FDOT) performed mock-up tests and recommended the vacuum grouting method for filling voided ducts when compared with the pressure grouting method (FDOT 2001a). They carried out the evaluation of effective grouting using horizontal mock-up specimens.

Figure 2-1. Vacuum Control and Grouting Equipment for Tendons with Defective Grouting (VSL 2002).

2.4. Inspection of PT Systems

The presence of voids in the grouted tendons in PT bridges have been identified on several bridges (ASBI 2000a; FDOT 1999; FDOT 2001a; FDOT 2001b; Hansen 2007; NCHRP 1998b). A study conducted on PT systems in Japan found that about 35% of PT systems contained voids (Woodward and Miller 1990). In another study, 30% of ducts in 1000 PT bridges in the United Kingdom (UK) contained voids while 19% of inspected PT bridges in the United States were found to have voids (Pearson-Kirk 2003). The inspection and detection of structural defects at an early stage could assist engineers in ensuring public safety, taking necessary actions to prevent further damage, and optimizing future inspection, maintenance, and repair costs.

In recent years, a considerable amount of research has been conducted in utilizing nondestructive testing and evaluation (NDT&E) methods to detect and locate damage and its severety in concrete structures. However, the implementation of NDT&E methods has limitations, especially because of the noise generated during the field measurements, multiple interfaces between various elements of a structural system, and other reasons. To develop an effective NDT&E method, the following criteria should be satisfied: 1) high speed measurement, 2) ease of application, and 3) low cost. Following is a review of various NDT&E methods used in civil engineering applications.

2.4.1. Computerized tomography technique

The computerized tomography (CT) is a technique used to reconstruct images of an object projected by X-rays or Gamma (γ)-rays. This technology is used to determine several cross-sectional images of an object under projection where the intensity of the transmitting rays vary with the object's density. It has revolutionized the medical diagnostic field and has been expanding in industrial fields (Herman 1980). The application of CT in concrete samples was performed by Martz et al. (1991). They applied the X-ray CT system to inspect voids and reinforcement bars in small concrete

samples. In 1993, the authors studied the use of the γ-ray CT to perform more accurate inspections for voids and reinforcement bars in concrete specimens (Martz et al. 1993). Figure 2-2 shows a CT scanned image for a sample of grouted ducts with three strands. The image exhibits the existence of voids inside the ducts, but the size of voids can be affected by beam hardening near high density materials. Although CT is capable of producing detailed images of the structure, the device is expensive and requires accessibility to the concrete specimen from both sides which limits its application in the field.

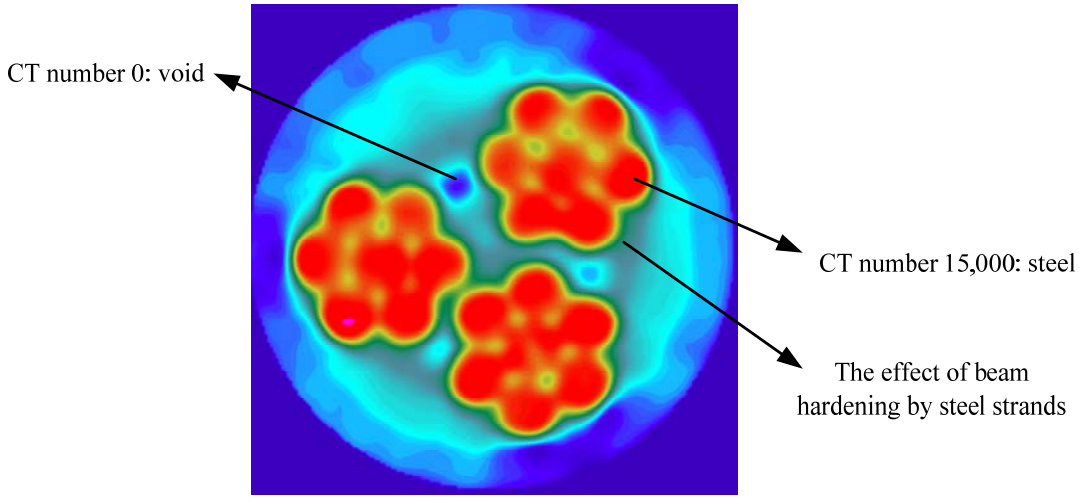

Note: CT number of air is -1000 (low CT number is related with low density of projected rays)

Figure 2-2. CT Scan Image of a Sample of Grouted Ducts with Strands.

2.4.2. Impact-echo technique

The impact-echo (IE) method uses mechanical impacts to generate stress pulses in concrete. This method has been studied by several researchers (Carino and Sansalone 1990; Carino and Sansalone 1992; Pessiki and Carino 1988; Sansalone and Carino 1989) and yielded successful measurements for flaw detection. Because the impact generates a high energy pulse and can penetrate deep into the concrete, the IE method is particularly promising. Moreover, it produces a better signal-to-noise ratio than other ultrasonic techniques because of its low attenuation in composite materials such as concrete

(Karaoğuz et al. 1998). Carino and Sansalone (1992) applied the IE method to detect simulated voids in grouted post-tensioning ducts located in a 3.3 ft (1 m) thick concrete wall specimen. Although the IE method can detect small voids, it is difficult to produce an image of the structure and to directly apply in small grouted ducts such as external tendons. Moreover, the IE method is rather time intensive for inspection of large specimens. To resolve this limitation a movable IE scanner system was developed by Tinkey et al. (2005). The scanning system was applied to internal ducts. However, it was difficult to detect voids when the concrete cover was thicker than the diameter of the embedded ducts. Also, the IE scanner system is incapable of identifying voids when the ducts are partially filled with water (Tinkey et al. 2005). The authors concluded that a scanning system could not detect voids well when the diameter of the ducts was small and the concrete covers were large.

2.4.3. Magnetic flux leakage technique

The magnetic flux leakage (MFL) technique is a promising technique in the NDT&E field because it is capable of detecting corrosion in embedded steels or metallic materials. This technique employs the use of magnetic field sensors called superconducting quantum interference devices (SQUIDS). These sensors are relatively sensitive and have a large dynamic range for inspection. Krause et al. (2001) studied the inspection of ruptured tendons in pre-stressed concrete structures using a SQUID system. It was reported that the MFL method was applied successfully to the detection of corrosion in external polymer ducts (Tilly 2002). Although the MFL technique is effective in detecting corrosion in metallic materials, it cannot evaluate other discontinuities such as voids and cracks. To prevent tendons from corroding, it is necessary to identify the existence of voids before severe corrosion in tendons occurs.

2.4.4. Ultrasonic technique

Ultrasonics is defined as the study dealing with sound, having a frequency of 18 kHz and higher (Blitz and Simpson 1996). The ultrasonic technique can be used in concrete structures to identify concrete thickness (Krause et al. 1995), elastic modulus, and detecting flaws such as cracks, voids etc. (Schickert 1995). Martin et al. (2001) performed tests on 1.6-inch (40 mm) grouted duct specimens with simulated voids by measuring the time-of-flight of transmitted pulses. These tests required the use of several receivers in a grid pattern on the surface of specimens. Although this technique exhibited successful results for detecting voids in PT concrete beams, it is relatively time-consuming and costly because of the large number of transducers required. Iyer et al. (2003; 2005) evaluated the ultrasonic C-scan imaging system to verify the detection of corrosion and voids in specimens. The specimens were grouted in square PVC ducts with one strand in the center. They identified two different levels of corrosion and voids in specimens using the C-scan.

In general, ultrasonic testing systems can be classified into three types: ultrasonic pulse echo (UPE) method, ultrasonic pulse velocity (UPV) method, and pitch catch method (Kundu 2000). The UPE method employs a single transducer that generates pulses and measures reflected pulses. This method consists of having a transducer on the surface of a specimen that transmits ultrasonic pulses. The emitted pulses are then reflected from layers or discontinuities in the concrete such as cracks and voids. The reflected pulse waves are then recorded at the transducer on the surface for further processing. The UPE transducer is moved over the entire surface of the specimen in small increments to monitor the inside condition continuously. In the UPV method, two transducers are utilized: one for excitation and the other for detection. Usually, these transducers are located on opposite sides of a specimen to measure signals directly. Alternatively, for the pitch catch method, the transducers are on the same side of the specimen. In these three methods, contact transducers are normally used, so a couplant, such as water, is needed between the transducers and the surface of the specimen.

Although the application of ultrasonic techniques is limited in real structures, these methods could be promising if these limitations are resolved. Alternatives have been studied that involve non-contact ultrasonic systems such as air-coupled ultrasound (Martínez et al. 2003; Mendelsohn and Wiener-Avnear 2002) or laser ultrasound (Kil et al. 1998; Scruby and Drain 1990). Air-coupled ultrasound works typically in the frequency range of 50 to 100 kHz for application in concrete structures; however, it has the disadvantage of low signal amplitudes due to the impedance mismatch between the interfaces (transducer-air-specimen). The input source is easy to reflect at the boundary between air and the specimen. However, Blum (2003) studied the increased signal amplitude using several combined air-coupled ultrasonic transducers into an array for generation of ultrasound. Laser ultrasonics, the technique involving laser generated surface wave pulses, may be used for inspecting defects of structures by means of the generation and detection of elastic waves. Also, these laser ultrasonic techniques provide lots of benefits while applying with conventional piezoelectric techniques (Hurlebaus et al. 1998). The laser ultrasonics methods based on non-contacting techniques do not require a couplant, so they are free of any errors associated with couplant thickness and/or applied pressure for coupling in piezoelectric transducers during the process being monitored (Silk 1984). The thickness of couplant and coupling pressure applied on the specimen can affect arrival times of elastic waves. Another advantage of the laser methods is that they can be applied to any size and kind of specimen because they are point techniques. Also, the laser ultrasound techniques can generate broadband signals and provide absolute measurements with high fidelity (resonance free). However, laser ultrasonics is expensive and difficult to apply in the field due to the laser safety issues.

2.4.5. Sounding technique

For the inspection of external PT ducts, the sounding inspection is generally performed to identify the existence of voids in ducts (FDOT 2001a). Although the sounding

inspection might contain errors, it is easy to execute in the field and is a very rapid method for detecting voids in ducts. Also, this inspection is particularly effective in the field because it can be applied without a power supply. In addition, sounding inspection findings can be supported by a borescope survey.

2.4.6. Borescoping

An inspection using a borescope can be utilized near the location having an "irregular sounding" in order to inspect voids and corrosion directly (FDOT 2001a). A borescope consists of flexible optic fibers with a small eyepiece (the diameter is less than 0.16 inches (4 mm)) at one end. This equipment has been used mainly in the field of medicine and inspection of small equipment. Although void inspections using a borescope require access holes, it can give a clear and concise image of hidden areas within ducts.

2.4.7. Summary

Most non-destructive inspection techniques detect structural defects using the propagation of elastic waves. However, the shrinkage of class A grout causes problems for typical damage detection. The shrinkage of class A grout creates a gap between the interface of the grout and the duct, and as a consequence does not transmit elastic waves. This shrinkage separation does not increase the risk of corrosion while strands are fully covered with grouts; however, it does increase the errors associated with void detection. Therefore, further research is required to reduce the negative effects of the shrinkage gap in ducts.

2.5. Repair Grouting of External PT System

Currently, a vacuum method is recommended by the FDOT to fill voids in PT ducts. This is due to the ineffectiveness of PG method (FDOT 2001a). FDOT personnel compared the PG and VG methods using a mock up test specimen as shown in Figure 2-3. Both methods were performed from the grout ports located on the anchor plate (or bearing plate) without a grout outlet.

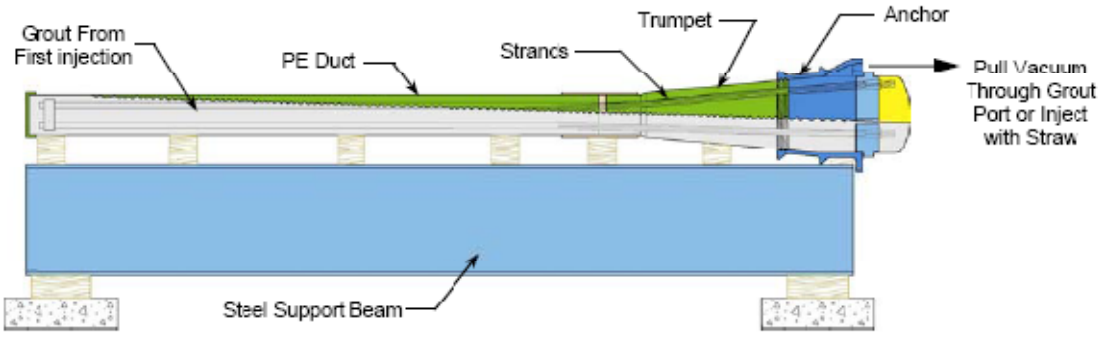

Figure 2-3. Mock-up Test Specimen of FDOT Report (FDOT 2001a).

Figure 2-4 shows the cut-off section of repaired ducts by using each grouting injection method. The figure shows that the VG method completely filled the voids in the specimen but the PG method did not. Thus, FDOT concluded that the VG method is better than the PG method in void-filling capability of the ducts.

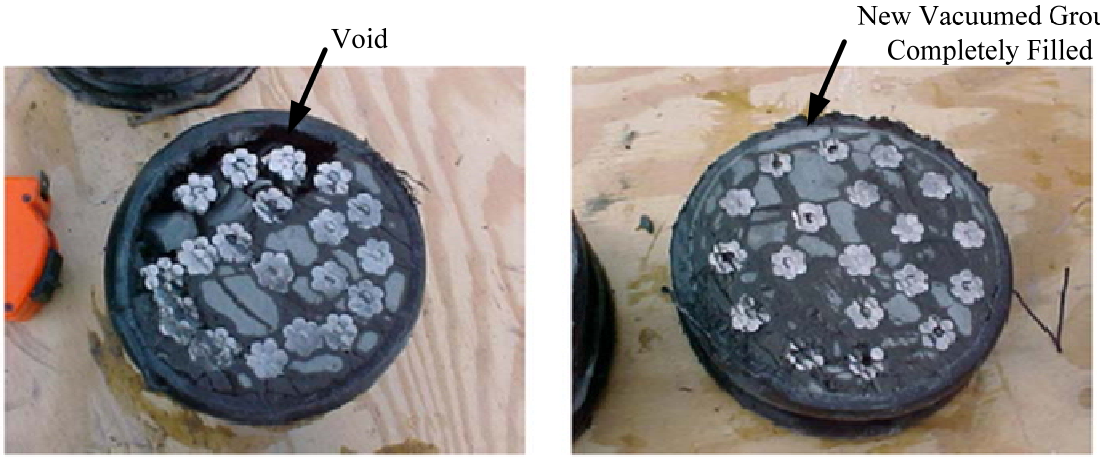

Figure 2-4. Mock-up Test Sections after Repair: Pressure Injection (a) and Vacuum Injection (b) (FDOT 2001a).

Although the VG method is effective for filling voids, it is time-consuming and costly. To perform the VG method, a vacuum system is connected to the duct and the pressure in the duct is decreased. Once the pressure stabilizes, the vacuum pump is closed off from the system and fresh grout flows into the duct, filling the voids. This method is effective for filling voids; however it is difficult to form an air-tight seal in PT ducts such that a constant vacuum pressure is held. Significant preparation time is required to make the ducts air-tight, often taking months. This makes the application of the VG method difficult and the economic viability questionable.

In addition, using the PG method without a grout outlet (or air outlet) makes it difficult to fill the voids in the ducts. The reason for this is that the injecting grout compresses the air in the sealed duct, and these air pockets prevent the repair grout from filling the void completely. Therefore, the re-evaluation of the PG method with an air outlet is needed to determine if this method produces better filling of the voids and is economical.

Unlike the VG method, the application of the PG method is quite simple. The PG method consists of injecting the repair grout under pressure. In the past, pressure

grouting was applied on tendons under air-tight conditions; however, this repair method does not require a system to be air-tight. In fact, relief valves or air outlets typically have to be installed for the method to be effective. This requires less preparation work and could make this procedure more cost-effective. However, further research is needed to evaluate (1) the effectiveness, (2) the performance, and (3) the economic feasibility of this method to fill the voids.

In addition to the typical VG method and PG method, an alternative repair grouting method is considered as well. Thus, the pressure-vacuum grouting (PVG) method, which is a repair method considering the advantages of the VG and PG methods, will be designed and evaluated.

Therefore, the current grouting repair method (VG method) has to be assessed with other proposed grouting repair methods with respect to effectiveness, performance, and economic feasibility.

2.6. Simulation of Filling and Flows in Ducts

Computational Fluid Dynamics (CFD) utilizes a numerical approach and algorithms to predict overall behavior of fluids. The CFD approach has been developed and widely used to simulate various conditions of fluid flow. Although the CFD approach still presents challenges to predicting flow pattern due to several simplifications included in the analysis, such as a discretization problem, boundary conditions, and modeling error, it can provide several advantages (Kundu and Cohen 2008). The CFD method can inexpensively replace experiments for fluid flows and provide more accurate results with rapidly advancing computer performance. Also, it can easily perform various parametric studies and get detailed information about fluid flows through the analysis. In addition, the CFD is capable of simulating an ideal condition if experimental conditions are difficult to establish. Because of these advantages, CFD is quickly developing and being applied in various research fields. The CFD approaches are mostly applied in simulations of mold injection and flow phenomenon in pipelines. However, limited work

has been performed on grout flow using CFD, and more studies of simulations for filling voided ducts are needed to verify better methods and materials for repair grouting. The grout flow in voided ducts seems to be analogous to the flow of mold injection and bubbly flow in pipelines.

For several decades, researchers have been studying the simulation of mold injection and flow. Through the simulation of mold injection, engineers can reduce the cost and time needed for designing an appropriate mold and mold process by reducing trial and errors of experiments. The flow in mold injection is influenced by material characteristics, geometric conditions of the mold, and material flow characteristics in the molding process.

In the 1970s, several researchers developed a simulation of one-dimensional flow based on studies of theoretical principles of fluids (Kamal and Kenig 1972; Wu et al. 1974; Stevenson 1976; Nunn and Fenner 1977). They simulated 1-D flow of circular tube flow. Kamal and Kenig (1972) compared numerical results with experimental data, and successfully predicted the front flow in the cavity. Also, Stevenson (1976) assessed a relation between pressure and injection rates and provided the minimum pressure for filling cavities. However, one dimensional flow had a drawback for simulation of branch flow, so a 2-D approach was adopted in a thin layer using the classical Hele-Shaw flow (Tadmor et al. 1974; Broyer et al. 1975a; Broyer et al. 1975b; Krueger and Tadmor 1980). Tadmor et al. (1974) proposed the flow analysis network method as a common flow solution using a spatial finite difference approach. They applied the method to the injection filling process of cavity and simulated front flow as a function of time (Broyer et al. 1975b). Hieber and Shen (1980) studied the 2-D flow simulation using finite element analysis considering inelastic and non-Newtonian fluid under non-isothermal conditions at generalized Hele-Shaw flow. They successfully predicted a location of weld line which is the conjunction by two injection points in the thin plate mold. In the early 1980s, Moldflow Corporation developed a finite element analysis applying 2-D element to 3-D space, which is called 2.5-D modeling, and then introduced a commercial

finite element program for analyzing mold filling (Jaworski 2003). In 1986, Wang et al. (1986) presented a numerical simulation method combining 1-D elements and triangular elements. They considered the temperature field in the flow simulation by making discretized layers in the gap-wise direction. Based on this study, they advanced the Computer-Aided Engineering (CAE) analysis program (CIMP-FLOW 3D), developed at the Cornell Injection Molding Program (CIMP) (Yeung and Lau 1997). Wu (1989) evaluated three commercial packages for simulating flow and cooling in mold injection: Moldflow MFL3, Moldtemp, and Cflow. Moldflow MFL3 and Cflow showed similar sensitivities for different pressures, but Moldflow MFL3 was much more sensitive to mesh size than Cflow.

The study of 3-D simulation has rapidly developed since the mid 1990s as computer performance advanced and computing prices dropped. In 1996, Friedl (1996) presented the necessity for 3-D simulation and discussed practical progress toward true 3-D CAE analysis to achieve more accurate solutions for injection molding. Rajupelem et al. (1997) advanced 3-D simulation of injection molding by developing the discrete equation of flow theory. In the following year, they proposed the packing equation that reflects the behavior of compressive fluid, and simulated packing stages using a 3-D analysis program (Talwar et al. 1998). The packing phase was considered in compressible fluid and the initial time step of the analysis was regarded as small steps due to the rapid change of cavity pressure. In the process, they neglected inertia effects, and assumed that the velocity was proportional to the gradient of pressure. Pichelin and Coupez (1998) simulated the advancing front flow of injection using discontinuous Galerkin interpolation and Tayler expansion. They demonstrated that this approach is applicable in complex geometries and flows and showed a presence of weld-lines by simulation. In this approach, they presented a general solution of 3-D mold filling for incompressible non-Newtonian fluids and the solution was based on the combination of a Stoke solver and the solution of a transport equation.

Moldflow Corporation introduced the commercial 3-D flow analysis program in 1998. A 3-D mesh needed fewer assumptions than meshes of 2.5-D modeling and modified 2.5-D modeling. The 3-D mesh uses the full 3-D Navier-Stoke solvers and reflects heat conduction in all directions. Each node in meshes can evaluate pressure, temperature, and three-directional velocity components. Options in the 3-D simulation provide considerations of inertia and gravity effect in mold flow (Shoemaker 2006). Furthermore, a 3-D simulation model can provide more detailed information concerning flow characteristics and stress distributions in the mold injection process than the 2.5-D simulation (Tie et al. 2006). Although 3-D simulation can reflect complex geometries, thick structures, inertia and gravitational effect, and imbalanced flow due to non-uniform temperature distribution (Talwar et al. 1998; Kim and Turng 2004), it takes significant time for analysis and memory for computation. Also, 3-D modeling has trouble simulating mesh in the gap-wise direction (thickness direction). The fine mesh size in the gap-wise direction leads to a poor aspect ratio of mesh elements and can cause numerical instability and analysis errors (Kim and Turng 2004).

Many researchers have been dealing with CAE analysis program in the mold injection fields. Han et al. (2000) performed flow analysis of thermoset material using the 3-D finite element method. They analyzed the compressibility of the material in the post-filling stage and compared the numerical results with experimental data in a simple rectangular cavity. However, pressure results from the analysis program showed some differences with experimental data due to the inaccurate consideration of materials and measurement errors.

The Metal Injection Molding (MIM) requires an accurate analysis for mold design to prevent powder segregation in the molding process. Barriere et al. (2002) proposed a new explicit algorithm based on a bi-phasic model to consider the specific behavior of MIM flow. They also developed the explicit 3-D software considering a new algorithm to examine the suitability of MIM design. The new approach showed reasonable results in the simulations of the filling phase as well as powder segregation.

In 2002, a full 3-D finite element analysis of the Powder Injection Molding (PIM) was performed by Hwang and Kwon (2002). They introduced the slip boundary condition and slip law in the 3D finite element formulation to predict the PIM filling process. Based on a nonlinear penalty-like parameter, the new approach was successfully adopted to steady state circular pipe flow. The new method accurately predicted a flow front of PIM and prevented numerical troubles in the sharp corner. They also proved that the simulation results were in close agreement with the experimental short shot.

Courbebaisse (2005) introduced an optimization strategy for performing the propagation simulation using fast algorithm and for finding the best injection location to minimize the end-filling pressure. To find optimized injection points, he introduced a pseudo circle concept considering an optimal centering and skeleton concept. However, his work was based on the Hele-Shaw model, so this approach cannot reflect the 3-D effects.

In 2005, Cao et al. (2005) developed a 3-D simulation program of injection flow for viscous, incompressible, non-isothermal, and non-Newtonian fluids. They introduced an iterative method that analyzes a flow at each time step to reduce the memory of computation and to increase the stability of analysis. They advanced the study of Rajupalem et al. (1997) for both Stokes and Navier-Stokes problems. They employed the implicit scheme, combined with the "up-wind" method in the energy equation, to avoid thermal oscillations and to obtain accurate results. Tie et al. (2006) applied a 3-D finite element method using an equal-order velocity-pressure interpolation method. They also employed a 3-D control volume scheme to simulate front flow during the filling stage. They applied the 3-D Finite Element Method (FEM) program to the analysis of the flow in cavities and showed more exact results of pressure and temperature distribution of complex geometry in the filling process. Tavakoli et al. (2006) performed the numerical simulation of complex flows having liquid/gas phase flow. To analyze the behavior of the liquid-gas free surfaces, they employed the Volume of Fluid (VOF) method considering the piecewise linear interface calculation.

They analyzed the filling process of 2-D complex and S-shaped channels by numerical simulation and compared filling states and the existence of air bubbles with experimental results. They also performed 3-D analysis considering gravity effects and simulated entrapped gas bubbles in the filling process.

To simulate a bubbly flow in pipes, especially in oil pipes, a two-phase VOF approach is usually applied to predict flow pattern inside pipelines. Banerjee et al. (2002) simulated an oil filler pipe to study air entrainment and vapor emission while injecting gasoline. They also compared the simulation with experimental results using images produced by neodymium-doped yttrium aluminium garnet (Nd:YAG) pulsed laser beam. Banerjee and Isaac (2006) performed a parametric study in the simulation of an oiler and analyzed the effect of fluid velocity, fluid pressure, and inclined angle to optimize the design of oiler. Several researchers analyzed the characteristics of flow patterns in horizontal and inclined pipes using the VOF approach (Sampaio et al. 2008; Ragab et al. 2008; Ekambara et al. 2008). Their analyses were focused on fully-developed stratified flow inside pipes and they used the turbulence flow model. However, the appropriate determination of values of k, ε, or ω in the trubulence flow model is significant to obtain better simulation results (Sampaio et al. 2008) and, for grout flows in voided ducts, it is difficult to determine flow characteristics for turbulence.

The grout flow in voided ducts seems to be close to laminar flow because the grout flow is expected to have low Reynolds number less than 1200 (Armaly et al. 1983). For the VOF approach with laminar flow, Lima et al. (2008) performed numerical studies for flow in the sudden expansion joint in rectangular pipes. They also compared Finite Volume Method (FVM) and FEM in the analysis and both methods showed similar trends in the analysis. The numerical analysis showed good agreement with experimental results in low Reynolds number. Also, many researchers examined the "Taylor bubble" problem, a bubble occurring in slug flow, and the simulations have been carried out using the VOF approach with laminar flow (Taha and Cui 2002; Ndinisa et al. 2005; Xiong et al. 2007; Shao et al. 2008). Taha and Cui (2002) used FLUENT, a

commercial CFD code, to analyze a slug flow with a bubble in tubular membranes. The simulation had reasonable accuracy in experiments predicting bubble and permeate flux. Xiong et al. (2007) simulated bubbly flow pattern where air and water were separately injected in a micro-channel and the shape of the bubble and the parametric effects were compared with experiments. In this simulation, air was injected in the channel filled with water.

In sum, all these numerical analyses were performed in the pressure condition and simulated water, oil, or plastic flow. Although previous research was not applied for grout flow, the VOF approach with laminar flow is expected to predict grout filling where grouts having high viscosity are injected in voided ducts filled with air. Also, it is expected that vacuum condition can be created by applying negative pressure at boundary condition.

3. DETECTION OF VOIDS IN POST-TENSIONED BRIDGES: EXPERIMENTAL PROGRAM AND RESULTS

3.1. Introduction and Objectives

The literature review provided in Subsection 2.4 found that an effective inspection method is required to identify voids and their locations in post-tensioned (PT) systems. This section describes the experimental program and results of research performed on void detection and measurement methods. At first, preliminary testing and results are discussed. Details of test specimens, test methodologies, and the analysis plan are then described. The results from this study are then presented.

The objectives of this section are:

- to develop an effective method for identifying voids in PT system, and;
- to develop a method to estimate the volume of voids in PT system.

3.2. Preliminary Testing and Results

Based on the literature review, the Impact-Echo (IE) and Ultrasonic Pulse Velocity (UPV) techniques are selected for preliminary testing. Small-scale test specimens are fabricated and tested using the IE and UPV methods (Figure 3-1). In the preliminary testing, the IE and UPV techniques are found to be ineffective in detecting voids in PT systems. This is because the gap between the high-density polyethylene (HDPE) ducts and cementitious grout obstructs the elastic waves used in these techniques. The IE technique is sensitive to vibration. The IE technique is generally useful in detecting voids in thick concrete webs of box girders. However, This method is not effective in detecting voids in the 4-inch (102 mm) diameter tendon specimens evaluated in this study. The UPV method requires a couplant between the transducers and the surface of

the specimens and it needs a considerable time to place and clean the couplant. This is a time-consuming process and impractical to be used on long tendon systems in PT bridges. As a result, IE and UPV techniques are not effective for field applications.

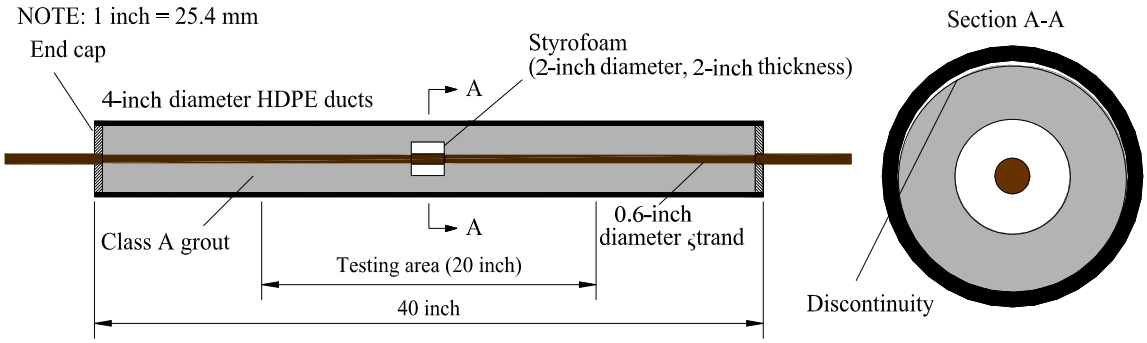

Figure 3-1. Small-scale Test Specimen for Preliminary Test.

3.3. Void Detection and Assessment: Experimental Program

This section first presents the details of prototype external tendon (PET) test specimens and explains how to fabricate the artificial voids in PET specimens. The visual and sounding inspection methods are then presented. Finally, a procedure to estimate the effectiveness of the sounding inspection method in estimating void volume is discussed.

3.3.1. Experimental setup

PET specimens were designed, fabricated, and used to evaluate the sounding inspection method. The schematic of a PET specimen is shown in Figure 3-2.

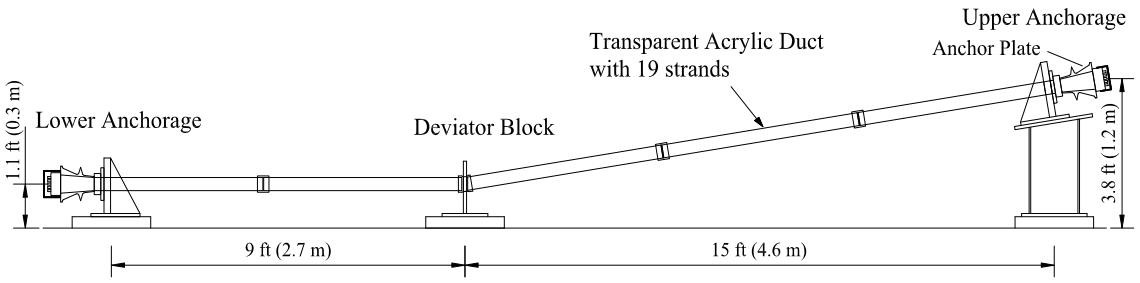

Note: For clarity the 19 strands inside the acrylic duct are not shown.

Figure 3-2. Prototype External Tendon Speicmen.

This PET specimen consists of a lower anchorage, a deviator block, an upper anchorage, and 19 strands inside a transparent acrylic duct. The inside diameter of the acylic duct is 4 inches (0.1 m). To straighten the strands and mimic field conditions, the 19 strands were tensioned to 0.8 ksi (5.52 MPa), which is equal to 0.3% of their ultimate strength. After stressing the strands, the interstitial spaces between the stands and duct were filled with Class A grout (cement and water with a water-cement ratio (w/c) of 0.44) to consider the effect of bleeding. The grout was injected through the grout hole near the lower anchorage using a hand grout pump (Figure 3-3). The hand grout pump was used to better control the grout level and void size in the PET specimens. Artificial voids were then formed in the top anchorage zone and at five locations along the duct to simulate improper grouting procedures. A schematic of these voids and their locations are shown in Figure 3-4.

The main void near the top anchorage zone is formed by filling the grout only to the 'initial grout level' as indicated in Figure 3-5. The five void locations along the tendon system were fabricated by extracting grout from these locations using a vacuum pump and flask. This vacuum pump and flask setup is shown in Figure 3-6. Through preliminary studies an appropriate time for making the voids was determined to be 2 hours after the initial grouting. To insert the vacuum tube to extract the fresh grout at

each void location, a 1-inch (0.025 m) diameter hole was drilled into the duct before initial grouting. After removing the grout, the duct was later sealed with a pipe saddle tap to prevent the leakage of repair grout (Figure 3-7).

Figure 3-3. Hand Grout Pump (www.chemgrout.com).

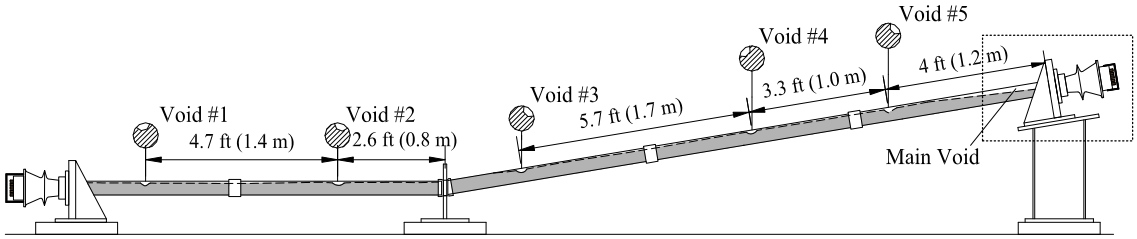

Figure 3-4. Void Locations on the PET Specimen.

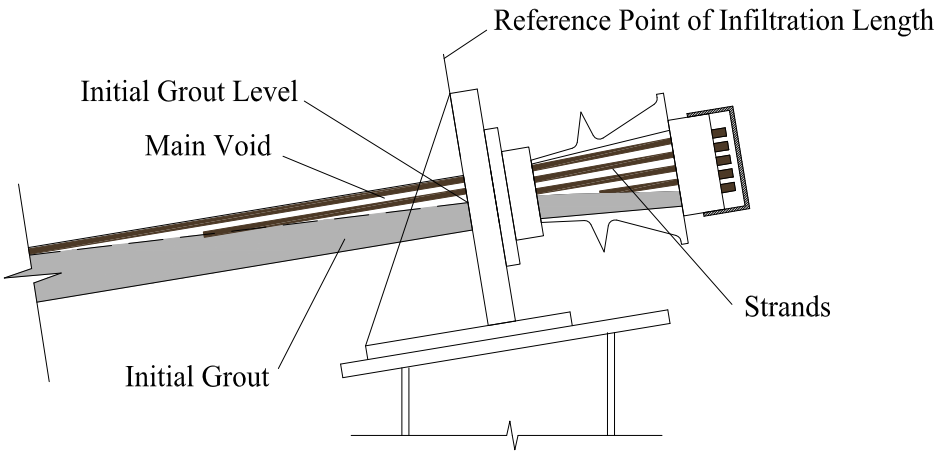

Figure 3-5. Close-up View of the Main Void Near the Top Anchorage of the PET Specimen.

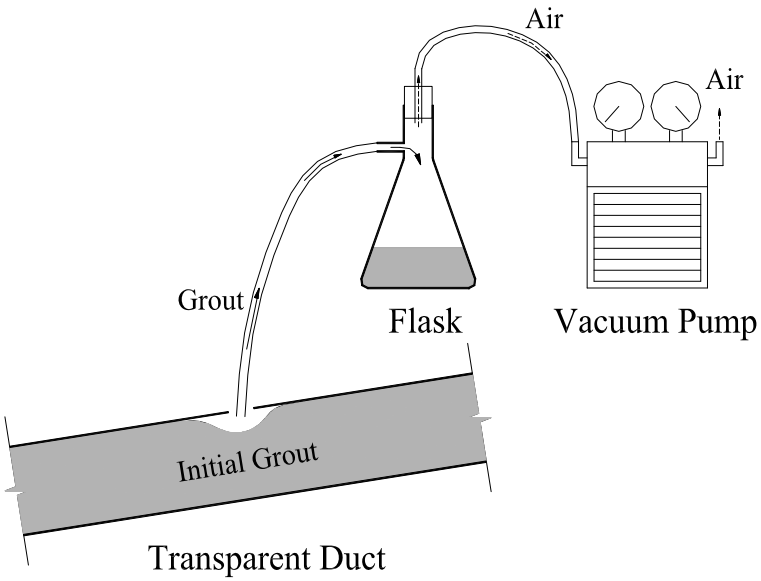

Figure 3-6. Schematic Showing the Setup Used for Making Making Artificial Voids in PET Specimen.

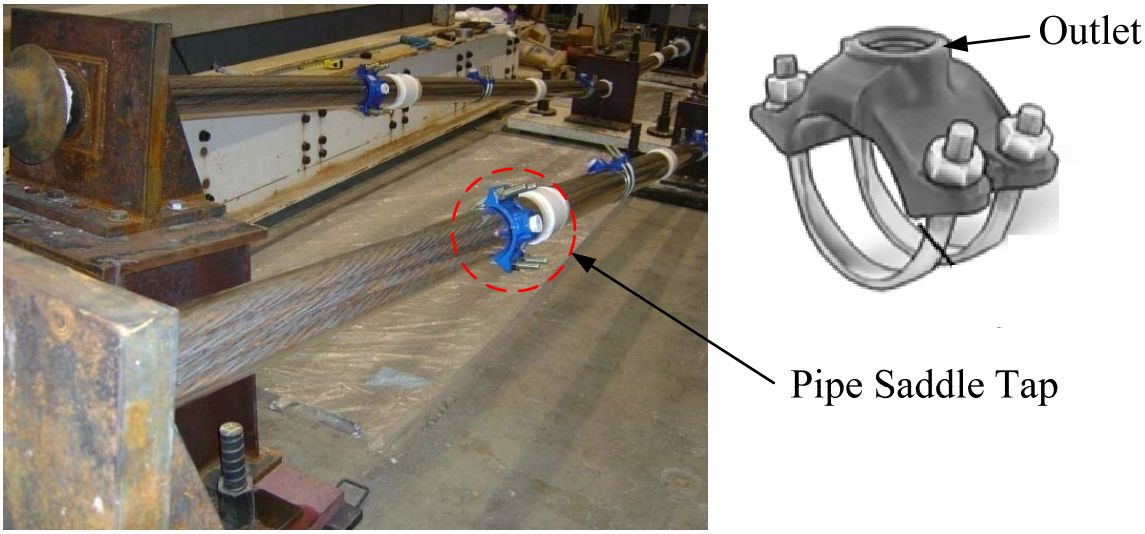

Figure 3-7. Transparent Acrylic Ducts and Pipe Saddle Tap Used on PET Specimens.

As shown in Figure 3-4, the main void at the top anchorage zone and the five other small voids along the duct are connected by a top surface void line along the duct. These void lines are called “bleed lines” (also known as “bug holes”) and are formed by the evaporation of bleed water from the grout and entrapped air pockets (PCI 1997). A total of 16 PET specimens were fabricated and tested in this research.

3.3.2. Visual inspection

Transparent acrylic ducts were used to facilitate visibility during the initial and repair grouting procedures. The voids in the PET specimens were visually inspected and drawn on a “void mapping sheet.” The “void mapping sheet” will be discussed later.

3.3.3. Sounding inspection

The sounding inspection method used in this study used a steel impactor to identify the existence of voids in ducts. Figure 3-8 shows these steel impactors. The presence of voids was identified by detecting a high pitch and irregular sound while tapping. In this research, soundings were recorded at every inch (25.4 mm) in the surveyed intervals (1 ft, 0.305 m) of specimens. Although the assessment of sounding is subjective and depends on the inspector's judgement, it was classified as high and low pitch sounds. Following this method, void profiles of PET systems were drawn on "void mapping sheets."

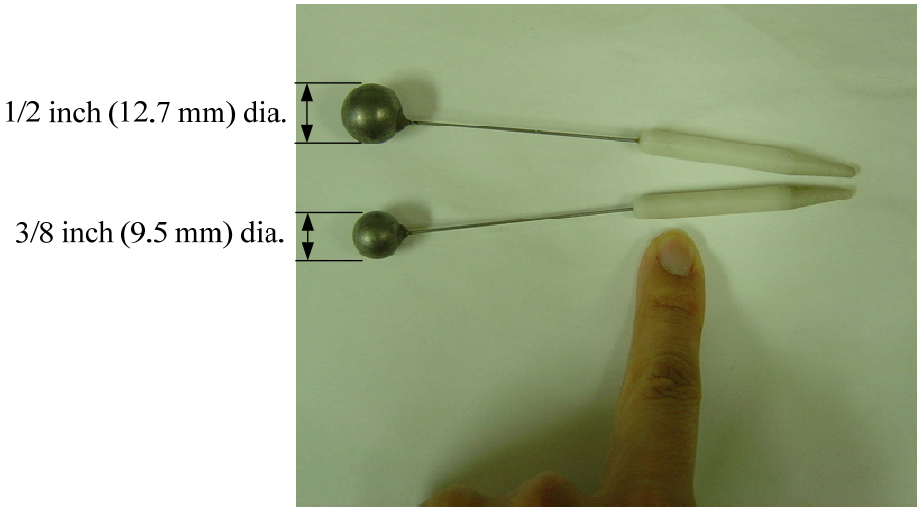

Figure 3-8. Steel Impactors for Sounding Inspection.

3.3.4. Void mapping sheet

Void profiles developed from the sounding and visual inspections were mapped on scaled sheets called "void mapping sheets." Irregular soundings are recorded on the "unrolled drawing" of PT ducts as shown in Figure 3-9 and Figure 3-10. Black areas indicate voids in Figure 3-10.

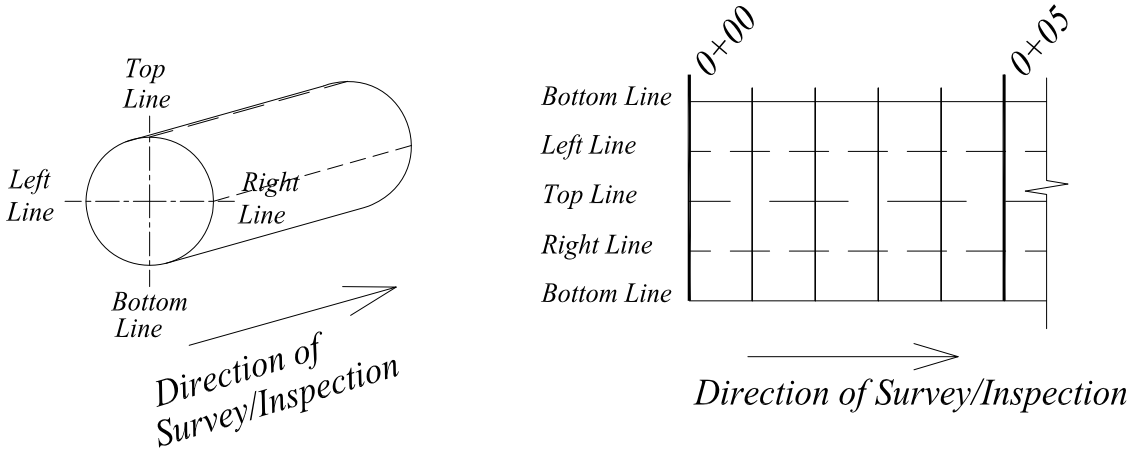

Figure 3-9. Unrolled Drawing of PT Ducts in the "Void Mapping."

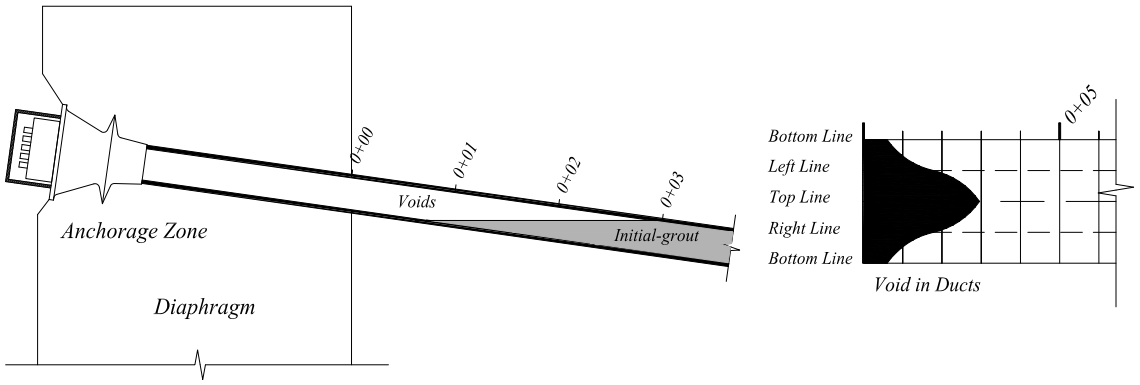

Figure 3-10. Marking Voids on the "Void Mapping Sheet."

3.3.5. Comparison of void profiles obtained using visual and sounding inspections

A comparison of void profiles obtained using the sounding and visual inspections was performed to assess the accuracy of the sounding inspections.

The void maps obtained from the visual and sounding inspection were drawn in AutoCAD® and the area at every one-foot (0.305 m) interval was determined. The calculated areas were then used to compare the effectiveness of the sounding inspection method.

3.3.6. Nomenclature of specimen

For the experimental specimens, both sounding and visual inspections are first performed and repair work described in Section 4 is then carried out in this research. Thus, each specimen is identified here using repair grouting methods and materials. Specimen identification and notation consists of three character groups with each group separated by a hyphen. The first character set denotes the name of the repair grouting method (VG, PG, or PVG) while the grout type is assigned to the second group (C1, C2, or C3). The third and final number represents the specimen number (1 or 2). For example, the classification VG-C1-2 denotes that it is the second specimen using the vacuum grouting procedures with C-1 grout.

3.4. Void Detection and Assessment: Results

This section provides the detailed results of sounding inspections of specimen VG-C1-2. Although some errors were identified with the sounding technique, this research shows that the sounding technique is relatively accurate and there exists a correlation between irregular soundings and the existence of voids. This section also provides a summary of a procedure on how to estimate repair grout volumes from sounding inspection data. The

detailed results of all other specimens are shown in Appendix A. However, it might be not practical in bridges having low height (under 6 feet [1.8 m]) of inside box girder because they are not appropriate to perform a walkthrough inspection.

3.4.1. Effectiveness of sounding inspection

A sounding inspection is generally performed to identify the existence of voids in ducts (FDOT 2001a). Because of the general uncertainty associated with sounding inspections, a detailed inspection using a borescope can be conducted to confirm the existence of a void. To evaluate the effectiveness of sounding inspections, a *t*-test is performed that compares the differences between sounding and visual inspections. Void profiles found by both sounding and visual inspection methods are provided in the form of void maps for every specimen. The difference between the sounding inspection and the void inspection was estimated at intervals of one per foot (0.305 m) for the entire specimen. Figure 3-11 shows the initial void profiles found by the sounding inspection and the visual inspection before repairing the specimen (VG-C1-2). The areas of both void profiles were estimated using AutoCAD® and are provided in Table 3-1.

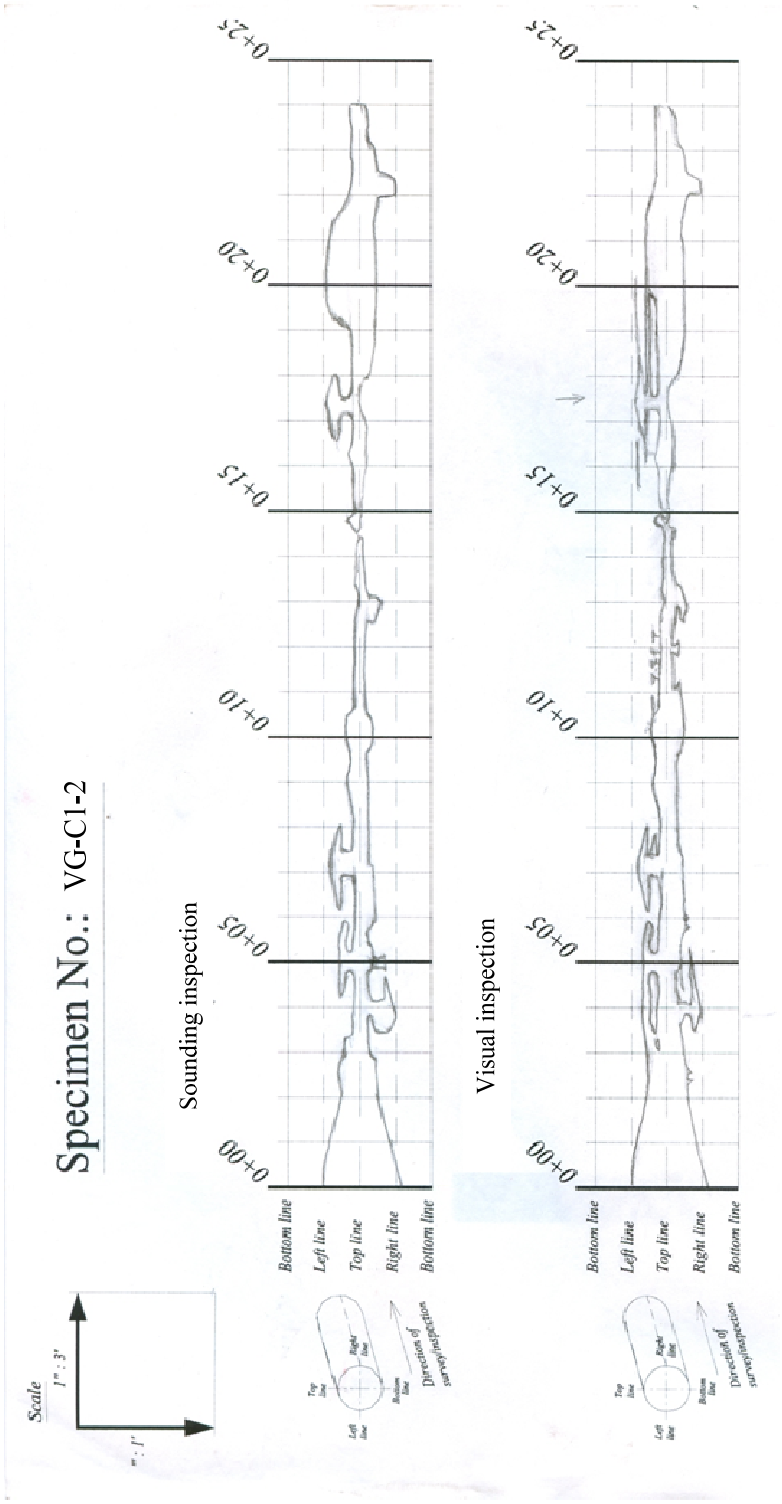

Figure 3-11. Void Map of Specimen VG-C1-2.

Table 3-1. Estimation of Void Profile in Specimen VG-C1-2.

Section, ft (m)	Sounding Inspection (SI), inch^2 (10^{-4} m^2)	Visual Inspection (VI), inch^2 (10^{-4} m^2)	SI - VI, inch^2 (10^{-4} m^2)
0~1 (0~0.3)	73.60 (474.9)	73.20 (472.2)	0.41 (2.6)
1~2 (0.3~0.6)	50.58 (326.3)	53.34 (344.2)	-2.76 (-17.8)
2~3 (0.6~0.9)	38.69 (249.6)	41.93 (270.5)	-3.25 (-20.9)
3~4 (0.9~1.2)	31.94 (206.1)	41.46 (267.5)	-9.52 (-61.4)
4~5 (1.2~1.5)	30.48 (196.7)	37.46 (241.7)	-6.98 (-45.0)
5~6 (1.5~1.8)	28.80 (185.8)	34.93 (225.3)	-6.13 (-39.6)
6~7 (1.8~2.1)	29.49 (190.2)	31.78 (205.0)	-2.29 (-14.8)
7~8 (2.1~2.4)	32.32 (208.5)	35.88 (231.5)	-3.55 (-22.9)
8~9 (2.4~2.7)	19.04 (122.8)	20.34 (131.2)	-1.30 (-8.4)
9~10 (2.7~3.0)	21.75 (140.3)	24.93 (160.8)	-3.18 (-20.5)
10~11 (3.0~3.4)	20.76 (133.9)	30.52 (196.9)	-9.77 (-63.0)
11~12 (3.4~3.7)	11.59 (74.7)	20.07 (129.5)	-8.49 (-54.7)
12~13 (3.7~4.0)	17.75 (114.5)	18.33 (118.3)	-0.58 (-3.7)
13~14 (4.0~4.3)	11.31 (73.0)	14.30 (92.3)	-2.99 (-19.3)
14~15 (4.3~4.6)	7.50 (48.4)	10.33 (66.6)	-2.83 (-18.3)
15~16 (4.6~4.9)	11.10 (71.6)	12.19 (78.7)	-1.09 (-7.0)
16~17 (4.9~5.2)	19.93 (128.6)	22.50 (145.2)	-2.57 (-16.6)
17~18 (5.2~5.5)	26.44 (170.6)	27.76 (179.1)	-1.32 (-8.5)
18~19 (5.5~5.8)	23.16 (149.4)	33.98 (219.3)	-10.83 (-69.9)
19~20 (5.8~6.1)	46.90 (302.6)	39.19 (252.8)	7.72 (49.8)
20~21 (6.1~6.4)	51.61 (333.0)	39.85 (257.1)	11.76 (75.9)
21~22 (6.4~6.7)	41.21 (265.9)	37.33 (240.8)	3.88 (25.0)
22~23 (6.7~7.0)	35.74 (230.6)	37.21 (240.0)	-1.47 (-9.5)
23~24 (7.0~7.3)	19.61 (126.5)	21.06 (135.9)	-1.45 (-9.4)

The void profiles and the area estimates for all other specimens are provided in Appendix A. In the analysis, void maps generated from visual inspections are

considered to represent the actual existence of voids as it was possible to confirm their existence through the transparent acrylic ducts. The differences between the void quantities from the sounding inspections and the visual inspections were compared using the null and alternate hypotheses (H_0 and H_1) as follows:

$$H_0 : \mu_{\text{Sounding Inspection - Visual Inspection}} = 0$$
$$H_1 : \mu_{\text{Sounding Inspection - Visual Inspection}} \neq 0 \quad (3.1)$$

where, $\mu_{\text{Sounding Inspection – Visual Inspection}}$ is the mean of the population for differences between void areas detected from the sounding inspections and visual inspections.

The results of the *t*-test are provided in Table 3-2. Figure 3-12 shows the data distributions. From the analysis, the null hypothesis is rejected at the 0.05 level of significance; therefore, the voids identified from the sounding inspection do not accurately represent the existence of voids in ducts.

Table 3-2. The *t*-test for Difference between Sounding and Visual Inspections.

Difference	Mean	Standard Deviation	Sample Size	*t*-test	*p*-value
Sounding - Visual	-1.0743	7.7295	360	-2.637	0.002

However, a correlation analysis between sounding and visual inspections reveals a highly positive linear correlation (correlation coefficient is 0.906) between the actual voids in the test specimens and sounding inspections. Interpretation of this correlation reveals that the voids detected by sounding inspections are inaccurate when considering the magnitude of a void, but are relatively accurate at determining the location and existence of a void. This relationship will be shown in the next section. While the sounding inspection lacks the ability to detect extremely small voids and requires

experienced personnel, it can be an effective tool for inspecting voids because of its ease of application and relative accuracy.

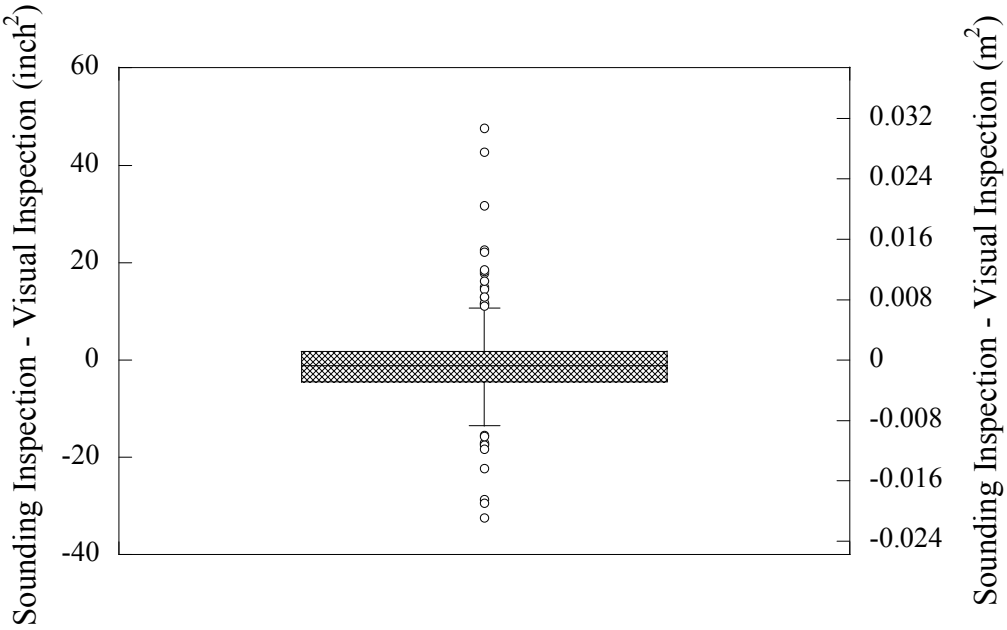

Figure 3-12 Box and Whisker Plot for the Difference between Sounding Inspection and Visual Inspection.

3.4.2. Volume estimation of voids in ducts by sounding inspection

The volume of repair grout can be estimated using a volumeter, an instrument that measures the volume of voids in ducts, using air pressure (FHWA 2004). However, using a volumeter requires that ducts are in sealed conditions to correctly estimate void volumes. While volumeters are equipped with some leak compensation abilities, errors might be occurred. A volumeter is capable of estimating the entire volume of an external tendon. Based on the experimental results in Section 4, however, for this to be accomplished in the field the repair grouting might be performed twice from each end because test results indicate that repair grouts cannot fill all the voids in the entire tendon

at one time. Therefore, alternative methods for measuring the volume of voids are required for repair methods in ducts.

In this research, estimates of the required volume for repair grout were made using the data obtained from sounding and visual inspections. However, the experimental specimens are too short to provide the required grout volume in the field. Thus, this research estimated void volume in bleed line and assumed partially filled parts, void areas that exceed the "Left Line" and "Right Line" on void mapping sheets, as empty. The void areas per foot obtained from visual and sounding inspection ($A_{VI/ft}$ and $A_{SI/ft}$) were found to be linearly correlated (Figure 3-13). The corresponding equation is as follows:

$$A_{VI/ft} = 0.85A_{SI/ft} + 4.5$$
$$(A_{VI/ft} = 0.85A_{SI/ft} + 30 \text{ for SI unit}) \quad (3.2)$$

where $A_{VI/ft}$ is the estimated by visual inspection, which is assumed here to be the actual void area per foot estimated on void mapping sheet, in inch^2 (10^{-4} m^2 for SI unit) and $A_{SI/ft}$ is the estimated by the sounding inspection in inch^2 (10^{-4} m^2 for SI unit). To prevent the underestimation of voids, the upper limit (U.L.) equation for a 0.05 level of significance can be used as follows:

$$A_{VI/ft} = 0.85A_{SI/ft} + 19 \text{ (U.L.)}$$
$$(A_{VI/ft} = 0.85A_{SI/ft} + 120 \text{ (U.L.) for SI unit}) \quad (3.3)$$

Through the sounding inspection $A_{SI/ft}$ is obtained as follows:

$$A_{SI/ft} = A_{SI} / l_{void}$$
$$(A_{SI/ft} = 0.3048 A_{SI} / l_{void} \quad \text{for SI unit}) \tag{3.4}$$

where A_{SI} is the total void area estimated by the sounding inspection in inch^2 (10^{-4} m^2 for SI unit) and l_{void} is total void length on void mapping sheet in foot (m for SI unit).

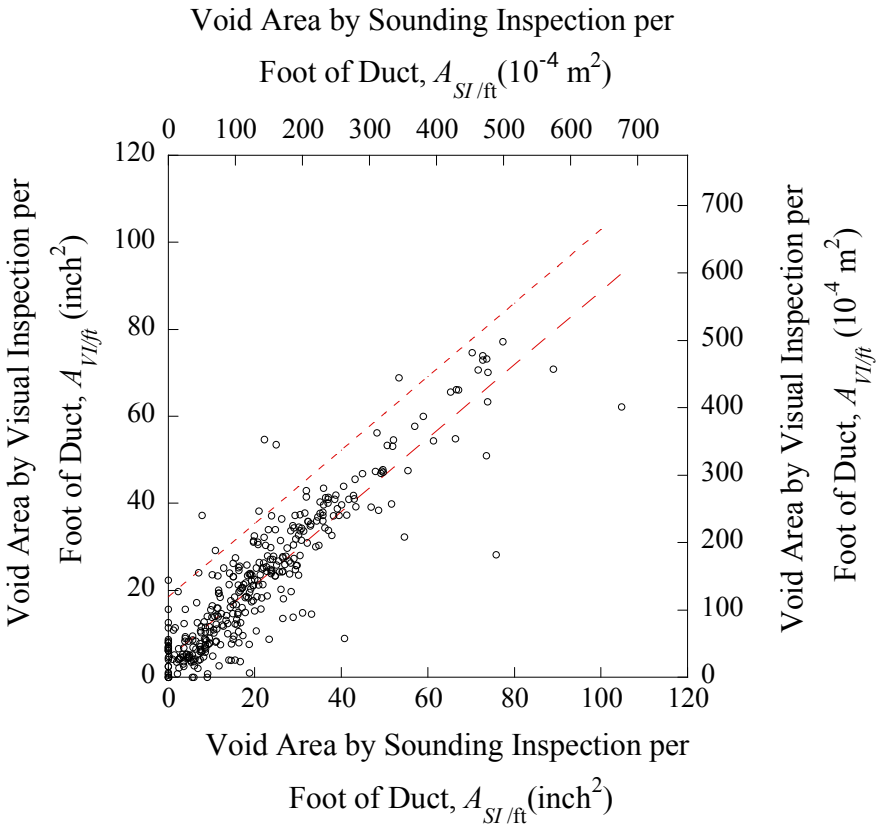

Figure 3-13. Scatter Plots between the Void Areas Per Foot Obtained from Sounding and Visual Inspections.

From volumetric estimations of repaired grouts from the test specimens, the relationship between void areas per foot by visual inspection and the volume of repair grouts per foot used for the specimens are provided in Figure 3-14. The repaired volume per foot of each specimen was obtained from the sections of the cut tendon. For cut

sections, the approximate repaired volume was determined using the average void area at both ends multiplied by the cut length. The equation for the relationship between void areas per foot determined from the visual inspections and the grout volume per foot is estimated as follows:

$$V_{req/ft} = 1.2\exp(0.45A_{VI/ft})$$
$$(V_{req/ft} = 10\exp(0.03A_{VI/ft}) \text{ for SI unit}) \quad (3.5)$$

where, $A_{VI/ft}$ is the estimated area per foot by visual inspection in inch^2 (10^{-4} m^2 for SI unit) and $V_{req/ft}$ is the estimated repair volume per foot of the specimen in inch^3 (10^{-6} m^3 for SI units). To ensure enough grout for repair, the upper limit equation (95% confidence limit) for this relationship is given by:

$$V_{req/ft} = 1.5\exp(0.5A_{VI/ft}) \text{ (U.L.)}$$
$$(V_{req/ft} = 11\exp(0.03A_{VI/ft}) \text{ (U.L.) for SI unit}) \quad (3.6)$$

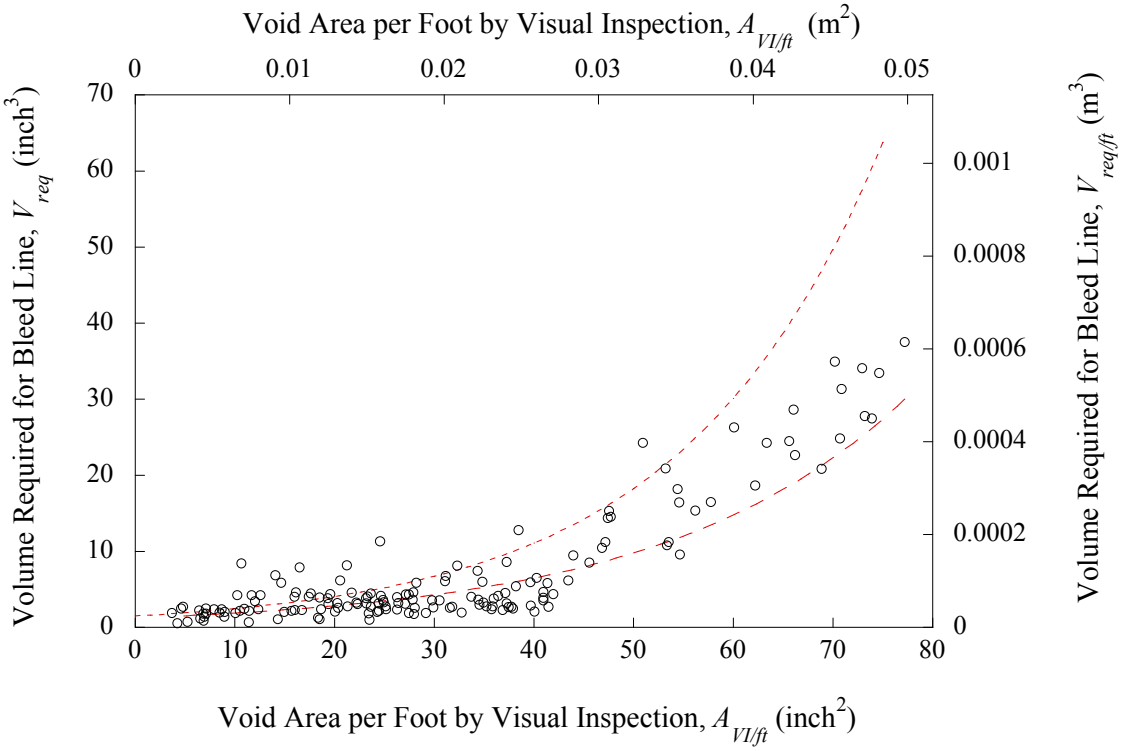

Figure 3-14. Scatter Plot between the Void Areas per Foot from Visual Inspection and the Void Volume Repaired per Foot.

From Equations (3.3) and (3.6), the repair volume per foot can be approximately estimated from the sounding inspection. The equation of the repair volume per foot for bleed line, which does not contain the volume of bearing plate and embedded ducts, is defined as follows:

$$V_{req/ft} = 1.5\exp(0.4A_{SI/ft} + 20)$$
$$(V_{req/ft} = 11\exp(0.03A_{SI/ft} + 4) \text{ for SI unit}) \quad (3.7)$$

Thus, tatal required volume can be estimated multiplying the total length of voids:

$$V_{req} = V_{req/ft} \times l_{void}$$
$$(V_{req} = V_{req/ft} \times l_{void} / 0.3048 \quad \text{for SI unit}) \tag{3.8}$$

Based on the cross sections of each test specimen the repair volume per foot of each specimen was obtained for estimating void volume of bleed lines. However, this relationship does not include the void volume contained in the embedded ducts and the bearing plate in the diaphragm; the embedded duct and bearing plate in the concrete diaphragm in the field cannot be examined using the sounding inspection method. To ensure sufficient grout is prepared, the volume estimates of the repair grout should be performed assuming that the embedded ducts and bearing plate contain no grout. From bearing plate designs and diaphragm thicknesses, bridges have different grout volume requirements for anchorage zones. Thus, the void volume in bearing plate and embedded ducts has to be added to Equation (3.8) to apply in the field.

Figure 3-15 provides examples of the void profiles obtained from sounding inspections. While this inspection shows the existence of voids, it lacks the ability to show void size and the condition of the strands inside. Hence, a detailed inspection using a borescope would be beneficial to assess voids and strand corrosion. From a detailed inspection using a borescope, it might be determined whether tendons need repair work or not. In both examples in Figure 3-15, it was assummed that repair grouting might be needed. Although this volume may be different in actual structures, the obtained volume can be simply determined from the sounding inspection and ensures sufficient volumes for repair.

In the case of the example in Figure 3-15 (a), the value of A_{SI} can be estimated from 3 ft (0.91 m) to 10.2 ft (3.07 m). Note that the void profile between 0 ft (0 m) and 3 ft (0.91 m) represents a nearly empty duct. To ensure sufficient amounts of repair grout void areas that exceed the “Left Line” and “Right Line” (see Figure 3-15 (a)) are considered as empty. Thus, the bearing plate, the embedded ducts in the diaphragm, and

an additional 3 ft (0.91 m) along the ducts are considered to be empty in this case (see Figure 3-15). To estimate the area per foot of the sounding inspection, $A_{SI/ft}$, total void area, A_{SI}, from 3 ft (0.91 m) to 10.3 ft (3.14 m) is divided by the total length of voids, l_{void}. The repair grout volume per foot, $V_{req/ft}$, can be obtained from Equation (3.7). Thus, the total required volume, V_{req}, is determined using (3.8) The volume of the empty bearing plate and ducts has to be estimated and added to V_{req} to provide the total required volume for repair grouting.

In the case of the example in Figure 3-16 (b), the value of A_{SI} can be estimated from 0 ft (0 m) to 9.7 ft (2.92 m) - the bearing plate and embedded ducts in the diaphragm are considered to be empty. The estimated A_{SI} can be used to determine $A_{SI/ft}$ in Equation (3.4) and V_{req} can be estimated using Equations (3.7) and (3.8). The volume of the bearing plate and duct embedded in the diaphragm is estimated assuming it is empty. The total volume required can again be obtained by adding these two volumes.

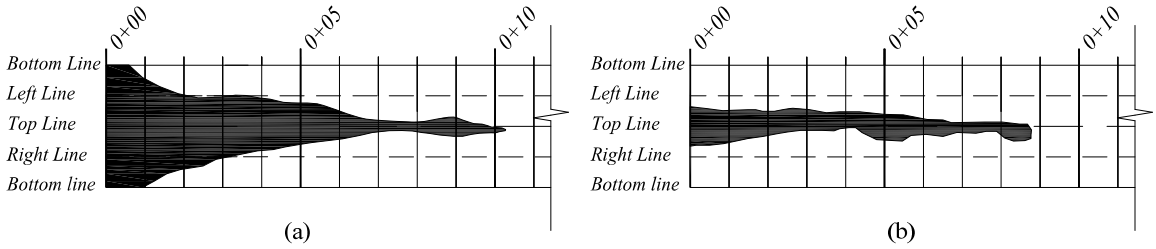

Figure 3-15. Examples of Void Profiles Obtained from Sounding Inspection Method.

The Equation (3.7) for estimating volume required for repair can be applied in the field when external tendons are contained in 4-inch (0.1-m, inside diameter) ducts and void profiles are determined using sounding inspections. Therefore, a void profile developed using a sounding inspection method can be used to predict the grout volume required for repair as well as the appropriate locations for detailed inspections using a borescope.

3.5. Application of Sounding Inspection in the Field

To verify the effectiveness of the sounding inspection method, the method was applied to the San Antonio "Y" bridge, which is a segmental PT bridge including external PT systems. With permission from the Texas Department of Transportation (TxDOT), two spans (No. 24 and 25) of Spine CC (IH 35 South Bound) were selected for the sounding inspection. Figure 3-16 and Figure 3-17 show the outside and inside views of Span 25.

Figure 3-16. Outside View of Box Girder (Span 25, Spine CC).

Figure 3-17. Inside View of Box Girder (Span 25, Spine CC).

Walk-through inspections were performed first in both selected spans and two external tendons in Span 25 were then selected for applying detailed sounding inspections. The tendons selected for in-depth inspection needed to be surveyed such that inspectors can quickly determine the location of voids or other damaged areas. Thus, the selected tendons were cleaned for marking and then surveyed for the sounding inspection. Survey stations were marked at every foot interval along the ducts using a paint marking pen. The sounding inspections were then performed on the selected tendons in the same manner of experiments in the laboratory. The void profiles in the field are shown in Figure 3-18 and Figure 3-19.

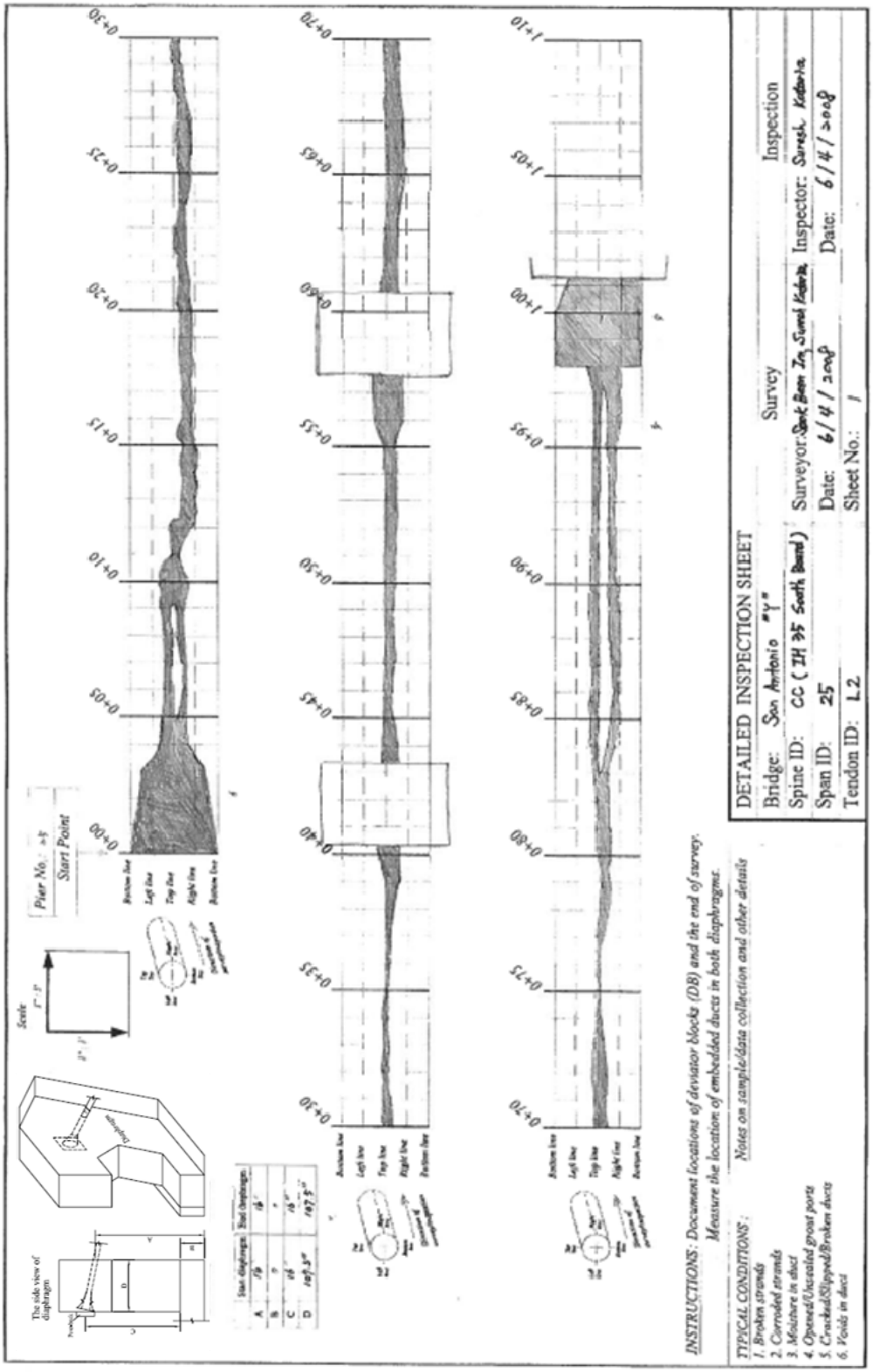

Figure 3-18. A Void Profiles in San "Y" Bridge (Tendon L2 in Span 25).

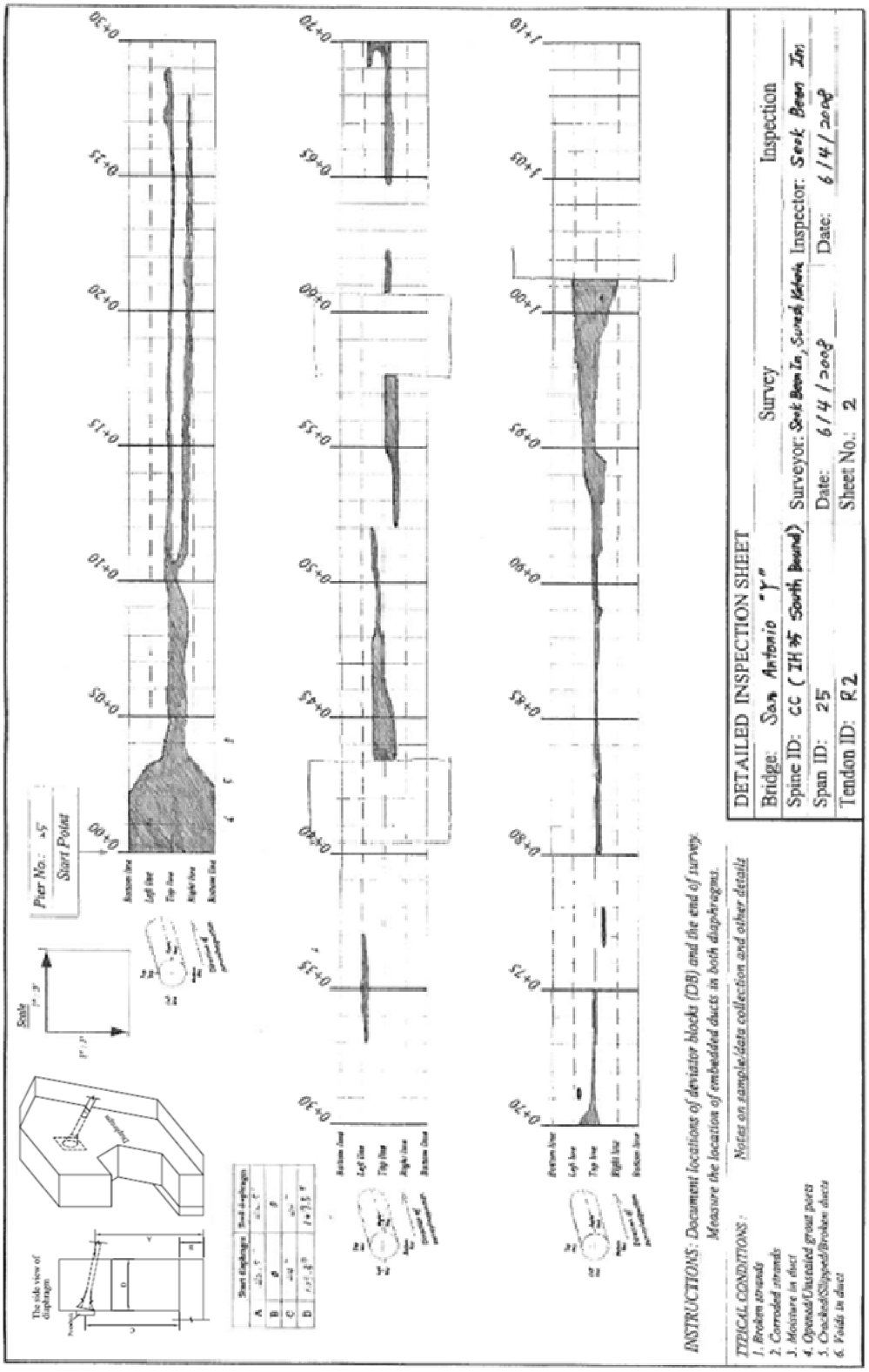

Figure 3-19. A Void Profiles in San "Y" Bridge (Tendon R2 in Span 25).

The void profiles in the selected tendons (Figure 3-18 and Figure 3-19) show the same trends as the laboratory samples, and indicate that large voids are present in ducts near both end diaphragms. To verify the effectiveness of the sounding inspection, the locations of both end diaphragms were directly inspected using a borescope. The inspection was performed using a borescope and introduced through the grout inlet of each selected tendon and the inside of the tendon near the end diaphragm was investigated. Figure 3-20 and Figure 3-21 show the inside view of tendons near the end diaphragms and grout-void interface is identified in these locations. Thus, it can be concluded that the sounding inspection identifies grout-void interface inside ducts. Although the sounding inspection cannot assess the exact size of voids and the presence of corrosion, it is effective to simply apply in the field and provide void locations in ducts.

Figure 3-20. Inside View Using Borescope of Ducts near an End Diaphragm (Tendon R2, Span 25, Spine CC).

Figure 3-21. Inside View Using Borescope of Ducts near an End Diaphragm (Tendon L2, Span 25, Spine CC).

3.6. Inspection of PT Bridges

Based on the experiments and field inspection, this research developed a manual of the inspection and repair of PT bridges for field engineers. This manual is provided in Appendix B. The reader is encouraged to review that document if procedures on inspecton or repair are needed. An overview of inspection is provided here.

The corrosion of tendons has been a long-standing issue in PT structures because the PT tendons perform a significant role in the structural integrity of the system. In addition, severe tendon corrosion can lead to the collapse of a bridge. Thus, it is critical to proactively protect tendons from corrosion. For PT tendons with severe corrosion, tendon replacement may be required; however, this can be expensive. Therefore, it would be advantageous to detect tendon corrosion in its early stages, not only to ensure public safety, but also to prevent severe damage and to reduce structural maintenance and repair costs.

Ideally, bridge inspection should be performed at regular intervals to ensure bridge performance. As with most bridges, PT bridges are inspected every two years. However, more detailed inspections may be needed – these can be expensive and time consuming and inspecting all bridges in great detail may not be necessary. Detailed bridge inspections should be able to be performed in a timely manner and repairs should be dependent on damage levels. This research provides an inspection manual that provides strategies for inspection and analysis of external PT tendon system to maintain bridge performance when corrosion is present (Appendix B). This inspection manual categorizes bridges and spans based on environmental conditions, factors inducing corrosion, and structural/non-structural damage caused by corrosion. This approach can reduce the time for bridge inspection significantly; thus enabling bridge management to be performed more effectively.

4. MITIGATION AND REPAIR STRATEGIES: EXPERIMENTAL PROGRAM AND RESULTS

4.1. Introduction and Objective

The objective of the research presented in this section is to develop and propose an effective method for repairing voids in tendons on PT bridges. Three different repair grouting methods were evaluated for determining the 1) filling capability in voided ducts, 2) repair performance, and 3) economic feasibility of the method. In addition to evaluating grouting methods, various grout types were assessed as possible repair materials.

4.2. Mitigation or Repair Strategies: Experimental Program

This section describes the experimental program including the test materials, the test methodologies, and the analysis. This section first introduces the descriptions of the test materials and test procedures. Next, the proposed methodologies for repairing tendons are presented. The analysis plan of the data obtained from the test program is then presented and effective repair methods for filling voids in ducts are proposed.

4.2.1. Experimental setup

In this research 16 prototype external tendon (PET) specimens were fabricated. These specimens contained inclined and horizontal tendons. This tendon set-up was designed, fabricated, and used to evaluate different repair grouting methods and different grouting materials (refer to Figure 3-2 in Subsection 3.3.1).

4.2.2. Grouting techniques

4.2.2.1. Grout types

In this research, the initial grout used to fill ducts is a Class A grout. The repair grouts used are commercially available pre-packaged grouts, classified as Class C grouts. Three high performance grouts are being assessed in this program and are labeled C-1, C-2, and C-3. Table 4-1 shows how each grout is labeled and Table 4-2 shows the experimental design. The research evaluated three different grouts and three different repair methods. Duplicate tests were planned for each combination but the C-3 grout was found to be difficult to use in the repair methods assessed in this program. As a result of this, only one PET specimen each with the C-3 grout in the VG and PVG repair methods (discussed later). The w/p (water-powder ratio*) of each repair grout was based on the manufacturer's recommendation. The color of the A and C grouts are similar. To distinguish between the initial grout and repair grout a small amount of colorant was added to the grouts.

Table 4-1. Labels of Pre-packaged Grouts.

Grout	Label
ASTM Type I cement	A
Masterflow 816	C-1
Sika grout 300PT	C-2
Euco Cable grout PTX	C-3

* Water-powder ratio is the ratio of water and all ingredients in the pre-packaged grout bag.

Table 4-2. Repair Materials and the Test Matrix.

Grout Materials		No. of Specimens for Each Repair Grouting Method		
Repair Grouts	**w/p**	**PG**	**VG**	**PVG**
C-1	0.30	2	2	2
C-2	0.26	2	2	2
C-3	0.27	2	1	1

4.2.2.2. Grout mixer and mixing procedures

Two types of mixers are used to prepare The A grout. The A grout was first mixed (for 5 minutes) using an air-powered paddle mixer as shown in Figure 4-1. Then, mixing was stopped to add colorant. This was following by further mixing (for one additional minute) using a 2500 rpm drill with a mixing paddle (Figure 4-2). Further mixing was then performed with the air-powered grout mixer for an additional 5 minutes. The total mixing time was 11 minutes for the A grout.

Figure 4-1. Grout Mixer for Initial Grouts and Grout Pump.

To mix the C grouts used for the repairs, portable drills and mixing paddles were used to mimic field practices when small amounts of grout are required for tendon repairs (see Figure 4-2). The amount of grout required for each repair was 1500 cubic inches (0.025 cubic meters); therefore, the grout was divided into two batches, mixed separately for the recommended mixing time, then combined in 15-gallon (56.8-liter) buckets. The grout was then mixed for an additional 2 minutes. Mixing times for each repair grout is provided in Table 4-3.

Figure 4-2. Drill and Mixing Paddle.

Table 4-3. Recommended Mixing Time and Drill for Repair Grouts.

Repair grouts	Mixing Time (minutes)	Mixing Drill (rpm)
C-1	5	2500
C-2	6	2500
C-3	20	4000

4.2.2.3. Material tests for grouts

Because small changes in environmental conditions can have a significant influence on grout flow, the flow cone test was performed to measure the efflux time of the grouts. Procedures provided in Tex-437-A Method 2 (TxDOT 1999) were followed. In addition, the wick-induced bleed test was conducted following Tex-441-A (TxDOT 2003). The flow cone test and wick-induced bleed test are provided in Figure 4-3. The compressive strength test of cubic molds was carried out to verify the strength of hardened grouts. Three cubes were cast for each grout and were tested for compressive strength at 7 and 28 days following Tex-442-A (TxDOT 2006). The results of the compressive strength test are shown in Appendix C. All grout materials exceeded the TxDOT required strength (4 ksi at 7 days and 4.6 ksi at 28 days).

(a) (b)

Figure 4-3. (a) Flow Cone and (b) Wick-induced Bleed Test.

4.2.3. Methodology of repair grouting

FDOT (2001a) reported that the VG method is more effective than the PG method. However, the FDOT did not employ the use of air outlets for the PG method and grout was injected by pressure into sealed specimens. This can significantly reduce the effectiveness of the PG method, making it more difficult to fill the voids in the tendon. In this research, the PG method is applied with an air outlet on the voided duct.

A preliminary test using the PG method was performed to determine an appropriate location for grout injection. The first injection location for the repair grout is grout vent #1 (Figure 4-4). This location was selected because grout should be injected from a low point to reduce the amount of entrapped air inside the tendon. When injected at this point the grout filled the voids below the injection hole and did not fill the void above the injection point. As a result of this, the repair grout was injected into grout vent #2. The grout infiltrated the ducts below this point and did not fill the void above this point. Finally, the repair grout is injected into grout vent #3. The grout filled the lower voids up to grout vent #2. Although grout can be injected near the anchorage zone in this setup where the large voids were located, in actual structures the anchorage

diaphragms will likely prevent access to these areas. In most cases, diaphragms range from 5 to 9 ft (1.52 to 2.74 m) long, so they will prevent the access of ducts where large voids are present near anchorage areas.

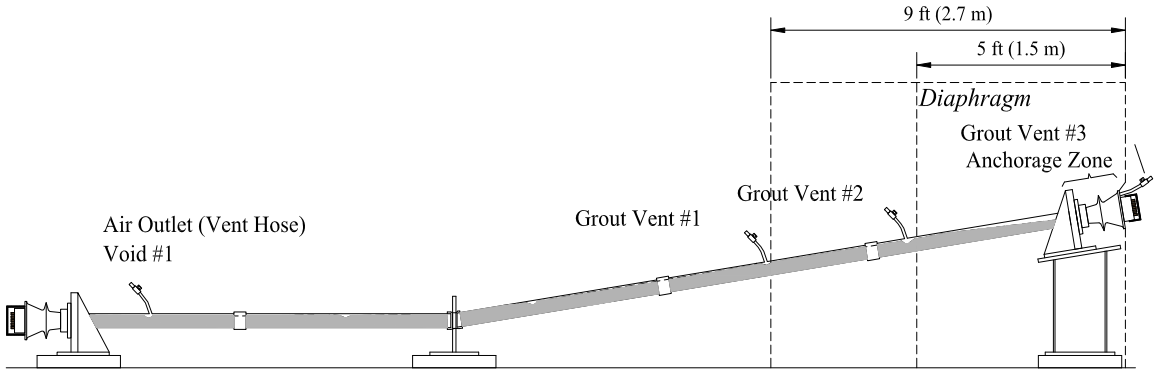

Figure 4-4. Preliminary Test for the PG Method.

Therefore, the injection location and the air outlet for the PG method were developed based on preliminary testing and industry practices. The test set-ups for the different methods are shown in Figure 4-5. All the injection grout inlets for each repair grouting method are at the ports located in the anchor plate of the upper anchorage (Figure 3-2).

4.2.3.1. Pressure-grouting method

The grout injection in the PG method can be applied by using an air-powered grout pump. However, a sealed portion of the ducts could burst when this pressure is applied. To prevent sealed ducts from bursting while under pressure, a hand grout pump (Figure 3-3) was used which does not typically increase the pressure inside the duct to a high level.

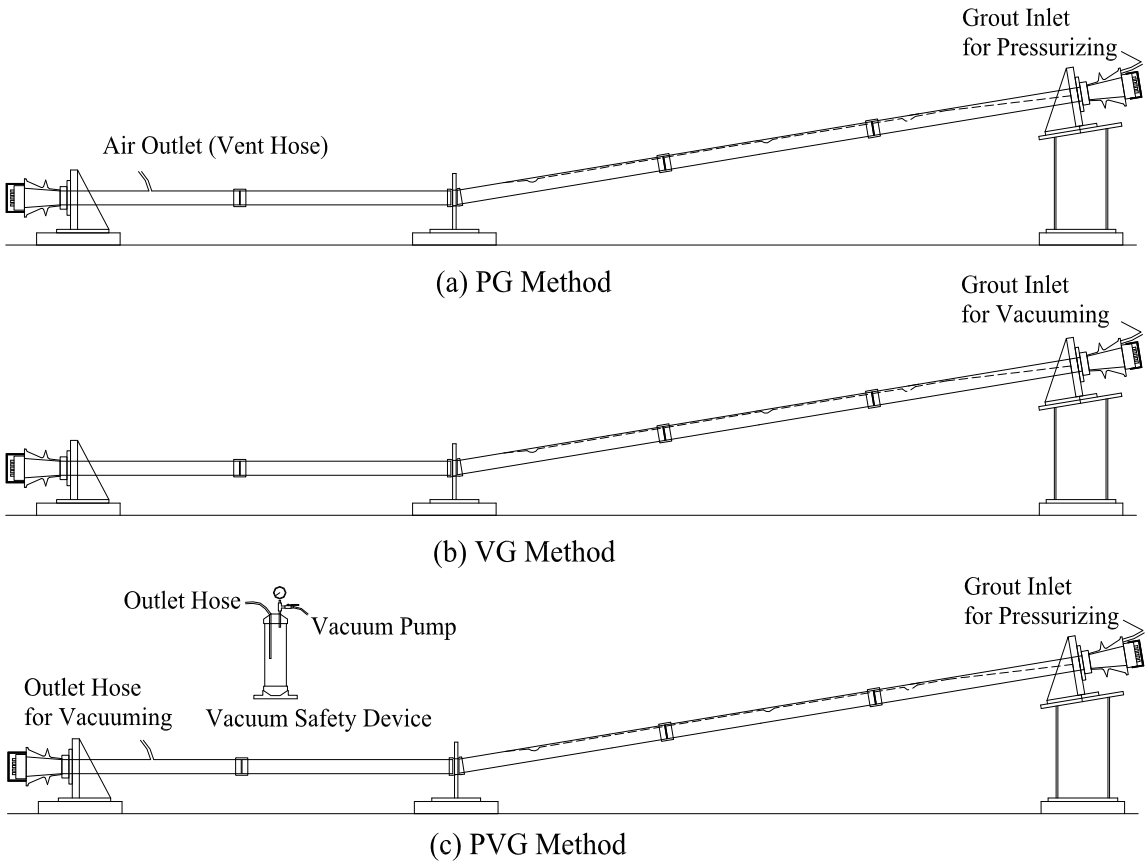

Figure 4-5. Schematic of PET Specimens Showing the Inlet and Outlet Holes.

4.2.3.2. Vacuum-grouting method

The VG method uses only one grout port and no outlet port. The vacuum pump is connected to one end of a T-connection valve and the grout storage tank is connected to the other end (Figure 4-6). The vacuum grout inlet is connected to the third opening of the T-connection valve. When activating the vacuum pump the valve connecting the storage tank has to be closed. After a vacuum is created inside the tendon the valve for the vacuum pump is closed and the storage tank valve is opened. Repair grout will flow into the duct due to the reduced pressure in the duct. However, to create the reduced pressure required to fill the voids an air-tight condition is required. This has been a challenge of using the VG method in the field.

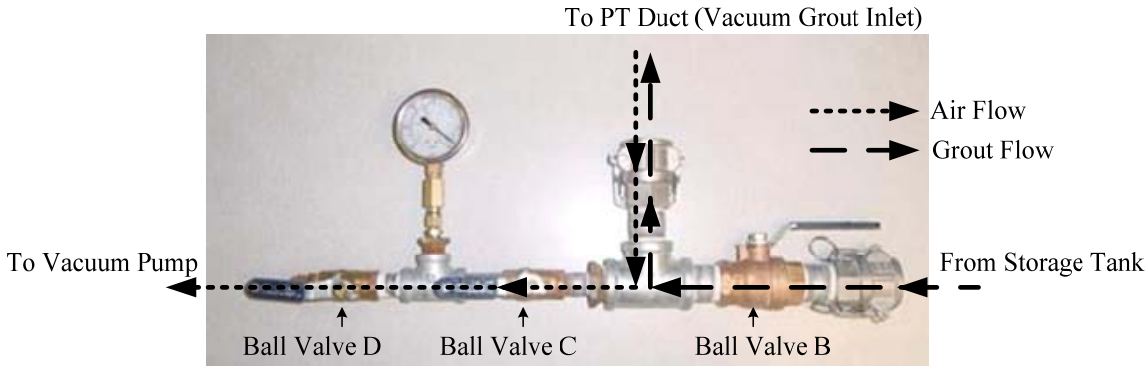

Figure 4-6. T-connection Valve for Vacuum Grouting Method.

4.2.3.3. Pressure-vacuum-grouting method

The PVG method requires the simultaneous use of a hand grout pump and a vacuum pump. The use of a vacuum pump is required to avoid the potential pressure build-up inside the duct. The vacuum pump is connected to the air outlet near the lower anchorage of the test specimen. Because the PVG method does not require an air-tight duct, it may be more practical for field applications than the VG method. To protect the vacuum pump from being contaminated with repair grout, a safety device was connected between the outlet hose and the vacuum pump (see Figure 4-7). If grout does flow from the duct the grout will be retained in the vacuum pump container.

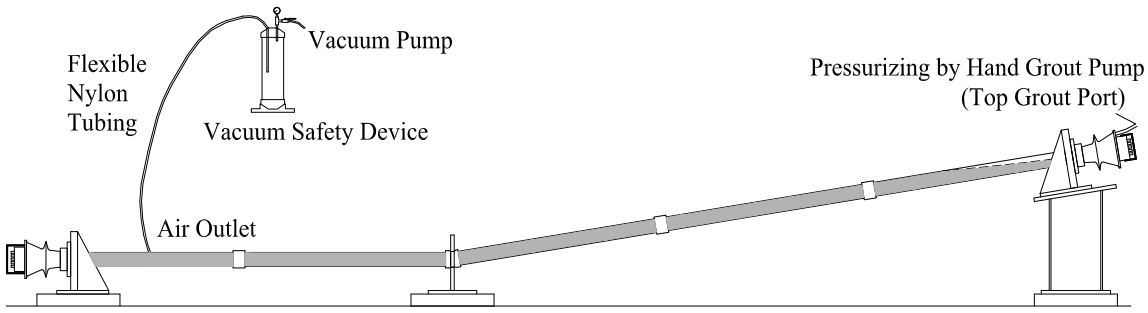

Figure 4-7. Set-up of the PVG Method.

4.2.4. Step-wise procedures for repair grouting methods

The detailed procedures for using PG, VG, and PVG repair methods are described in the following sub-sections.

4.2.4.1. Pressure-grouting method

This method requires an injection port and an air outlet. After these are connected, the following procedure was performed.

- Make connections and apply pressure grout with hand grout pump from top grout port (Figure 4-8).
- Inject repair grout until resistance on hand pump is significant (75 psi [517 kPa]).
- If the repair grout flows from air outlet, close valve at air outlet and then pump until resistance on hand pump is significant (75 psi [517 kPa]).
- If the repair grout does not flow out until resistance on hand pump is significant, close valves at grout inlet and outlet.
- Remove connection to valves and clean equipment.

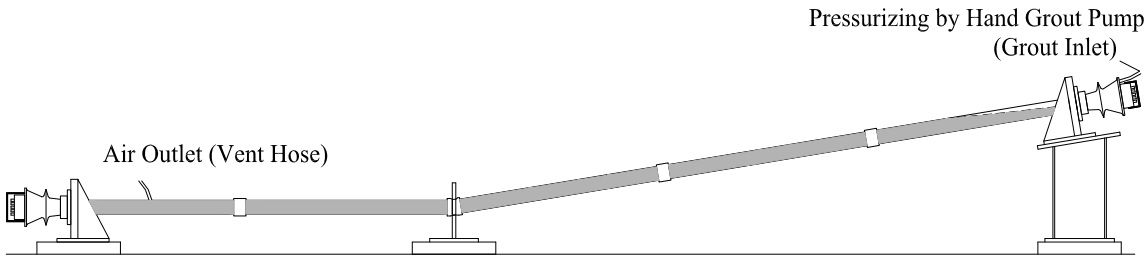

Figure 4-8. Set-up of the PG Method.

4.2.4.2. Vacuum-grouting method

This procedure assumes that all leaks in the system have been sealed. Methods include applying epoxy, chalking, and other materials to leaking areas. After sealing, the researchers used the following procedure:

- Close ball valve B and open storage tank valve (Figure 4-9).
- Open ball valves A, C, and D (not B).
- Turn on the vacuum pump to reduce pressure by 92% of the atmospheric pressure (27.5 in Hg).
- Close ball valve D and check air-tight status of ducts (by reading vacuum gage).
- If vacuum is held, close ball valve C. If vacuum is not maintained, repair leak and start process again.
- Pour repair grout into storage tank.
- Open ball valve B (repair grout will flow into duct).
- Close ball valve A after grout stops flowing.
- Close ball valve B and storage tank valve.
- Remove connection and clean equipment.

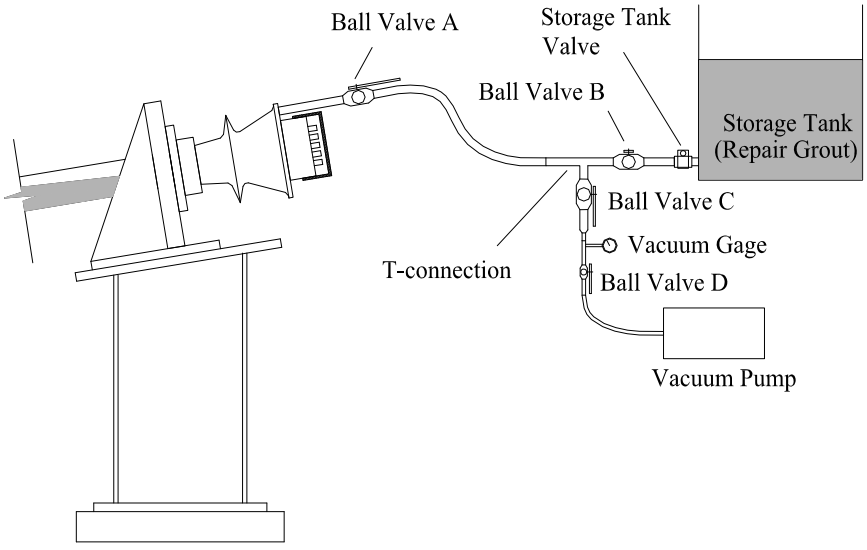

Figure 4-9. Set-up of the VG Method.

4.2.4.3. Pressure-vacuum-grouting method

This method uses both vacuum and pressure to inject repair grout into ducts containing voids. The advantages of this method include not having to repair all vacuum leaks and relatively easy repair procedures. To perform the PVG grouting method the following steps are performed.

- Connect vacuum safety device to air outlet and to vacuum pump (Figure 4-7).
- Connect hand grout pump to top grout port.
- Apply vacuum pump to reduce pressure by approximately 80% (or as much as possible) of the atmospheric pressure (23.9 in Hg)
- Open grout inlet and inject repair grout with hand grout pump
- If the repair grout flows from the air outlet, close valve B at air outlet, close valve A at safety device, and then pump until resistance on hand pump is significant (75 psi [517 kPa]).
- If the repair grout does not flow out from the air outlet, close valve A at safety device, and then pump until resistance on hand pump is significant (75 psi [517 kPa]).
- Close valve at top grout port.
- Turn off vacuum pump.
- Disconnect tubing from valves and clean equipment.

4.2.5. Methodology to evaluate the repair methods and materials

To examine the effectiveness of each grouting method and each grout material, this study performs the following analysis to assess the filling capability (FC), performance, and economic feasibility. The term FC is defined as the ability of the repair method-material combination to fill the voids.

4.2.5.1. Filling capability of repair methods and materials

To compare the FC of each specimen the length that the repair grout infiltrated the duct was investigated. The infiltration length is measured from the reference point at the upper anchorage and measured along the inclined ducts (Figure 4-10 and Figure 4-11).

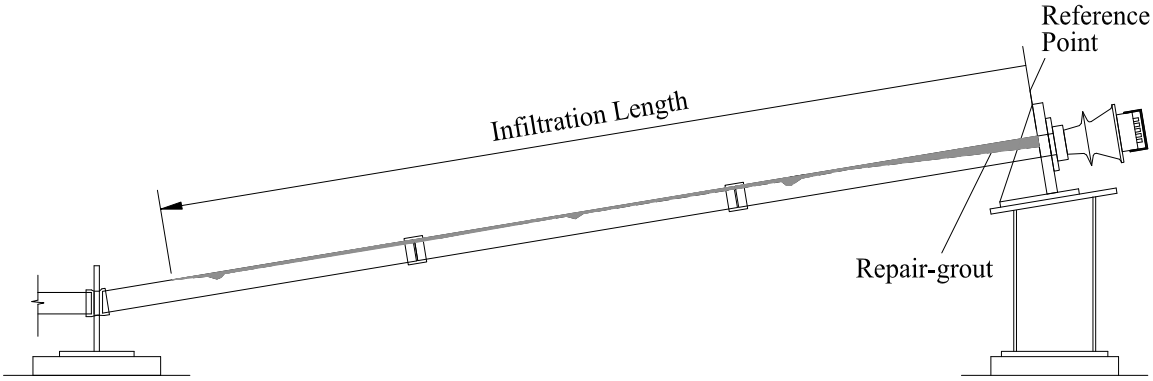

Figure 4-10. The Infiltration Length Measured from the Reference Point.

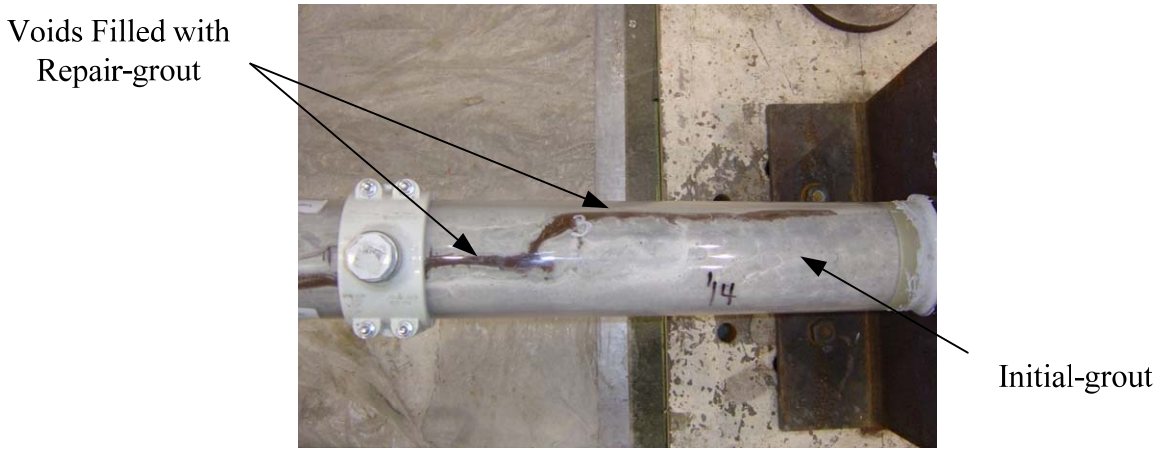

Figure 4-11. Top View of the PET Specimen Showing the Infiltration of Repair Grouts.

The path and width of the bleed line and the shape of the voids varied from one PET specimen to another. This research compares the amount of voids filled by a repair grout using an analysis of cut sections, as presented in Figure 4-12 (a) and discussed earlier. Sections were cut using a band saw at the locations shown in Figure 4-12 (a). The following subsection discusses how these were analyzed.

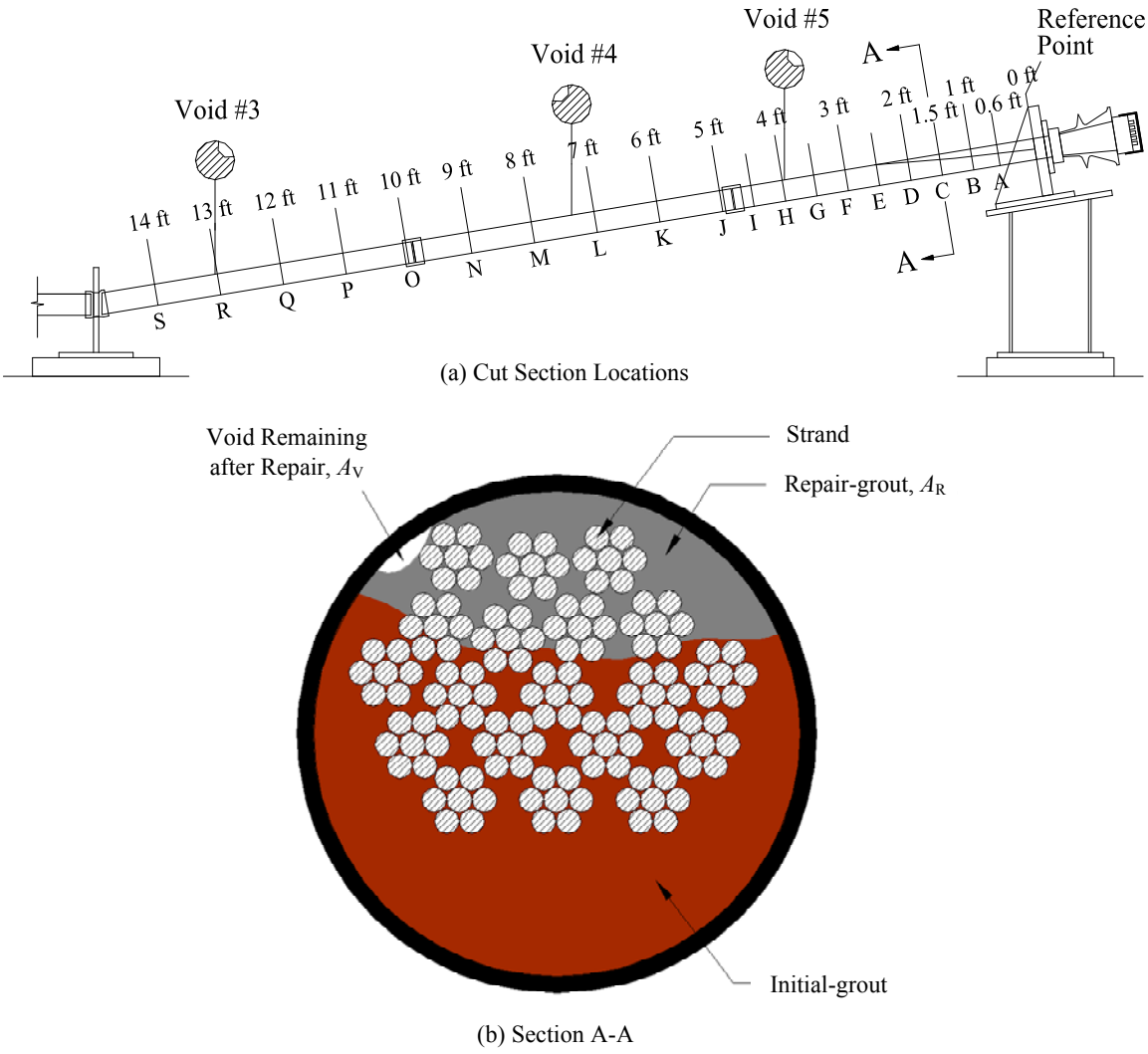

Figure 4-12. (a) Cut Section Locations of Repaired Ducts (b) and Cut Section of A-A.

4.2.5.2. Performance of repair grouts

As already noted the repair grouting was performed by three different methods using three different grout materials such that recommendation in an appropriate and economical repair grouting method for external PT systems can be developed. Figure 4-12 (b) shows an example of cut sections in a repaired duct. Note that small and sometimes isolated voids remain after grouting and these remaining voids could still leave the tendon vulnerable to corrosion. Therefore, this study evaluated and compared the performance of repair grouts using remaining void ratios from cut sections. The void ratio, η, in the repair grout was defined as follows:

$$\eta = \frac{A_V}{A_R} 100\ \% \tag{4.1}$$

where A_V is remaining voids in repair grouts and A_R is net area of repair grouts.

The remaining void ratio can be obtained using the following procedure. First, the cut-section area of a repair grout, A_R, is estimated using figures in AutoCAD®. The area of the remaining voids after repair in the cut section, A_V, is then estimated by outlining the voids in AutoCAD®. After the pre- and post-repair sections are generated, comparisons are made to assess the effectiveness of each repair-grout combination.

4.2.5.3. Economic feasibility

One objective of this research is to propose the most practical repair grouting method to use in the field. Therefore, the preparation time required for each repair method is a critical factor because of its close relationship with the overall repair costs. As mentioned in Section 4.2.3, each repair method requires different amounts of sealing and preparation time. Each grout material also has dissimilar times for mixing. Thus, a time

analysis of the sealing and mixing procedure will be performed to compare the economic feasibility of each repair method - grout combination.

4.3. Mitigation or Repair Strategies: Results

This section contains the experimental results and analyses of the repair methods and materials. The objective of this analysis is to provide details on an appropriate repair method and repair grout for field applications. Using test results from the infiltration length and cut sections from each specimen, the analysis was performed to evaluate the FC and performance for each repair method and grout type. The economic feasibility for the study for the different combinations were also analyzed using estimates of preparation and grout mixing time.

As mentioned in Subsection 3.3.6, specimen identification and notation consists of three character groups with each group separated by a hyphen. The first character set denotes the name of the repair grouting method (VG, PG, or PVG) while the grout type is assigned to the second group (C1, C2, or C3). The third and final number represents the specimen number (1 or 2).

4.3.1. Filling capability of repair grouts

To assess the FC of the different systems the infiltration length and minimum repaired area in cut sections, which means how small the voids were in the repaired specimens, were analyzed. The following section provides a description of the analysis procedure.

4.3.1.1. Analysis of infiltration length of repair method - grout combination

The FC of the repair methods and repair grouts is analyzed using the infiltration length measurements assuming that all of the specimens are subjected to the same initial conditions.

The infiltration lengths for all other specimens are provided in Appendix A. The infiltration length is measured through the transparent duct (Figure 4-13). From Table 4-4, it can be seen that the VG and PVG methods using The C-1 and C-2 grouts have a better FC than the other combinations. The infiltration lengths also resulted in similar trends when comparing the average value of each repair method and grout. Figure 4-14 and Figure 4-15 show average infiltration lengths and their standard deviations. It can be seen that the VG and PVG methods have higher infiltration lengths than the PG method, on average. Also, the C-1 and C-2 grouts, on average, have better infiltration lengths than does the C-3 grout.

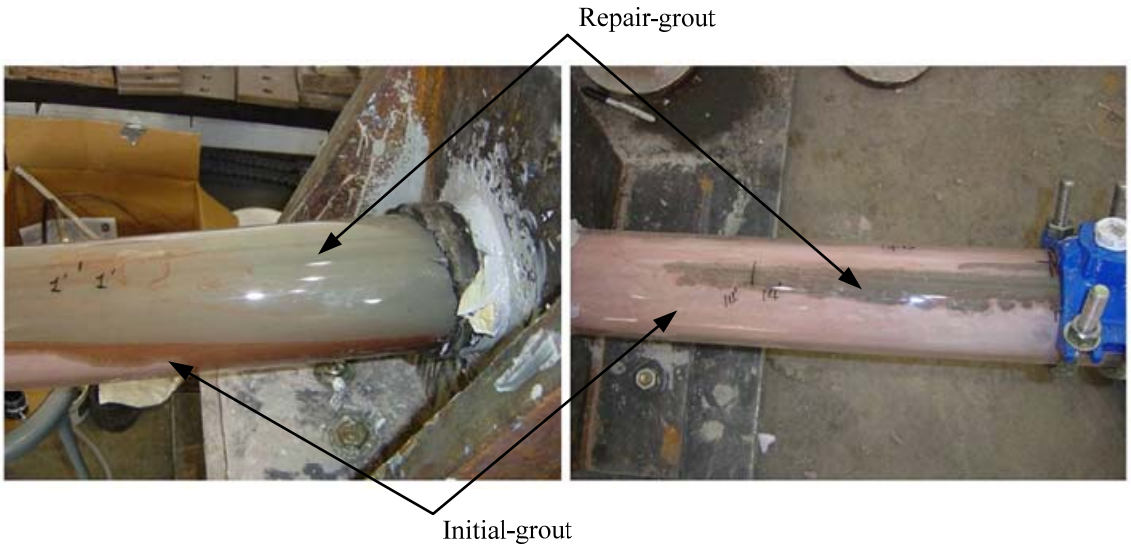

Figure 4-13. Specimen VG-C1-2 Showing Initial and Repair Grouts.

Table 4-4. Results of Repair (Infiltration Length from the Reference Point).

Repair grouts		Infiltration Length of Repair Grouts, ft (m)		
Type	**w/p**	**PG**	**VG**	**PVG**
C-1	0.30	11.5 (3.51) / 9.3 (2.83)	14.5 (4.42) / 14.3 (4.36)	15.0 (4.57) / 14.5 (4.42)
C-2	0.26	4.6 (1.40) / 14.4 (4.39)	13.4 (4.08) / 14.4 (4.39)	14.4 (4.39) / 14.3 (4.36)
C-3	0.27	7.3 (2.23) / 13.2 (4.02)	4.8 (1.46)	3.9 (1.19)

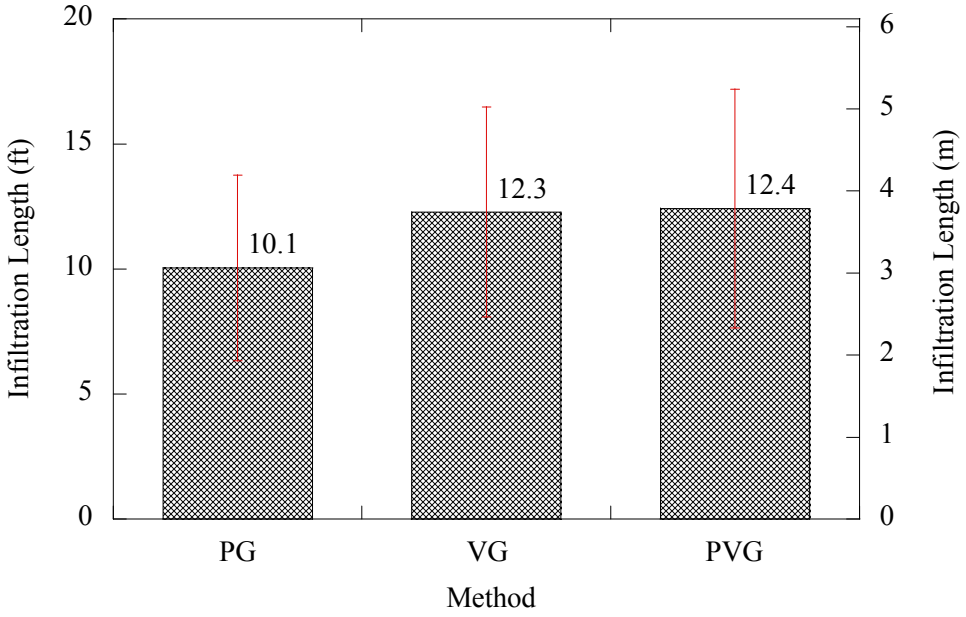

Figure 4-14. Comparison of Infiltration Lengths Obtained with Different Repair Methods.

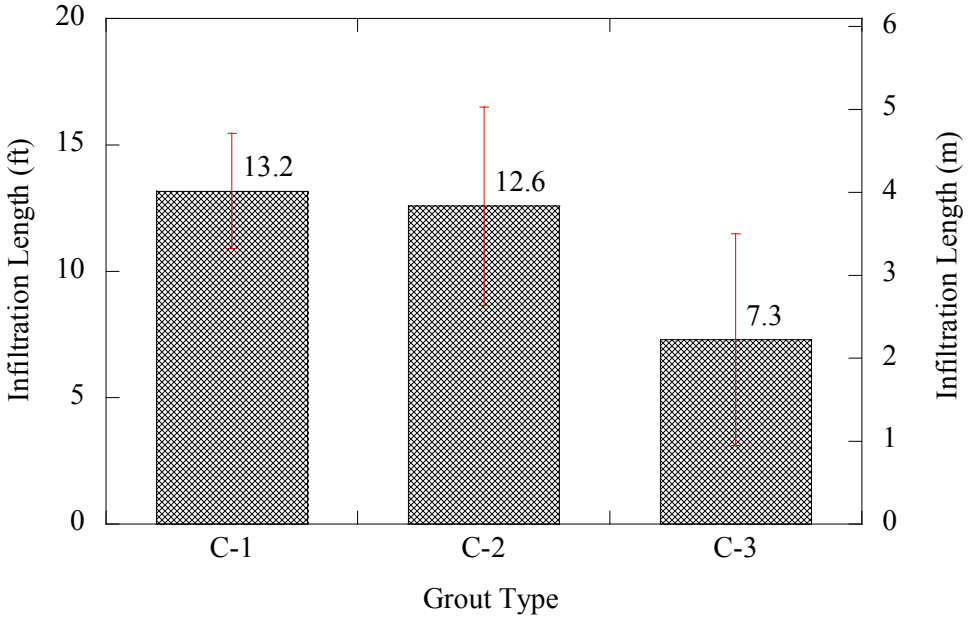

Figure 4-15. Comparison of Infiltration Lengths Obtained with Different Repair Grouts.

A two-factor factorial experiment design was used to analyze the differences between infiltration lengths of the various repair methods and repair grouts. In this experiment the two factors are repair methods (PG, VG, and PVG) and repair grout materials (C-1, C-2, and C-3). The linear statistical model of the two-factor factorial is defined by

$$Y_{ijk} = \mu + \tau_i + \beta_j + (\tau\beta)_{ij} + \varepsilon_{ijk} \begin{cases} i = 1,2,3 \\ j = 1,2,3 \\ k = 1 \text{ or } 1,2 \end{cases}, \tag{4.2}$$

where μ is the overall mean effect, τ_i is the effect of the repair methods, β_j is the effect of the repair grout materials, $(\tau\beta)_{ij}$ is the effect of the interaction between repair methods and repair grouts, and ε_{ijk} is a random error component having a normal

distribution with a mean zero and variance σ^2. The null and alternate hypotheses are defined as:

$$
\begin{aligned}
&1.\ H_0 = \tau_1 = \tau_2 = \tau_3 = 0 && \text{(no main effect of repair methods)} \\
&\quad H_1 = \tau_i \neq 0 \ \text{ at least one } i && \\
&2.\ H_0 = \beta_1 = \beta_2 = \beta_3 = 0 && \text{(no main effect of repair grouts)} \\
&\quad H_1 = \beta_j \neq 0 \ \text{ at least one } j && \\
&3.\ H_0 = (\tau\beta)_{11} = (\tau\beta)_{12} = \cdots = (\tau\beta)_{33} = 0 && \text{(no interaction)} \\
&\quad H_1 = \text{at least one } (\tau\beta)_{ij} \neq 0 &&
\end{aligned}
\tag{4.3}
$$

The analysis of variance (ANOVA) is performed to test these hypotheses. Table 4-5 shows the ANOVA results for the infiltration length. At the 0.05 level of significance, the ANOVA results show that different grouts affect the FC of repair grouting (*p*-value of repair grouts is less than 0.05) while the repair methods do not reveal a significant difference for filling voids (*p*-value of repair grouts is not less than 0.05).

Table 4-5. ANOVA for the Infiltration Length.

Source	Type III Sum of Square	Degree of Freedom	Mean Square	F Statistic	*p*-value
Repair Methods	3.367	2	1.683	0.172	0.845
Repair grouts	120.492	2	60.246	6.157	0.029
Methods×Grouts	77.792	4	19.493	1.992	0.200
Error	68.495	7	9.785		
Total	250.398	15			

While the ANOVA tests are capable of showing that different repair grouts have an influence on filling voids in ducts, it is not capable of identifying which grout is superior. Hence, Fisher's *least significant difference* (LSD) method using the 0.05 level

of significance is applied to determine which repair grout is preferred (Montgomery and Runger 2007). The mean values for each repair grout are compared with the null hypothesis:

$$H_0:\ \mu_i = \mu_j \ \text{for all}\ i \neq j \tag{4.4}$$

According to the Fisher's LSD the pair of means for infiltration length would be concluded to be significantly different if:

$$|\bar{y}_{i.} - \bar{y}_{j.}| > \text{LSD}$$

$$\text{where, LSD} = t_{\alpha/2,N-a}\sqrt{MS_E\left(\frac{1}{n_i}+\frac{1}{n_j}\right)} \tag{4.5}$$

where $t_{\alpha/2,a(n-1)}$ is a two sided *t*-statistic with α level of significance; *a* is the number of treatments applied (repair grouts); *N* is the total sample number; and MS_E is the mean square error when the sample sizes are different. The mean values for the repair grouts are compared in Table 4-6.

Table 4-6. The Comparisons of Void Ratios Corresponding to the Repair Grouts.

Comparison	Difference of Means	LSD	Results
(C-1)-(C-2)	0.6	3.901	No difference
(C-1)-(C-3)	5.883	4.361	C-3 is lower than C-1
(C-2)-(C-3)	5.823	4.361	C-3 is lower than C-2

However, Fisher's LSD test is susceptible to a high probability of Type I errors (also, known as α-error) because of its inability to consider multiple comparisons. Thus, Tukey's Honestly Significantly Differences (HSD) test and Student-Newman-Keuls (SNK) test were performed using the program SPSS, a statistical software package. Tukey's HSD test is a fairly conservative measure of differences among groups while the SNK test is a more sensible alternative to Duncan's test, which is designed for comparing samples with significantly different means. The results of both tests are provided in Table 4-7. The results show that the C-3 grout has a lower FC than the C-1 grout in Tukey's HSD test. The C-3 grout also shows a lower FC than both the C-1 and C-2 grouts in the SNK test.

Table 4-7. The Grouping Results of Tukey's HSD and SNK Tests.

Method	Source	N	Subset	Source	N	Subset	
			1			1	2
Tukey's HSD Test	PG VG PVG	6 5 5	10.050 12.280 12.420	C-1 C-2 C-3	6 6 4	13.183 12.583 -	- 12.583 7.300
Student-Newman-Keuls Test	PG VG PVG	6 5 5	10.050 12.280 12.420	C-1 C-2 C-3	6 6 4	13.183 12.583 -	- - 7.300

From the results shown in Table 4-7 it can be reasonably concluded that the C-3 grout has a lower FC than the other grouts. In addition, the C-3 grout has different infiltration lengths when used in conjunction with the VG and PVG methods, compared to the C-1 and C-2 grouts. Thus, the FC of each repair method will be further evaluated to identify if one repair method has a better FC using the C-1 and C-2 grouts. Figure 4-16 shows the comparison of average infiltration lengths for the C-1 and C-2 grouts. The graph shows that the PG method seems to have a lower FC than the VG and PVG methods.

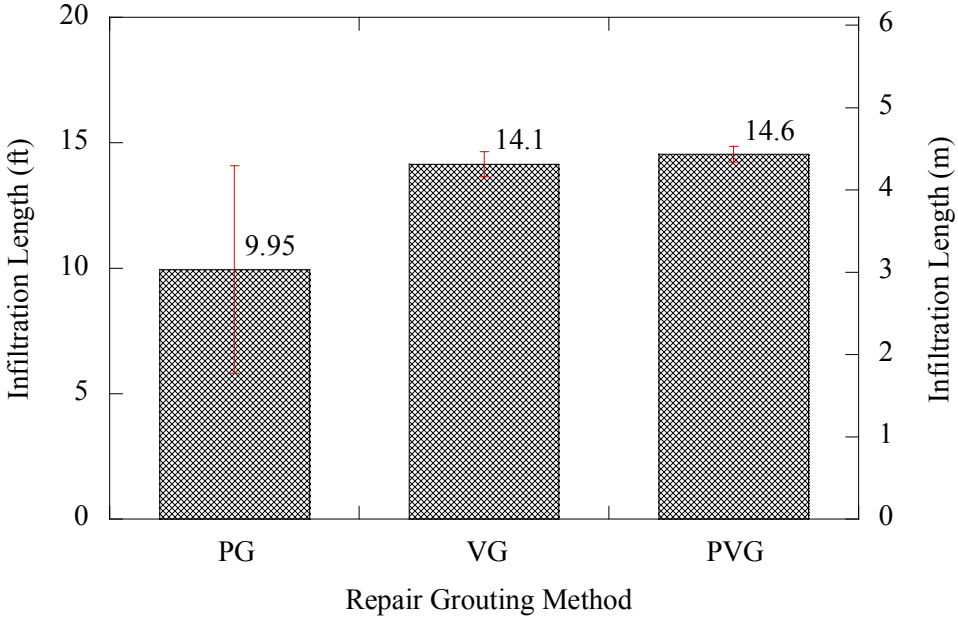

Figure 4-16. Comparison of Infiltration Length in Each Repair Method (Based on Results from C-1 and C-2 Grouts).

To compare the repair grouting methods in more detail, a two-factor factorial experiment was applied (the C-3 grout is not considered in this analysis). The two factors considered are the repair methods (PG, VG, and PVG) and the repair grouts (C-1 and C-2). The linear statistical model of the two-factor factorial is provided in Equation (4.2), where j is 1 and 2 because The C-3 grout is not considered. The null and alternate hypotheses are defined as follows:

$$
\begin{aligned}
&1.\ H_0 = \tau_1 = \tau_2 = \tau_3 = 0 && \text{(no main effect of repair methods)} \\
&\quad H_1 = \tau_i \neq 0 \ \text{ at least one } i \\
&2.\ H_0 = \beta_1 = \beta_2 = 0 && \text{(no main effect of repair grouts)} \\
&\quad H_1 = \beta_j \neq 0 \ \text{ at least one } j \\
&3.\ H_0 = (\tau\beta)_{11} = (\tau\beta)_{12} = \cdots = (\tau\beta)_{32} = 0 && \text{(no interaction)} \\
&\quad H_1 = \text{at least one } (\tau\beta)_{ij} \neq 0
\end{aligned}
\qquad (4.6)
$$

The ANOVA tests are performed again to test these hypotheses. Table 4-8 shows the ANOVA results for the infiltration results. For the 0.05 level of significance, the ANOVA shows that the repair methods do not affect the FC of the repair grouts. It should be noted that these results do not consider the amount of preparation work required to perform each repair method. They simply indicate that once prepared correctly, each method has the same potential to fill the voids.

Table 4-8. ANOVA Table for the Infiltration Results (Only Grouts C-1 and C-2 are Considered).

Source	Type III Sum of Square	Degree of Freedom	Mean Square	F Statistic	*p*-value
Repair Methods	51.947	2	25.973	3.050	0.122
Repair grouts	1.080	1	1.080	0.127	0.734
Methods×Grouts	0.140	2	0.070	0.008	0.992
Error	51.090	6	8.515		
Total	104.257	11			

4.3.1.2. Analysis of minimum repaired area in cut sections.

Another way to evaluate the FC of the repair grouts is to analyze the minimum repaired area of each specimen from its cut sections. An improved FC should be represented by a reduced value in the minimum repaired area of the cut sections. In another way, a grout-method combination exhibiting a low FC cannot fill small voids in ducts. Figure 4-17 shows the cross-sectional views of the cut sections obtained from specimen VG-C1-2. From the cut sections, it is noted that the repair grout successfully filled the main voids and the #3, #4, and #5 large voids (see Figure 4-12). However, small voids still exist inside the repaired ducts, especially in-between strands (see cut sections, C, D, E, and F in Figure 4-17). However, those voids cannot be repaired because the voids are isolated from the "bleed lines" which are routes for the repair grouts.

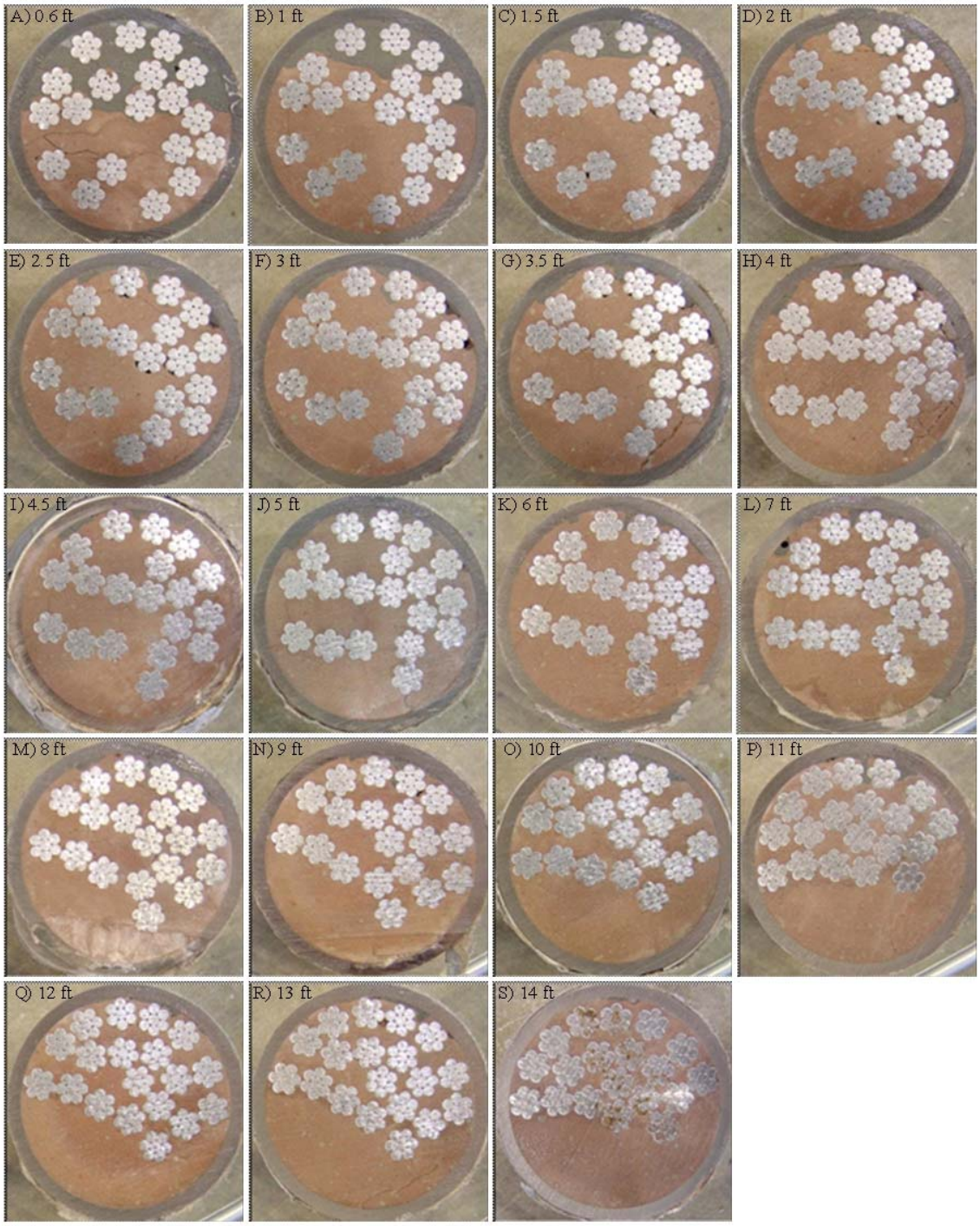

Figure 4-17. Cut Sections of Specimen VG-C1-2 for the FC of Repair Method–Grout Combination (Note: See top left corner of each figure for the location of cross-section; 1 ft=0.3 m).

To compare the minimum repaired area in cut sections, repaired areas in each cut section are provided in Table 4-9. The repaired area was calculated using AutoCAD® (see Subsection 4.2.5.2 for details).

Table 4-9. The Void Area Remaing after Repair of Specimen VG-C1-2.

Cut Sections, ft (m)		Repaired Area, A_R, inch^2(10^{-4} m^2)	Void Area, A_V, inch^2(10^{-4} m^2)	Void Ratio, η (%)
A	0.6 (0.18)	2.528 (16.31)	0.0095 (0.061)	0.38
B	1 (0.30)	1.525 (9.84)	0.0045 (0.029)	0.30
C	1.5 (0.46)	0.783 (5.05)	0.0044 (0.028)	0.56
D	2 (0.61)	0.515 (3.32)	0.0066 (0.043)	1.28
E	2.5 (0.76)	0.333 (2.15)	0.0111 (0.072)	3.33
F	3 (0.91)	0.288 (1.86)	0.0024 (0.015)	0.83
G	3.5 (1.07)	0.216 (1.39)	0.0012 (0.008)	0.56
H	4 (1.22)	0.198 (1.28)	0.0099 (0.064)	5.01
I	4.5 (1.37)	0.185 (1.19)	0.0020 (0.013)	1.08
J	5 (1.52)	0.339 (2.19)	0.0060 (0.039)	1.77
K	6 (1.83)	0.202 (1.30)	0.0009 (0.006)	0.45
L	7 (2.13)	0.254 (1.64)	0.0184 (0.119)	7.24
M	8 (2.44)	0.212 (1.37)	0.0042 (0.027)	1.98
N	9 (2.74)	0.223 (1.44)	0.0027 (0.017)	1.21
O	10 (3.05)	0.331 (2.13)	0.0056 (0.036)	1.69
P	11 (3.35)	0.261 (1.68)	0.0088 (0.057)	3.38
Q	12 (3.66)	0.096 (0.62)	0.0069 (0.045)	7.23
R	13 (3.96)	0.119 (0.77)	0.0082 (0.053)	6.87
S	14 (4.27)	0.060 (0.39)	0.0029 (0.019)	4.81
Sum		8.667 (55.92)	0.1162 (0.750)	1.34

The minimum repaired area of specimen VG-C2-1 is provided in cut section S in Table 4-9 (0.060 inch^2 [0.39×10^{-4} m^2]). Table 4-10 shows the minimum repaired area for every PET specimen. The values from the other specimens are given in Appendix A.

Table 4-10. Results of Repair Grouts (Minimum Repaired Area in Cut Sections).

Grout Type	Minimum Repaired Area in Cut Sections, inch^2 (10^{-4} m^2)		
	PG	VG	PVG
C-1	0.033 (0.21) / 0.181 (1.17)	0.030 (0.19) / 0.060 (0.39)	0.051 (0.33) / 0.021 (0.13)
C-2	0.040 (0.26) / 0.120 (0.77)	0.019 (0.12)	0.053 (0.34) / 0.031 (0.20)
C-3	0.186 (1.20) / 0.141 (0.91)	0.094 (0.61)	0.074 (0.48)

Figure 4-18 and Figure 4-19 show the average and standard deviation of the minimum repaired area for each repair method and repair grout, respectively. Through the comparison of the minimum repaired area in each grout method it was determined that the VG and PVG methods have better FC than the PG method, on average. It can also be seen that, from the comparison of the repair grouts, the C-1 and C-2 grouts have better FC than the C-3 grout, on average.

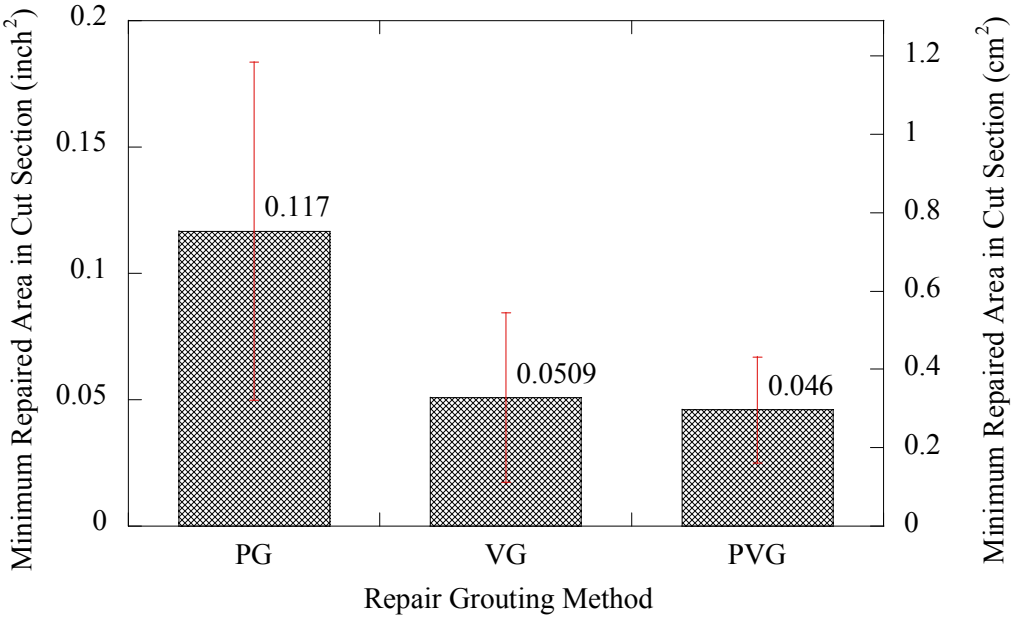

Figure 4-18. Comparison of Minimum Repaired Area for Different Repair Methods.

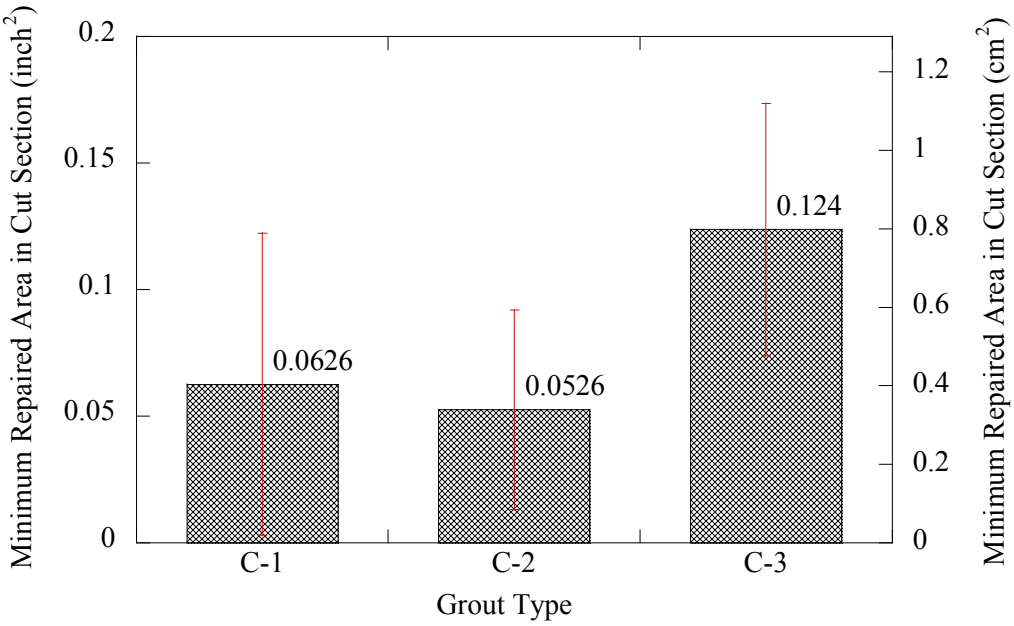

Figure 4-19. Comparison of Minimum Repaired Area Corresponding to Different Grouts.

The two-factor factorial experiment was again used to analyze the differences between the minimum repaired area of each specimen with respect to the repair method and repair grout. The two factors used are the repair methods (PG, VG, and PVG) and repair grout materials (C-1, C-2, and C-3 grouts). The linear statistical model of the two-factor factorial design is provided in Equation (4.2) and the null and alternative hypotheses were shown earlier in Equation (4.3).

The ANOVA tests were performed to test these hypotheses. Table 4-11 shows the results of the ANOVA table for the minimum repaired area in the sections. For the 95% confidence limit, the ANOVA shows that different repair methods and grouts do not significantly affect the FC (minimum repaired area in specimen) of the repair grouting. However, based on the comparisons of the graphs and results of the ANOVA, the PG method seems to have a lower FC value than the VG and PVG methods.

Table 4-11. ANOVA for the Minimum Repaired Area in Cut Sections.

Source	Type III Sum of Square	Degree of Freedom	Mean Square	F Statistic	*p*-value
Repair Methods	0.015	2	0.007	2.690	0.147
Repair grouts	0.009	2	0.004	1.589	0.279
Methods×Grouts	0.001	4	0.000	0.117	0.972
Error	0.016	6	0.003		
Total	0.044	14			

4.3.1.3. Analysis of influencing factors in filling capability

Although significant efforts have been made to ensure consistency between the specimens, the grout levels from test setups do have slight differences from specimen to specimen. Also, void shapes in ducts could have formed differently due to differences in bleed water and entrapped air. Different void shapes and sizes in specimens have an

influence on the resistance force, P, generated against the flow of repair grout. For the flow of a fluid element in a void a constant cross sectional area, A, a perimeter, U, and length, dx, (Figure 4-20), the term P is evaluated. The unit resistance pressure, p, in a small void is estimated as follows:

$$\left(p+\frac{1}{2}\mathrm{d}p\right)A-\left(p-\frac{1}{2}\mathrm{d}p\right)A=\tau_0 U\,\mathrm{d}x$$
$$\mathrm{d}p=\frac{U}{A}\tau_0\,\mathrm{d}x \tag{4.7}$$

For an arbitrarily shaped void, the resistance stresses, τ_0, are generated opposite to the direction of grout flow around the perimeter U of the void (Figure 4-20). For the unit length, dx, the relation between the unit resistance pressure, p, and the resistance force, P, for a given length, l, are given by:

$$P=\int_0^l \mathrm{d}p=\int_0^l \frac{U}{A}\tau_0\,\mathrm{d}x \tag{4.8}$$

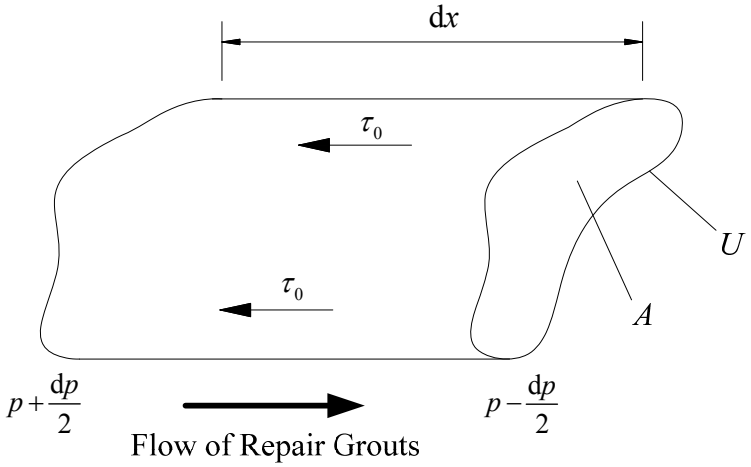

Figure 4-20. Schematic of Resistance Stresses for Grout Flow in Voids.

Because the resistance stresses in repair grouts are analogous to shear stress in a fluid flow, the principles of fluid mechanics are used to estimate this stress for a steady uniform flow (Cruise et al. 2007):

$$\tau_0 = \frac{f \rho V^2}{8} \tag{4.9}$$

where, V is the fluid velocity, f, is a dimensionless parameter representing the roughness between the fluid flow and the ducts, and the factor, ρ, represents the density of the fluid. Substituting Equation (4.9) into Equation (4.8) and then integrating results in:

$$P = \frac{U}{A} l \frac{f \rho V^2}{8} \tag{4.10}$$

where the specific weight of the fluid, γ, can be expressed as $\gamma = \rho g$. Thus, the term P can be determined as follows:

$$P = \frac{l}{R_h} f \frac{\gamma V^2}{8g} \tag{4.11}$$

where the hydraulic radius R_h is defined as A/U and l is the infiltration length when the applied force is P. In Equation (4.11), the friction factors are considered constant in this case due to the slow rate of flow. However, R_h and V are critical parameters that directly affect the infiltration length, l, in the repair grouts. From the basic principles of fluid motion, the mass flow rate is as follows:

$$Q = AV = \text{constant} \tag{4.12}$$

A fluid with a constant mass flow rate will have a velocity that is inversely proportional to the cross-sectional area, A, of the void. Therefore, A directly impacts the resistance force, P, in ducts. Summarizing the infiltration length, l, can be determined as follows:

$$l = 8 \cdot \frac{P}{f} \frac{g}{\gamma} R_h \frac{A^2}{Q^2} \tag{4.13}$$

when the applied force is constant in the duct. The value of P/f is a constant that represents an applied force divided by the friction factor in the duct.

To analyze the factors affecting the filling of voids, correlations between infiltration length and varying geometric and material conditions across the specimens were evaluated. For the geometric conditions of specimens, the average square area, A^2, of the voids and hydraulic radius, R_h, are considered in the analysis. The efflux time of each repair grout is estimated by considering the different fluidity conditions of the

grouts. Table 4-12 was generated using estimates from section cuts and the results of the flow cone test. Table 4-13 shows the correlation matrix for all of the specimens.

Table 4-12. Description of Experimental Data on Influence Factors.

Specimen	Infiltration Length, ft (m)	Average R_h of Voids, inch (10^{-2} m)	Average A^2 of Voids, inch^2 (10^{-4} m^2)	Efflux Time of Repair Grout (s)
VG-C1-1	14.5 (4.4)	0.066 (0.17)	0.43 (2.8)	9.91
VG-C1-2	14.3 (4.4)	0.044 (0.11)	0.46 (2.9)	8.34
VG-C2-2	14.4 (4.4)	0.037 (0.09)	0.41 (2.6)	12.06
VG-C3-1	4.8 (1.5)	0.053 (0.14)	0.81 (5.2)	22.57
PG-C1-1	11.5 (3.5)	0.084 (0.21)	0.95 (6.1)	7.8
PG-C1-2	9.3 (2.8)	0.057 (0.14)	0.59 (3.8)	8.72
PG-C2-1	4.6 (1.4)	0.040 (0.10)	0.35 (2.3)	15.31
PG-C2-2	14.4 (4.4)	0.054 (0.14)	0.49 (3.2)	12.59
PG-C3-1	7.3 (2.2)	0.049 (0.13)	0.76 (4.9)	19.12
PG-C3-2	13.2 (4.0)	0.088 (0.22)	1.04 (6.7)	23.14
PVG-C1-1	15 (4.6)	0.061 (0.15)	0.57 (3.7)	9.97
PVG-C1-2	14.5 (4.4)	0.061 (0.16)	0.63 (4.1)	8.75
PVG-C2-1	14.4 (4.4)	0.053 (0.13)	0.82 (5.3)	14.16
PVG-C2-2	14.3 (4.4)	0.047 (0.12)	0.44 (2.8)	10.84
PVG-C3-1	3.9 (1.2)	0.056 (0.14)	0.68 (4.4)	25.63

Table 4-13. Correlation Matrix of Repaired Specimens.

	Infiltration Length	Average A^2 of Voids	Average R_h of Voids	Efflux Time of Repair grouts
Infiltration Length	1	-0.121	0.166	-0.646
Average A^2 of Voids	-0.121	1	0.755	0.441
Average R_h of Voids	0.166	0.755	1	0.073
Efflux Time of Repair grouts	-0.646	0.441	0.073	1

From Table 4-13, the geometric conditions of voids (R_h and A^2) in cut locations do not show positive correlation with infiltration length of the repair grouts; however, the efflux time has a slight negative correlation with the infiltration length of the repair grouts. The correlation coefficient factors show different trends in Table 4-13 when they are estimated by each repair grouting method.

The correlation coefficient factors obtained are shown in Table 4-14, Table 4-15, and Table 4-16. Table 4-14 shows that the correlation coefficient between the infiltration length and A^2. This correlation is highly negative when using the VG method. However, this correlation conflicts with the theory involving resistance force in ducts derived in Equation (4.13). The reason for this is that the flow rate Q in the VG method is not constant; thus, the velocity of the fluid in a small void is not inversely proportional to the flow rate. Therefore, the A^2 does not affect the infiltration length when using the VG method. From Table 4-15, the average R_h has a slight linear correlation with infiltration length obtained when using the PG method, but not when using the VG and PVG methods. The efflux time of the repair grouts has a negative correlation with the infiltration length for the VG and PVG methods, but not in the PG method. Therefore, the correlation matrix for the PG method is obtained separately as shown in Table 4-17. The VG and PVG methods are assessed together to estimate the correlation matrix (Table 4-18).

Table 4-14. Correlation Coefficient between Infiltration Length and Average A^2 of Voids.

Average A^2 of Voids	Infiltration Length		
	PG	**VG**	**PVG**
PG	0.458	-	-
VG	-	-0.998	-
PVG	-	-	-0.166

Note: "-" indicates no correlation between factors.

Table 4-15. Correlation Coefficient between Infiltration Length and Average R_h of Voids.

Average R_h of Voids	Infiltration Length		
	PG	**VG**	**PVG**
PG	0.654	-	-
VG	-	-0.169	-
PVG	-	-	0.012

Note: "-" indicates no correlation between factors.

Table 4-16. Correlation Coefficient between Infiltration Length and Efflux Time of Grouts.

Efflux Time of Repair grouts	Infiltration Length		
	PG	**VG**	**PVG**
PG	-0.032	-	-
VG	-	-0.970	-
PVG	-	-	-0.961

Note: "-" indicates no correlation between factors.

Table 4-17. Correlation Matrix of PG Methods.

	Infiltration Length	**Average A^2 of Voids**	**Average R_h of Voids**	**Efflux Time of Repair grouts**
Infiltration Length	1	0.458	0.654	-0.032
Average A^2 of Voids	0.458	1	0.920	0.336
Average R_h of Voids	0.654	0.920	1	0.083
Efflux Time of Repair grouts	-0.032	0.336	0.083	1

From Table 4-17 one can conclude that the average R_h has a slightly positive and linear relationship with infiltration length when using the PG method. However, the infiltration length for the PG method does not reveal any correlation with the efflux time of the repair grouts. Figure 4-21 shows the scatter plot between infiltration length and the average R_h value when using the PG method. Although the correlation coefficient between these variables is not highly positive, they can be rationalized based on the fact that the FC of the PG method is dominated by geometric conditions.

Table 4-18. Correlation Matrix of VG and PVG Methods.

	Infiltration Length	Average A^2 of Voids	Average R_h of Voids	Efflux Time of Repair grouts
Infiltration Length	1	-0.538	-0.073	-0.958
Average A^2 of Voids	-0.538	1	0.248	0.619
Average R_h of Voids	-0.073	0.248	1	0.023
Efflux Time of Repair grouts	-0.958	0.619	0.023	1

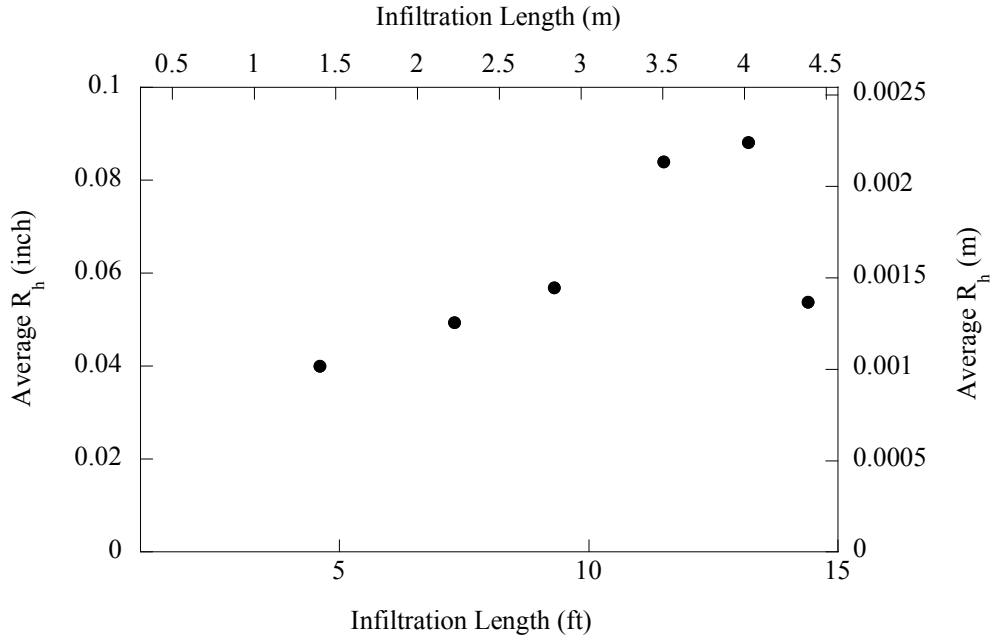

Figure 4-21. Scatter Plot between Infiltration Lengths and Average R_h.

When the VG and PVG methods were used (Table 4-18), the correlation between the infiltration length and the efflux time of the repair grouts was highly negative. Thus, it is shown that when the efflux time is lower the FC is higher. However, the FC of these methods does not have any correlation with the geometric condition, R_h. Figure 4-22 shows the scatter plot between infiltration length and the initial efflux time of repair grouts when applying the VG and PVG methods. Although the correlation coefficient between the infiltration lengths and the initial efflux time is highly negative, the scatter plot shows that there are no data points between low infiltration lengths and high infiltration lengths. In addition, the two data points with low infiltration lengths are from the C-3 grout. When considering only the C-1 and C-2 grouts, the relationships between infiltration length and efflux time do not show negative correlations, and therefore it is difficult to conclude that the FC of the VG and PVG methods are dominated by the initial efflux time of the repair grouts.

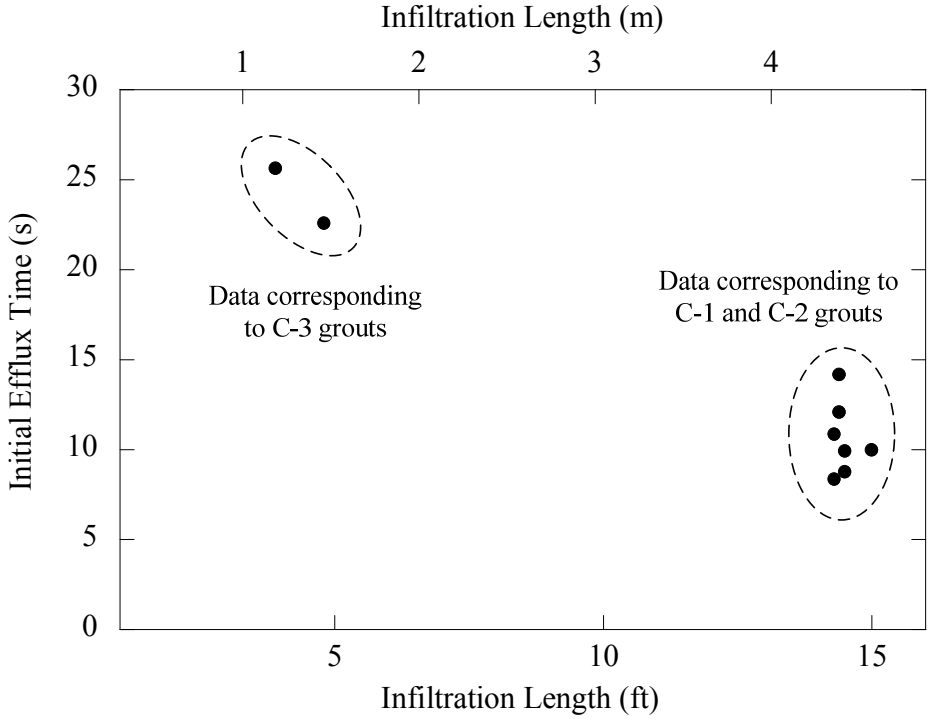

Figure 4-22. Scatter Plots between Infiltration Lengths and Initial Efflux Time.

In summary, the PG method seems to be significantly affected by the geometric condition, R_h, when filling voided ducts. Conversely, the VG and PVG methods' filling capabilities are shown to be relatively unaffected by a void's geometric conditions, leaving the engineer few options in optimizing the repair process.

4.3.2. Filling performance of repair grouts

The C grouts tested in this research do not show any signs of having bleeding water when the wick-induced bleed test was performed. However, entrapped air may be introduced when repairing. Although isolated voids created by entrapped air are not typically associated with strand corrosion in ducts, these voids can be used as an index for evaluating the filling performance of repair grouts. To compare the performance of repair grouts, the void ratio, η, (defined as A_V / A_R) is estimated. The A_R and A_V are calculated using AutoCAD® tools (Section 4.2.5.2). Table 4-9 shows the values of A_R and A_V for each cut section. From Table 4-9, the value of η, obtained from the analysis, is 1.34% for Specimen VG-C1-2. The void ratios for all other specimens are provided in Appendix A, and all the results are summarized in Table 4-19.

The remaining voids in repaired specimens were estimated using the cut-section analysis. However, the value of η can be magnified when the remaining voids exist only in small repaired area. Thus, the filling performance for each specimen is provided considering the summation over all of the cut sections for each specimen. The results of the filling performance of each specimen are shown in Table 4-19.

Table 4-19. Results of Filling Performance in Each Specimen.

Grout Type	Void Ratio, η, in Each Specimen (%)		
	PG	VG	PVG
C-1	0.22 / 1.76	0.60 / 1.34	0.66 / 0.67
C-2	1.13 / 0.78	0.99	0.92 / 0.51
C-3	1.56 / 0.98	0.57	2.16

Figure 4-23 and Figure 4-24 show the average and the standard deviation of the η for each repair method and repair grout, respectively.

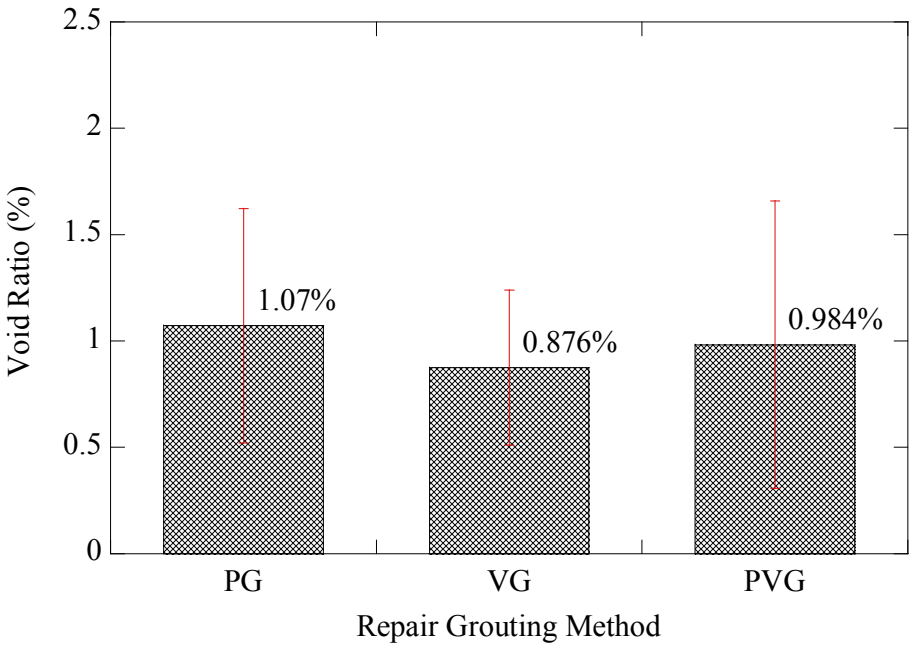

Figure 4-23. Comparison of Void Ratio, η, in Each Repair Method.

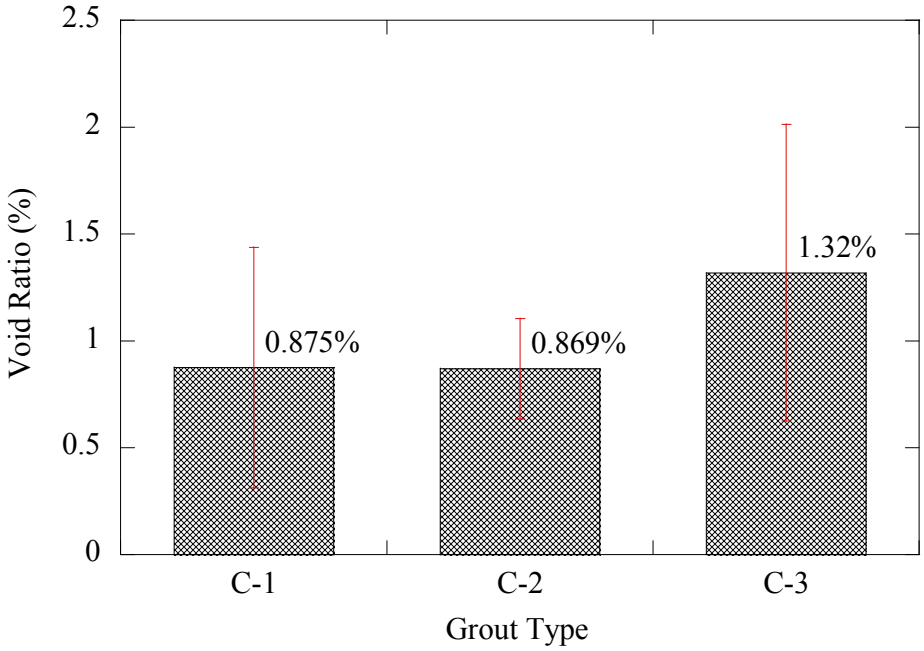

Figure 4-24. Comparison of Void Ratio, η, in Each Repair Grout.

Comparing the values η obtained from each grouting method, all repair methods seem to have similar amounts of remaining voids (Figure 4-23). The comparison of the repair grouts indicate that the specimens repaired with the C-3 grout show slightly more voids than the C-1 and C-2 grouts, on average (Figure 4-24).

A two-factor factorial experiment was again considered to analyze the differences between void performance of repair methods and repair grouts. The two factors used are repair methods (PG, VG, and PVG) and repair grout materials (C-1, C-2, and C-3). The linear statistical model of the two-factor factorial was provided in Equation (4.2), and the null and alternative hypotheses were shown in Equation (4.3).

An ANOVA test was performed to test these hypotheses. Table 4-20 shows the ANOVA table for the η of the test specimens. For the 0.05 level of significance, the

ANOVA table concludes that different repair methods and grouts do not significantly affect filling performance.

Table 4-20. ANOVA Table for the Void Ratio, η, of Test Specimens.

Source	Type III Sum of Square	Degree of Freedom	Mean Square	*F* Statistic	*p*-value
Repair Methods	0.231	2	0.116	0.396	0.690
Repair grouts	0.554	2	0.277	0.948	0.439
Methods×Grouts	1.425	4	0.356	1.219	0.394
Error	1.754	6	0.292		
Total	3.833	14			

4.3.3. Economic feasibility based on repair methods and grouts

The economic feasibility of each repair method and grout can be represented by the time required to effectively apply each method and grout. Longer repair time increases the demands on labor which can lead to higher costs. Also, leaving a structure under repair for longer periods of time increases the chance of failures as other sections of the structure may become overstressed in order to accommodate the area under repair. Therefore, the optimal repair method and grout should be selected based on its required time to implement and the performance of the repaired system.

4.3.3.1. Feasibility of repair grouts

From the data collected on mixing time for the repair grouts, the C-3 grout was found to have the least feasibility for field applications. The C-3 grout required 20 minutes of mixing time and as a consequence led to overheating and breakdown of mixers (Table 4-3). Furthermore, in some cases the efflux time did not satisfy the requirements of Tex-437-A Method 2. The C-1 and C-2 grouts required relatively shorter mixing times,

and both grouts met the requirements of Tex-437-A Method 2. Considering the grout mixing times, efflux requirements, and required equipment, the C-1 and C-2 grouts are considered to be feasible for filling voids.

4.3.3.2. Feasibility of repair grouting methods

For the assessment of repair grouting methods, the preparation time for each specimen was documented. Table 4-21 shows the time schedule for sealing ducts for Specimen VG-C1-2. It also shows the steps required to achieve an air-tight condition. The total sealing time for Specimen VG-C1-2 was three working days or 5 hours. Because sealing requires curing time working days and time are different.

Table 4-21. Sealing Time Schedule of Specimen VG-C1-2.

Sealing Procedure	Working Day	Working Time (min.)
Connect hose and silicone	Day 1	11
Installing pipe saddle tap with grease	Day 1	35
Setting end rubber cover and silicone	Day 1	11
Mixing epoxy and sealing	Day 1	35
Wait	1 day	
Connect T-connection and check air-tight	Day 2	65
RTV silicone sealing	Day 2	12
Check air-tight condition	Day 2	11
RTV silicone sealing	Day 2	10
Mixing epoxy and sealing	Day 2	30
Wait	1 day	
Check air-tight and seal with RTV silicone	Day 3	80
Sum	**3 days**	**300 (5 hours)**

The preparation time for all other specimens are provided in Appendix A. The time estimates for the required sealing time for each specimen is shown in Table 4-22. The preparation times for specimens VG-C1-1 and VG-C2-1 were not considered in this

analysis because both these specimens required a considerable amount of trial and error before it was possible to create an air-tight condition in the test specimens. On specimen PVG-C1-2 even after working for 12.5 hours an air-tight condition could not be created. Table 4-22 and Table 4-23 show the required preparation time and schedule for applying each method. The term "sealing schedule" in the following discussions is defined as the laboratory work-days required to prepare each PET specimen. Although the sealing schedule was delayed occasionally due to lab conditions and scheduling, the delayed time is not considered in Table 4-22 and Table 4-23.

Table 4-22. Sealing Time Required for Each PET Specimen.

Repair Methods	Sealing Time for Repair (hours)						Average
	PET Specimen No.						
	1	2	3	4	5	6	
PG	1.03	0.88	0.85	0.65	0.97	0.88	0.88
VG	10.92	5	12.53	3.63			8.02
PVG	2.83	2.33	2.25	1.57	1.50		2.10

Table 4-23. Sealing Schedule Required for Each PET Specimen.

Repair Methods	Sealing Schedule for Repair (days)						Average
	PET Specimen No.						
	1	2	3	4	5	6	
PG	3	2	2	2	2	2	2.17
VG	7	3	9	3			5.50
PVG	4	1	2	2	2		2.20

Figure 4-25 is provided to compare the mean time requirements needed to repair the lab specimens using each method. The results show that the VG method requires significantly more sealing time than the other methods. Also, the PG method requires

much less preparation time than the PVG method. Figure 4-26 shows the preparation schedule required before applying each repair method. This figure also shows that the VG method seems to involve more preparation than the PG and PVG methods.

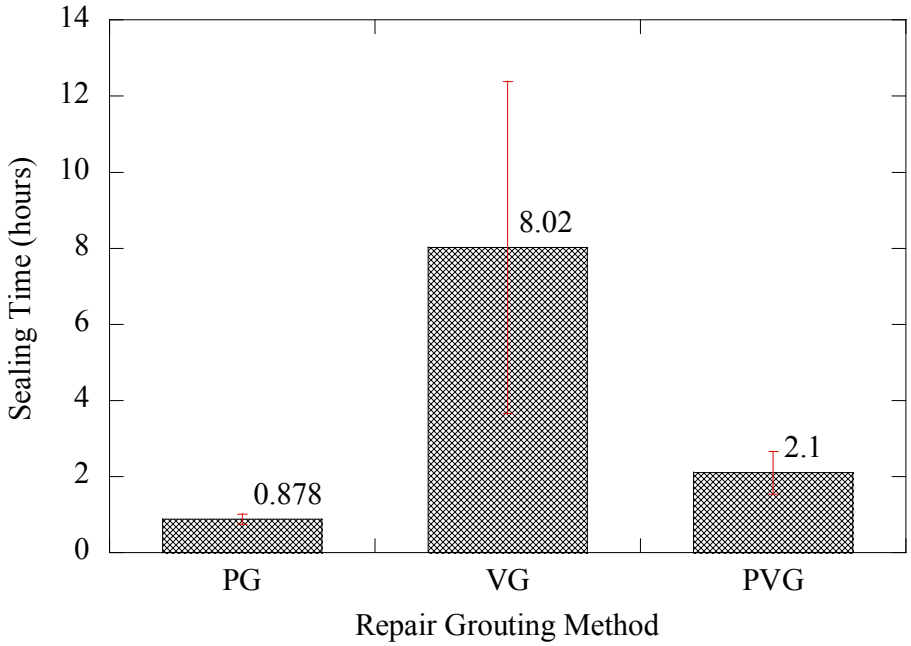

Figure 4-25. Sealing Time Required for Applying Repair Methods.

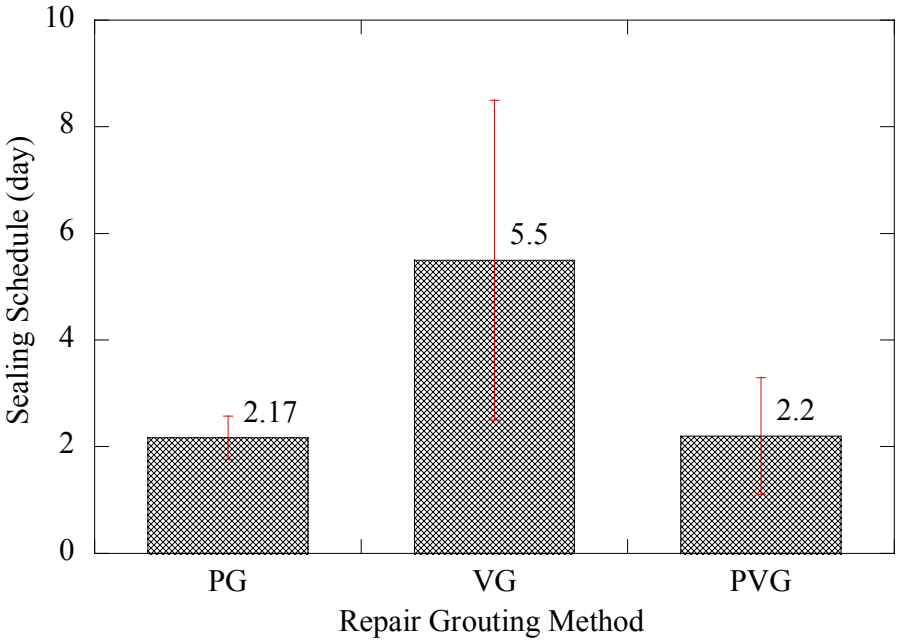

Figure 4-26. Sealing Schedule Required for Applying Repair Methods.

To further analyze the time required for each repair method, a single-factor factorial experiment was performed to compare the differences of preparation time and scheduling among repair methods. The single factor is the repair methods (PG, VG, and PVG), where the response for each repair method is considered as a random variable. The linear statistical model of a single-factor experiment is defined by:

$$Y_{ij} = \mu + \tau_i + \varepsilon_{ij} \begin{cases} i = 1,2,3 \\ j = 1,2,\cdots,n_i \end{cases} , \tag{4.14}$$

where μ is the overall mean effect, τ_i is the effect of the repair methods, and ε_{ij} is a random error component having a normal distribution with mean of zero and a variance σ^2. The null and alternate hypotheses are defined as:

$$H_0 = \tau_1 = \tau_2 = \tau_3 = 0 \quad \text{(no main effect of repair methods)}$$
$$H_1 = \tau_i \neq 0 \text{ at least one } i \tag{4.15}$$

An ANOVA test was performed to test these hypotheses. Table 4-24 and Table 4-25 show the ANOVA results for sealing time and scheduling for the application of the repair methods, respectively. For the 0.05 level of significance, the analysis shows that different repair methods require different preparation times and schedules.

Table 4-24. The ANOVA table for the Sealing Time for Preparing Repair.

Source	Type III Sum of Square	Degree of Freedom	Mean Square	*F* Statistic	*p*-value
Repair Methods	131.409	2	65.704	13.483	0.001
Error	58.476	12	4.873		
Total	189.885	14			

Table 4-25. ANOVA for the Sealing Schedule for Preparing Repair.

Source	Type III Sum of Square	Degree of Freedom	Mean Square	*F* Statistic	*p*-value
Repair Methods	32.300	2	16.150	5.939	0.016
Error	32.633	12	2.719		
Total	64.933	14			

Tukey's HSD test and Student-Newman-Keuls (SNK) test were performed using SPSS. The results of both tests are shown in Table 4-26 and Table 4-27. Table 4-26 and Table 4-27 shows that the VG method requires a longer sealing time for conducting repairs than the other methods. However, the tables also reveal that there is no significant difference in preparation time between the PG and PVG methods. Thus, the PG and PVG methods are more economical and feasible for repairing voids in the field than the VG method.

Table 4-26. Grouping Results of Tukey's HSD and SNK Tests for Preparation Time.

Method	Source	N	Subset	
			1	2
Tukey's HSD Test	PG	6	52.67	-
	PVG	5	125.80	-
	VG	4	-	481.25
Student-Newman-Keuls Test	PG	6	52.67	-
	PVG	5	125.80	-
	VG	4	-	481.25

Table 4-27. Grouping Results of Tukey's HSD and SNK Tests for Preparation Schedule.

Method	Source	N	Subset	
			1	2
Tukey's HSD Test	PG	6	2.167	-
	PVG	5	2.200	-
	VG	4	-	5.500
Student-Newman-Keuls Test	PG	6	2.167	-
	PVG	5	2.200	-
	VG	4	-	5.500

4.4. Effect of Particle Size and Viscosity of Repair Grouts

The fillability index (FI) of three different repair grouts was determined using the fillability test (Kataria 2008). Kataria (2008) designed the fillability test to evaluate particle sizes of repair grouts that can significantly affect their ability to fill voided ducts. Repair grouts are filtered by ten different 2-inch (51-mm) diameter pore size filters in fillability meters under 20 psi (138 kPa) of pressure. The FI is obtained by measuring grout volumes retained in each filter. Table 4-28 shows the FI for the three type C grouts.

Table 4-28. Fillability Index of Repair Grouts (Kataria 2008).

Grouts	Fillability Index			
	1	2	3	Average
C-1	4.1	4.3	4.2	4.2
C-2	5.3	5.2	5.2	5.2
C-3	7.5	6.4	6.3	6.7

From this fillability tests, the C-3 grout shows higher FI values than others, and this indicates that the C-3 grout includes larger sized particles than the C-1 and C-2 grouts. Although the fillability tests are not performed with the experiments conducted in this research, the effect of FI for filling voids is considered here with the results of infiltration length because the FI values of each grout show consistent values. Thus, the relationship between the averaged values of FIs and infiltration lengths is obtained and shown in Figure 4-27.

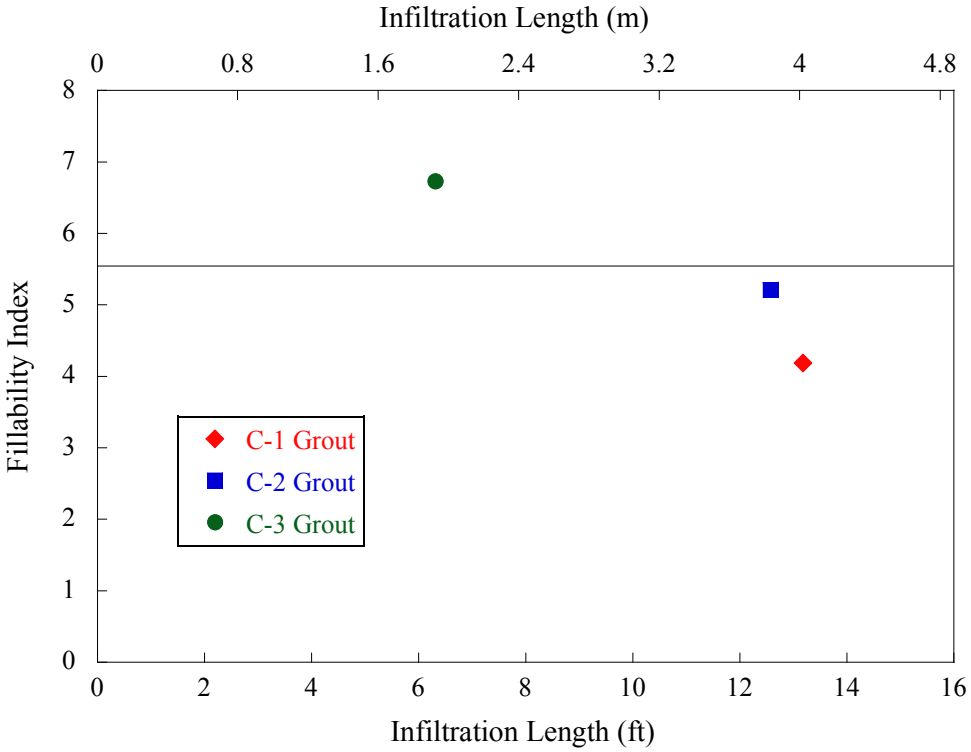

Figure 4-27. Relationship between Fillability Index and Infiltration Length(Kataria 2008).

Based on the relationship obtained between the fillability index and infiltration length, it is observed that the C-1 and C-2 grouts have lower fillability indices and higher infiltration lengths than the C-3 grout. Based on these results, it is recommended that the grouts with a fillability index of 5.5 or less will be appropriate for filling voided ducts in PT systems (Kataria 2008).

In addition, the viscosity of repair grouts may affect filling voids inside ducts. In this research, the dynamic viscosity tests are not performed simultaneoulsy with experiments for repairing voids. Thus, the relation between efflux time and viscosity for type C grouts is obtained from Kataria (2008). The relations of each C grout are shown in Figure 4-28, Figure 4-29, and Figure 4-30.

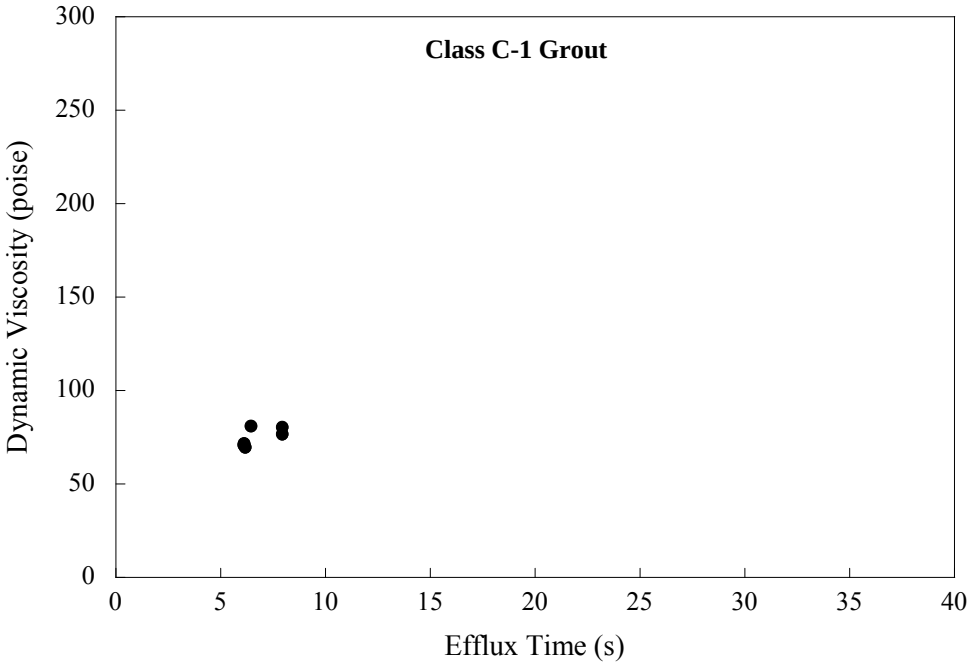

Figure 4-28. The Relation between Efflux Time and Viscosity for C-1 Grout (Kataria 2008).

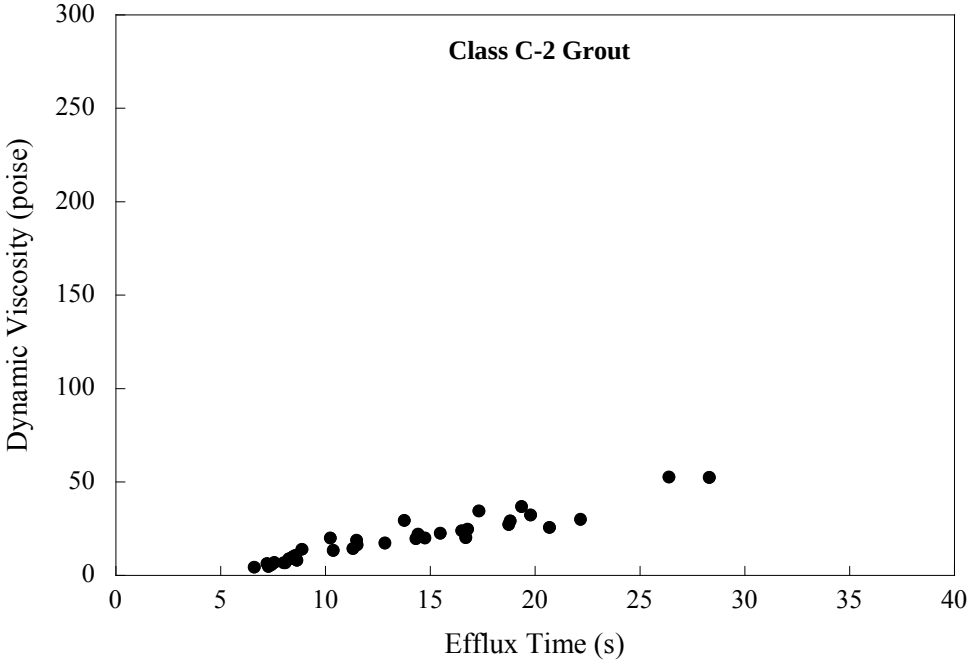

Figure 4-29. The Relation between Efflux Time and Viscosity for C-2 Grout (Kataria 2008).

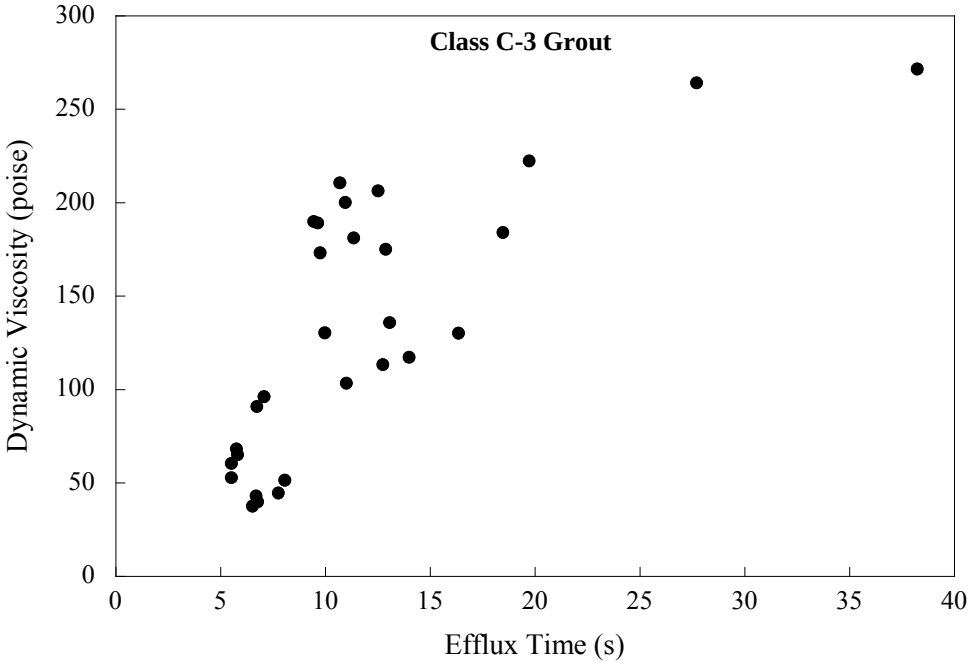

Figure 4-30. The Relation between Efflux Time and Viscosity for C-3 Grout (Kataria 2008).

Although the relation for The C-1 grout does not provide many data points, it is used for estimating the viscosity of experiments here, because the six data points exactly cover the efflux times of experiments in this research. Based on the relations above, the effect of viscosity for filling voids is considered with the results of infiltration length. Thus, the relation between the efflux time and infiltration length is obtained and shown in Figure 4-31.

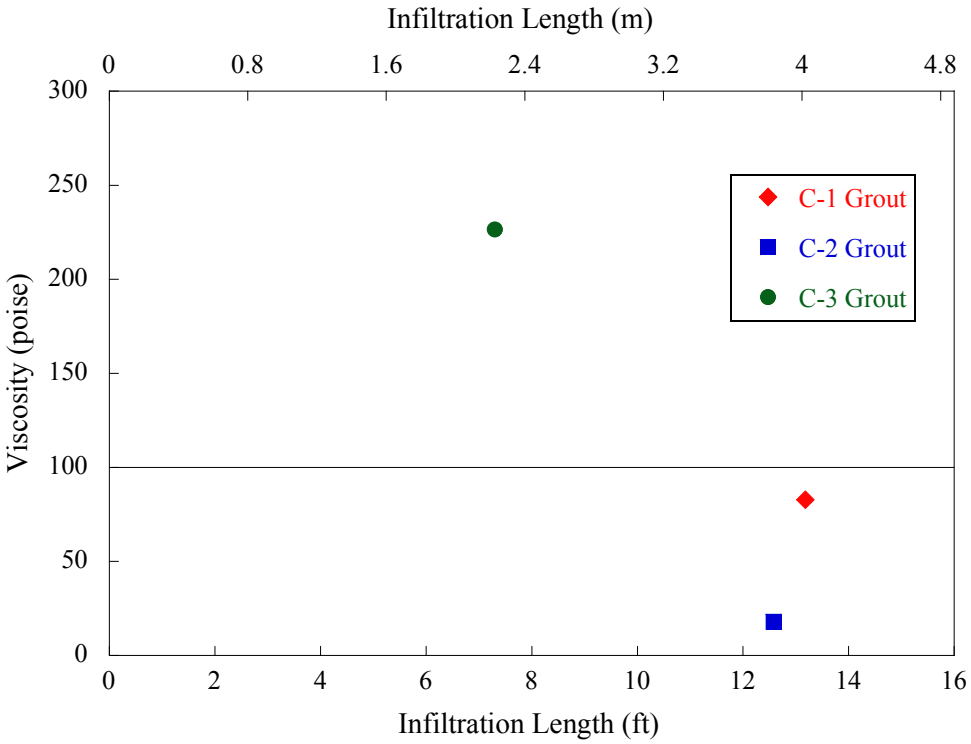

Figure 4-31. Relation between Viscosity and Infiltration Length.

Based on the relation obtained between the viscosity and infiltration length, it is observed that the C-1 and C-2 grouts, having lower viscosity, exhibit better filling capabilities in voids. Thus, it is advised that the grouts with a viscosity of 100 or more are not appropriate for filling voided ducts in PT systems.

4.5. Recommendation

Repairing voids before severe corrosion occurs may be an important factor for reducing maintenance cost as well as targeting potential factors of corrosion failure. Based on the results of this research, the PVG method is recommended for filling voids in the field while the PG method has lower FC and the VG method is less constructable. This method exhibits good filling capability and better economic feasibility. Application of the PVG method for repairing voids can reduce the time and costs while providing good fillability of the voids. For identifying an appropriate grout for repair, the C-1 and C-2 grouts show better filling capability with the PVG method, and it seems that grouts having lower fillability indices and viscosities are better materials for filling voids in PT systems.

5. SIMULATION OF REPAIR GROUT FLOW: ANALYSIS AND RESULTS

5.1. Introduction and Objectives

In experimental tests, prototype specimens of external PT tendons were fabricated and evaluated using different repair grouting methods and materials. However, experimental conditions cannot cover all void conditions in the field. Therefore, it is difficult to propose the most effective repair grouting method and materials based on experimental results. The reason for using simulation is that it is easier to make a parameter study to consider different effects such as repair methods, inclined angles of voided ducts, viscosities of repair grouts, and pressurizing. The basic numerical analysis model is verified using the experimental results and then the parameter study is performed.

This section describes the analysis and results on the research performed on simulations of repair grout flow. At first, the numerical program and analysis conditions are introduced. Preliminary analysis and results are then discussed. Details of the numerical analysis models are then described. The results of the analysis are then presented.

The objectives of this section are to:

- Develop a numerical model;
- Validate the numerical program and models with experimental results, and;
- Estimate the filling capability (FC) of repair grouting methods for different parameters such as repair methodologies, inclined angles of voided ducts, viscosities of repair grouts, and pressuring effects.

5.2. Simulation of Repair Grout Flow: Numerical Program and Conditions

This section briefly introduces the numerical program and then explains the details of the analysis conditions for the numerical model, mesh type, solver, etc. The material characteristics of repair grouts are then presented for viscosity and surface tension. Finally, the boundary conditions of the numerical analysis models representing an external voided tendon system are discussed.

5.2.1. Numerical program for simulating grout flow

In this research, a commonly-used computational fluid dynamics (CFD) program, FLUENT version 6.3.26, is used to simulate grout flow. To predict fluid flow for various conditions, the FLUENT solver computes the mass and momentum conservation equations (FLUENT 2006a). It can also consider the energy conservation equation when flows are affected by heat or compression. In this research, however, the mass and momentum conservation equations are considered to predict the flow of repair grouts.

The general mass conservation equation is:

$$\frac{\partial \rho}{\partial t} + \nabla \cdot (\rho \vec{v}) = S_m \tag{5.1}$$

where ρ is the density of fluid, $\vec{v}$ is the vector of fluid velocity, and S_m is the mass added from the second phase of the fluid.

The general momentum conservation equation is:

$$\frac{\partial}{\partial t}(\rho \vec{v}) + \nabla \cdot (\rho \vec{v}\vec{v}) = -\nabla p' + \nabla \cdot (\bar{\bar{\tau}}) + \rho \vec{g} + \vec{F} \tag{5.2}$$

where p' is the static pressure, $\bar{\bar{\tau}}$ represents the stress tensor considering the viscosity of fluid, $\rho \vec{g}$ is the gravitational body force, and $\vec{F}$ is the external body force applied in the fluid model.

The FLUENT program is based on the Finite Volume Method (FVM) which considers conservation equations at discretized cells of fluid model. Therefore, less cells in the model are required to predict the exact flow of fluid, but the analysis requires considerable computation time.

5.2.2. Numerical conditions in FLUENT

From the literature reivew, the Volume of Fluid (VOF) model can be used to track air/grout phase in the flow analysis because the VOF approach is usually used for slug flow and filling flow (2006b). To analyze fractions of air/grout phases in flows using the VOF model, the general mass conservation equation is revised (2006a). The equation shows a continuity equation considering the volume fraction of the q^{th} phase as follows:

$$\frac{1}{\rho_q}\left[\frac{\partial}{\partial t}(\alpha_q \rho_q) + \nabla \cdot (\alpha_q \rho_q \vec{v}_q) = S_{\alpha_q} + \sum_{p=1}^{n}(\dot{m}_{pq} - \dot{m}_{qp})\right] \tag{5.3}$$

where α_q is the q^{th} fluid's volume fraction in the meshed element and $\dot{m}_{pq}$ is the transferred mass from phase p to phase q.

The volume fraction of the primary phase can be computed while satisfying the requirement:

$$\sum_{q=1}^{n} \alpha_q = 1 \tag{5.4}$$

For choosing a solver in FLUENT, the pressure-based solver has to be selected to use a VOF scheme. The solver is appropriate for analyzing flows because it can analyze a wide range of fluid and needs less memory size for data storage. Also, Non-Iterative Time Advancement (NITA) schemes in the pressure-based solver are applied with the fractional-step method which considers pressure-velocity coupling in order to reduce computation time of analysis.

5.2.3. Material properties

To reflect the material characteristics of the grouts, the density and viscosity are considered in the FLUENT program. However, grout hardening due to cement hydration is not considered because the repair work can be completed before the hydration significantly affects the flow characteristics. The experimental data for the wet density and viscosity of the repair grouts was obtained from Kataria (2008). The wet density of the C-1 and C-2 grouts was 8.2 lb/ft^3 (2.1 g/cm^3) and the C-3 grout was 7.7 lb/ft^3 (2.0 g/cm^3). In this simulation, the material characteristics of the C-1 and C-2 grouts are considered because it was concluded that the C-3 grout is not applicable for repair grouting of small voids. Also, several dynamic viscosity tests using Brookfield rheometer were performed in this research to determine the range of viscosity in numerical approach. Figure 5-1 shows the viscosity results for the C-1, C-2, and C-3 grouts and some of results were obtained from Kataria's experiments (Kataria 2008). Although Brookfield rheometer can be an option for estimating dynamic viscosity of fluid, it might not represent the viscosity of grouts exactly.

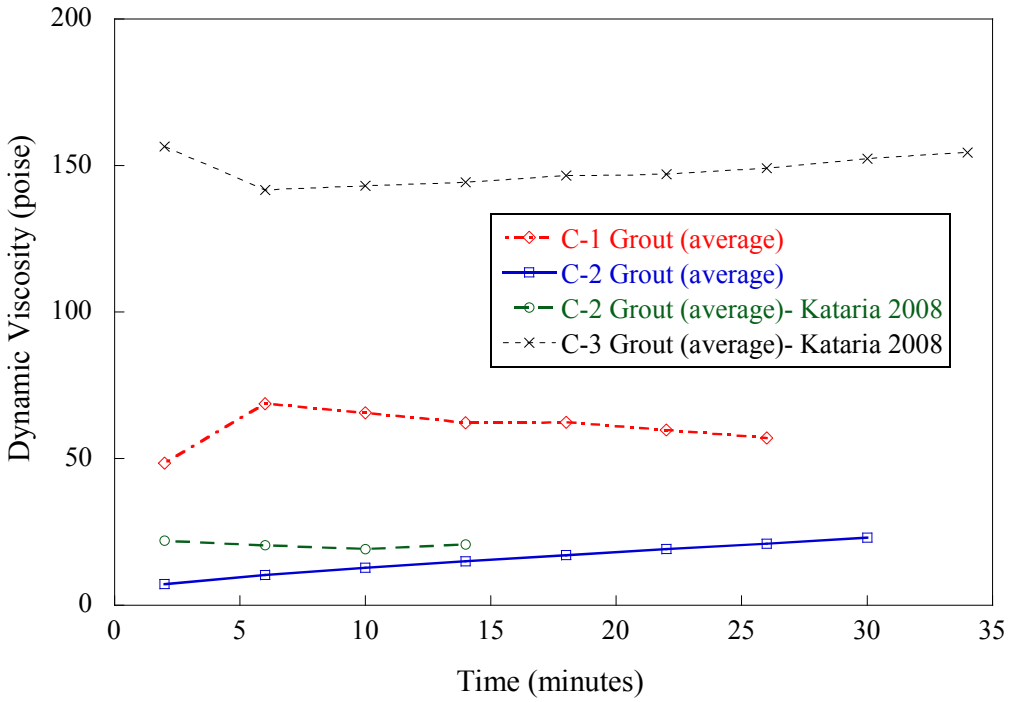

Figure 5-1. Dynamic Viscosities of C-1 and C-2 Grouts (Kataria 2008).

In the VOF approach, surface tension of fluids needs to be applied in the model. Thus, surface tension of grouts is computed using the equation (Kim and Corapcioglu 2002);

$$\sigma_{ST} = \frac{100}{\ln(100\mu_m + 7.5)} + 25 \tag{5.5}$$

where σ_{ST} is the surface tension (dyne/cm) of grouts and μ_m is the viscosity (centi poise) of the grouts. Therefore, the C-2 grout has a dynamic viscosity of 22 poise (average) and a surface tension of 33.13 dyne/cm in the analysis.

5.2.4. Modeling and boundary conditions

To construct a numerical model representing voided external tendon system, the pre-processor of FLUENT, Gambit version 2.3.16, is employed. The hexagonal (Hex) element was applied to the numerical analysis model. The numerical model was built with a half-model of voided ducts, assuming that the geometry of voids is symmetric. Thus, boundary conditions consist of a grout inlet, grout outlet, wall surface, and surface reflecting symmetric conditions. In the wall surface, options of no-slip condition and wall adhesion are evaluated in the numerical model. Repair grouts are injected at the grout inlet by applying a constant pressure. The vacuum condition is simulated using an exhaust fan model at the grout outlet, which can extract air inside the duct. Although the fan model can create a vacuum condition in the model, the vacuum condition is slightly different from experimental conditions; small amount of grouts can be continuously extracted through the fan model.

5.3. Simulation of Repair Grout Flow: Preliminary Analysis and Results

Preliminary 3-D analysis is performed to verify whether the FLUENT program can predict grout flow in voided ducts and to simulate experimental methodologies for repair grouting. This section describes a model of the preliminary analysis. Pressurizing

conditions of three different methods are then discussed to consider real vacuum condition in the analysis. The three repair methods, VG, PG, and PVG methods, are then compared in this analysis.

5.3.1. A model for preliminary analysis

The 3-D model for the preliminary analysis is simplified based on the experimental specimens. To apply appropriate elements in the numerical model the model is created with 4-inch-wide rectangular-shape ducts. The model simulates voided parts inside the tendon and strands in voids are not considered in the model. Furthermore, the model has an incline of 9 degrees, the same as the experimental specimens. The model is shown in Figure 5-2.

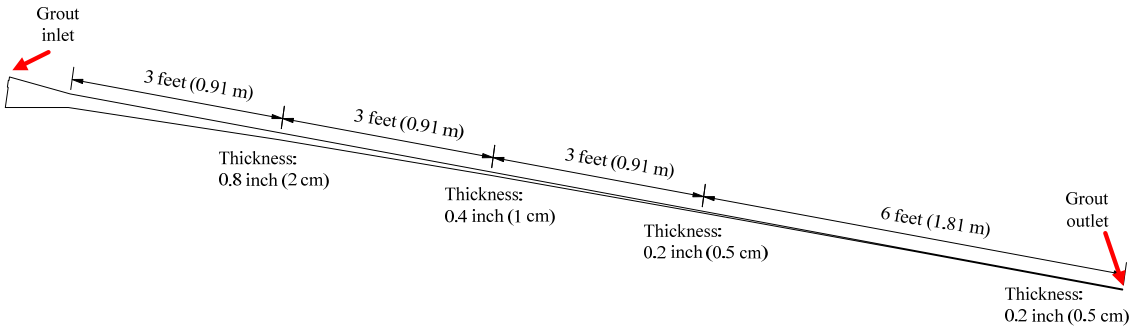

Figure 5-2. Side View of Void Model for Preliminary Analysis.

5.3.2. Pressure conditions of repair methods

For the pressurizing of the PG method at the grout inlet, the pressure of the analysis was temporarily determined as 50 psi (345 kPa) because grout should be injected by a pressure of less than 75 psi (517 kPa) at the inlet (FHWA 2004). Based on the experiments, the initial negative pressure inside the ducts of the VG method was -13.5 psi (-93 kPa, 92% of atmospheric pressure). However, the negative pressure may be reduced as repair grouts fill the voided ducts. The reduced pressure cannot be considered in the analysis, so the following three conditions were compared to determine an appropriate boundary condition for the VG method (Figure 5-3).

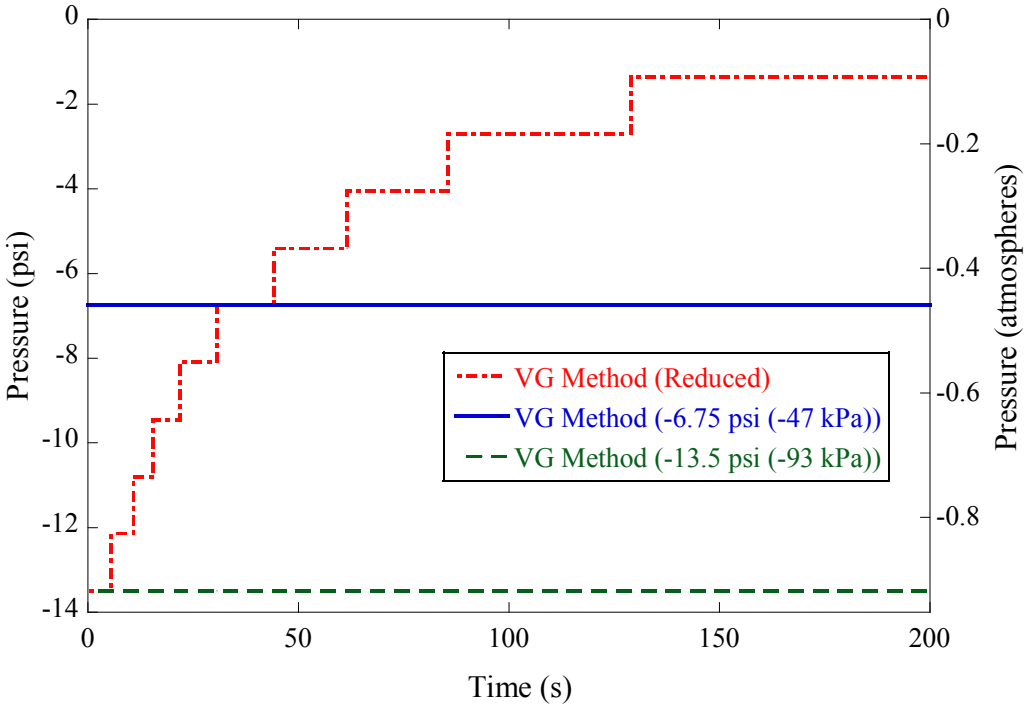

Figure 5-3. Pressure Conditions in VG Method.

In the condition of VG method (reduced), negative pressures at the grout outlet are manually applied, and 10% of intial vacuum pressure is reduced whenever grouts for 10% of initial voided volume are injected. Half of the initial vacuum pressure (-6.75 psi, -47 kPa) is compared with the reduced pressure and the filling capability (FC) of each condition is compared in Figure 5-4. Figure 5-4 shows that the filling with the half pressure is slightly different from the filling of reduced pressure in the beginning, but both fillings are converging. Thus, half pressure will be used in further analyses.

For the PVG method, both pressure and vacuum are applied simultaneously. Unlike the VG method, the vacuuming in the PVG method is continuously applied at the grout outlet; thus, 50 psi (345 kPa) of positive pressure at the inlet and -13.5 psi (-93 kPa) of the negative pressure at the outlet are used in the numerical model.

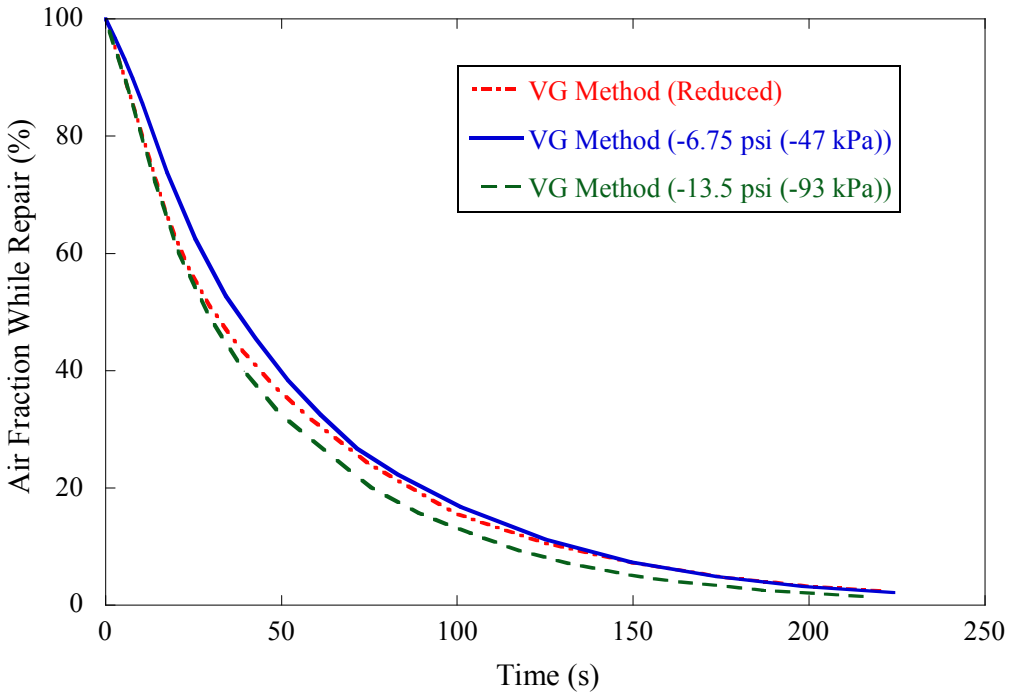

Figure 5-4. Filling Capabilities in Different Pressure Conditions.

The properties of the C-2 grout are used in this analysis; a dynamic viscosity of 22 poise and a wet density of 8.2 lb/ft^3 (2.1 g/cm^3).

5.3.3. Preliminary analysis results

Based on the experimental results, three different repair grouting methods, PG, VG, and PVG methods, are compared for filling voided ducts. Figure 5-5 shows the FC of each repair grouting method from the analysis. The PVG method fills voids fast inside ducts and exhibits a better FC than the PG and VG methods. However, the VG method has a lower FC value than the other methods and slowly fills the voided ducts.

From the preliminary analysis results shown in Figure 5-5, the numerical results seem to be similar to the experimental results for the VG and PVG methods. However, the PG method exhibits a good FC in the analysis while the PG method in experiments does not.

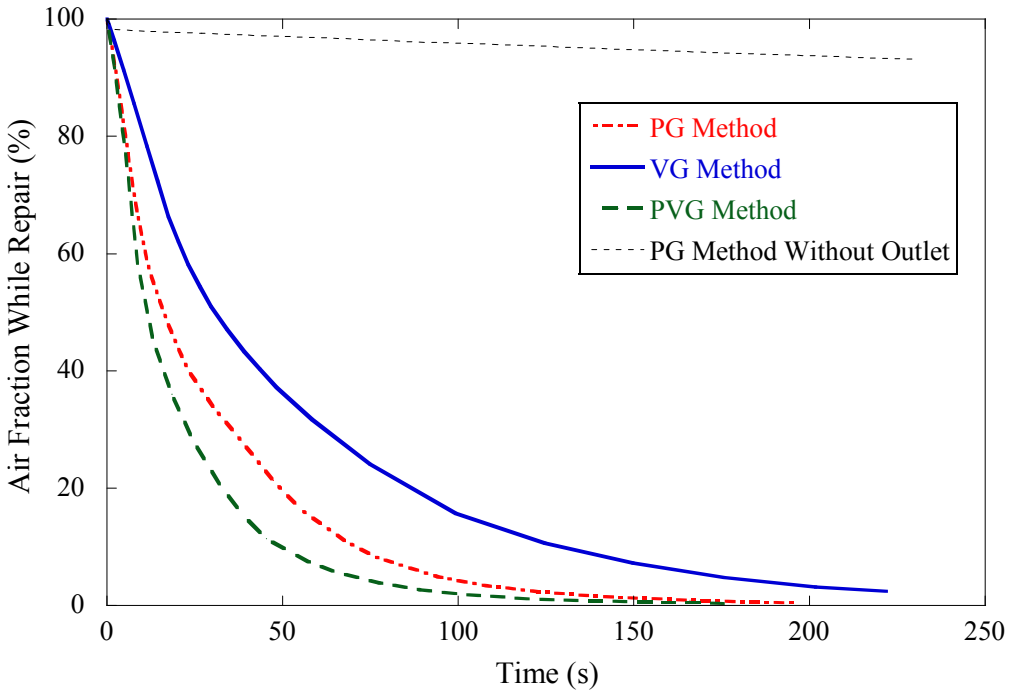

Figure 5-5. Comparison of Filling Capability for Different Repair Grouting Methods Using Preliminary Analysis.

From the experiments, an air outlet for the PG method was built at the end of each specimen but the air outlet may not be present in some specimens because voids in experiments may not be interconnected. To verify the effect of an air outlet in the PG method, the PG method without an air outlet is also analyzed and compared in Figure 5-5 and Figure 5-6. Figure 5-6 shows contour of grout volume around 150 seconds after injecting. Figure 5-6 (b) exhibits that the repair grouts do not effectively fill the voids when applying the PG method without an air outlet. Therefore, the PG method exhibits better FC in the analysis but it requires more attention for applying in the field because bleed line might not be interconnected between the grout inlet and outlet.

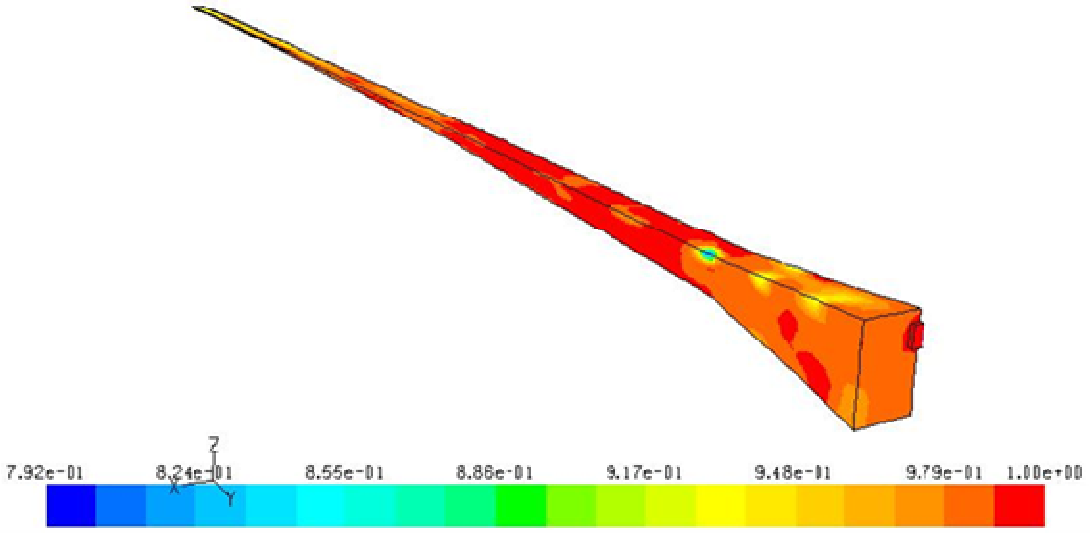

(a) Volume Fraction (Grouts) – PG Method With Air Outlet

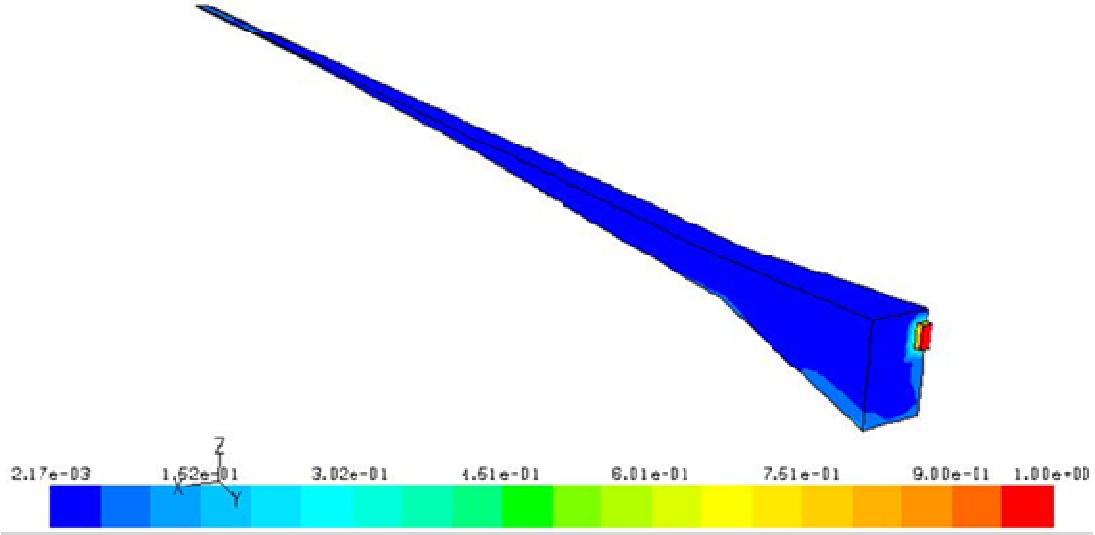

(b) Volume Fraction (Grouts) – PG Method Without Air Outlet

Figure 5-6. Contour of Grout Volume Fraction in Different Boundary Conditions.

5.4. Simulation of Repair Grout Flow: Numerical Analysis Models

The section first presents how to design a numerical analysis model and verify it. The numerical analysis model is simplified here because the geometric conditions inside the voids are complicated. This section proposes a simplified numerical model reflecting the geometry of voids and then verifies the model with experimental results.

5.4.1. Simplification of numerical analysis model

The geometric conditions of voided ducts are complicated as the voids usually have irregular shapes. In addition, due to the curved surface of the round-shaped duct, voids are difficult to model in the analysis program. To simplify the ducts with voids in the experiments, three models (Model 1, Model 2, and Model 3) are evaluated as described in Table 5-1. Simplified rectangular models are designed to match the hydraulic radius, R_h, and cross sectional area, A, of the round-shaped model. The repair grouts are injected into 10-ft (3.05 m) long empty ducts with three different sections and the FC of each model is compared in the analysis (Figure 5-7).

Table 5-1. Geometric Conditions for Simplifying Ducts.

Model No.	Duct Shape	Size	Area of Section	R_h of Section
1	Round	4-inch (10.16 cm) Diameter	12.57 inch^2 (81.10 cm^2)	1.00 inch (2.54 cm)
2	Rectangular	4 × 4 inches	16.00 inch^2 (103.23 cm^2)	1.00 inch (2.54 cm)
3	Rectangular	3.54 (8.99 cm)× 3.54 inches	12.53 inch^2 (80.84 cm^2)	0.89 inch (2.25 cm)

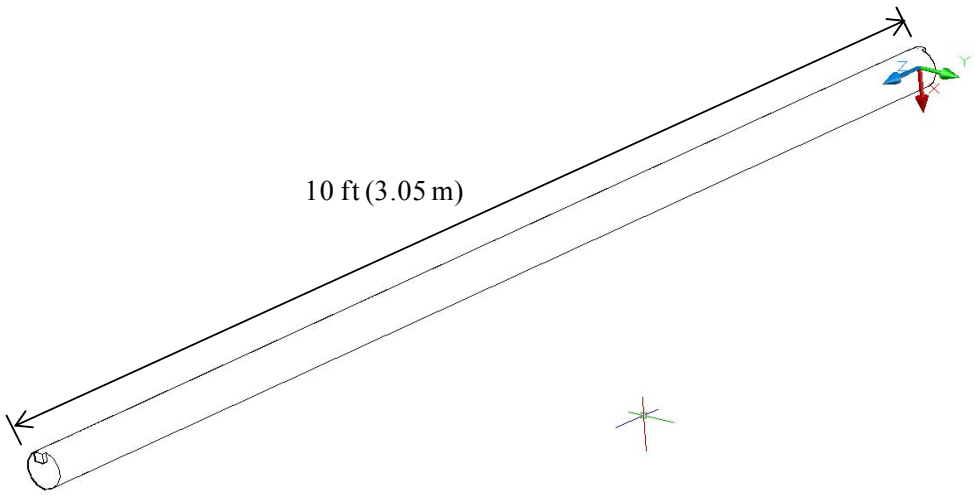

Figure 5-7. Model of Round-shape Ducts.

From the analysis, the remaining air fraction, which means that remaining voids are divided by the initial volume, while injecting repair grouts was assessed as shown in Figure 5-8. Assuming that the round-shape duct represents the real-case scenario, it can be seen that Models 2 and 3 may be representing Model 1. After approximately 150 seconds all models converge and likely can be used to assess the filling capability of grouts. It should be noted that although the round-shape duct likely represents actual conditions, modeling the placement of repair grout in voids in the round-shape duct is challenging. Therefore, the rectangular system would be more useful for modeling the repair procedure. In this research, Model 3 will be used for further analyses.

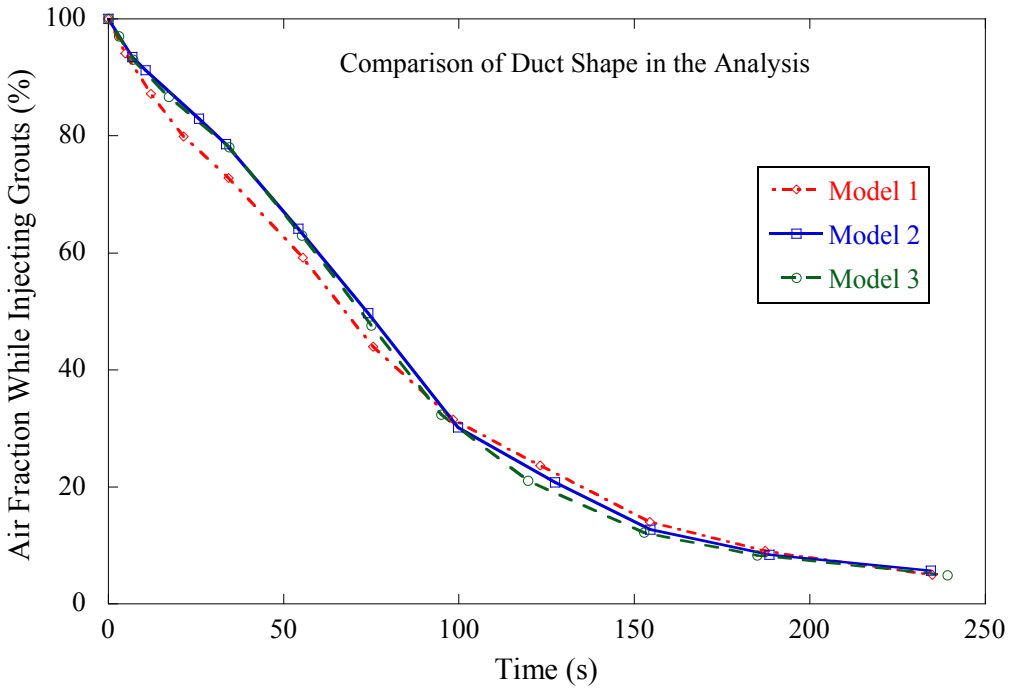

Figure 5-8. Air Fraction While Injecting Grouts for Different Duct Shapes.

This result also shows that the rectangular model, whose section has a different void size but the same hydraulic radius as the round-shape ducts, is similar to the round-shape model for the analysis of filling voids when considering air fraction. For an arbitrary shaped void, the resistance stresses, τ_0, are generated opposite to the direction of grout flow around the perimeter U of the void (Figure 4-20). From Equation (4.8) the relation between geometric conditions of voids (U and A) and the resistance force P for a given length, l, are given by:

$$P = \frac{U}{A} l \cdot \tau_0$$
$$\therefore\ l = \frac{1}{\tau_0} P \cdot R_h \qquad (5.6)$$

where τ_0 is related to velocity and viscosity of flow.

From the Equation (5.6) the FC can be affected by the hydraulic radius of the voids in the model. Based on cut sections of experiments the void area and perimeter at each cut section are assessed and then the hydraulic radius can be obtained. Therefore, the simplified rectangular models considering the area and perimeter of voids are analyzed, and one of these models is shown in Figure 5-9.

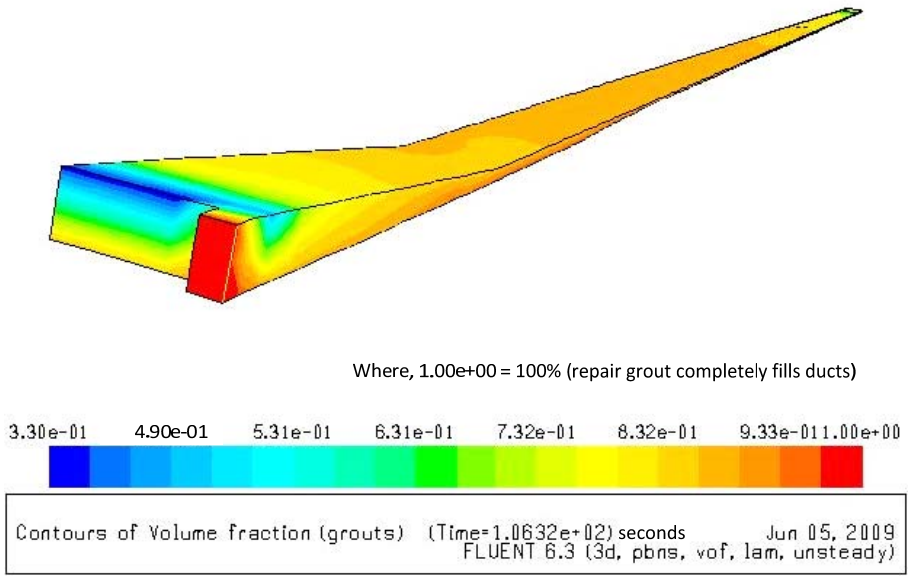

Figure 5-9. Analysis Results of Grout Fraction Using a Simplified Model.

The simplified models are considered to void profiles of VG-C2-2, PG-C2-2, and PVG-C2-2 to validate the numerical analysis model with experimental results. The voids in the experimental specimens are fabricated by voids due to the bleed water and artificial voids caused by extracting grout using a vacuum pump. In some cases, these voids might have a biased trend in an experimental specimen. Thus, the uni-model obtained from the averaged void profile of experiments was considered to reduce the error caused by biased results. Thus, analyses are carried out to the model reflecting one of the general void profiles in the field. The details of the section for the uni-model are shown in Table 5-2.

Table 5-2. Details of Section for Uni-model.

Cut Section Locations from the Reference Points, ft (m)	R_h, in (cm)	Width, in (cm)	Thickness, in (cm)
-0.88 (-0.27) / Grout Inlet	0.381 (0.968)	4.96 (12.60)	0.900 (2.287)
0 (0) / Reference Point	0.122 (0.310)	3.54 (8.99)	0.262 (0.666)
0.60 (0.18)	0.101 (0.258)	3.54 (8.99)	0.215 (0.547)
1.00 (0.30)	0.081 (0.207)	3.54 (8.99)	0.171 (0.433)
1.50 (0.46)	0.066 (0.168)	3.54 (8.99)	0.137 (0.349)
2.00 (0.61)	0.060 (0.152)	3.54 (8.99)	0.124 (0.314)
2.50 (0.76)	0.055 (0.139)	3.54 (8.99)	0.113 (0.287)
3.00 (0.91)	0.053 (0.135)	3.54 (8.99)	0.109 (0.278)
3.50 (1.07)	0.055 (0.141)	3.54 (8.99)	0.115 (0.291)
3.75 (1.14)	0.055 (0.141)	3.54 (8.99)	0.115 (0.292)
4.00 (1.22)	0.074 (0.189)	3.54 (8.99)	0.155 (0.394)
4.25 (1.30)	0.052 (0.132)	3.54 (8.99)	0.107 (0.272)
4.50 (1.37)	0.052 (0.132)	3.54 (8.99)	0.107 (0.272)
5.00 (1.52)	0.053 (0.136)	3.54 (8.99)	0.110 (0.280)
6.00 (1.83)	0.046 (0.117)	3.54 (8.99)	0.095 (0.240)
7.00 (2.13)	0.049 (0.123)	3.54 (8.99)	0.100 (0.254)
7.25 (2.21)	0.070 (0.178)	3.54 (8.99)	0.146 (0.370)
7.50 (2.29)	0.041 (0.105)	3.54 (8.99)	0.085 (0.215)
8.00 (2.44)	0.041 (0.105)	3.54 (8.99)	0.085 (0.215)
9.00 (2.74)	0.042 (0.106)	3.54 (8.99)	0.085 (0.216)
10.00 (3.05)	0.038 (0.097)	3.54 (8.99)	0.078 (0.199)
11.00 (3.35)	0.035 (0.088)	3.54 (8.99)	0.071 (0.180)
12.00 (3.66)	0.035 (0.090)	3.54 (8.99)	0.072 (0.184)
12.75 (3.89)	0.035 (0.090)	3.54 (8.99)	0.072 (0.184)
13.00 (3.96)	0.066 (0.167)	3.54 (8.99)	0.136 (0.346)
13.25 (4.04)	0.028 (0.071)	3.54 (8.99)	0.057 (0.144)
14.00 (4.27)	0.028 (0.071)	3.54 (8.99)	0.057 (0.144)
14.50 (4.42)	0.028 (0.071)	3.54 (8.99)	0.057 (0.144)
15.00 (4.57)	0.024 (0.060)	3.54 (8.99)	0.048 (0.122)

5.4.2. Element sizes in the model

In the CFD analysis, the size of mesh can significantly affect the accuracy of the numerical analysis because continuity equations are computed using discretized scheme; thus, a fine-mesh model is required for obtaining better results. However, the finer-mesh model significantly increases the analysis time. Thus, mesh convergence has to be checked to determine an appropriate mesh size.

The model of voided ducts here is a tapered shape, and the mesh type has to be used by the Hex element which is hexagonal in shape. Thus, mesh size gets finer as the size of the void gets smaller. To identify mesh convergence of the analysis, the model needs to be meshed with the same size. However, it is a challenge to perform the analysis for mesh convergence in the tapered geometry. To obtain a good shaped element the tapered model for voided ducts can be meshed as a coarse model and a fine model. However, only two models cannot ensure the appropriate mesh size for the analysis and the following model (4 inch × 4inch × 10 ft rectangular-shape ducts [10.2 cm × 10.2 cm × 3.05 m]) is then considered to ensure mesh convergence of the analysis (Figure 5-10). The mesh size and the corresponding numbers of elements are provided in Table 5-3.

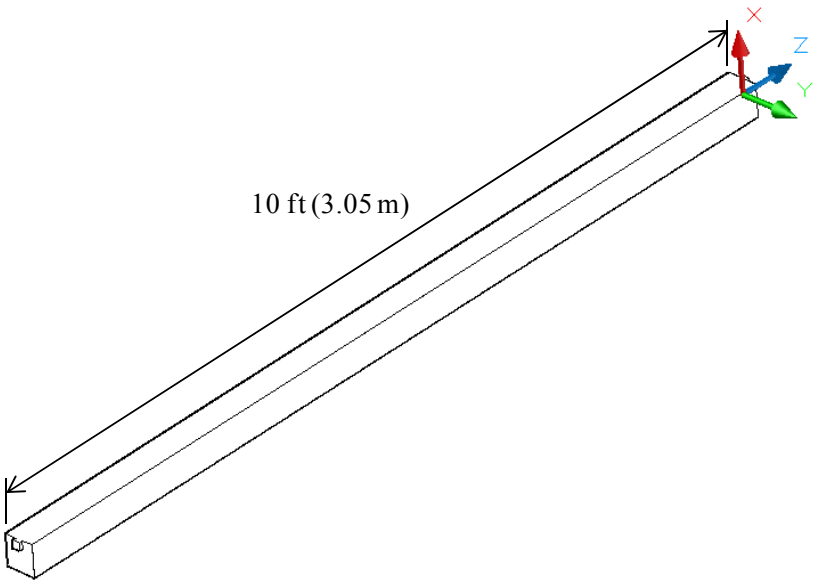

Figure 5-10. The Model of 4 inch × 4 inch (10.2 cm × 10.2 cm) Reactangular Ducts.

Table 5-3. Mesh Sizes and Corresponding Numbers of Elements of Numerical Analysis Models.

Mesh Size, inch (cm)	No. of Elements
1 (2.54)	2402
0.5 (1.27)	15,356
0.4 (1.02)	33,018
0.3 (0.76)	67,636
0.25 (0.64)	122,944

In this analysis, the PG method with an injecting pressure of 50 psi (345 kPa) is applied to the model and the repair grouts have a dynamic viscosity of 22 poise.

Figure 5-11 shows the analysis results. These results converge when the mesh number is 67,636 and larger (mesh size is 0.3 inch and less). Thus, a mesh size of less than 0.3 inch (0.76 cm) is required for the tapered voided model.

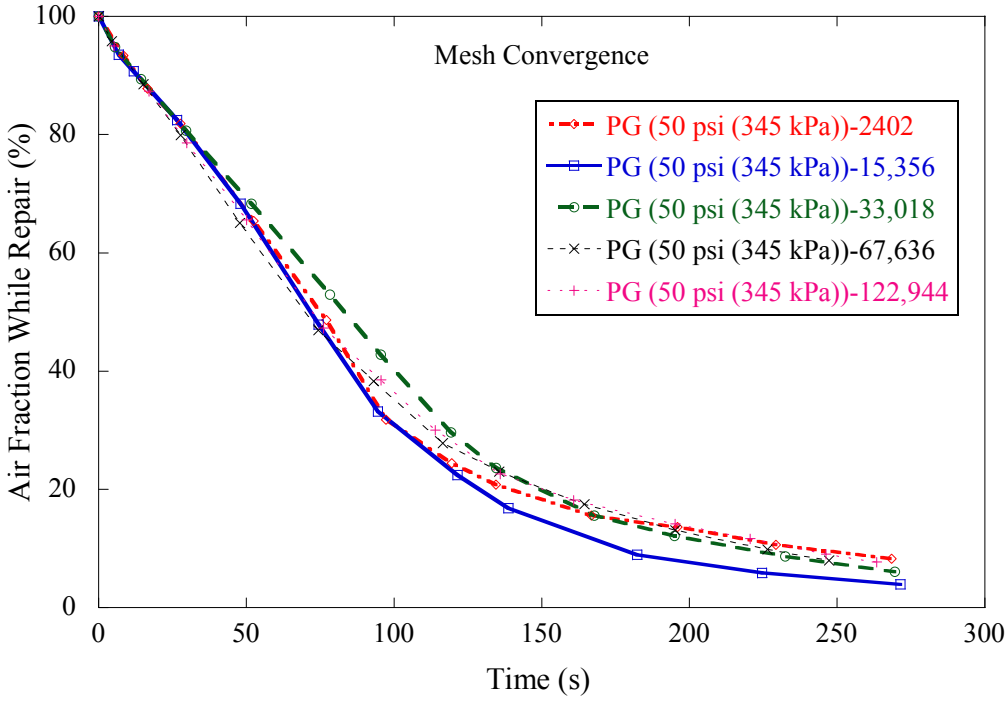

Figure 5-11. Comparison of Grout Filling for Different Mesh Sizes.

As mentioned above, the tapered model for voided ducts can be meshed as coarse and fine models. The coarse model ranges from 0.5 inches (1.27 cm) to 0.025 inches (0.06 cm) and the fine model ranges from 0.3 inches (0.76 cm) to 0.012 inches (0.03 cm). Based on the analysis for mesh convergence it is better to use the fine model; however, analysis of both models does not have critical differences from using the uni-model (Figure 5-12).

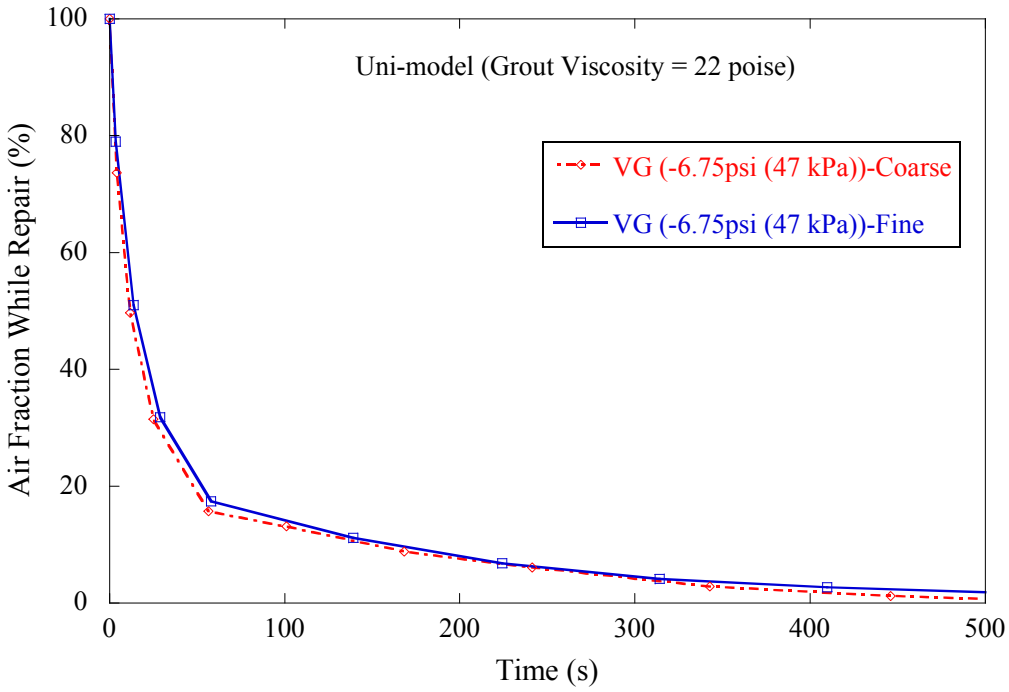

Figure 5-12. Comparison of Filling Capability Using Coarse and Fine Model.

5.4.3. Validation of simplified numerical analysis model

To validate the applicability of the simplified model, analysis results for filling capability are compared with experimental results. Based on the video analysis of filling voided ducts and cut section analysis after repair, the amount of filling voids is estimated. From the cut section analysis, the approximate initial void volume of each experimental specimen is assessed. Also, the video recordings show the filling speed of each experiment for repair through the transparent ducts (Figure 5-13) and the estimated void volume can be obtained from the cut section analysis. Thus, the air fractions while filling voids in experiments are obtained and compared with the numerical results. Figure 5-14, Figure 5-15, and Figure 5-16 show that the simplified numerical model just considering hydraulic radius in each cut section has slightly different results from the experimental results but the trends of filling voids look similar.

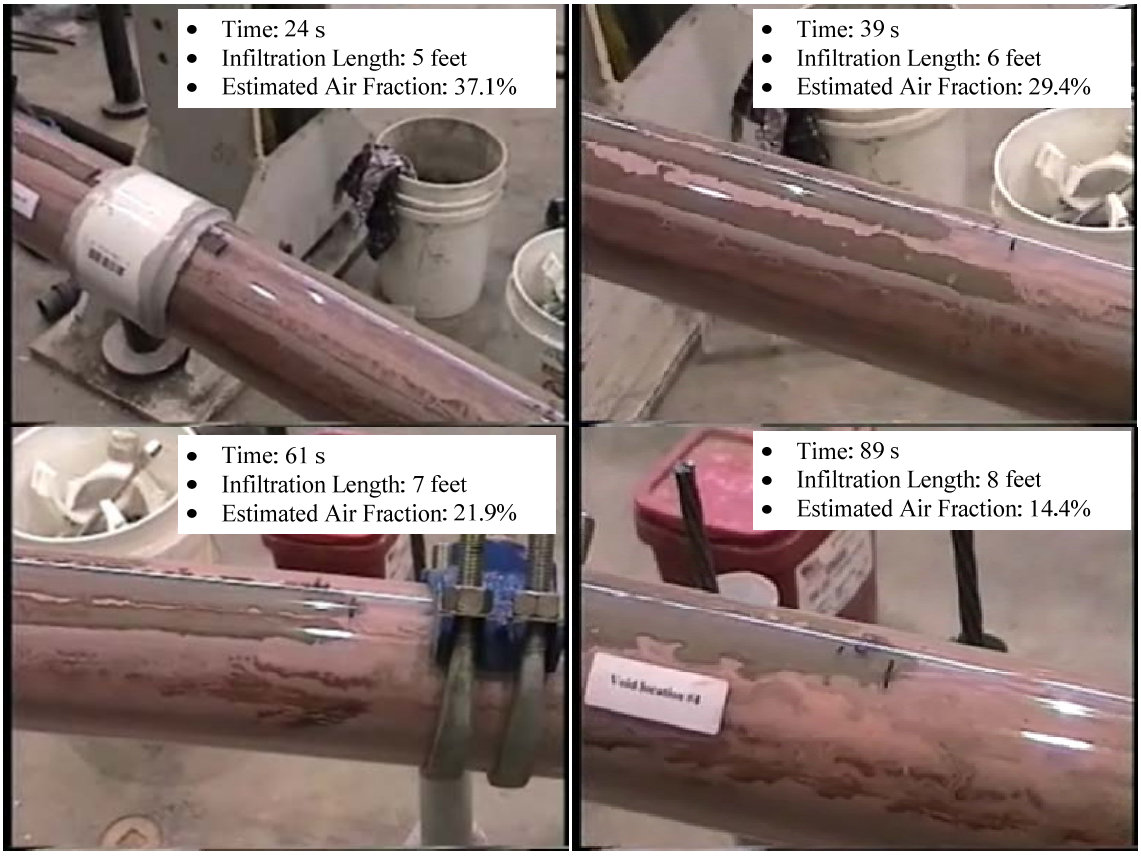

Figure 5-13. Video Frames of Specimen VG-C2-2.

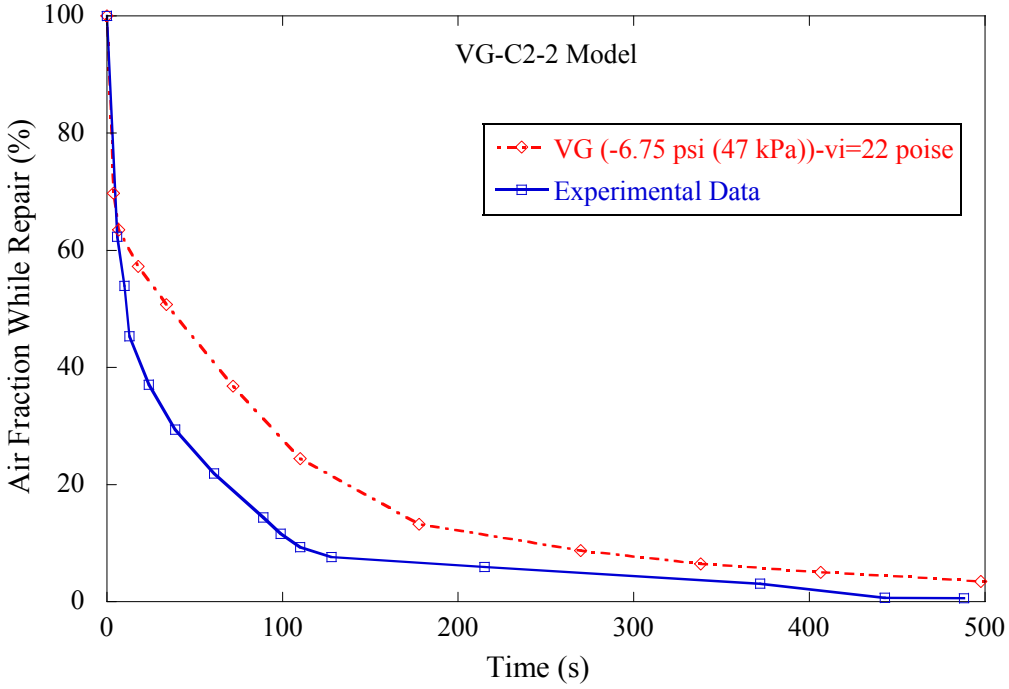

Figure 5-14. Comparison of Filling Capability between Analysis and Experimental Data for VG-C2-2 Specimen.

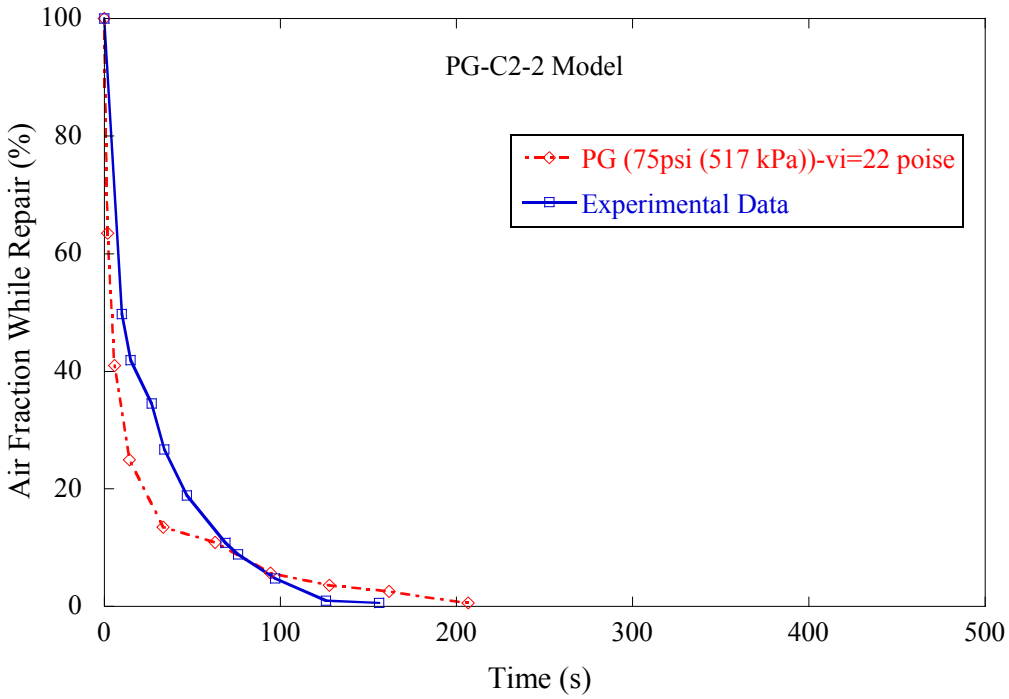

Figure 5-15. Comparison of Filling Capability between Analysis and Experimental Data for PG-C2-2 Specimen.

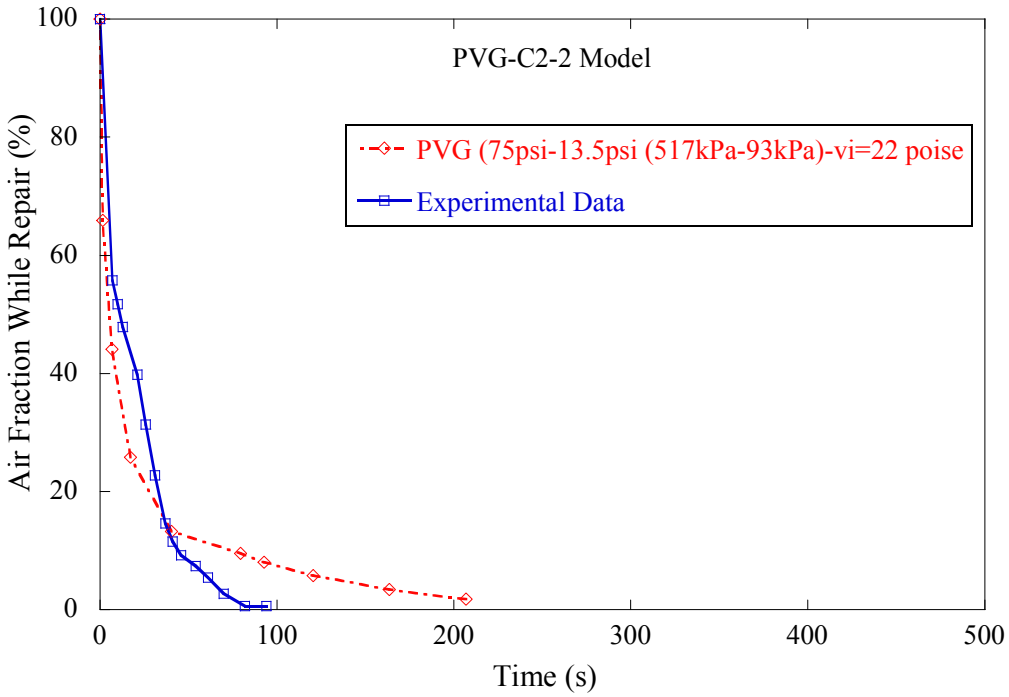

Figure 5-16. Comparison of Filling Capability between Analysis and Experimental Data for PVG-C2-2 Specimen.

In addition, the experimental results of filling performance after repair are compared with the analysis results using the simplified model. The void ratios after repair at each cut section location are compared and shown in Figure 5-17, Figure 5-18, and Figure 5-19. The void ratio from the experiments shows the entrapped air while repairing voids. The entrapped air is usually distributed along the repaired area and it is not continuously connected. Thus, the experimental results have 0% of void ratio depending on the cut locations. Therefore, the void ratio of experiments seems to be less than the analysis results. Also, the void ratio from the analysis exhibits a larger void ratio than the experimental data after 5 feet (1.5 m) of cut section location. However, the void ratio can be magnified when the remaining voids exist only in a small repaired area. Figure 5-20 exhibits the comparison of the remaining voids after repair for specimen PVG-C2-2. Thus, the difference between experimental data and analysis may not be critical after 5 feet (1.5 m) of cut section locations and the analysis results for filling

performance seem to be reasonable. Therefore, the simplified model is used for further analyses predicting grout flow in voided ducts.

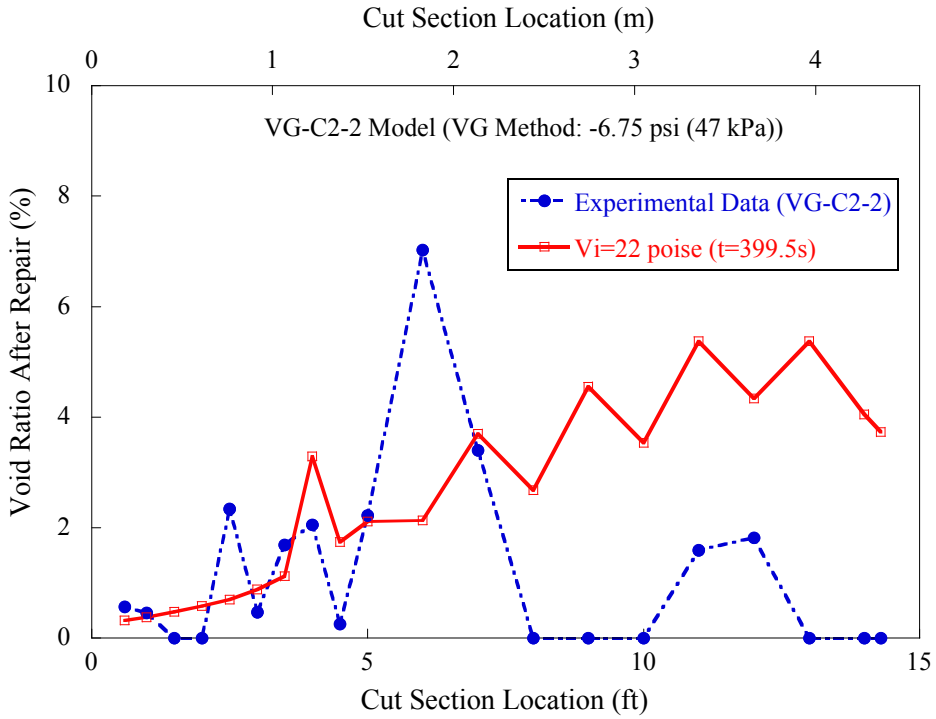

Figure 5-17. Comparison of Filling Performance between Analysis and Experimental Data for VG-C2-2 Specimen.

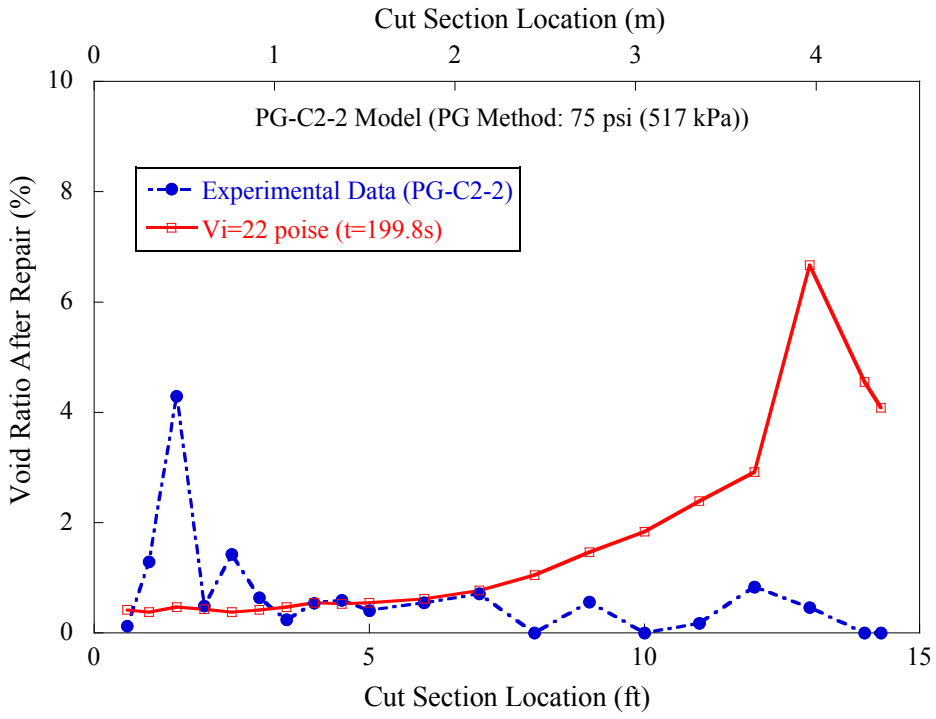

Figure 5-18. Comparison of Filling Performance between Analysis and Experimental Data for PG-C2-2 Specimen.

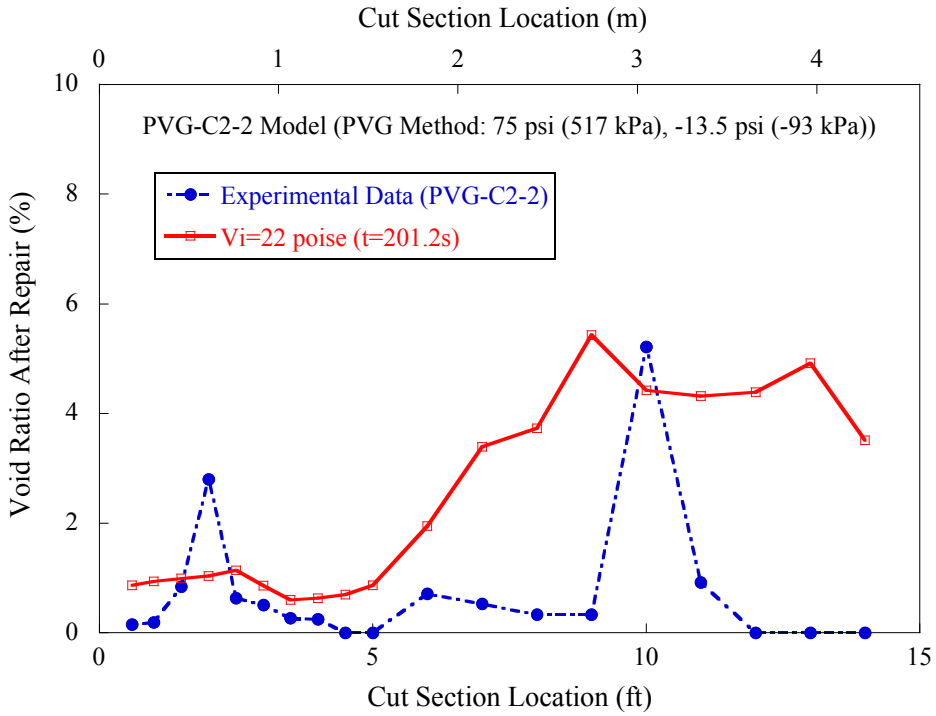

Figure 5-19. Comparison of Filling Performance between Analysis and Experimental Data for PVG-C2-2 Specimen.

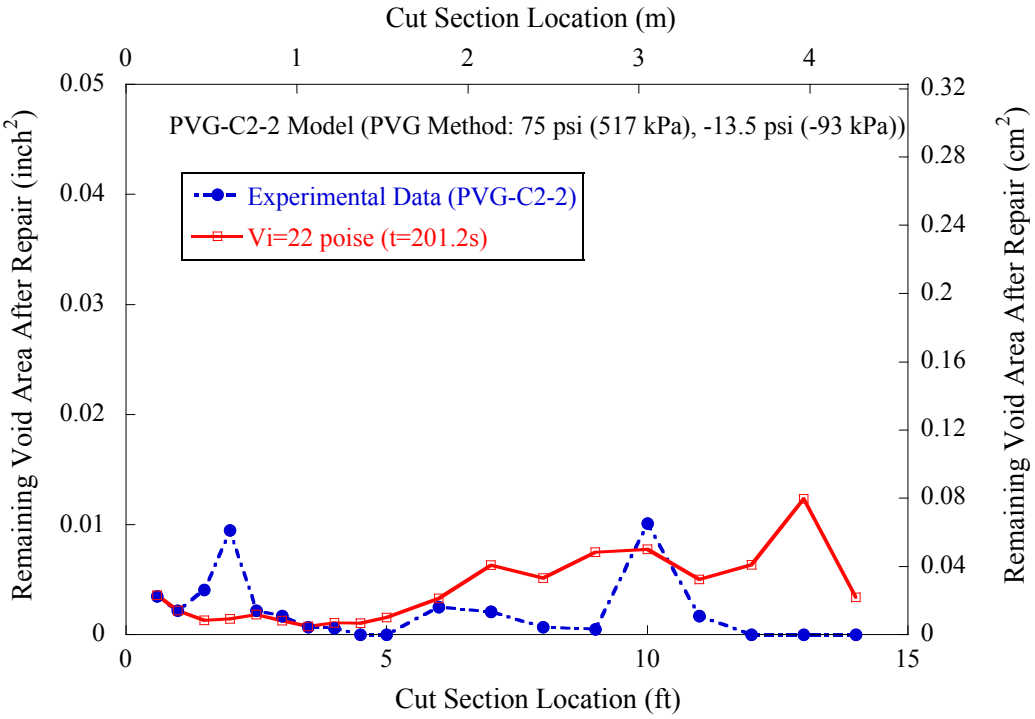

Figure 5-20. Comparison of Remaining Void Area between Analysis and Experimental Data for PVG-C2-2 Specimen.

5.5. Simulation of Repair Grout Flow: Analysis and Results

This section provides results for simulating grout flow in voided ducts. First, three different repair grouting methods, VG, PG, and PVG methods, are assessed to identify an effective method for filling voids. Then, a parametric study is performed to verify the effects of filling voids in various conditions. This study is expected to suggest an appropriate condition for repair grouting methods.

5.5.1. Comparison of repair grouting methods

The analysis is carried out using the uni-model with fine meshed elements and a grout having a dynamic viscosity of 22 poise. Figure 5-21 shows that the PG and PVG methods show slightly better FC than the VG method, and both methods fill voided ducts more quickly than the VG method. For the PG method without an outlet, however,

the FC is significantly reduced. The analysis of the PG method without an outlet was stopped at approximately 80 seconds after injecting the grouts because of the divergence of numerical solution. Thus, the application of the PG method is not appropriate for filling voided ducts without air outlets.

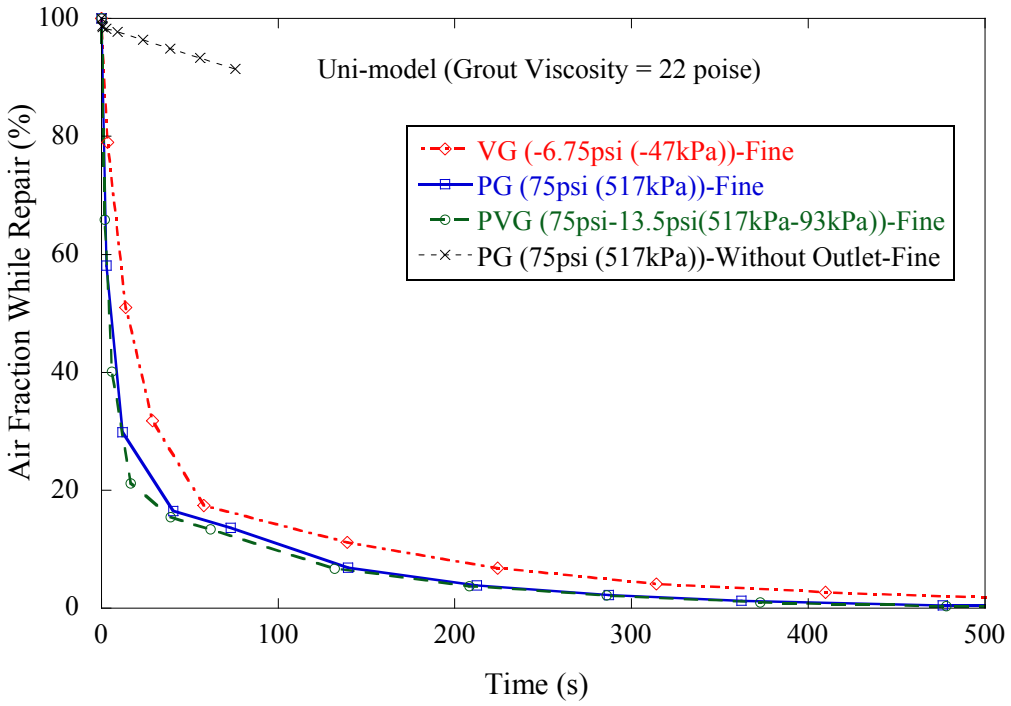

Figure 5-21. Comparison of Filling Capability for Different Repair Grouting Methods Using Uni-model.

Figure 5-22 shows the void ratio in the cut section locations from the experiments. The results also show that the PG and PVG methods have slightly better filling performance than the VG method.

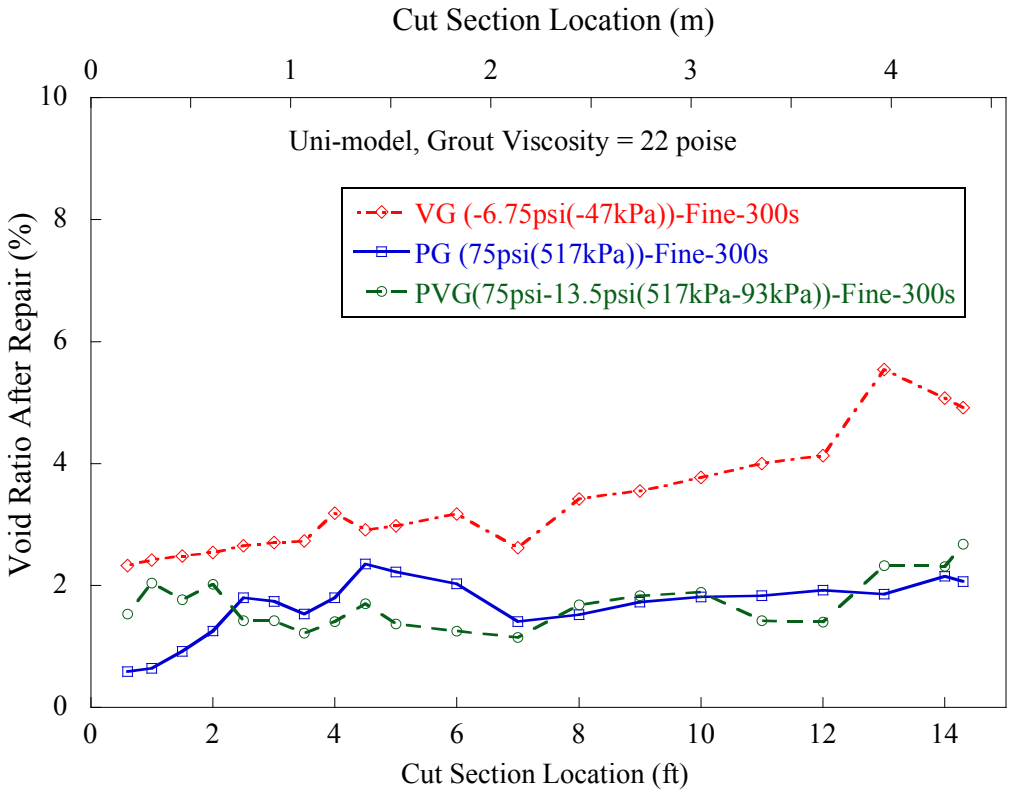

Figure 5-22. Comparison of Filling Performance in Cut Sections for Different Grouting Methods.

For other void conditions before repair, the FC may have different trends than the results using the uni-model. Thus, the initial conditions of the VG-C2-2 model, PG-C2-2 model, and PVG-C2-2 model are also assessed for the FC of three repair grouting methods. Figure 5-23, Figure 5-24, and Figure 5-25 shows the comparison of the FC for different repair grouting methods for specific experimental void conditions. The PG and PVG methods generally have better FC than the VG method, and they have much better FC than the VG method in the PVG-C2-2 model.

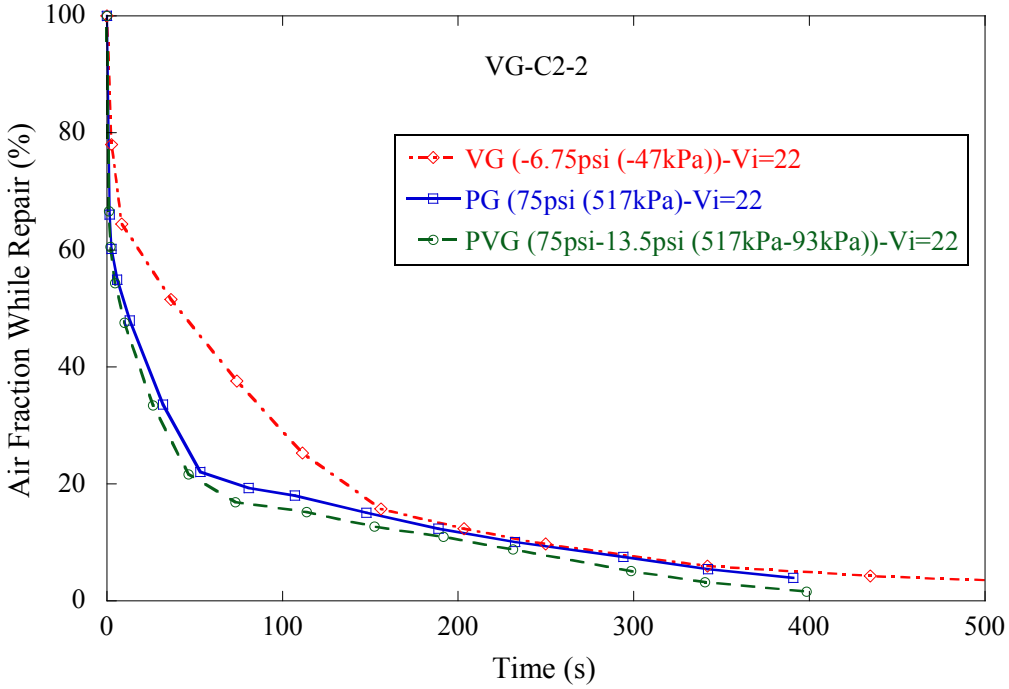

Figure 5-23. Comparison of Filling Capability for Different Repair Grouting Methods Using VG-C2-2 Model.

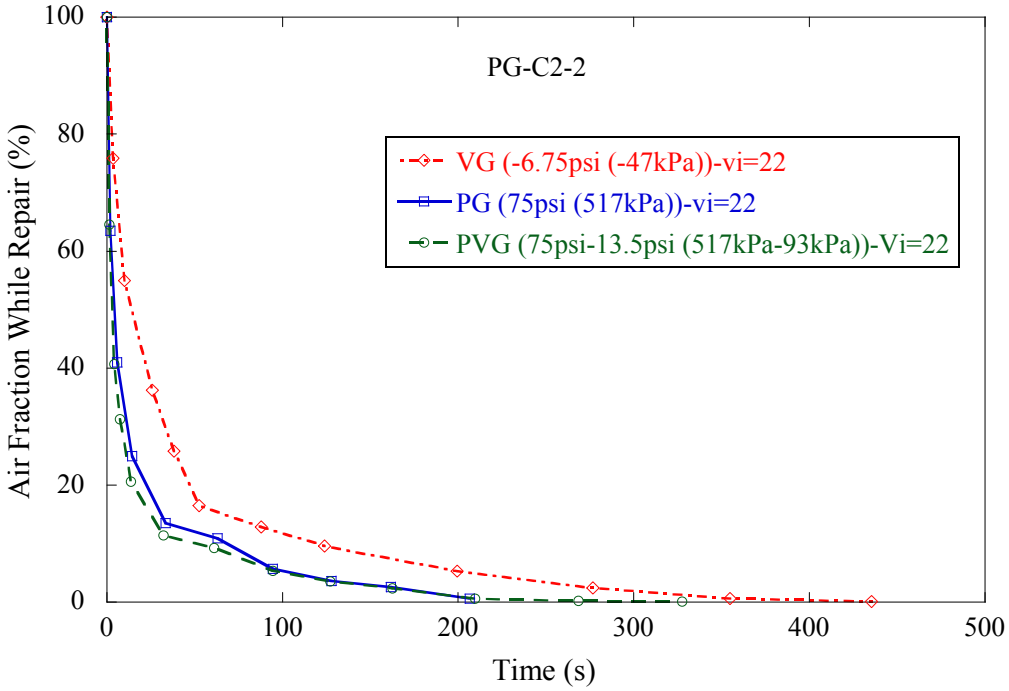

Figure 5-24. Comparison of Filling Capability for Different Repair Grouting Methods Using PG-C2-2 Model.

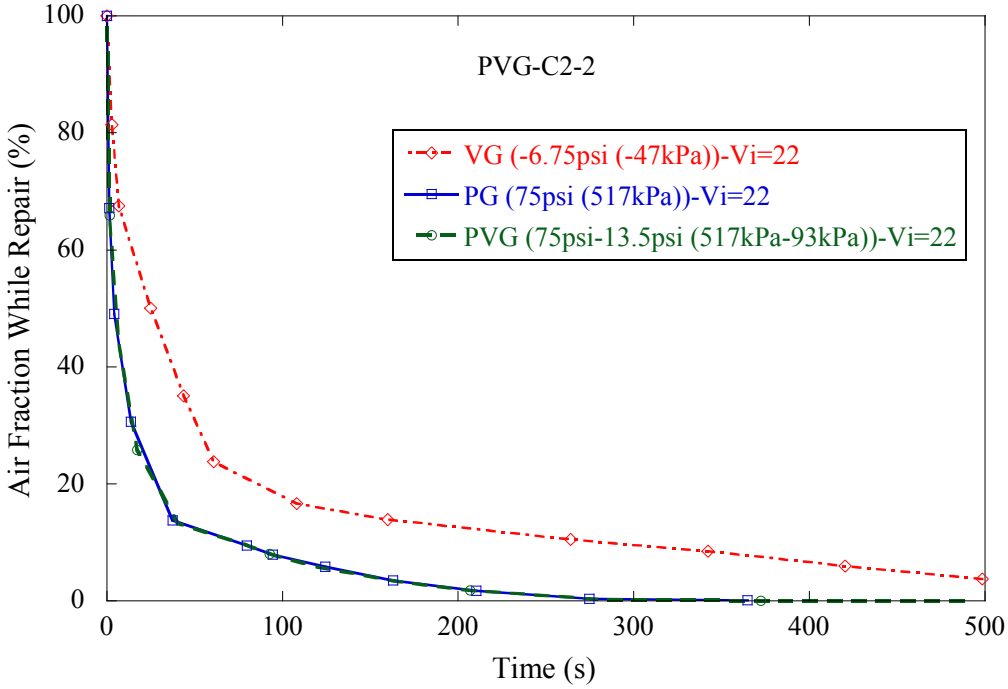

Figure 5-25. Comparison of Filling Capability for Different Repair Grouting Methods Using PVG C2-2 Model.

In the field, various sizes of voids can exist. Thus, the FCs of repair grouting methods are assessed in ducts including larger voids. Additionally, 6-ft empty ducts and 12-ft empty ducts are added to the uni-model. The analyses are performed using coarse meshed element because the added empty ducts excessively increase the number of elements. As with the other models the grout is assumed to have a viscosity of 22 poise.

The results are shown in Figure 5-26 and Figure 5-27. Like the analysis using the uni-model, the PG and PVG methods have better FC than the VG method in both models with larger voids. However, Figure 5-27 shows that air fractions of all the repair methods converge at 200 seconds after starting the injection of grout. It seems that the void volume of empty ducts is larger than the void volume of partially voided ducts; that is, the empty ducts can be easily filled by all the repair methods.

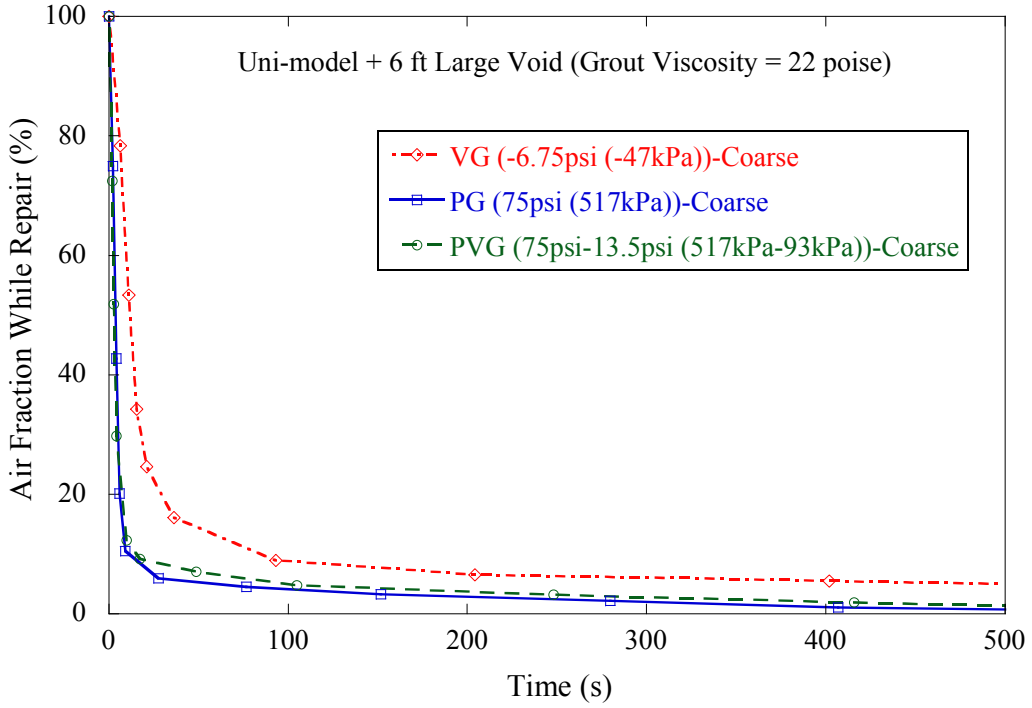

Figure 5-26. Comparison of Filling Capability for Different Repair Grouting Methods Using Uni-model + 6 ft Large Void.

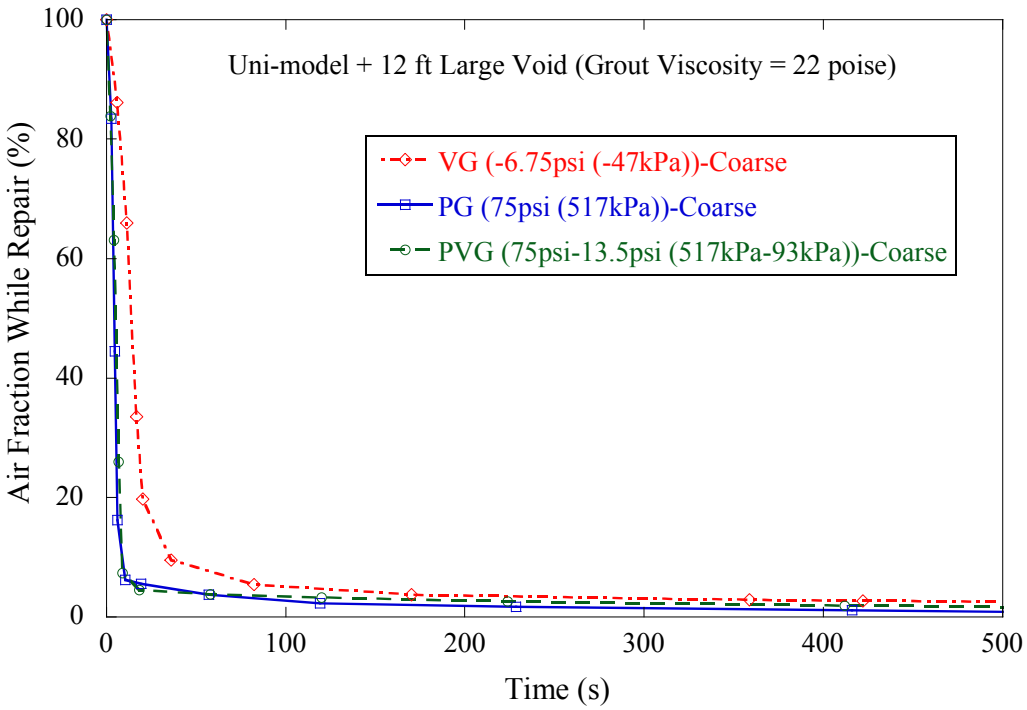

Figure 5-27. Comparison of Filling Capability for Different Repair Grouting Methods Using Uni-model + 12 ft Large Void.

5.5.2. Parametric study

To identify parametric effects of grout flow in voided ducts, analyses using the uni-model are performed for various conditions. Filling voided ducts can be affected by repair methodologies, geometric conditions of the voids, material characteristics, and pressurizing conditions of each method. Thus, the following parameters are assessed in the analysis:

- Repair Methodology
  - VG, PG, and PVG methods
- Inclined angles of voided ducts
  - 0˚, 9˚, and 18˚
- Viscosity of repair grouts
  - 22, 50, 100, and 200 poise
- Effect of pressurizing
  - VG method
    - Inlet: 0 psi
    - Outlet: -1, -2, -4, and -6.75 psi
  - PG method
    - Inlet: 25, 50, and 75 psi
    - Outlet: 0 psi
  - PVG method
    - Inlet: 25, 50, and 75 psi
    - Outlet: -13.5 psi

The analyses are performed using the uni-model and fine meshed models. To consider the parametric effects for filling voids, air fractions at 300 seconds after injecting repair grouts are obtained and compared. The results of the analysis for each

repair method are shown in the Table 5-4, Table 5-5, Table 5-6, Figure 5-28, Figure 5-29, and Figure 5-30.

Table 5-4. Air Fraction at 300 Seconds after Injecting Grouts for VG Method.

t=300 s		Air Fraction of VG Method (%)											
Pressurizing		-1 psi (-7 kPa)			-2 psi (-14 kPa)			-4 psi (-28 kPa)			-6.75 psi (-47 kPa)		
Inclined Angle		0˚	9˚	18˚	0˚	9˚	18˚	0˚	9˚	18˚	0˚	9˚	18˚
Visc-osity (poise)	22	30.9	4.3	0.7	25.7	5.0	0.5	18.9	4.5	0.6	14.0	4.4	0.6
	50	40.2	8.7	5.9	36.6	8.8	6.1	30.1	8.8	5.5	25.2	8.4	5.2
	100	47.2	13.5	10.9	43.4	13.5	10.6	37.2	12.4	9.7	32.6	12.5	10.8
	200	50.5	20.9	15.0	47.3	21.5	14.8	43.4	19.5	14.2	38.7	18.6	14.3

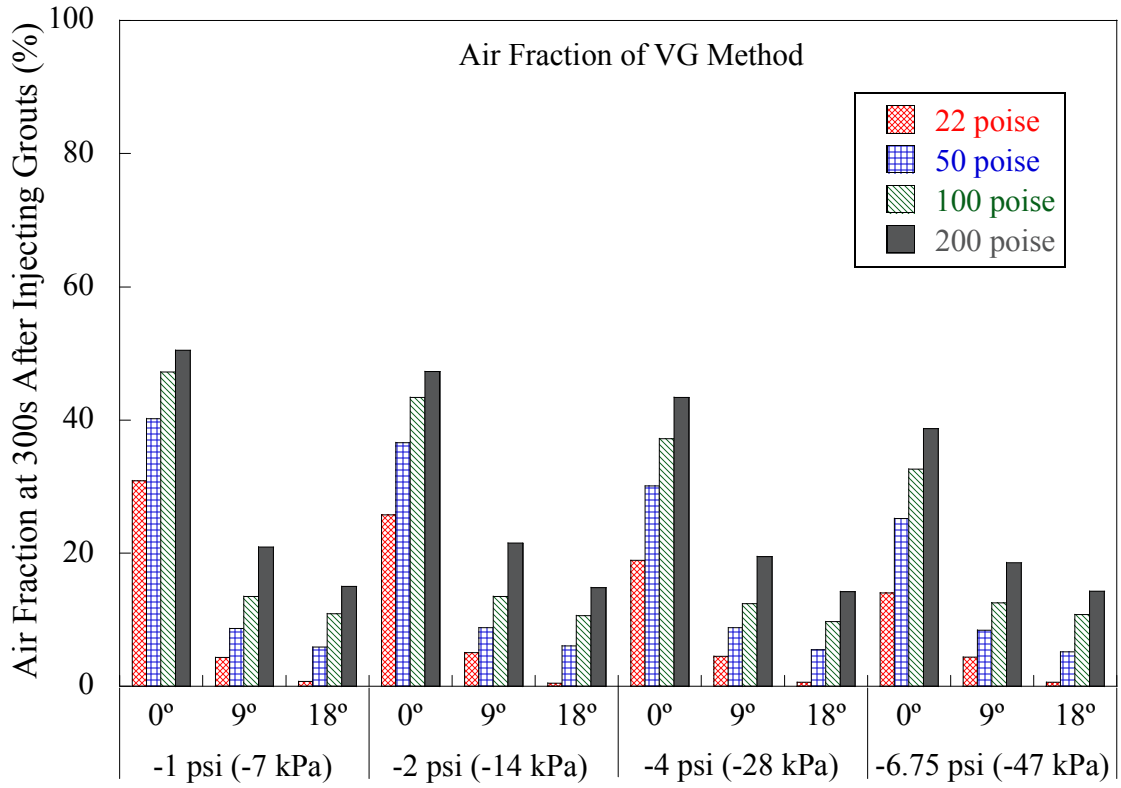

Figure 5-28. Air Fraction at 300 Seconds after Injecting Grouts for VG Method.

Table 5-5. Air Fraction at 300 Seconds after Injecting Grouts for PG Method.

t=300 s		Air Fraction of PG Method (%)								
Pressurizing		25 psi (172 kPa)			50 psi (345 kPa)			75 psi (517 kPa)		
Inclined Angle		0˚	9˚	18˚	0˚	9˚	18˚	0˚	9˚	18˚
Visc-osity (poise)	22	9.9	3.9	0.3	7.6	2.6	0.4	5.2	2.0	0.2
	50	14.2	7.7	5.0	10.2	6.3	4.0	8.7	5.4	3.5
	100	16.4	12.7	9.0	14.4	11.0	8.8	11.3	9.8	7.8
	200	24.4	14.7	14.1	19.9	14.3	14.1	14.9	14.2	13.5

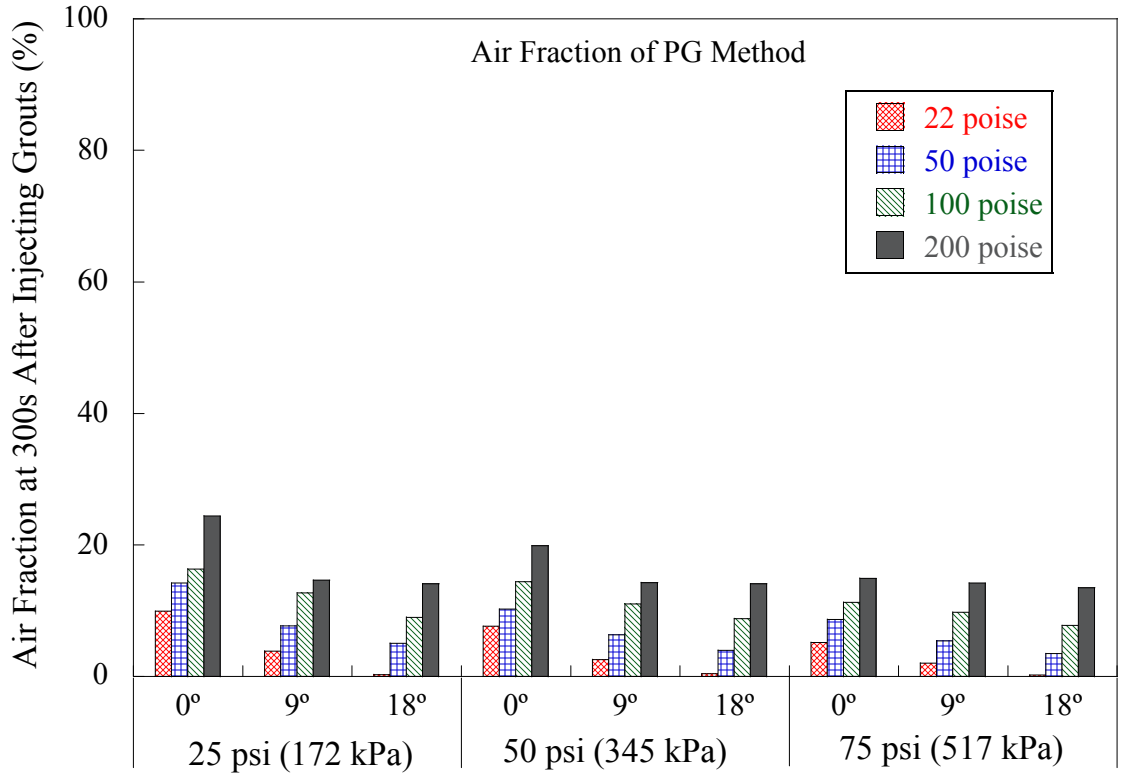

Figure 5-29. Air Fraction at 300 Seconds after Injecting Grouts for PG Method.

Table 5-6. Air Fraction at 300 Seconds after Injecting Grouts for PVG Method.

t=300 s		Air Fraction of PVG Method (%)								
Pressurizing		25 psi (172 kPa)			50 psi (345 kPa)			75 psi (517 kPa)		
Inclined Angle		0˚	9˚	18˚	0˚	9˚	18˚	0˚	9˚	18˚
Visc-osity (poise)	22	8.9	3.7	0.3	6.3	2.2	0.3	4.6	1.9	0.2
	50	11.8	7.2	4.9	9.5	5.6	3.5	7.9	4.3	3.0
	100	16.1	12.4	9.6	12.5	10.4	8.2	10.9	9.0	7.6
	200	22.8	14.6	13.7	16.0	14.0	13.2	14.7	13.1	13.3

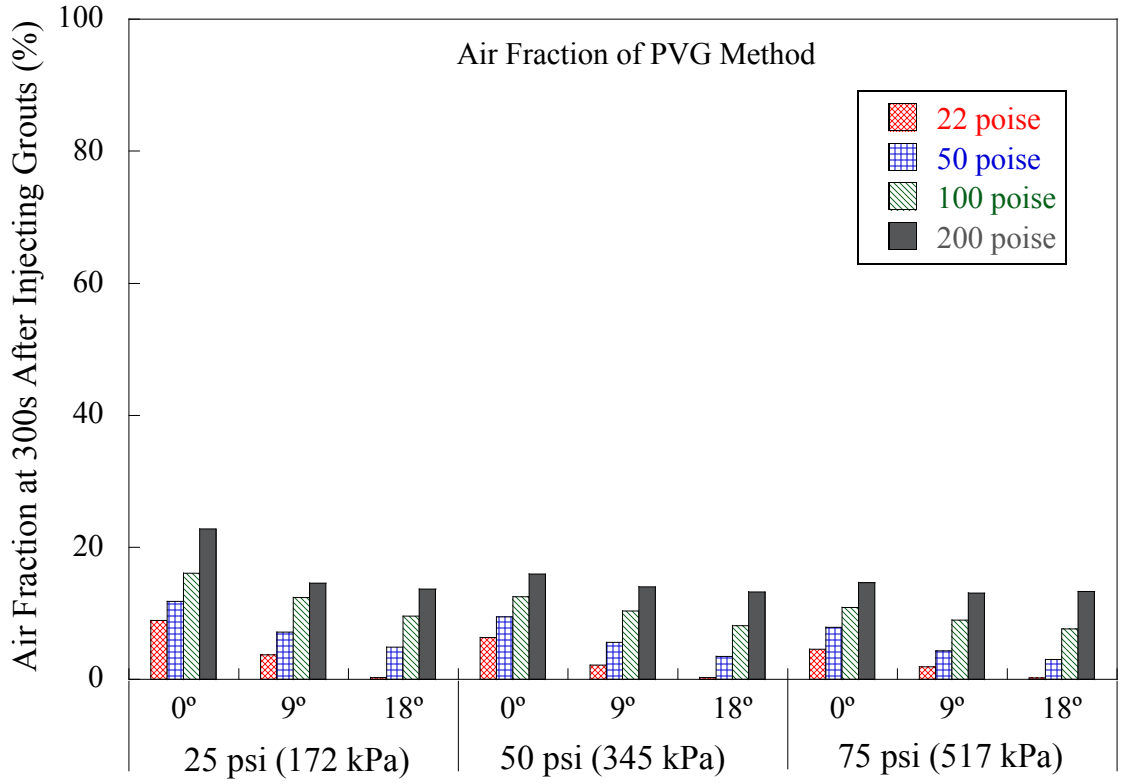

Figure 5-30. Air Fraction at 300 Seconds after Injecting Grouts for PG Method.

The results show that the vacuum pressure does not affect FC when using models with inclined angles (9˚ and 18˚). For 9-degree inclined ducts in the VG method, the air fractions at 300 seconds are 4.3, 5.0, 4.5, and 4.4 % with respect to different vacuum pressures (Table 5-4). It seems that the inclined angles have a larger affect on filling

voids than the vacuum in the VG method. Figure 5-31 shows the FCs of the inclined models for different vacuum pressures, and it shows that vaccum pressurizing does not have influence on filling voids in the inclined ducts.

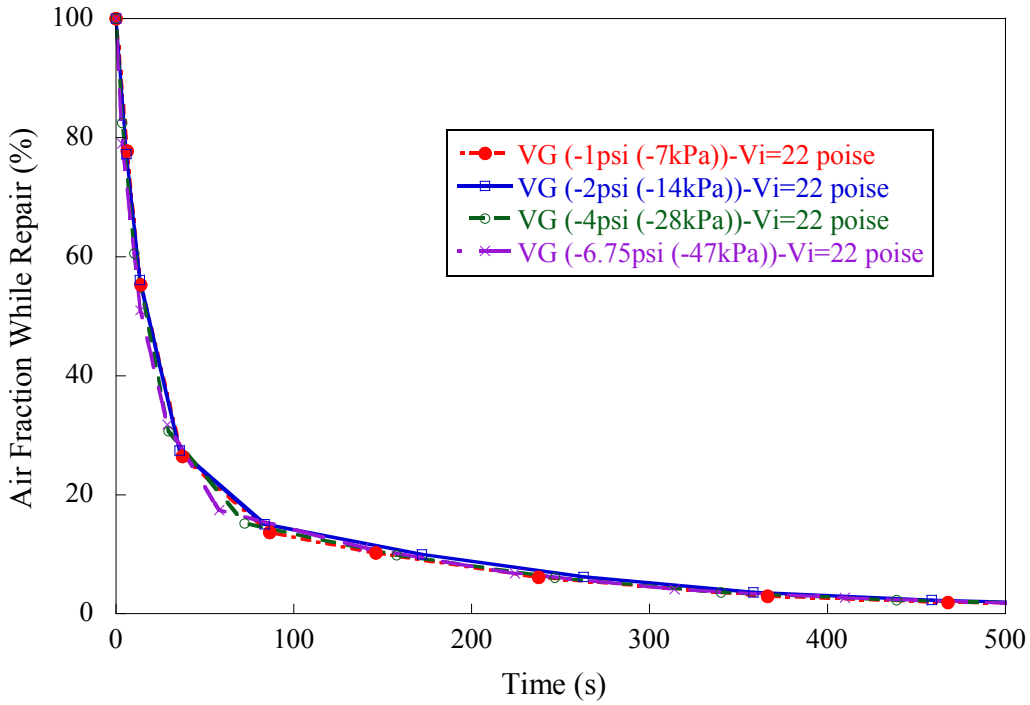

Figure 5-31. Effect of Vacuum Pressure in VG Method for 9 Degree Inclined Voided Ducts.

On the other hand, the vacuum pressure significantly affects the FC of the VG method when being applied to the 0˚ inclined angle (horizontal) ducts. Figure 5-32 shows filling voided ducts while repairing for horizontal ducts. Therefore, loss of vacuum pressurizing due to leaking of ducts may critically reduce the FC in horizontal voided ducts.

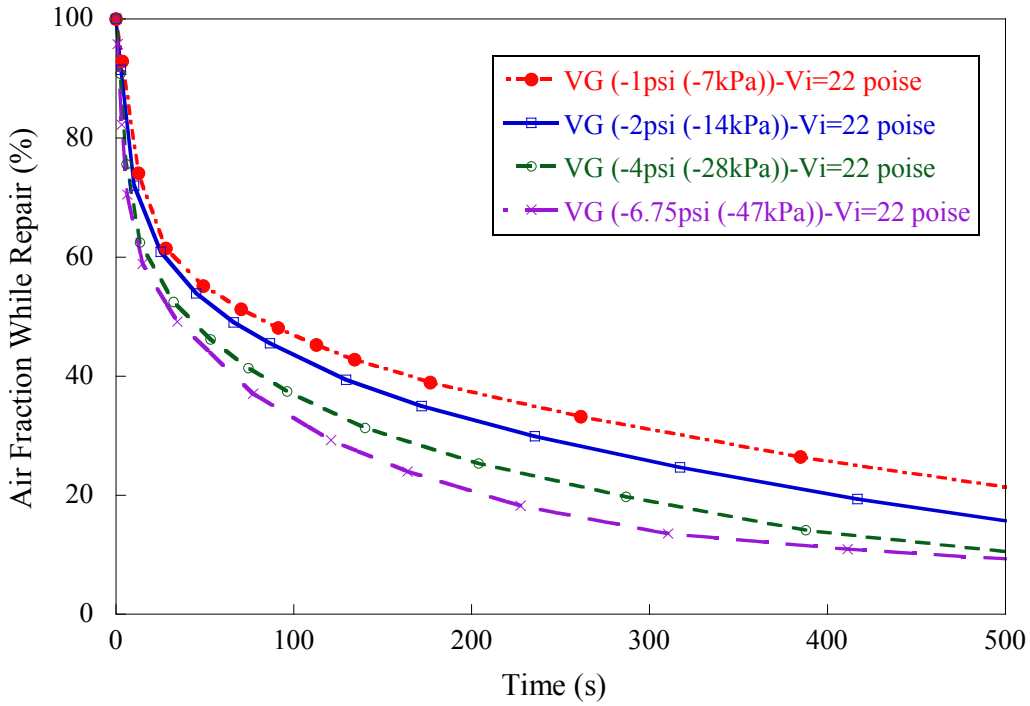

Figure 5-32. Effect of Vacuum Pressure in VG Method for Horizontal Voided Ducts.

The results also show that the viscosity of grouts has a significant impact on the FC of the VG method while the higher pressure in the PG and PVG methods can reduce the effects of the higher viscosity. From the -6.75 psi (-47 kPa) pressure case for horizontal ducts in the VG method, the difference of air fraction for grout with a viscosity of 22 and 200 poise is 24.7% while the PVG method has 10.1% at 75 psi (517 kPa) (Table 5-4 and Table 5-6). Thus, the VG method should be used with grouts having lower viscosity. Even using lower viscosity materials (22 poise), however, the air fraction in the voided ducts is still high in the 0˚ inclined angle ducts. Therefore, the VG method may be ineffective for repairing voids inside ducts in the field.

From the results, the FC of the PG and PVG methods is similar. The PG and PVG methods with higher pressures (75 psi, 517 kPa) and lower viscosity materials (22 poise) show better FC in this analysis. For the PG method with horizontal ducts, the difference in air fractions between the grout with 22 and 200 poise is 14.5% at 25 psi

(172 kPa) pressurizing case while the 75 psi (517 kPa) pressurizing case has 9.7% (Table 5-5). Thus, the higher pressures in both methods slightly reduce the effect of viscosity when using the 0˚ inclined angle ducts. Unlike the VG method, the inclined angle in the PG and PVG methods does not have a significant impact on filling voids inside the duct. For the PVG method using a grout with a viscosity of 22 poise, the air fractions of 9-degree inclined ducts are 3.7, 2.2, and 1.9% with respect to different pressures; that indicates that the pressures in the PVG method is still effective for filling voids in the inclined angle (Table 5-6). Figure 5-33 exhibits FCs of inclined models for different pressures of the PVG method, and it shows that higher pressurizes slightly improve the FCs of repair grouts.

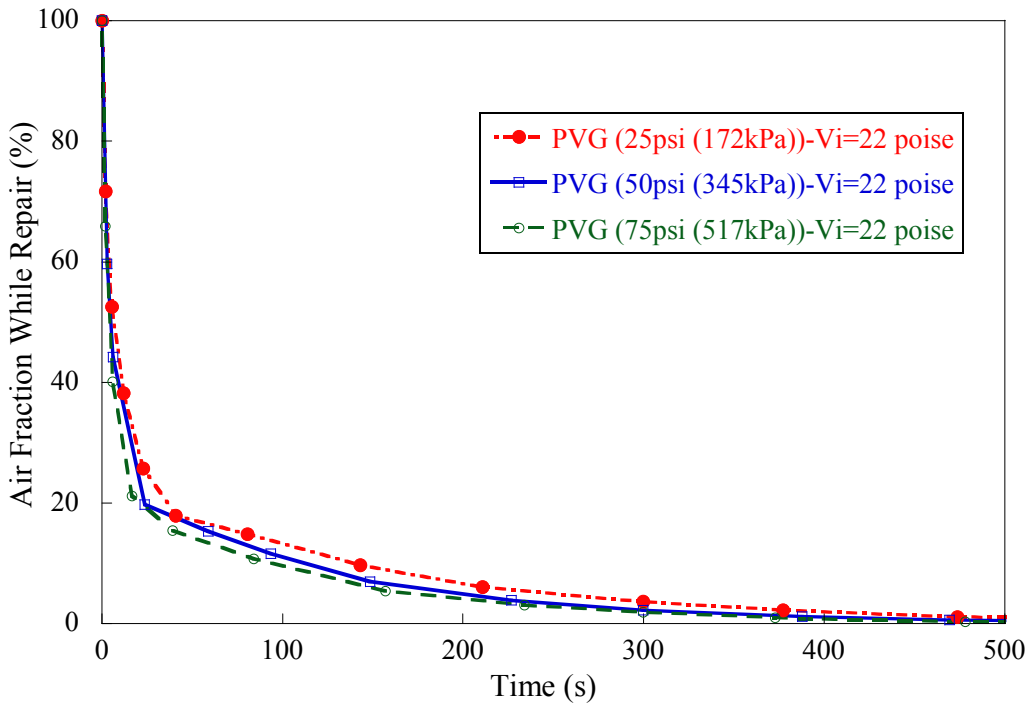

Figure 5-33. Effect of Pressurizing in PVG Method for 9 Degree Inclined Voided Ducts.

In addition, the pressures in PVG method does not significantly affect the FC of repair grouts while the vacuum pressures in VG method has great influence on filling voids when being applied to the 0˚ inclined angle (horizontal) ducts. Figure 5-34 exhibits

filling voided ducts while repairing for horizontal ducts. Therefore, the PVG method is effective to apply in the field because possible loss of pressures in the field does not significantly affect the FC in horizontal voided ducts.

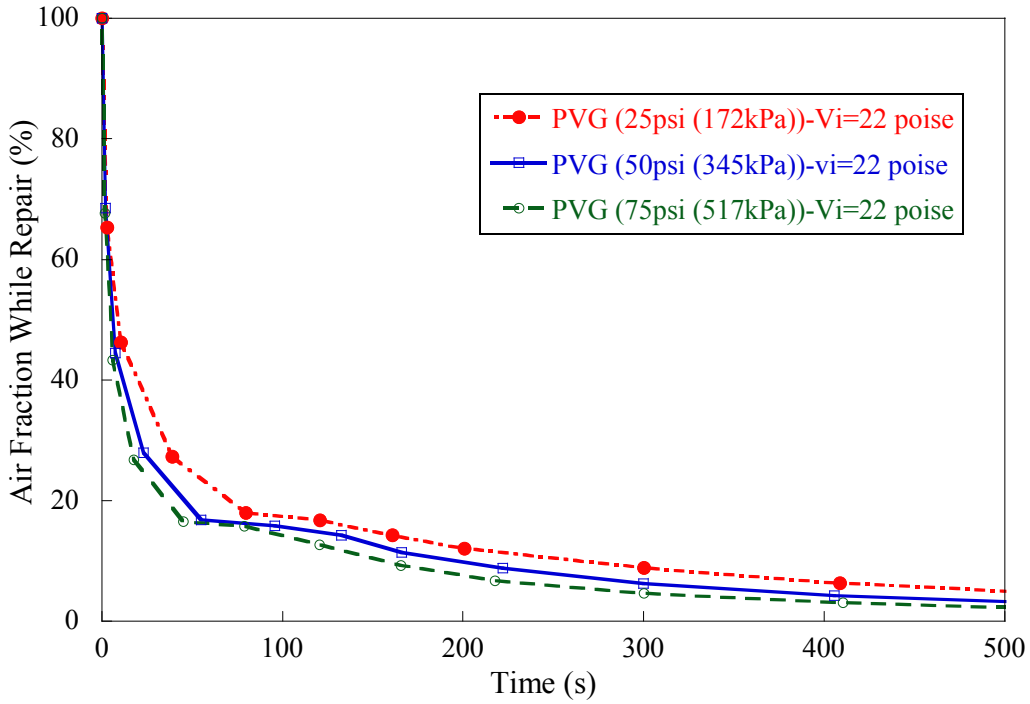

Figure 5-34. Effect of Pressurizing in PVG Method for Horizontal Voided Ducts.

For all cases in this analysis, the PVG and PG methods show significantly better FC than the VG method. However, the PG method needs more attention for applying in the field because an application of the PG method without ensuring an air outlet may critically reduce the filling voided ducts. Based on the numerical analysis, therefore, the PVG method is recommended for filling voids in the field.

6. CONCLUSIONS, RECOMMENDATIONS, AND FUTURE RESEARCH

Recent investigations of PT bridges have uncovered problems related to tendon failure due to excessive corrosion. The failure of an individual tendon due to corrosion means that other tendons will have to resist additional loads which may lead to failure of the tendons or structural failure. PT structures are designed with the intention of having at least a significant portion of the post-tensioning force in place throughout its design life. Thus, the loss of tendons may cause total failure of PT structures. Even if the consequences of a PT tendon are not catastrophic, they still involve costly repairs and could affect the bridge's safety and performance. Thus, it is extremely critical to protect tendons using an appropriate repair method from deterioration caused by corrosion. For grout repair applications, the recommended repair method is the vacuum grouting method. This method requires an air-tight tendon which can be extremely difficult to achieve in the field. In this research, tests on an external PT tendon system were conducted to assess applicable NDT methods for inspecting voids inside external tendon systems, and repair methods for filling voids in ducts.

Sounding inspections are commonly used to inspect voided ducts in the field. This inspection method is appropriate for employing in the field because it can be applied without a power supply and is simple to perform. While most non-destructive inspection methods are sensitive to ambient vibrations resulting from wind and traffic, the sounding inspection is not affected by these field conditions. This research evaluated the effectiveness of the sounding inspection method using a tendon system with transparent ducts. Voided areas were identified using soundings and were compared with visual measurements at the void conditions. Although the voids identified with the sounding inspection were not identical to the voids found with the visual inspection, statistical analysis shows that both inspections are highly correlated. The analysis results show that the sounding inspection method underestimates the size of the voids; however, the inspected locations have a close correlation with actual voids in ducts. Thus, the

sounding inspection method can be applied as an effective inspection tool in the field to assess void volume. However, this approach may not be cost effective for performing inspections of large bridges.

This research also provides an alternative way of estimating the repair volume required in voided ducts using a sounding inspection. Although the currently used volumeter can estimate the void volume in ducts accurately, significant preparation may be needed for sealing ducts to ensure accurate estimates of the entire duct volume. Thus, this research estimates the relationship between void profiles through visual inspections and the volume of repair grout in ducts. The repair grout volume was assessed using cut section analysis. Through discovered relationships between sounding and visual inspections, the void profile found by a sounding inspection can provide the approximate required volume of repair grouting.

The proposed repair grouting methods− pressure grouting (PG), pressure-vacuum grouting (PVG), and vacuum grouting (VG) − were evaluated with respect to their filling capabilities, filling performance, and economic feasibility. To estimate the filling capabilities of these repair methods, the infiltration length and minimum repaired area in cut sections were estimated. Although the different grouting repair methods did not show significant differences in their filling capability at a 95 percent confidence limit, the PG method seems to have a lower filling capability than the VG and PVG methods. To evaluate the filling performance, the void ratio of repair grouts was estimated using cut sections; however, no significant differences were identified between the different grouting methods.

Preparation time and scheduling for each repair grouting method have been estimated to evaluate the economic feasibility of each method. The analysis contained in this dissertation concludes that the VG method requires more sealing time than the PG and PVG methods. Thus, the PG and PVG methods are more economical methods for repairing voids than the VG method. Because the PG method exhibited lower filling capability and the VG method requires extensive preparation time, the PVG method is

recommended for filling voids. Note that this method should only be used if it is determined that galvanic cells do not form at existing-new grout interfaces.

The mock-up test for filling voids in ducts was fabricated and commercially available pre-packaged grouts were assessed. The three grouts, identified as C-1, C-2, and C-3, were assessed in this research. The filling capability of repair grouts was evaluated by using the infiltration length and the minimum repaired area in cut sections. The C-3 grout shows a significantly lower filling capability for infiltration length than the C-1 and C-2 grouts. For assessment of the minimum repaired area in cut sections, the different grouts do not have a significant difference at a 95% confidence limit; however, the C-3 grout seems to again have lower filling capability than the others. The statistical analysis for the filling performance has been assessed using a 95% confidence limit, and there is no significant difference among repair grouts. However, the C-3 grout shows a slightly higher ratio of voids in cut sections. In addition, the C-3 grout requires more mixing time than the other grouts, which could increase to cost and time. Therefore, the C-1 and C-2 grouts are recommended for repairing voided ducts because of their better filling capabilities and performance. The C-1 and C-2 grouts are also more appropriate grouts for application in the field because of their decreased required mixing time.

For these grouts, the effect of viscosity and particle size are compared with the results of infiltration length to identify a better grout for repair. Based on the experiments for repair grouting and material tests obtained from Kataria (2008), the effect of viscosity and particle size were assessed. The effect of material characteristics for filling voids was assessed using results from the flow cone tests. The results show that higher viscosity and larger particle size critically reduce the filling capability of voids. Thus, a grout having lower viscosity and smaller particle sizes is recommended for filling voided ducts.

A numerical analysis using FLUENT, a commercial Computational Fluid Dynamics (CFD) program, was conducted to assess three repair grouting methods. In this research, the simplified model reflecting voided ducts was designed and its

applicability with experimental results was verified. Although the numerical analysis may have some errors while simulating geometric conditions, the results showed similar trends with experimental results. Also, the effects of various parameters in repair grouting methods were assessed. From the analysis results, the PG and PVG methods exhibited better filling capabilities than the VG method, but the PG method is not recommended for the field because blocked voids in the middle of void profiles can rapidly generate a built-up pressure inside the tendons and significantly reduce the filling of voids. However, the PVG method may not be influenced by the blocked voids because the pre-applied vacuum inside the tendons can create negative pressure and reduce the built-up pressure by pressurizing. Thus, the results conclude that the PVG method with grouts having lower dynamic viscosity values is better for repairing voids.

In summary, this research recommends that the PVG method is the most effective method for filling voids in PT tendons. A sounding inspection can assess void locations in ducts. Also, it can provide the information of the required volume of repair grout material although it may not be appropriate for a small box-girder bridge. It should be noted that grouting of voided tendons was not performed in the field as part of this research because of potential issues with accelerated corrosion at the existing-repair-grout interface. Until this issue can be resolved, repairing with grouts should not be performed.

Future research should be conducted to simulate a real duct condition and to consider the effect of particle size of repair grouts.

REFERENCES

Armaly, B. F., Durst, F., Pereira, J. C. F., and Schonung, B. (1983) “Experimental and Theoretical Investigation of Backward-facing Step Flow”, *Journal of Fluid Mechanics*, 127, 473-496.

ASBI. (2000). “American Segmental Bridge Institute Grouting Committee: Interim Statement on Grouting Practices.” American Segmental Bridge Institute (ASBI), Phoenix, AZ.

Banerjee, R., Isaac, K. M., Oliver, L., and Breig, W. (2002) "Features of Automotive Gas Tank Filler Pipe Two-phase Flow: Experiments and Computational Fluid Dynamics Simulations", *Jounal of Engineering for Gas Turbines and Power*, 124, 412-420.

Banerjee, R. and Isaac, K. M. (2006) "A Study to Determine Vapor Generation from the Surface of Gasoline Flowing in an Inclined Channel Using a Continuous Thermodynamics Approach", *Numerical Heat Transfer, Part A*, 50, 705-729.

Barriere, T., Gelin, J. C., and Liu, B. (2002) “Improving Mould Design and Injection Parameters in Metal Injection Moulding by Accurate 3D Finite Element Simulation”, *Journal of Materials Processing Technology*, 125-126, 518-524.

Blitz, J. and G. Simpson (1996). *Ultrasonic Methods of Non-destructive Testing*, Chapman and Hall, London.

Blum, F. (2003). "A Focused, Two Dimensional, Air-coupled Ultrasonic Array for Non-Contact Generation," MS Thesis, Georgia Institute of Technology, Atlanta, GA.

Broyer, E., Gutfinger, C., and Tadmor, Z. (1975a) “Evaluating Flows of Non-Newtonian Fluids by the Method of Equivalent Newtonian Viscosity”, *AIChE Journal*, 21(1), 198-200.

Broyer, E., Gutfinger, C., and Tadmor, Z., (1975b) “A Theoretical Model for the Cavity Filling Progress in Injection Molding”, *Transactions of the Society of Rheology*, 19(3), 423-444.

Cao, W., Shen, C., and Wang, R. (2005) “3D Flow Simulation for Viscous Nonisothermal Incompressible Fluid in Injection Molding”, *Polymer Plastics Technology and Engineering*, 44, 901-917.

Carino, N. J., and Sansalone, M. (1990) "Impact-echo: A New Method for Inspecting Construction Materials." *Proc., Conference on NDT&E for Manufacturing and Construction*, Urbana, IL, 209-223.

Carino, N. J., and Sansalone, M. (1992). "Detection of Voids in Grouted Ducts Using the Impact-echo Method." *ACI Material Journal*, 89(3), 296-303.

Courbebaisse, G. (2005) “Numerical Simulation of Injection Moulding Process and the Pre-modelling Concept”, *Computational Materials Science*, 34, 397-405.

Cruise, J. F., Sherif, M. M., and Singh, V. P. (2007). *Elementary Hydraulics*, Nelson Education, Toronto, Ontario.

Della Vedova, M., and Elsener, B. (2006) "Enhanced Durability, Quality Control and Monitoring of Electrically Isolated Tendons." *Proc. of the 2nd FIB International Congress*, Naples, Italy, 1-12.

Ekambara, K., Sanders, R. S., Nandakumar, K., and Masliyah, J. H. (2008) “CFD Simulation of Bubbly Two-phase Flow in Horizontal Pipes”, *Chemical Engineering Journal*, 144, 277-288.

Elsener, B. (2004) "Experience with Electrically Isolated Tendons in Switzerland." *Proc. of the first workshop of COST 534 on NDT Assessment and New Systems in Prestressed Concrete Structures*, Zurich, Switzerland, 89-97.

FDOT. (1999). "Corrosion Evaluation of Post-Tensioned Tendons on the Niles Channel Bridge." Florida Department of Transportation, Tallahassee, FL, USA.

FDOT. (2001a). "Mid-Bay Bridge Post-tensioning Evaluation – Final Report." Florida Department of Transportation, Corven Engineering, Inc., Tallahassee, FL.

FDOT. (2001b). "Sunshine Skyway Bridge Post-tensioned Tendons Investigation." Florida Department of Transportation, Parsons Brinckerhoff Quade and Douglas, Inc., , Tallahassee, FL.

FHWA. (2004). "Post-Tensioning Tendon Installation and Grouting Manual." Federal Highway Administration, Washington, DC.

FLUENT (2006a), “FLUENT 6.3 Documentation.” Ansys Inc., Lebanon, NH.

FLUENT (2006b). “Introductory FLUENT Notes.” Ansys Inc., (www.fluentusers.com).

Friedl, C. (1996) “Progress Towards True 3D CAE Analysis for Injection Molding”, *ANTEC, Conference Proc.*, 1, 731-735.

Ganz, H. R. (2001). "Evolution of Prestressing Systems." *Durability of Post-Tensioning Tendons*. *fib*-IABSE Technical Report, Bulletin 15, Convener, Belgium, 155-171.

Han, S., Costa, F. S., and Ray, S. R. (2000) "Integrated Flow Analysis During Filling and Post-filling Stage of Thermoset Molding", *Journal of Electronic Packaging*, 122(1), 20-27.

Hansen, B. (2007) "Tendon Failure Raises Questions about Grout in Posttensioned Bridges." *Forensic Engineering: Civil Engineering News*, 17-18.

Henrikson, C. F., Knudsen, A., Braestrup, M. W. (1998). "Cable Corrosion: Undetected?" *Concrete International* 20(10), 69-72.

Herman, G. T. (1980). *Image Reconstruction from Projections: The Fundamentals of Computerized Tomography.* Academic Press, New York.

Hieber, C. A. and Shen, S. F. (1980) "A Finite-element/Finite-difference Simulation of Injection-molding Filling Process" *Journal of Non-Newtonian Fluid Mechanics*, 7, 1-32.

Hope, B. B. and Ip, A. K. C. (1988). "Grout for Post-tensioning Ducts." *ACI Materials Journal* 85(4), 234-240.

Hurlebaus, S., Jacobs, L. J., and Jarzynski, J. (1998). "Laser Techniques to Characterize the Effect of Geometry on Acoustic Emission Signals." *Journal of Nondestructive Testing and Evaluation*, 14, 21-37.

Hwang, C. J. and Kwon, T. H. (2002) “A Full 3D Finite Element Analysis of the Powder Injection Molding Filling Process Including Slip Phenomena”, *Polymer Engineering and Science*, 42(1), 33-50.

Iyer, S., Schokker, A. J., and Sinha, S. K. (2003). "Ultrasonic C-Scan Imaging: Preliminary Evaluation for Corrosion and Void Detection in Posttensioned Tendons " *Transportation Research Record: Journal of the Transportation Research Board*, 1827, 44-52.

Iyer, S. R., Sinha, S. K., and Schokker, A. J. (2005). "Ultrasonic C-Scan Imaging of Post-tensioned Concrete Bridge Structures for Detection of Corrosion and Voids." *Computer-Aided Civil and Infrastructure Engineering*, 20(2), 79-94.

Jaworski, M. J. (2003) “Theoretical and Experimental Comparison of Mesh Types Used in CAE Injection Molding Simulation Software”, University of Massachusetts Lowell.

Kamal, M. R. and Kenig. S. (1972) "The Injection Modeling of Thermoplastics Part I: Theoretical Model." *Polymer Engineering and Science*, 12, 294-301.

Karaoğuz, M., Bilgütay, N., Akgül, T., and Popovics, S. (1998). "Defect Detection in Concrete Using Split Spectrum Processing." *IEEE Ultrasonics symposium*, 1, 843-846.

Kataria, S. (2008) “Assessment of grouts for constructability and durability of post-tensioned bridges.” Master Thesis, Texas A&M University, College Station, TX.

Kil, H.-G., Jarzynski, J., and Berthelot, Y. H. (1998). "Wave decomposition of the vibrations of a cylindrical shell with an automated scanning laser vibrometer." *Journal of the Acoustic Society of America*, 104(6), 3161-3168.

Kim, M. and Corapcioglu, M. Y. (2002) "Cel barrier formation in unsaturated porous media." *Journal of Contaminant Hydrology*, 56, 75-98

Kim, S. W. and Turng, L. S. (2004) "Developments of Three-dimensional Computer-aided Engineering Simulation for Injection Moulding", *Modelling and Simulation in Materials Science and Engineering*, 12, S151-S173.

Krause, H.-J., Wolf, W., Glaas, W., Zimmermann, E., Faley, M. I., Sawade, G., Neudert, G., Gampe, U., and Krieger, J. (2001). "SQUID System for Magnetic Inspection of Prestressed Tendons on Concrete Bridges." *Insight Nondestructive Testing and Condition Monitoring*, 43(7), 458-461.

Krause, M., Maierhofer, C., and Wiggenhauser, H. (1995) "Thickness Measurement of Concrete Elements Using Radar and Ultrasonic Impulse Echo Techniques." *Proc. International Conference on Structural Faults and Repair-95*, London, UK, 17-24.

Krueger, W. L. and Tadmor, Z. (1980) "Injection Modeling into a Rectangular Cavity with Insert." *Polymer Engineering and Science* 20, 426-431.

Kundu, T. (2000). "Chapter 12: Nondestructive Testing Techniques for Material Characterization." *Modeling in Geomechanics*, M. Zaman, G. Gioda, and J. Booker, eds., John Wiley & Sons, New York, 267-298.

Kundu, P. K. and Cohen, I. M. (2008) *Fluid Mechanics (4th edition)*, Academic Press, Elsevier, Boston.

Lima, R. C., Andrade, C. R., and Zaparoli, E. L. (2008) “Numerical Study of Three Recirculation Zones in the Unilateral Sudden Expansion Flow”, *International Communications in Heat and Mass Transfer*, 35, 1053-1060.

Martin, J., Broughton, K. J., Giannopolous, A., Hardy, M. S. A., and Forde, M. C. (2001). "Ultrasonic Tomography of Grouted Duct Post-Tensioned Reinforced Concrete Bridge Beams." *NDT&E International*, 34, 107-113.

Martínez, O., Akhnak, M., Ullate, L. G., and Espinosa, F. M. (2003). "A Small 2D Ultrasonic Array for NDT Application." *NDT&E International*, 36(1), 57-63.

Martz, H. E., Roberson, G. P., Skeate, M. F., Schneberk, D. J., and Azevedo, S. G. (1991). "Computerized Tomography Studies of Concrete Samples." *Nuclear Instruments and Methods in Physics Research Section B*, 58(2), 216-226.

Martz, H. E., Schneberk, D. J., Roberson, G. P., and Monteiro, P. J. M. (1993). "Computerized Tomography Analysis of Reinforced Concrete." *ACI Materials Journal*, 90(3), 259-264.

Mendelsohn, Y., and Wiener-Avnear, E. (2002). "Simulations of Circular 2D Phase-array Ultrasonic Imaging Transducers." *Ultrasonics*, 39(9), 657-666.

Montgomery, D. C., and Runger, G. C. (2007). *Applied Statistics and Probability for Engineers*, 4th Edition, John Wiley & Sons, Inc, New York.

NCHRP. (1998). "Durability of Precast Segmental Bridges." *Project 20-7/Task 92*, National Cooperative Highway Research Program (NCHRP): Transportation Research Board: National Research Council,, Washington DC.

Ndinisa, N. V., Wiley, D. E., and Fletcher, D. F. (2005) "Computational Fluid Dynamics Simulations of Taylor Bubbles in Tubular Membranes Model Validation and Application to Laminar Flow Systems", *Chemical Engineering Research and Design*, 83(A1), 40-49.

Nunn, R. E. and Fenner, R. T. (1977) “Flow and Heat Transfer in the Nozzle of an Injection Molding Machine”, *Polymer Engineering and Science*, 17(11), 811-818.

O’Neil, E. F. and M. Schupack (1997). “Steel Post-tensioning Tendon Behavior – up to 35-year Marine Exposure.” *ASCE Structures Congress – Proc.*, 324-328

Park, R. (1975). "Post-tensioned Tendons in Prestressed Concrete – to Grout or Not to Grout?" *New Zealand Engineering* 30(11), 315-319.

PCI (1997). "Chapter 3: Fabrication and Construction." PCI Bridge Design Manual., Prestressed Concrete Institute, Chicago, IL.

Pearson-Kirk, D. (2003) "The Performance of Post-tensioned Bridge." *Role of Concrete Bridges in Sustainable Development – Proc. of the International Symposium,* UK. 129-140.

Pessiki, S. P., and Carino, N. J. (1988). "Setting Time and Strength of Concrete Using the Impact-Echo Method." *ACI Materials Journal*, 85(5), 389-399.

Pichelin, E. and Coupez, T. (1998) “Finite Element Solution of the 3D Mold Filling Problem for Viscous Incompressible Fluid”, *Computer Methods in Applied Mechanics and Engineering*, 163, 359-371.

Pielstick, B. (2002). "Grouting of Segmental Posttensioned Bridges in America." *Transportation Research Record*, 1813(1), 235-241.

Pillai, R. G. (2009) "Electrochemical Characterization and Time-variant Structural Reliability Assessment of Post-tensioned, Segmental Concrete Bridges." Ph.D dissertation, Texas A&M University, College Station, TX.

PTI. (1998). "Acceptance Standard for Post-Tensioning Systems*."* Post-tensioning Institute, Phoenix, AZ.

Qian, T., Wei, S., Jiaping, L., and Changwen, M. (2004). "Performance of Grouts for Post-tensioned Prestressed Structures." *Journal of Southeast University*, 20(4), 492-497.

Ragab, A., Brandstaetter, W., and Shalaby, S. (2008) "Numerical Simulation of Slug Flow Phenomena in Horizontal and Inclined Pipelines", *Oil Gas European Magazine*, 34, 194-199.

Raiss, M. (1995). "Post-tensioned Concrete Bridges: The UK Debate." *Concrete International*, 29(2), 23-26.

Rajupalem, V., Talwar, K., and Friedl, C. (1997) "Three-dimensional Simulation of the Injection Molding Process", *ANTEC, Conference Proc.*, 1, 670-673.

Sampaio, P. A. B., Faccini, J. L. H., and Su, J. (2008) "Modelling of Stratified Gas-liquid Two-phase Flow in Horizontal Circular Pipes" *International Journal of Heat and Mass Transfer*, 51, 2752-2761.

Sansalone, M., and Carino, N. J. (1989). "Laboratory and Field Studies of the Impact-Echo Method for Flaw Detection in Concrete." *ACI Special Publication*, 112, 1-20.

Schickert, M. (1995) "Towards SAFT-Imaging in Ultrasonic Inspection of Concrete " *Proc. International Symposium of Non-destructive Testing in Civil Engineering (NDT-CE)*, 411-418.

Schokker, A. J., Breen, J. E., and Kreger, M. E. (2001). "Grouts for Bonded Post-Tensioning in Corrosive Environments." *ACI Materials Journal*, 98(4), 296-305.

Scruby, C. B., and Drain, L. E. (1990). *Laser Ultrasonics: Techniques and Applications*, Adam Hilger, New York.

Shao, N., Salman, W., Gavriilidis, A., and Angeli, P. (2008) "CFD Simulations of the Effect of Inlet Conditions on Taylor Flow Formation", *International Journal of Heat and Fluid Flow*, 29, 1603-1611.

Shoemaker, J. (2006) *Moldflow Design Guide – A Resource for Plastics Engineers*, Hanser Gardner, Cincinnati.

Shoji, N., Noritaka, S., Yasushi, K., and Koichiro, S. (2003). "Development of Repair Method for Poorly Grouting of PC Structures." *Concrete Journal*, 41(11), 31-43.

Smith, L. J., and Wood, R. (2001). "Grouting of External Tendons: A Practical Perspective." *Proc. of the Institution of Civil Engineers: Structures & Buildings*, 146(1), 93-100.

Sprinkel, M., and Napier, C. S. (2008) "VDOT Experience with Grouted Tendons in Varina-enon Precast Segmental Post-tensioned Bridge." *Virginia Concrete Conference* (http://virginiadot.org/business/resources/Materials/Virginia_Concrete_Presentations/5B-Sprinkel_Napier-Varina_Enon.pdf).

Stevenson, J. F. (1976) "An Experimental Study and Simulation of Disk Filling by Injection Molding", *ANTEC, Technical papers*, 22, 282-288.

Tadmor, Z., Broyer, E., and Gutfinger, C. (1974) "Flow Analysis Network (FAN) – A Method for Solving Flow Problems in Polymer Processing", *Polymer Engineering and Science*, 14, 660-665

Taha, T. and Cui, Z. F. (2002) "CFD Modelling of Gas-sparged Ultrafiltration in Tubular Membranes", *Journal of Membrane*, 210, 13-27.

Talwar, K., Costa, F., Rajupalem, V., Antanovski, L., and Friedl, C. (1998) "Three-dimensional Simulation of Plastic Injection Molding", *Conference Proc. at ANTEC '98*, 1, 562-566.

Tavakoli, R., Babaei, R., Varahram, N., and Davami, P. (2006) "Numerical Simulation of Liquid/Gas Phase Flow During Mold Filling", *Computer Methods in Applied Mechanics and Engineering*, 196, 697-713.

Tie, G., Dequn, L., and Huamin, Z. (2006) "Three-dimensional Finite Element Method for the Filling Simulation of Injection Molding", *Engineering with Computers*, 21, 289-295.

Tilly, G. P. (2002). "Performance and Management of Post-tensioned Structures." *Proc. of the Institution of Civil Engineers*, 152(1), 3-16.

Tinkey, Y. and Olson, L. D. (2007). "Sensitivity Studies of Grout Defects in Posttensioned Bridge Ducts Using Impact Echo Scanning Method." *Transportation Research Record: Journal of the Transportation Research Board* 2028, 154-162.

Tinkey, Y., Olson, L. D., and Wiggenhauser, W. (2005). "Impact Echo Scanning for Discontinuity Detection and Imaging in Posttensioned Concrete Bridges and Other Sturctures." *Materials Evaluation* 63(1), 64-69.

TxDOT. (1999). "Tex-437-A: Test for Flow of Grout Mixtures (Flow Cone Method)." Texas Department of Transportation, Austin, TX.

TxDOT. (2003). "Tex-441-A, Wick-induced Bleed Test of Freshly Mixed Grouts." Texas Department of Transportation, Austin, TX.

TxDOT (2004). "Critical Evaluation and Condition Assessment of Post-Tensioned Bridges in Texas." Texas Department of Transportation, Austin, TX.

TxDOT. (2006). "Tex-442-A, Determining Compressive Strength of Grouts." Texas Department of Transportation, Austin, TX.

VSL. (2002). "Grouting of Post - Tensioning Tendons." *Report Series 5*, VSL International Ltd., Lyssach/ Switzerland.

Wang, V. W., Heiber, C. A., and Wang, K. K. (1986) "Mold-filling –Simulation in Injection Molding of Three-dimensional Thin Parts", *ATEC – Society of Plastic Engineers*, 32, 97-102.

Warner, J. (2004). *Practical Handbook of Grouting*, John Wiley & Sons, Inc, Hoboken, NJ.

Woodward, R. J. and E. Miller (1990). "Grouting Post-tensioned Concrete Bridges: the Prevention of Voids." *Highways and Transportation* 37(6), 9-17.

Wu, J. L. (1989) “Evaluations of Computer Flow and Cooling Simulation Programs in Injection Molding: A Comprehensive Study of Moldflow, Moldtemp, and Cflow”, Ph.D dissertation of University of Lowell, Mass.

Wu. P., Huang, C. F., and Gogos, C. G. (1974) "Simulation of the Mold Filling Process." *Polymer Engineering and Science*, 14, 223-230.

Xiong, R., Bai, M., and Chung, J. N. (2007) "Formation of Bubbles in a Simple Co-flowing Micro-channel", *Journal of Micromechanics and Microengineering*, 17, 1002-1011.

Yeung, V. W. S. and Lau, K. H. (1997) “Injection Moulding, “C-MOLD” CAE Package, Process Parameter Design and Quality Function Deployment: A Case Study of Intelligent Materials Processing”, *Journal of Materials Processing Technology*, 63, 481-487.

APPENDICES

APPENDIX A

EXPERIMENTAL RESULTS OF REPAIR GROUTING

The experimental results of repair grouting for analysis are summarized in this appendix. First, void profiles mapped by a sounding and visual inspection are provided to evaluate the effectiveness of sounding technique for detecting voids in ducts. Also, the infiltration length of repair grout and results obtained from the cut sections are represented to compare FC and performance of different repair methods and grouts. Finally, the sealing time and schedule are recorded to assess economic feasibility of different repair methods.

A.1. SPECIMEN VG-C1-1

Figure A-1 depicts the initial void profiles of the sounding inspection and of the visual inspection before grouting.

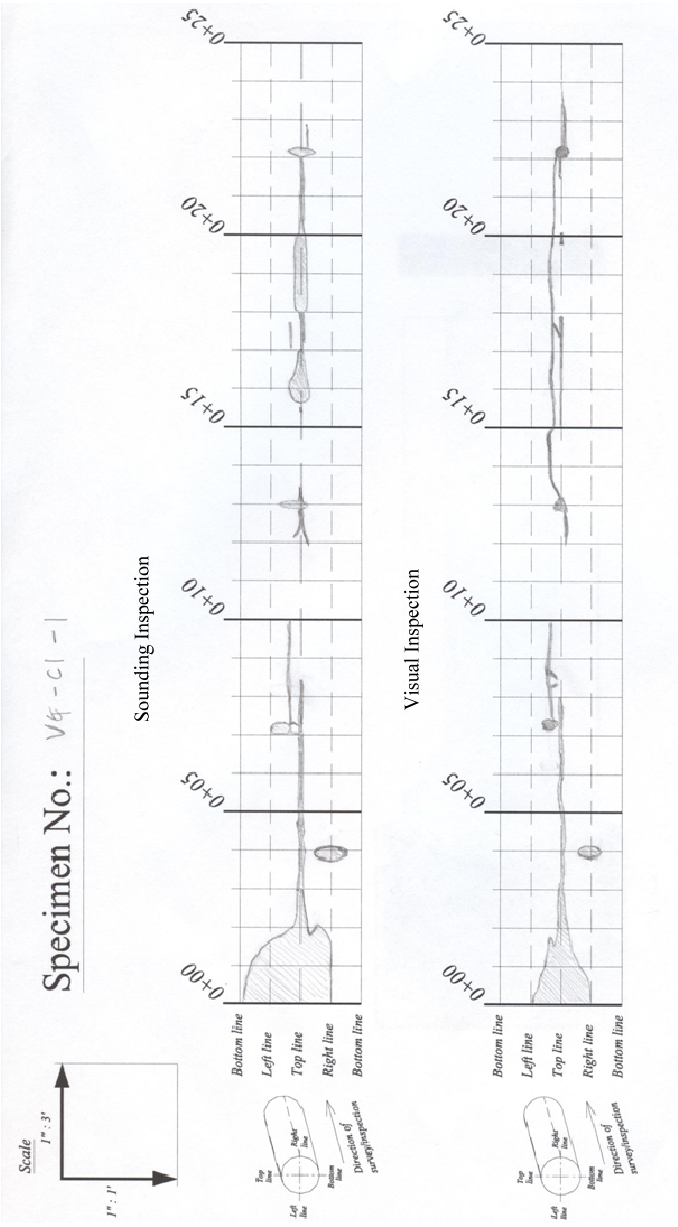

Figure A-1. Void Map of Specimen VG-C1-1.

The areas of both void profiles are estimated using AutoCAD® and provided in Table A-1.

Table A-1. Estimation of Void Profile in Specimen VG-C1-1.

Section, ft (m)	Sounding Inspection (SI), inch^2 (10^{-4} m^2)	Visual Inspection (VI), inch^2 (10^{-4} m^2)	SI - VI, inch^2 (10^{-4} m^2)
0~1 (0~0.3)	104.82 (676.2)	62.18 (401.2)	42.64 (275.1)
1~2 (0.3~0.6)	75.85 (489.3)	28.21 (182.0)	47.63 (307.3)
2~3 (0.6~0.9)	10.57 (68.2)	10.23 (66.0)	0.34 (2.2)
3~4 (0.9~1.2)	14.95 (96.5)	8.78 (56.7)	6.17 (39.8)
4~5 (1.2~1.5)	8.57 (55.3)	7.39 (47.7)	1.18 (7.6)
5~6 (1.5~1.8)	4.84 (31.2)	4.79 (30.9)	0.05 (0.3)
6~7 (1.8~2.1)	4.90 (31.6)	5.18 (33.4)	-0.28 (-1.8)
7~8 (2.1~2.4)	13.69 (88.3)	12.41 (80.1)	1.28 (8.3)
8~9 (2.4~2.7)	5.74 (37.0)	6.92 (44.6)	-1.18 (-7.6)
9~10 (2.7~3.0)	3.57 (23.1)	3.68 (23.8)	-0.11 (-0.7)
10~11 (3.0~3.4)	0.00 (0.0)	0.00 (0.0)	0.00 (0.0)
11~12 (3.4~3.7)	0.16 (1.0)	0.08 (0.5)	0.08 (0.5)
12~13 (3.7~4.0)	8.43 (54.4)	6.83 (44.0)	1.60 (10.3)
13~14 (4.0~4.3)	4.20 (27.1)	5.22 (33.7)	-1.03 (-6.6)
14~15 (4.3~4.6)	0.00 (0.0)	4.11 (26.5)	-4.11 (-26.5)
15~16 (4.6~4.9)	7.75 (50.0)	5.75 (37.1)	2.00 (12.9)
16~17 (4.9~5.2)	14.65 (94.5)	7.74 (50.0)	6.90 (44.5)
17~18 (5.2~5.5)	5.66 (36.5)	8.58 (55.4)	-2.92 (-18.8)
18~19 (5.5~5.8)	14.55 (93.9)	3.87 (25.0)	10.68 (68.9)
19~20 (5.8~6.1)	13.99 (90.3)	4.01 (25.9)	9.99 (64.4)
20~21 (6.1~6.4)	5.98 (38.6)	2.65 (17.1)	3.33 (21.5)
21~22 (6.4~6.7)	4.78 (30.9)	4.45 (28.7)	0.33 (2.1)
22~23 (6.7~7.0)	8.38 (54.1)	8.87 (57.2)	-0.48 (-3.1)
23~24 (7.0~7.3)	0.00 (0.0)	2.48 (16.0)	-2.48 (-16.0)

Repair grout is infiltrated from the top grout port and the main voids are filled successfully. The repair grout is infiltrated to 14.5 ft (4.42 m) from the reference point (Figure A-2).

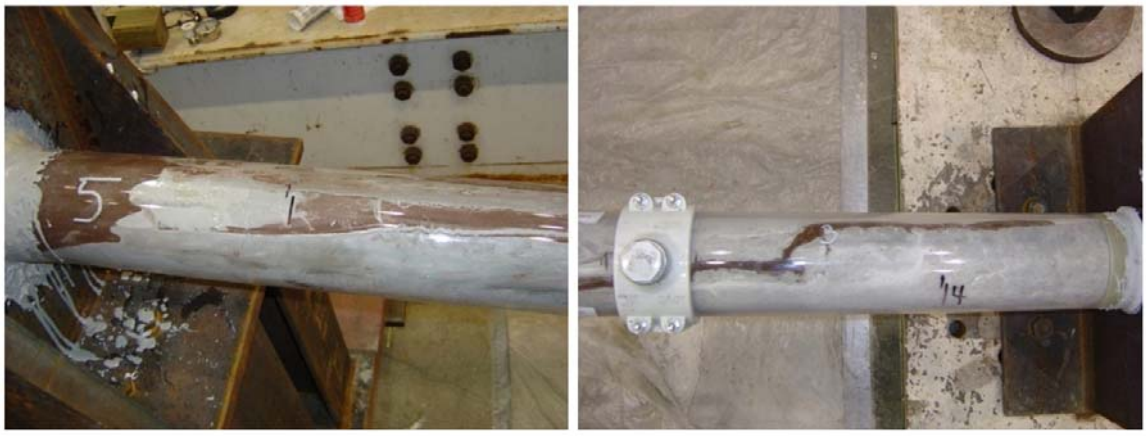

Figure A-2. Repair Grouted Ducts of Specimen VG-C1-1.

Figure A-3 shows the cross-sectional views of the cut sections obtained from Specimen VG-C1-1. For the Specimen VG-C1-1, a colorant is added in the repair grout. Through the preliminary test on Class C-1 grout, it is confirmed that the added colorant does not affect the fluidity of this grout. However, the colorant is added onward to the initial grout in order to minimize the effect in repair grouts.

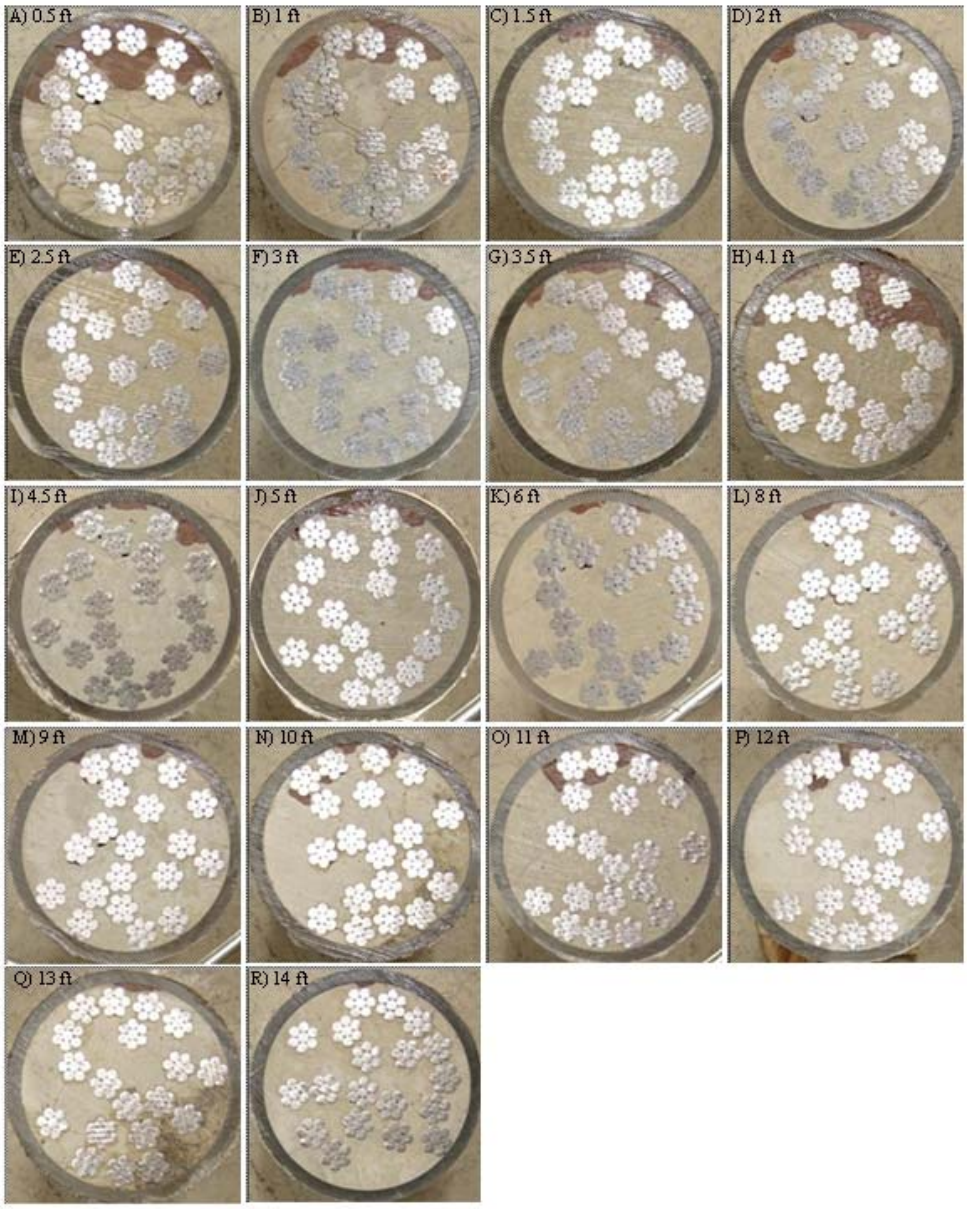

Figure A-3. Cut Sections of Specimen VG-C1-1 for the Filling Analysis of Repair Grout.

To compare the performance of repair grouts, the ratio of the remaining void area after repair to the repaired area is estimated. The repaired area and area of voids after repair are calculated using AutoCAD® (Table A-2)

Table A-2. Void Area of Specimen VG-C1-1.

Cut Sections, ft (m)		Repaired Area, A_R, inch^2(10^{-4} m^2)	Void Area, A_V, inch^2(10^{-4} m^2)	Void Ratio, η (%)
A	0.5 (0.15)	1.810 (12.20)	0.0031 (0.020)	0.17
B	1 (0.30)	0.797 (5.14)	0.0000 (0.000)	0.00
C	1.5 (0.46)	0.413 (2.67)	0.0000 (0.000)	0.00
D	2 (0.61)	0.339 (2.18)	0.0000 (0.000)	0.00
E	2.5 (0.76)	0.336 (2.17)	0.0010 (0.006)	0.30
F	3 (0.91)	0.402 (2.60)	0.0000 (0.000)	0.00
G	3.5 (1.07)	0.539 (3.48)	0.0012 (0.008)	0.22
H	4.1 (1.26)	1.200 (7.74)	0.0095 (0.061)	0.79
I	4.5 (1.37)	0.343 (2.21)	0.0052 (0.034)	1.52
J	5 (1.52)	0.350 (2.26)	0.0043 (0.028)	1.23
K	6 (1.83)	0.105 (0.68)	0.0022 (0.014)	2.10
L	8 (2.44)	0.113 (0.73)	0.0009 (0.006)	0.80
M	9 (2.74)	0.130 (0.84)	0.0020 (0.013)	1.54
N	10 (3.05)	0.187 (1.20)	0.0022 (0.014)	1.18
O	11 (3.35)	0.409 (2.64)	0.0060 (0.039)	1.47
P	12 (3.66)	0.212 (1.37)	0.0092 (0.059)	4.33
Q	13 (3.96)	0.091 (0.59)	0.0002 (0.001)	0.22
R	14 (4.27)	0.030 (0.19)	0.0000 (0.000)	0.00
Sum		**7.805 (50.36)**	**0.0470 (0.303)**	**0.60**

From the analysis, remaining voids in the repair grout are estimated in each cut section, but the void ratio in a section can be magnified when the remaining voids exist in a small repaired area. Thus, the filling performance for Specimen VG-C1-1 is evaluated using the summation of the estimated sections of Specimen VG-C1-1. The remaining void ratio after repair obtained from the analysis comes out to be 0.60% for Specimen VG-C1-1. The initial void area, the repaired area, as shown in Table A-2

ranges over 0.1 inch^2 (0.65×10^{-4} m^2) or more in Section P; however, these voids include small voids from Section Q.

The time analysis for repair preparation is not considered in Specimen VG-C1-1 and VG-C2-1 because both specimens required a significant amount of trial and error to find an appropriate way to seal the test specimens.

A.2. SPECIMEN VG-C2-1

Since Specimen VG-C2-1 is the first setup of its kind, a sufficient amount of grouts for initial grouting are mixed. The initial grouts are mixed separately in 2 batches using the air-powered grout mixer, and two high shear mixers are then used in the grout storage tank (Figure A-4) to ensure consistency between grouts mixed in two batches. The flow cone test (Method 1) is performed on both batches and the final batch according to the ASTM 939-02 (ASTM 2002) standard. The flow cone test for repair grouts is performed by Tex-437-A Method 2 (TxDOT 1999).

Figure A-4. Grout Storage Tank and High Shear Mixer.

The preparation for repair grouting in Specimen VG-C2-1 took a considerable of time (4 months) to construct since an air-tight PT system is required. While performing

sealing procedures a trial and error method is used in order to find a better sealing method.

Repair grout is infiltrated from the top grout port and the main voids are filled successfully. The repair grout is infiltrated to 13.4 ft (4.08 m) from the reference point (Figure A-5).

Figure A-5. Repair Grouted Ducts of Specimen VG-C2-1.

For the Specimen VG-C2-1, however, the colorant is not added in the initial grouting. Thus, the performance of repaired grout is not considered because the difference between initial grouts and repair grouts is difficult to identify.

A.3. SPECIMEN VG-C2-2

Figure A-6 depicts the initial void profiles of the sounding inspection and of the visual inspection before grouting for Specimen VG-C2-2.

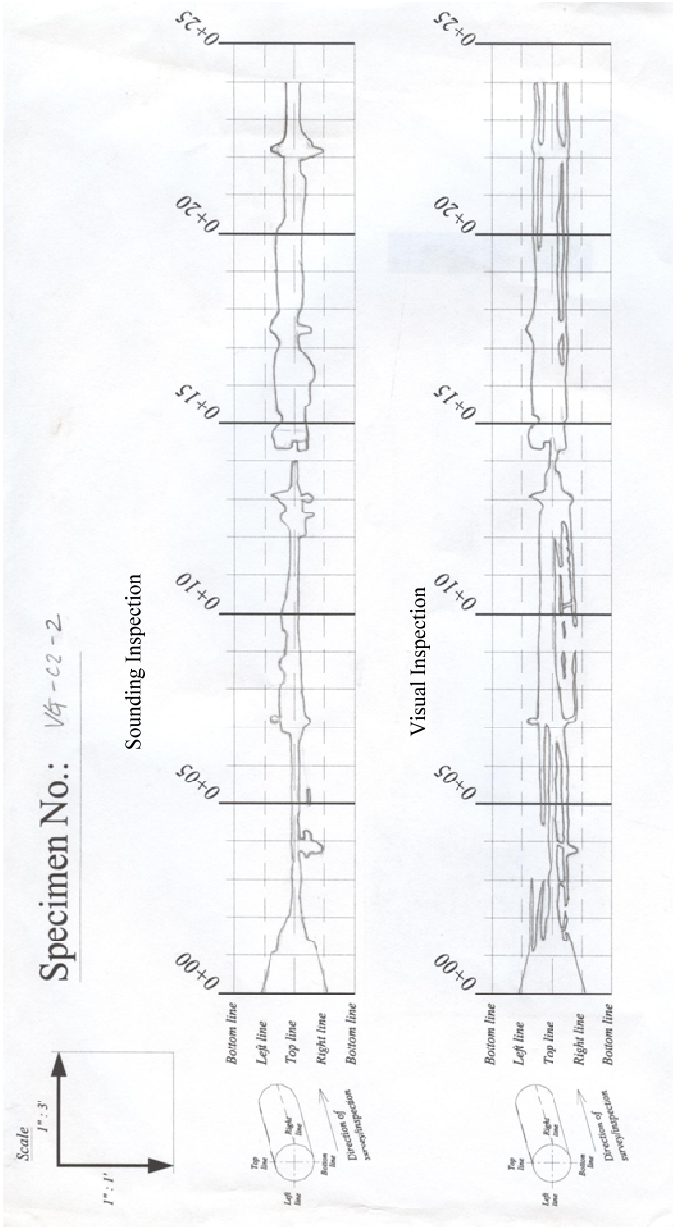

Figure A-6. Void Map of Specimen VG-C2-2.

The areas of both void profiles are estimated using AutoCAD® and provided in Table A-3.

Table A-3. Estimation of Void Profile in Specimen VG-C2-2.

Section, ft (m)	Sounding Inspection (SI), inch^2 (10^{-4} m^2)	Visual Inspection (VI), inch^2 (10^{-4} m^2)	SI - VI, inch^2 (10^{-4} m^2)
0~1 (0~0.3)	71.62 (462.1)	70.70 (456.2)	0.92 (5.9)
1~2 (0.3~0.6)	36.38 (234.7)	41.36 (266.8)	-4.98 (-32.1)
2~3 (0.6~0.9)	11.42 (73.7)	23.31 (150.4)	-11.89 (-76.7)
3~4 (0.9~1.2)	18.78 (121.2)	19.57 (126.3)	-0.79 (-5.1)
4~5 (1.2~1.5)	11.57 (74.6)	19.32 (124.7)	-7.76 (-50.0)
5~6 (1.5~1.8)	10.18 (65.7)	23.65 (152.6)	-13.46 (-86.9)
6~7 (1.8~2.1)	12.82 (82.7)	25.15 (162.3)	-12.34 (-79.6)
7~8 (2.1~2.4)	32.29 (208.3)	35.75 (230.7)	-3.46 (-22.4)
8~9 (2.4~2.7)	22.93 (147.9)	27.95 (180.3)	-5.02 (-32.4)
9~10 (2.7~3.0)	18.37 (118.5)	23.42 (151.1)	-5.05 (-32.6)
10~11 (3.0~3.4)	15.50 (100.0)	27.47 (177.2)	-11.97 (-77.2)
11~12 (3.4~3.7)	10.91 (70.4)	29.18 (188.2)	-18.27 (-117.9)
12~13 (3.7~4.0)	26.19 (168.9)	36.43 (235.0)	-10.24 (-66.1)
13~14 (4.0~4.3)	14.99 (96.7)	23.19 (149.6)	-8.19 (-52.9)
14~15 (4.3~4.6)	25.95 (167.4)	31.44 (202.8)	-5.49 (-35.4)
15~16 (4.6~4.9)	36.98 (238.6)	41.41 (267.1)	-4.43 (-28.6)
16~17 (4.9~5.2)	42.95 (277.1)	41.01 (264.6)	1.94 (12.5)
17~18 (5.2~5.5)	31.90 (205.8)	42.94 (277.1)	-11.04 (-71.2)
18~19 (5.5~5.8)	30.81 (198.8)	34.25 (221.0)	-3.45 (-22.2)
19~20 (5.8~6.1)	31.27 (201.8)	33.64 (217.1)	-2.37 (-15.3)
20~21 (6.1~6.4)	24.78 (159.9)	34.04 (219.6)	-9.26 (-59.7)
21~22 (6.4~6.7)	23.84 (153.8)	37.16 (239.8)	-13.32 (-86.0)
22~23 (6.7~7.0)	34.29 (221.2)	36.01 (232.4)	-1.72 (-11.1)
23~24 (7.0~7.3)	16.55 (106.8)	25.56 (164.9)	-9.01 (-58.1)

The repair grout is filled from the top grout port and infiltrated to 14.4 ft (4.39 m) from the reference point (Figure A-7).

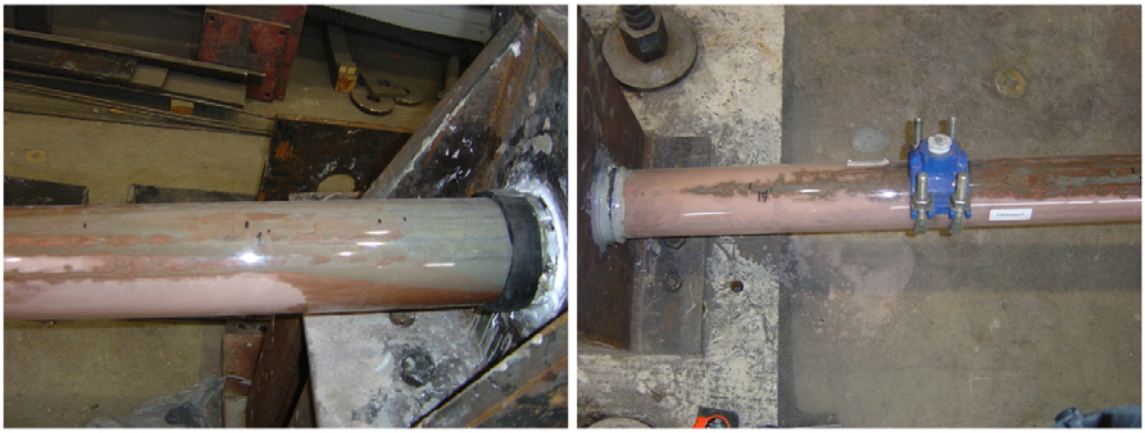

Figure A-7. Repair Grouted Ducts of Specimen VG-C2-2.

Figure A-8 shows the cross-sectional views of the cut sections obtained from Specimen VG-C2-2. From the cut sections, it is noted that the repair grouts successfully replaces the main voids and repairs local large voids #3, #4, and #5. The small voids still exist inside the initially grouted ducts, especially in-between strands.

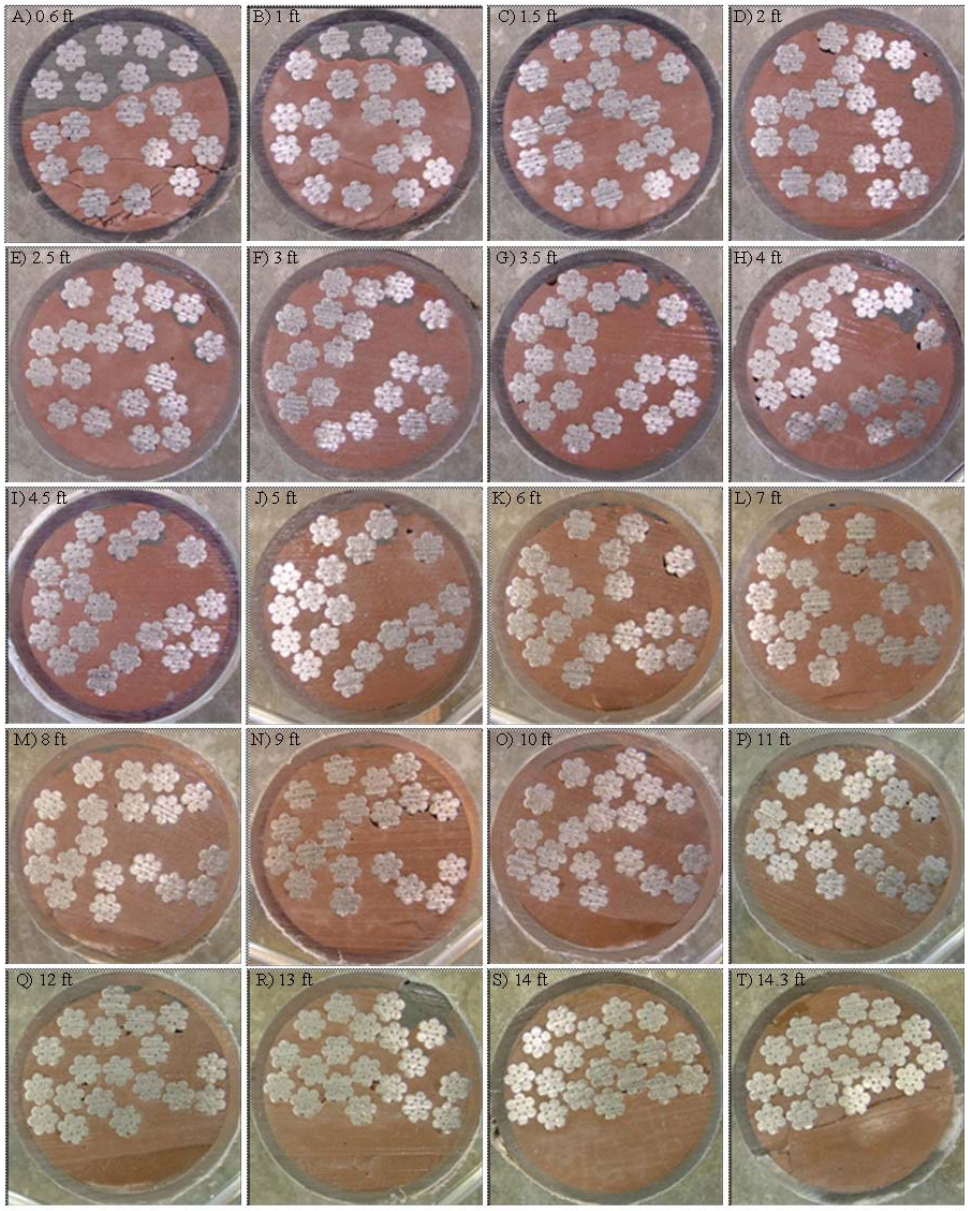

Figure A-8. Cut Sections of VG-C2-2 for the Filling Analysis of Repair Grout.

To compare the performance of repair grouts, the ratio of the remaining void area after repair to the repaired area is estimated. The repaired area and area of voids after repair are calculated using AutoCAD® (Table A-4).

Table A-4. Void Area of Specimen VG-C2-2.

Cut Sections, ft (m)		Repaired Area, A_R, inch^2(10^{-4} m^2)	Void Area, A_V, inch^2(10^{-4} m^2)	Void Ratio, η (%)
A	0.6 (0.18)	2.365 (15.26)	0.0134 (0.086)	0.57
B	1 (0.30)	0.952 (6.14)	0.0044 (0.028)	0.46
C	1.5 (0.46)	0.337 (2.17)	0.0000 (0.000)	0.00
D	2 (0.61)	0.325 (2.09)	0.0000 (0.000)	0.00
E	2.5 (0.76)	0.380 (2.45)	0.0089 (0.057)	2.34
F	3 (0.91)	0.278 (1.79)	0.0013 (0.008)	0.47
G	3.5 (1.07)	0.325 (2.10)	0.0055 (0.035)	1.69
H	4 (1.22)	0.542 (3.49)	0.0111 (0.072)	2.05
I	4.5 (1.37)	0.229 (1.48)	0.0006 (0.004)	0.26
J	5 (1.52)	0.279 (1.80)	0.0062 (0.040)	2.22
K	6 (1.83)	0.179 (1.16)	0.0126 (0.081)	7.03
L	7 (2.13)	0.223 (1.44)	0.0076 (0.049)	3.40
M	8 (2.44)	0.176 (1.14)	0.0000 (0.000)	0.00
N	9 (2.74)	0.117 (0.75)	0.0000 (0.000)	0.00
O	10 (3.05)	0.196 (1.26)	0.0000 (0.000)	0.00
P	11 (3.35)	0.119 (0.77)	0.0019 (0.012)	1.59
Q	12 (3.66)	0.198 (1.28)	0.0036 (0.023)	1.82
R	13 (3.96)	0.497 (3.20)	0.0000 (0.000)	0.00
S	14 (4.27)	0.033 (0.22)	0.0000 (0.000)	0.00
T	14.3 (4.37)	0.019 (0.12)	0.0000 (0.000)	0.00
Sum		**7.768 (50.12)**	**0.0771 (0.497)**	**0.99**

From the analysis of the cut sections, Specimen VG-C2-2 has the remaining void ratio, after repair, of 0.99% on average. The initial void area ranges over 0.1 inch^2 (0.65×10^{-4} m^2) or more from the reference point to Section R, however, these voids include a small contribution from Section S.

Table A-5 shows the time schedule for sealing ducts for Specimen VG-C2-2. Total sealing time for Specimen VG-C2-2 is 3 days and 3.63 hours before applying the repair grout.

Table A-5. Sealing Time Schedule of Specimen VG-C2-2.

Sealing Procedure	Working Day	Working Time (min.)
Installing pipe saddle tap with grease	Day 1	32
Setting rubber end caps and sealing hose	Day 1	5
Assembling T-connection, sealing with silicone, and checking air tight condition	Day 1	35
Sealing end rubber caps with silicone	Day 1	32
Sealing with epoxy	Day 1	27
Wait	1 day	
Checking air-tight condition and sealing	Day 2	13
Checking air-tight condition	Day 2	3
Sealing with epoxy	Day 2	45
Wait	1 day	
Checking air-tight condition	Day 3	5
Reassembling T-connection and checking air-tight condition	Day 3	16
Sealing with silicone	Day 3	5
Sum	**3 days**	**218 (3.6 hours)**

A.4. SPECIMEN VG-C3-1

Figure A-9 depicts the initial void profiles of the sounding inspection and of the visual inspection before grouting for Specimen VG-C3-1.

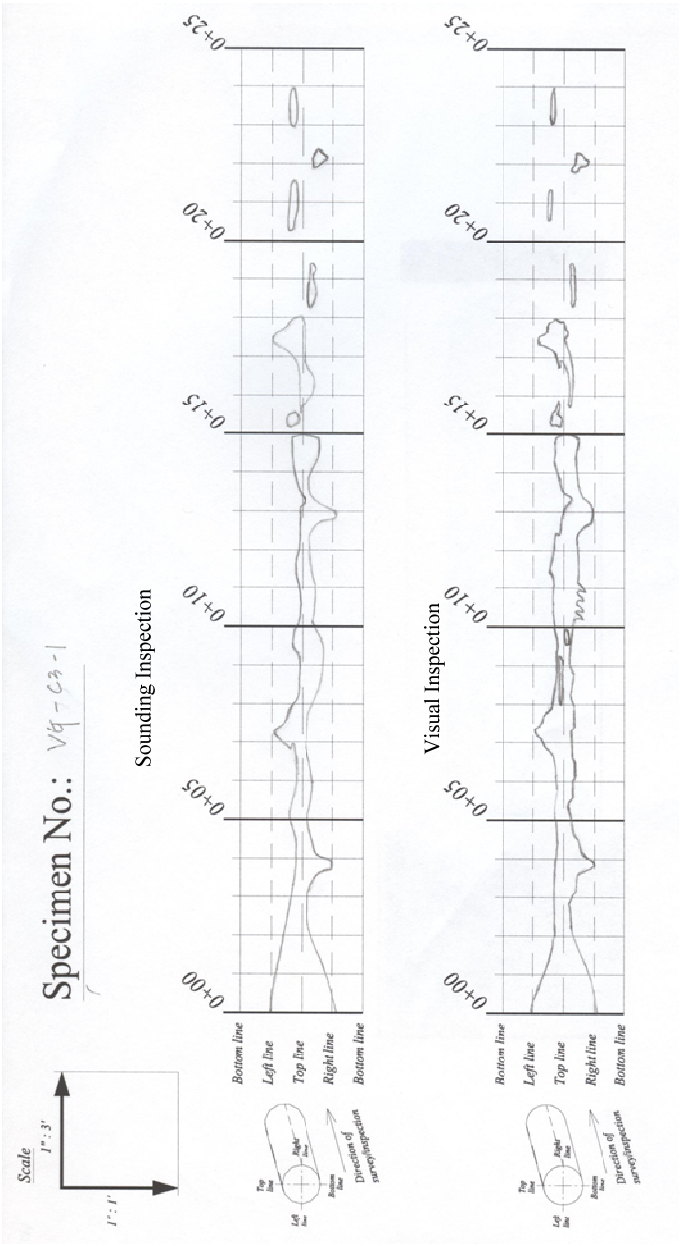

Figure A-9. Void Map of Specimen VG-C3-1.

The areas of both void profiles are estimated using AutoCAD® and provided in Table A-6.

Table A-6. Estimation of Void Profile in Specimen VG-C3-1.

Section, ft (m)	Sounding Inspection (SI), inch^2 (10^{-4} m^2)	Visual Inspection (VI), inch^2 (10^{-4} m^2)	SI - VI, inch^2 (10^{-4} m^2)
0~1 (0~0.3)	73.90 (476.8)	70.20 (425.9)	3.70 (23.9)
1~2 (0.3~0.6)	48.58 (313.4)	38.47 (248.2)	10.11 (65.2)
2~3 (0.6~0.9)	26.03 (167.9)	20.29 (130.9)	5.74 (37.0)
3~4 (0.9~1.2)	30.12 (194.3)	32.75 (211.3)	-2.63 (-17.0)
4~5 (1.2~1.5)	22.69 (146.4)	25.44 (164.1)	-2.75 (-17.8)
5~6 (1.5~1.8)	22.84 (147.3)	18.72 (120.7)	4.12 (26.6)
6~7 (1.8~2.1)	18.11 (116.8)	25.83 (166.7)	-7.72 (-49.8)
7~8 (2.1~2.4)	31.58 (203.7)	37.83 (244.1)	-6.25 (-40.3)
8~9 (2.4~2.7)	26.56 (171.4)	18.13 (117.0)	8.43 (54.4)
9~10 (2.7~3.0)	33.12 (213.7)	14.58 (94.1)	18.54 (119.6)
10~11 (3.0~3.4)	19.71 (127.2)	31.33 (202.1)	-11.62 (-75.0)
11~12 (3.4~3.7)	19.83 (128.0)	32.57 (210.1)	-12.74 (-82.2)
12~13 (3.7~4.0)	22.54 (145.4)	30.42 (196.3)	-7.88 (-50.8)
13~14 (4.0~4.3)	18.66 (120.4)	23.79 (153.5)	-5.13 (-33.1)
14~15 (4.3~4.6)	29.56 (190.7)	25.70 (165.8)	3.86 (24.9)
15~16 (4.6~4.9)	7.34 (47.4)	6.02 (38.8)	1.32 (8.5)
16~17 (4.9~5.2)	16.35 (105.5)	8.03 (51.8)	8.32 (53.7)
17~18 (5.2~5.5)	28.07 (181.1)	23.77 (153.3)	4.31 (27.8)
18~19 (5.5~5.8)	6.96 (44.9)	3.82 (24.6)	3.15 (20.3)
19~20 (5.8~6.1)	2.49 (16.1)	2.22 (14.3)	0.27 (1.8)
20~21 (6.1~6.4)	6.79 (43.8)	2.11 (13.6)	4.69 (30.2)
21~22 (6.4~6.7)	5.83 (37.6)	4.09 (26.4)	1.74 (11.2)
22~23 (6.7~7.0)	5.31 (34.2)	3.53 (22.8)	1.77 (11.4)
23~24 (7.0~7.3)	8.16 (52.7)	4.75 (30.6)	3.41 (22.0)

The repair grout is filled from the top grout port and infiltrated to 4.8 ft (1.46 m) from the reference point (Figure A-10).

Figure A-10. Repair Grouted Ducts of Specimen VG-C3-1.

Figure A-11 shows the cross-sectional views of the cut sections obtained from Specimen VG-C3-1. From the cut sections, it is noted that the repair grout successfully replaces the main voids up to 3 ft (0.91 m) from the reference point, but after that voids are only partially repaired. Also, this repair grout does not fill the #5 void, located in Section H. The small voids still exist inside the initially grouted ducts, especially in-between strands.

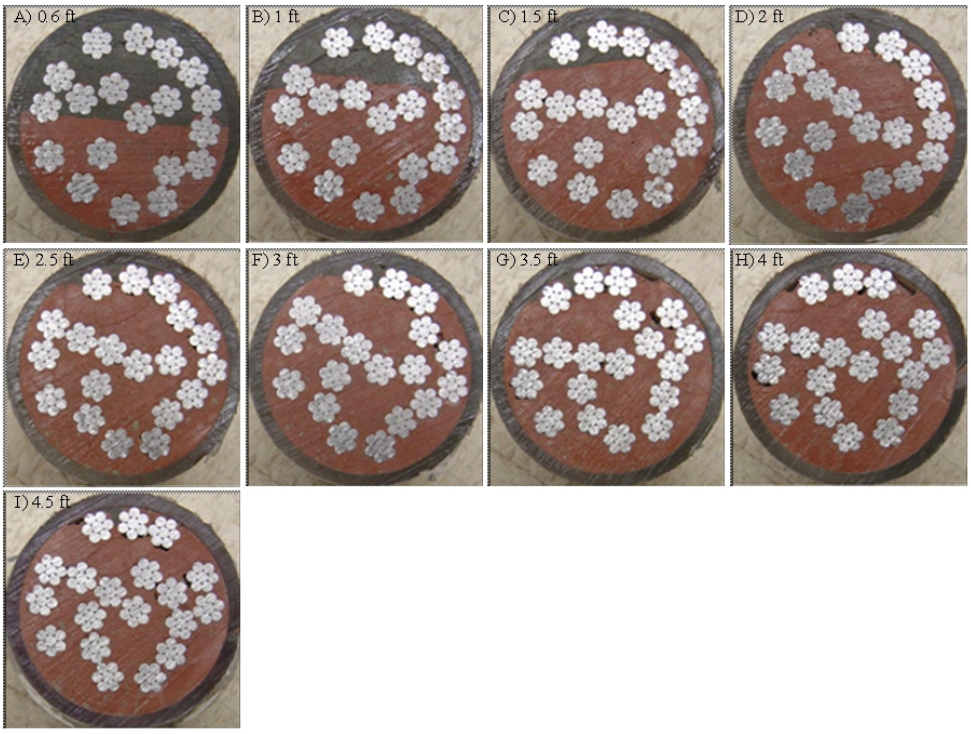

Figure A-11. Cut Sections of Specimen VG-C3-1 for the Filling Analysis of Repair Grout.

To compare the performance of repair grouts, the ratio of the remaining void area after repair to the repaired area is estimated. The repaired area and area of voids after repair are calculated using AutoCAD® (Table A-7).

Table A-7. Void Area of Specimen VG-C3-1.

Cut Sections, ft (m)		Repaired Area, A_R, inch^2(10^{-4} m^2)	Void Area, A_V, inch^2(10^{-4} m^2)	Void Ratio, η (%)
A	0.6 (0.18)	3.150 (20.32)	0.0117 (0.075)	0.37
B	1 (0.30)	2.019 (13.02)	0.0078 (0.050)	0.39
C	1.5 (0.46)	0.954 (6.16)	0.0004 (0.003)	0.04
D	2 (0.61)	0.336 (2.17)	0.0038 (0.025)	1.13
E	2.5 (0.76)	0.261 (1.69)	0.0020 (0.013)	0.77
F	3 (0.91)	0.216 (1.39)	0.0037 (0.024)	1.71
G	3.5 (1.07)	0.164 (1.06)	0.0120 (0.077)	7.32
H	4 (1.22)	0.104 (0.67)	0.0000 (0.000)	0.00
I	4.5 (1.37)	0.094 (0.61)	0.0002 (0.000)	0.21
Sum		**7.299 (47.09)**	**0.0416 (0.268)**	**0.57**

From the analysis of cut sections, Specimen VG-C3-1 has a remaining void ratio, after repair grouting, of 0.57% on average. The initial void area ranges over 0.1 inch^2 (0.65×10^{-4} m^2) or more from the reference point to Section H, however, the voids include small amount from Section I.

Table A-8 shows the time schedule of sealing ducts and preparation of repair grouting for Specimen VG-C3-1. Total sealing time of Specimen VG-C3-1 is 7 days and 10.92 hours before applying repair grout.

Table A-8. Sealing Time Schedule of Specimen VG-C3-1.

Sealing Procedure	Working Day	Working Time (min.)
Setting rubber end caps and sealing with epoxy	Day 1	55
Wait	1 day	
Installing pipe saddle tap with grease	Day 2	50
Assembling T-connection and checking air-tight condition	Day 2	110
Sealing with RTV silicone	Day 2	20
Checking air-tight condition	Day 3	50
Reassembling T-connection and checking air-tight condition	Day 4	150
Checking air-tight condition and sealing with epoxy	Day 5	60
Wait	1 day	
Checking air-tight condition and sealing	Day 6	30
Checking air-tight condition and sealing	Day 7	130
Sum	**7 days**	**655 (10.92 hours)**

A.5. SPECIMEN PG-C1-1

Figure A-12 depicts the initial void profiles of the sounding inspection and of the visual inspection before grouting for Specimen PG-C1-1.

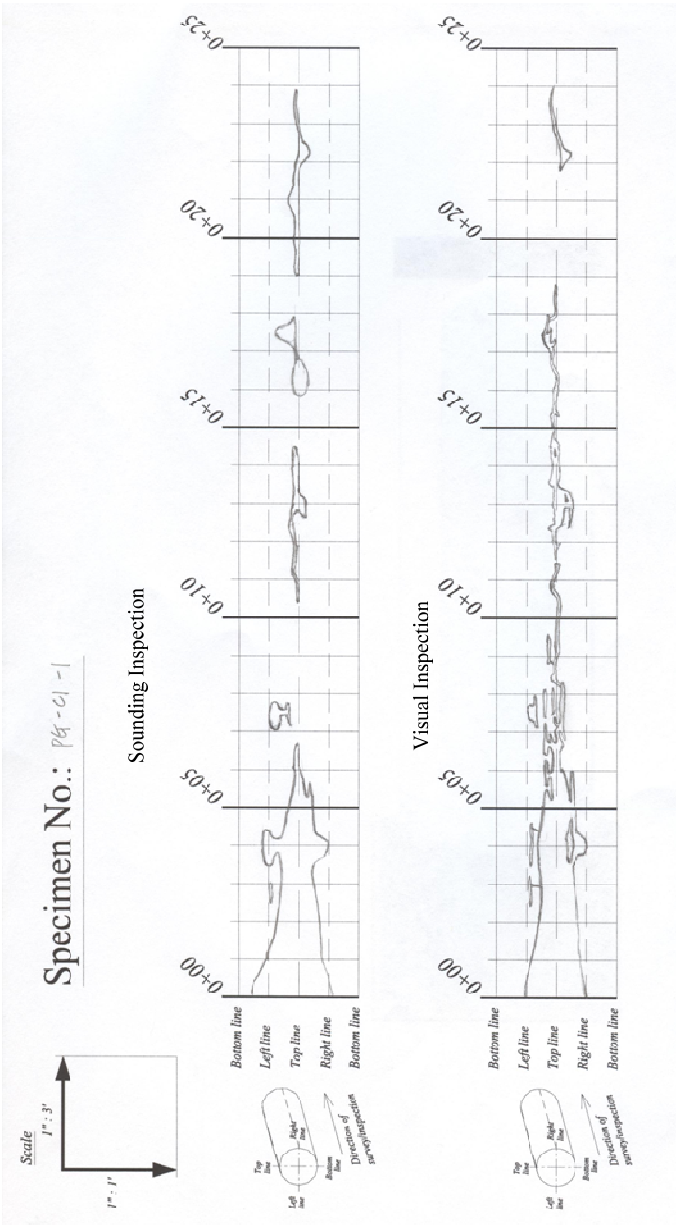

Figure A-12. Void Map of Specimen PG-C1-1.

The areas of both void profiles are estimated using AutoCAD® and provided in Table A-9.

Table A-9. Estimation of Void Profile in Specimen PG-C1-1.

Section, ft (m)	Sounding Inspection (SI), inch^2 (10^{-4} m^2)	Visual Inspection (VI), inch^2 (10^{-4} m^2)	SI - VI, inch^2 (10^{-4} m^2)
0~1 (0~0.3)	89.02 (574.3)	70.86 (457.1)	18.17 (117.2)
1~2 (0.3~0.6)	61.25 (395.2)	54.40 (351.0)	6.86 (44.2)
2~3 (0.6~0.9)	49.61 (320.0)	47.71 (307.8)	1.90 (12.2)
3~4 (0.9~1.2)	55.39 (357.4)	47.52 (306.6)	7.87 (50.7)
4~5 (1.2~1.5)	47.82 (308.5)	47.43 (306.0)	0.39 (2.5)
5~6 (1.5~1.8)	19.71 (127.1)	31.10 (200.6)	-11.39 (-73.5)
6~7 (1.8~2.1)	3.89 (25.1)	15.67 (101.1)	-11.78 (-76.0)
7~8 (2.1~2.4)	11.97 (77.2)	18.50 (119.4)	-6.53 (-42.2)
8~9 (2.4~2.7)	0.00 (0.0)	6.53 (42.1)	-6.53 (-42.1)
9~10 (2.7~3.0)	0.00 (0.0)	6.85 (44.2)	-6.85 (-44.2)
10~11 (3.0~3.4)	2.67 (17.2)	4.23 (27.3)	-1.56 (-10.1)
11~12 (3.4~3.7)	5.21 (33.6)	3.78 (24.4)	1.42 (9.2)
12~13 (3.7~4.0)	9.48 (61.2)	11.70 (75.5)	-2.21 (-14.3)
13~14 (4.0~4.3)	10.10 (65.1)	13.84 (89.3)	-3.74 (-24.2)
14~15 (4.3~4.6)	3.57 (23.0)	6.77 (43.7)	-3.21 (-20.7)
15~16 (4.6~4.9)	2.26 (14.6)	4.13 (26.6)	-1.87 (-12.1)
16~17 (4.9~5.2)	15.43 (99.5)	4.00 (25.8)	11.42 (73.7)
17~18 (5.2~5.5)	12.08 (77.9)	7.53 (48.6)	4.55 (29.3)
18~19 (5.5~5.8)	0.00 (0.0)	2.50 (16.1)	-2.50 (-16.1)
19~20 (5.8~6.1)	5.94 (38.3)	0.00 (0.0)	5.94 (38.3)
20~21 (6.1~6.4)	8.95 (57.8)	0.00 (0.0)	8.95 (57.8)
21~22 (6.4~6.7)	9.05 (58.4)	0.88 (5.7)	8.17 (52.7)
22~23 (6.7~7.0)	8.58 (55.4)	6.54 (42.2)	2.04 (13.1)
23~24 (7.0~7.3)	3.50 (22.6)	3.08 (19.9)	0.42 (2.7)

The repair grout is filled from the top grout port and infiltrated to 11.5 ft (3.51 m) from the reference point (Figure A-13).

Figure A-13. Repair Grouted Ducts of Specimen PG-C1-1.

Figure A-14 shows the cross-sectional views of the cut sections obtained from Specimen PG-C1-1. From the cut sections, it is noted that the repair grout successfully replaces the main voids and repairs local large voids #3, #4, and #5. The small voids still exist inside the initially grouted ducts, especially in-between strands. However, those voids cannot be repaired because the voids are isolated from the “bug holes” which is a route for repair grouts.

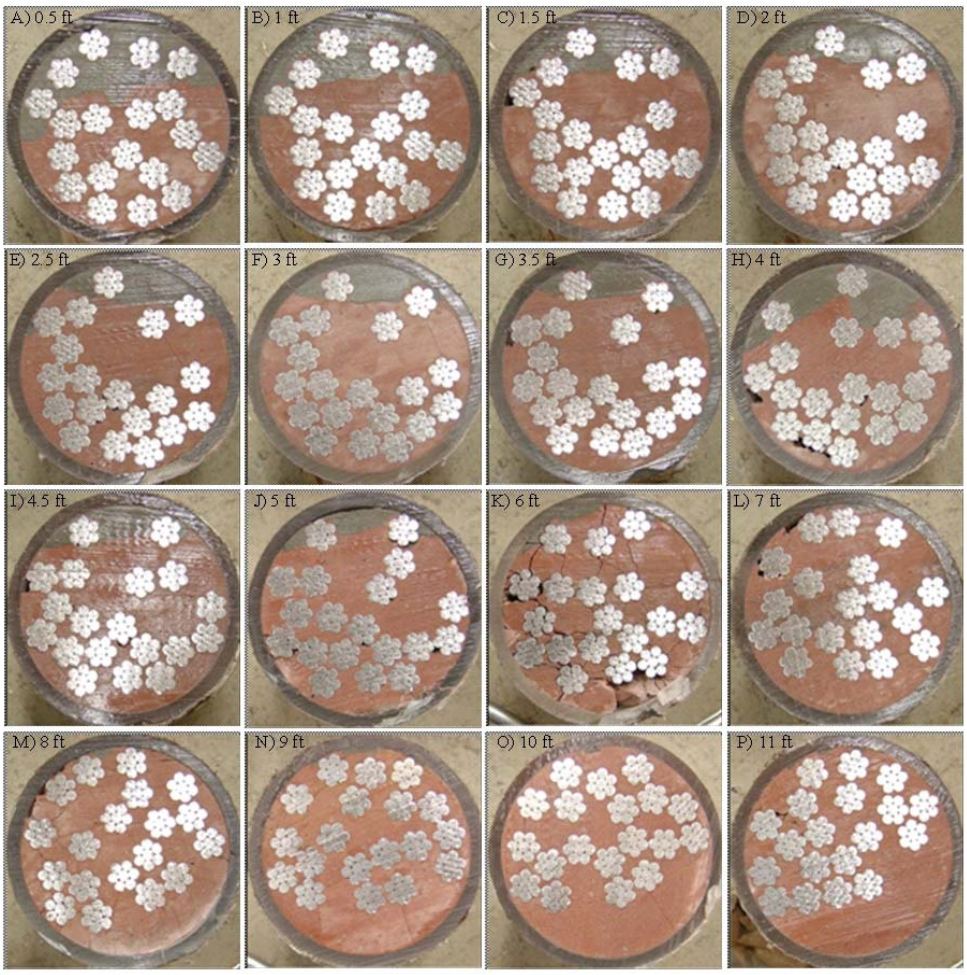

Figure A-14. Cut Sections of Specimen PG-C1-1 for the Filling Analysis of Repair Grout.

To compare the performance of repair grouts, the ratio of the remaining void area after repair to the repaired area is estimated. The repaired area and area of voids after repair are calculated using AutoCAD® (Table A-10).

Table A-10. Void Area of Specimen PG-C1-1.

Cut Sections, ft (m)		Repaired Area, A_R, inch^2(10^{-4} m^2)	Void Area, A_V, inch^2(10^{-4} m^2)	Void Ratio, η (%)
A	0.5 (0.15)	2.874 (18.54)	0.0118 (0.076)	0.41
B	1 (0.30)	1.825 (11.78)	0.0026 (0.017)	0.14
C	1.5 (0.46)	1.483 (9.57)	0.0078 (0.050)	0.53
D	2 (0.61)	1.272 (8.21)	0.0009 (0.006)	0.07
E	2.5 (0.76)	1.269 (8.19)	0.0008 (0.005)	0.06
F	3 (0.91)	1.050 (6.78)	0.0000 (0.000)	0.00
G	3.5 (1.07)	0.948 (6.11)	0.0000 (0.000)	0.00
H	4 (1.22)	2.158 (13.92)	0.0012 (0.008)	0.06
I	4.5 (1.37)	0.944 (6.09)	0.0000 (0.000)	0.00
J	5 (1.52)	0.753 (4.86)	0.0023 (0.015)	0.31
K	6 (1.83)	0.267 (1.73)	0.0000 (0.000)	0.00
L	7 (2.13)	0.099 (0.64)	0.0058 (0.037)	5.89
M	8 (2.44)	0.083 (0.53)	0.0000 (0.000)	0.00
N	9 (2.74)	0.113 (0.73)	0.0000 (0.000)	0.00
O	10 (3.05)	0.033 (0.21)	0.0008 (0.005)	2.43
P	11 (3.35)	0.064 (0.41)	0.0002 (0.001)	0.31
Sum		**15.234 (98.28)**	**0.0342 (0.221)**	**0.22**

The remaining void ratio after repair, obtained from the analysis, comes out to be 0.22% for Specimen PG-C1-1. The initial void area ranges over 0.1 inch^2 (0.65×10^{-4} m^2) or more from the reference point to Section K, however, the voids include a small contribution from Section L excluding Section N.

Table A-11 shows the time schedule for sealing ducts and preparation of repair grouting for Specimen PG-C1-1. Total sealing time for Specimen PG-C1-1 is 2 days and 0.88 hours before applying repair grout.

Table A-11. Sealing Time Schedule of Specimen PG-C1-1.

Sealing Procedure	Working Day	Working Time (min.)
Setting rubber end caps (one side)	Day 1	1
Installing pipe saddle tap	Day 1	20
Mixing epoxy and sealing (one side)	Day 1	20
Wait	1 day	
Connect pressure grout pump and reseal	Day 2	12
Sum	**2 days**	**53 (0.88 hours)**

A.6. SPECIMEN PG-C1-2

Figure A-15 shows depicts the initial void profiles of the sounding inspection and of the visual inspection before grouting for Specimen PG-C1-2.

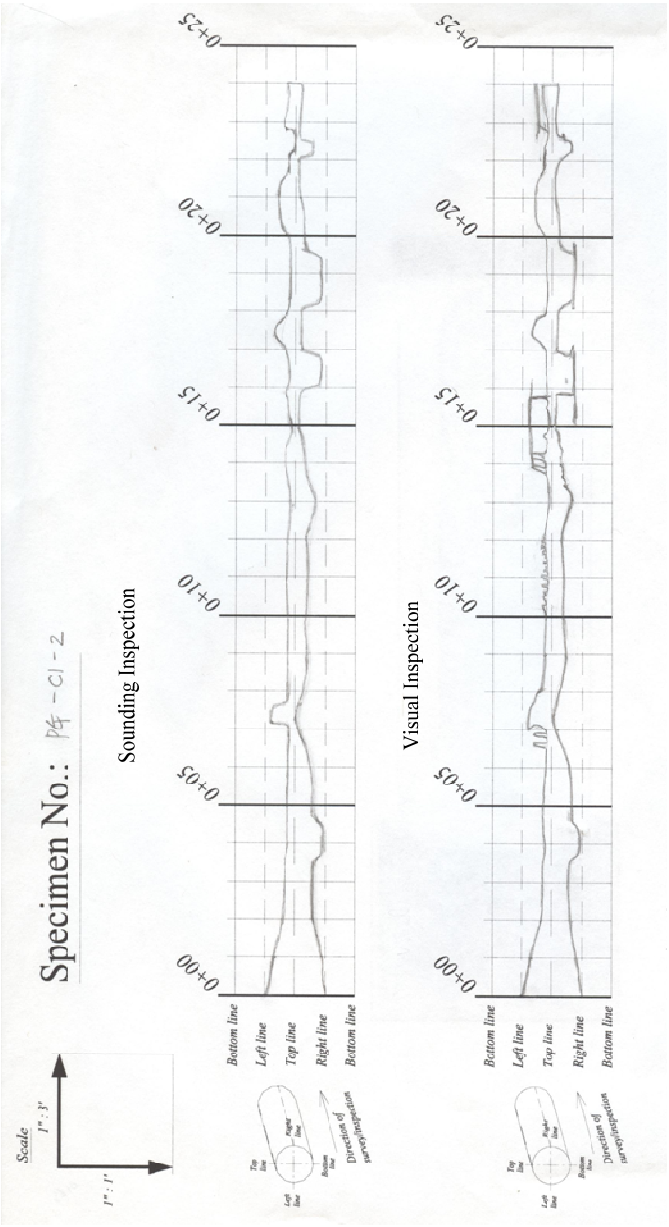

Figure A-15. Void Map of Specimen PG-C1-2.

The areas of both void profiles are estimated using AutoCAD® and provided in Table A-12.

Table A-12. Estimation of Void Profile in Specimen PG-C1-2.

Section, ft (m)	Sounding Inspection (SI), inch^2 (10^{-4} m^2)	Visual Inspection (VI), inch^2 (10^{-4} m^2)	SI - VI, inch^2 (10^{-4} m^2)
0~1 (0~0.3)	67.05 (432.6)	66.04 (426.1)	1.01 (6.5)
1~2 (0.3~0.6)	49.73 (320.9)	47.15 (304.2)	2.58 (16.7)
2~3 (0.6~0.9)	36.20 (233.6)	34.42 (222.0)	1.78 (11.5)
3~4 (0.9~1.2)	38.21 (246.5)	37.12 (239.5)	1.10 (7.1)
4~5 (1.2~1.5)	38.47 (248.2)	40.93 (264.1)	-2.47 (-15.9)
5~6 (1.5~1.8)	30.24 (195.1)	34.53 (222.8)	-4.30 (-27.7)
6~7 (1.8~2.1)	20.37 (131.4)	25.12 (162.1)	-4.76 (-30.7)
7~8 (2.1~2.4)	23.65 (152.6)	29.88 (192.8)	-6.23 (-40.2)
8~9 (2.4~2.7)	22.05 (142.2)	26.28 (169.6)	-4.24 (-27.3)
9~10 (2.7~3.0)	22.03 (142.1)	25.19 (162.5)	-3.17 (-20.4)
10~11 (3.0~3.4)	24.78 (159.9)	23.37 (150.7)	1.42 (9.2)
11~12 (3.4~3.7)	25.63 (165.4)	24.21 (156.2)	1.42 (9.2)
12~13 (3.7~4.0)	26.34 (169.9)	24.18 (156.0)	2.15 (13.9)
13~14 (4.0~4.3)	26.95 (173.9)	25.95 (167.4)	1.00 (6.5)
14~15 (4.3~4.6)	18.99 (122.5)	23.58 (152.1)	-4.59 (-29.6)
15~16 (4.6~4.9)	14.09 (90.9)	21.32 (137.5)	-7.22 (-46.6)
16~17 (4.9~5.2)	36.99 (238.6)	33.82 (218.2)	3.17 (20.5)
17~18 (5.2~5.5)	27.88 (179.9)	26.78 (172.8)	1.10 (7.1)
18~19 (5.5~5.8)	34.88 (225.0)	30.34 (195.8)	4.53 (29.2)
19~20 (5.8~6.1)	28.91 (186.5)	30.49 (196.7)	-1.58 (-10.2)
20~21 (6.1~6.4)	29.02 (187.2)	27.29 (176.1)	1.73 (11.1)
21~22 (6.4~6.7)	20.64 (133.2)	22.24 (143.5)	-1.60 (-10.3)
22~23 (6.7~7.0)	16.20 (104.5)	25.23 (162.8)	-9.02 (-58.2)
23~24 (7.0~7.3)	17.46 (112.6)	21.33 (137.6)	-3.88 (-25.0)

The repair grout is filled from the top grout port and infiltrated to 9.3 ft (2.86 m) from the reference point (Figure A-16).

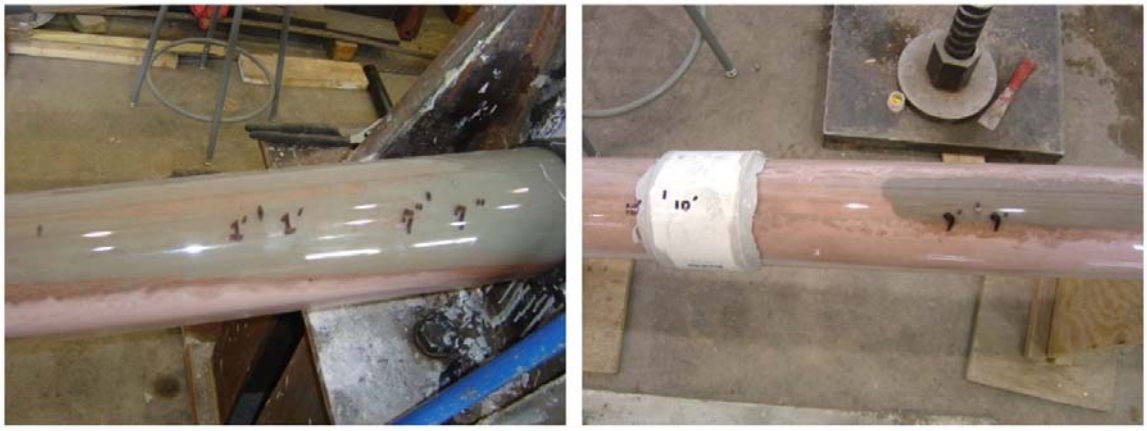

Figure A-16. Repair Grouted Ducts of Specimen PG-C1-2.

Figure A-17 shows the cross-sectional views of the cut sections obtained from Specimen PG-C1-2. From the cut sections, it is noted that the repair grouts successfully replaces the main voids up to 6 ft (1.83 m) from the reference point, but after that voids are only partially repaired. The local large void #5 is filled completely by repair grout; however, small voids still exist inside the initially grouted ducts, especially in-between strands.

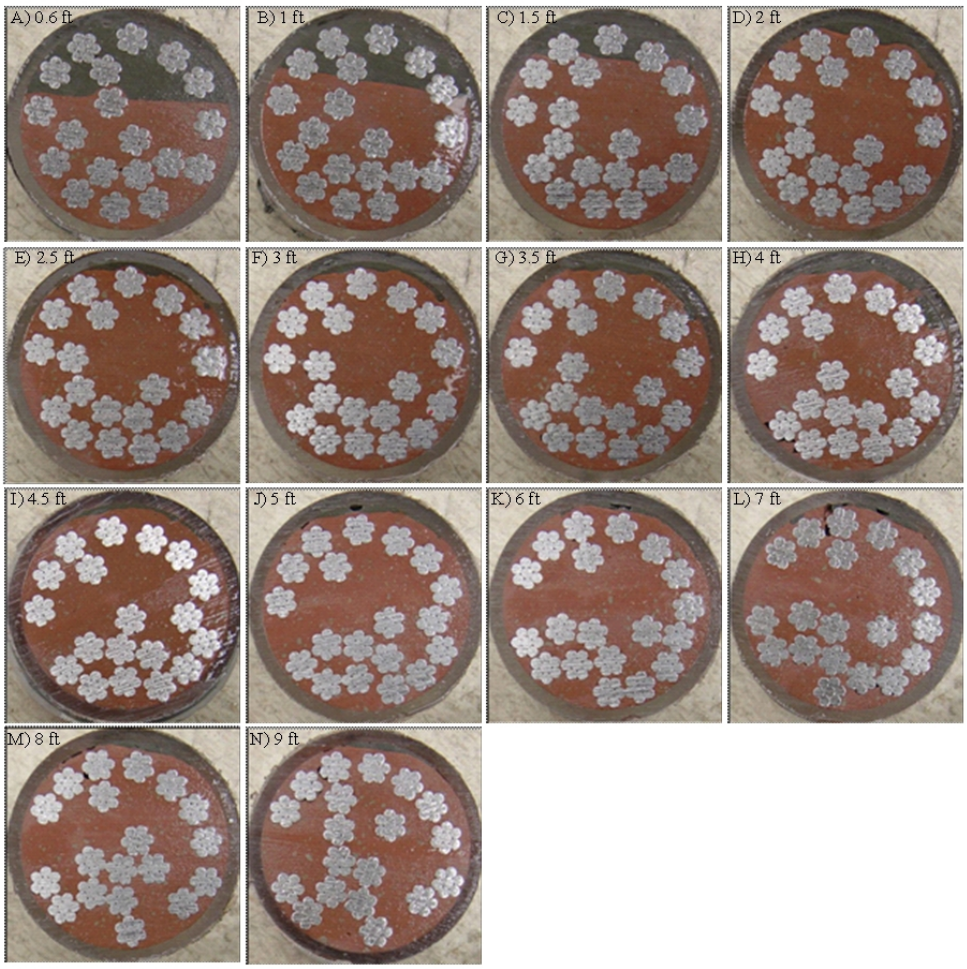

Figure A-17. Cut Sections of Specimen PG-C1-2 for the Filling Analysis of Repair Grout.

To compare the performance of repair grouts, the ratio of the remaining void area after repair to the repaired area is estimated. The repaired area and area of voids after repair are calculated using AutoCAD® (Table A-13).

Table A-13. Void Area of Specimen PG-C1-2.

Cut Sections, ft (m)		Repaired Area, A_R, inch^2(10^{-4} m^2)	Void Area, A_V, inch^2(10^{-4} m^2)	Void Ratio, η (%)
A	0.6 (0.18)	2.592 (16.72)	0.0063 (0.041)	0.24
B	1 (0.30)	1.614 (10.41)	0.0000 (0.000)	0.00
C	1.5 (0.46)	0.872 (5.62)	0.0039 (0.025)	0.45
D	2 (0.61)	0.384 (2.48)	0.0000 (0.000)	0.00
E	2.5 (0.76)	0.267 (1.72)	0.0008 (0.005)	0.30
F	3 (0.91)	0.301 (1.94)	0.0000 (0.000)	0.00
G	3.5 (1.07)	0.369 (2.38)	0.0000 (0.000)	0.00
H	4 (1.22)	0.467 (3.02)	0.0041 (0.026)	0.88
I	4.5 (1.37)	0.227 (1.46)	0.0021 (0.014)	0.93
J	5 (1.52)	0.264 (1.70)	0.0278 (0.179)	10.55
K	6 (1.83)	0.237 (1.53)	0.0300 (0.194)	12.68
L	7 (2.13)	0.225 (1.45)	0.0531 (0.343)	23.58
M	8 (2.44)	0.213 (1.37)	0.0135 (0.087)	6.35
N	9 (2.74)	0.181 (1.17)	0.0025 (0.016)	1.38
Sum		**8.211 (52.97)**	**0.1441 (0.930)**	**1.76**

From the analysis of the cut sections, Specimen PG-C1-2 has a remaining void ratio, after repair, of 1.76% on average. The initial void area ranges over 0.1 inch^2 (0.65×10^{-4} m^2) or more about all the repaired sections. Therefore, the PG method with Class C-1 grout in Specimen PG-C1-2 has a lower FC than other previously evaluated. Table A-14 shows the time schedule for sealing ducts for Specimen PG-C1-2. Total sealing time for Specimen PG-C1-2 is 2 days and 0.65 hours before applying repair grout.

Table A-14. Sealing Time Schedule of Specimen PG-C1-2.

Sealing Procedure	Working Day	Working Time (min.)
Installing pipe saddle tap	Day 1	22
RTV silicone sealing	Day 1	5
Wait	1 day	
Connect pressure grout pump and reseal	Day 2	12
Sum	**2 days**	**39 (0.65 hours)**

A.7. SPECIMEN PG-C2-1

The initial void profiles before repair grouting are represented and shown in Figure A-18.

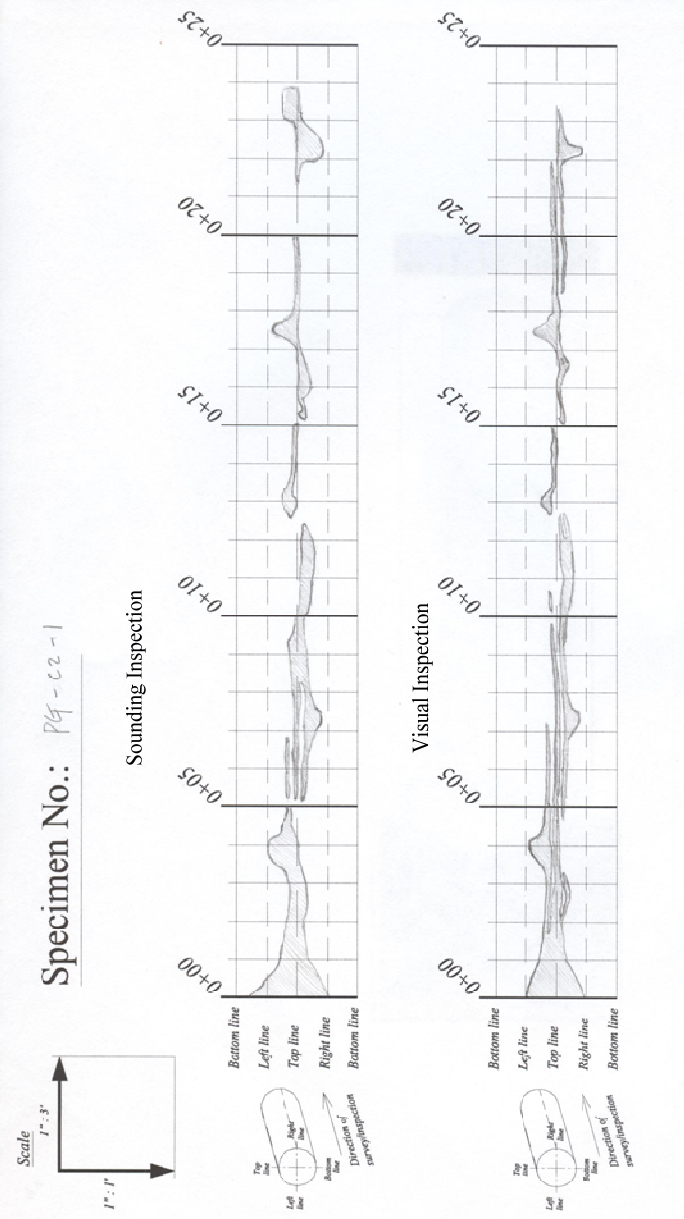

Figure A-18. Void Map of Specimen PG-C2-1.

The areas of both void profiles are estimated using AutoCAD® and provided in Table A-12.

Table A-15. Estimation of Void Profile in Specimen PG-C2-1.

Section, ft (m)	Sounding Inspection (SI), inch^2 (10^{-4} m^2)	Visual Inspection (VI), inch^2 (10^{-4} m^2)	SI - VI, inch^2 (10^{-4} m^2)
0~1 (0~0.3)	66.40 (428.4)	54.89 (354.1)	11.51 (74.3)
1~2 (0.3~0.6)	28.33 (182.7)	26.29 (169.6)	2.04 (13.1)
2~3 (0.6~0.9)	21.88 (141.2)	21.29 (137.3)	0.59 (3.8)
3~4 (0.9~1.2)	30.08 (194.0)	23.50 (151.6)	6.58 (42.4)
4~5 (1.2~1.5)	16.38 (105.7)	19.62 (126.6)	-3.24 (-20.9)
5~6 (1.5~1.8)	13.48 (87.0)	14.21 (91.7)	-0.73 (-4.7)
6~7 (1.8~2.1)	19.95 (128.7)	15.32 (98.8)	4.63 (29.9)
7~8 (2.1~2.4)	21.56 (139.1)	18.28 (117.9)	3.29 (21.2)
8~9 (2.4~2.7)	20.29 (130.9)	10.69 (69.0)	9.60 (62.0)
9~10 (2.7~3.0)	16.23 (104.7)	10.53 (68.0)	5.70 (36.8)
10~11 (3.0~3.4)	13.36 (86.2)	13.17 (85.0)	0.19 (1.2)
11~12 (3.4~3.7)	16.10 (103.9)	14.43 (93.1)	1.67 (10.8)
12~13 (3.7~4.0)	8.60 (55.5)	8.79 (56.7)	-0.20 (-1.3)
13~14 (4.0~4.3)	8.58 (55.3)	5.82 (37.5)	2.76 (17.8)
14~15 (4.3~4.6)	5.56 (35.9)	5.17 (33.4)	0.39 (2.5)
15~16 (4.6~4.9)	7.39 (47.7)	4.12 (26.6)	3.27 (21.1)
16~17 (4.9~5.2)	10.96 (70.7)	8.18 (52.8)	2.78 (17.9)
17~18 (5.2~5.5)	18.54 (119.6)	18.25 (117.8)	0.28 (1.8)
18~19 (5.5~5.8)	6.35 (40.9)	8.36 (54.0)	-2.02 (-13.0)
19~20 (5.8~6.1)	5.64 (36.4)	9.55 (61.6)	-3.91 (-25.3)
20~21 (6.1~6.4)	0.00 (0.0)	8.39 (54.1)	-8.39 (-54.1)
21~22 (6.4~6.7)	4.61 (29.8)	8.29 (53.5)	-3.68 (-23.7)
22~23 (6.7~7.0)	26.46 (170.7)	13.59 (87.7)	12.87 (83.0)
23~24 (7.0~7.3)	18.79 (121.2)	1.01 (6.5)	17.79 (114.7)

The repair grout is filled from the top grout port and infiltrated to 4.6 ft (1.40 m) from the reference point (Figure A-19).

Figure A-19. Repair Grouted Ducts of Specimen PG-C2-1.

Figure A-20 shows the cross-sectional views of the cut sections obtained from Specimen PG-C2-1. The repair grout successfully fills the voids up to 3.5 ft (1.07m) from the reference point, but it does not fill void #5 located at 4 ft (1.22 m) from the reference point since the void is isolated from the “bug hole”. Because the five local large voids are fabricated intentionally by vacuuming, in some cases, the voids are not connected with a void route located on the top surface. The small voids still exist inside the initially grouted ducts, especially in-between strands.

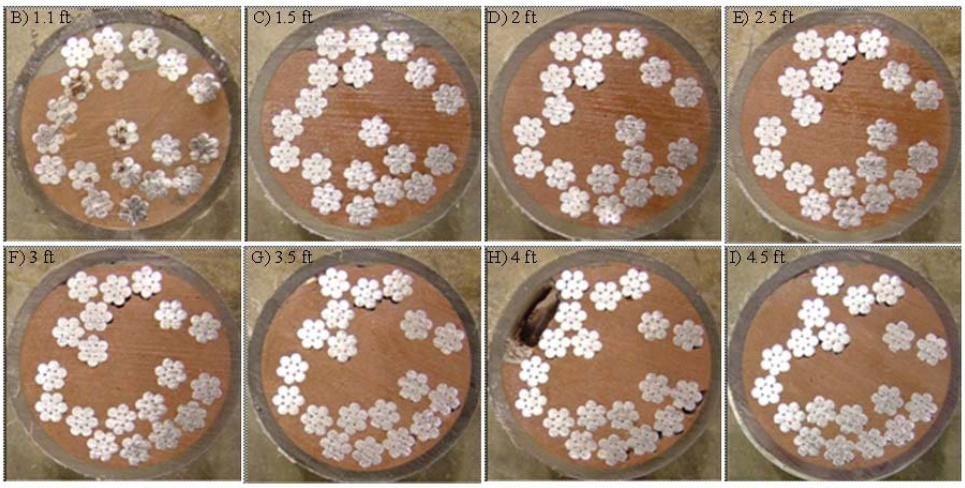

Figure A-20. Cut Sections of Specimen PG-C2-1 for the Filling Analysis of Repair Grout.

To compare the performance of repair grouts, the ratio of the remaining void area after repair to the repaired area is estimated. The repaired area and area of voids after repair are calculated using AutoCAD® (Table A-16).

Table A-16. Void Area of Specimen PG-C2-1.

Cut Sections, ft (m)		Repaired Area, A_R, inch^2(10^{-4} m^2)	Void Area, A_V, inch^2(10^{-4} m^2)	Void Ratio, η (%)
B	1.1 (0.34)	1.164 (7.51)	0.0079 (0.051)	0.68
C	1.5 (0.46)	0.436 (2.81)	0.0036 (0.023)	0.86
D	2 (0.61)	0.430 (2.77)	0.0021 (0.014)	0.49
E	2.5 (0.76)	0.182 (1.17)	0.0027 (0.017)	1.48
F	3 (0.91)	0.125 (0.81)	0.0057 (0.037)	4.56
G	3.5 (1.07)	0.081 (0.52)	0.0038 (0.025)	4.71
H	4 (1.22)	0.066 (0.43)	0.0026 (0.017)	3.92
I	4.5 (1.37)	0.040 (0.26)	0.0000 (0.000)	0.00
Sum		**2.524 (16.28)**	**0.0284 (0.183)**	**1.13**

From the analysis of the cut sections, Specimen PG-C2-1 has the remaining void ratio, after repair, of 1.13%. Since the initial void area is significantly less (under 0.1 $inch^2$ (0.65×10^{-4} m^2)) from Section G, the repair grouts cannot be depended on to adequately fill Specimen PG-C2-1 when compared to other specimens.

Table A-17 shows the time schedule for sealing ducts and preparation of repair grouting for Specimen PG-C2-1. Total sealing time for Specimen PG-C2-1 is 3 days and 1.03 hours before applying repair grout.

Table A-17. Sealing Time Schedule of Specimen PG-C2-1.

Sealing Procedure	Working Day	Working Time (min.)
Mixing epoxy and sealing	Day 1	25
Wait	1 day	
Setting rubber end cap (one side)	Day 2	2
Installing pipe saddle tap	Day 2	25
Connect pressure grout pump and reseal	Day 3	10
Sum	**3 days**	**62 (1.03 hours)**

A.8. SPECIMEN PG-C2-2

Figure A-21 depicts the initial void profiles of the sounding inspection and of the visual inspection before grouting for Specimen PG-C2-2.

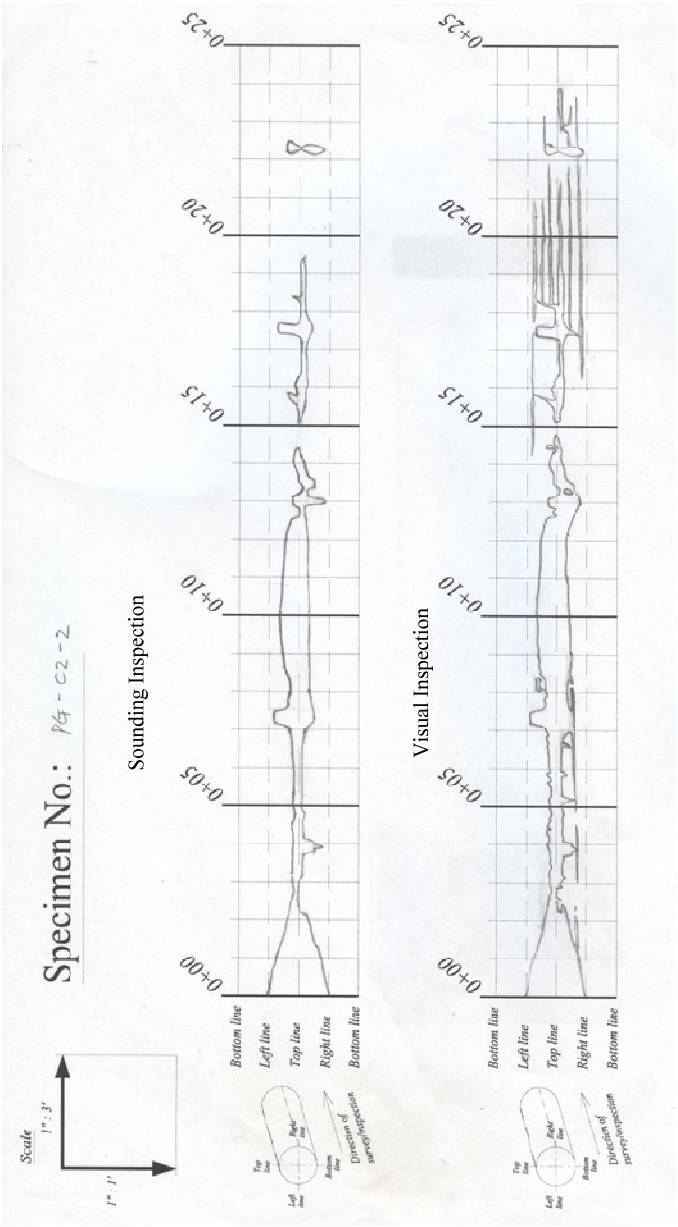

Figure A-21. Void Map of Specimen PG-C2-2.

The areas of both void profiles are estimated using AutoCAD® and provided in Table A-18.

Table A-18. Estimation of Void Profile in Specimen PG-C2-2.

Section, ft (m)	Sounding Inspection (SI), inch^2 (10^{-4} m^2)	Visual Inspection (VI), inch^2 (10^{-4} m^2)	SI - VI, inch^2 (10^{-4} m^2)
0~1 (0~0.3)	66.52 (429.1)	66.19 (427.0)	0.32 (2.1)
1~2 (0.3~0.6)	40.54 (261.5)	43.93 (283.4)	-3.39 (-21.9)
2~3 (0.6~0.9)	11.28 (72.8)	15.96 (103.0)	-4.68 (-30.2)
3~4 (0.9~1.2)	17.91 (115.5)	21.72 (140.1)	-3.81 (-24.6)
4~5 (1.2~1.5)	15.31 (98.8)	18.51 (119.4)	-3.20 (-20.6)
5~6 (1.5~1.8)	11.74 (75.7)	19.38 (125.0)	-7.64 (-49.3)
6~7 (1.8~2.1)	15.08 (97.3)	23.15 (149.3)	-8.07 (-52.1)
7~8 (2.1~2.4)	36.90 (238.0)	40.95 (264.2)	-4.05 (-26.1)
8~9 (2.4~2.7)	29.27 (188.8)	37.26 (240.4)	-7.99 (-51.6)
9~10 (2.7~3.0)	35.95 (231.9)	39.66 (255.9)	-3.71 (-24.0)
10~11 (3.0~3.4)	35.10 (226.5)	37.74 (243.5)	-2.64 (-17.1)
11~12 (3.4~3.7)	30.72 (198.2)	31.56 (203.6)	-0.84 (-5.4)
12~13 (3.7~4.0)	20.69 (133.5)	31.14 (200.9)	-10.45 (-67.4)
13~14 (4.0~4.3)	17.03 (109.9)	20.56 (132.7)	-3.53 (-22.8)
14~15 (4.3~4.6)	3.89 (25.1)	9.34 (60.3)	-5.45 (-35.2)
15~16 (4.6~4.9)	10.73 (69.2)	14.03 (90.5)	-3.30 (-21.3)
16~17 (4.9~5.2)	9.61 (62.0)	10.48 (67.6)	-0.87 (-5.6)
17~18 (5.2~5.5)	19.37 (125.0)	23.46 (151.3)	-4.09 (-26.4)
18~19 (5.5~5.8)	7.00 (45.2)	24.09 (155.4)	-17.09 (-110.3)
19~20 (5.8~6.1)	2.26 (14.6)	19.76 (127.5)	-17.50 (-112.9)
20~21 (6.1~6.4)	0.00 (0.0)	15.65 (101.0)	-15.65 (-101.0)
21~22 (6.4~6.7)	0.00 (0.0)	6.74 (43.5)	-6.74 (-43.5)
22~23 (6.7~7.0)	9.80 (63.2)	15.57 (100.4)	-5.76 (-37.2)
23~24 (7.0~7.3)	0.00 (0.0)	6.21 (40.1)	-6.21 (-40.1)

The repair grout is filled from the top grout port and infiltrated to 14.4 ft (4.39 m) from the reference point (Figure A-22).

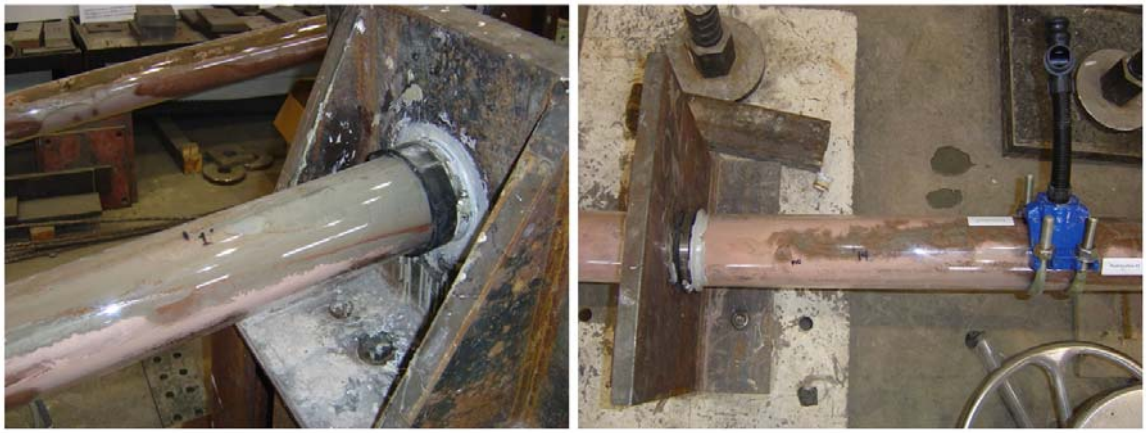

Figure A-22. Repair Grouted Ducts of Specimen PG-C2-2.

Figure A-23 shows the cross-sectional views of the cut sections obtained from Specimen PG-C2-2. From the cut sections, it is noted that the repair grouts successfully replaces the main voids and repairs local large voids #3, #4, and #5.

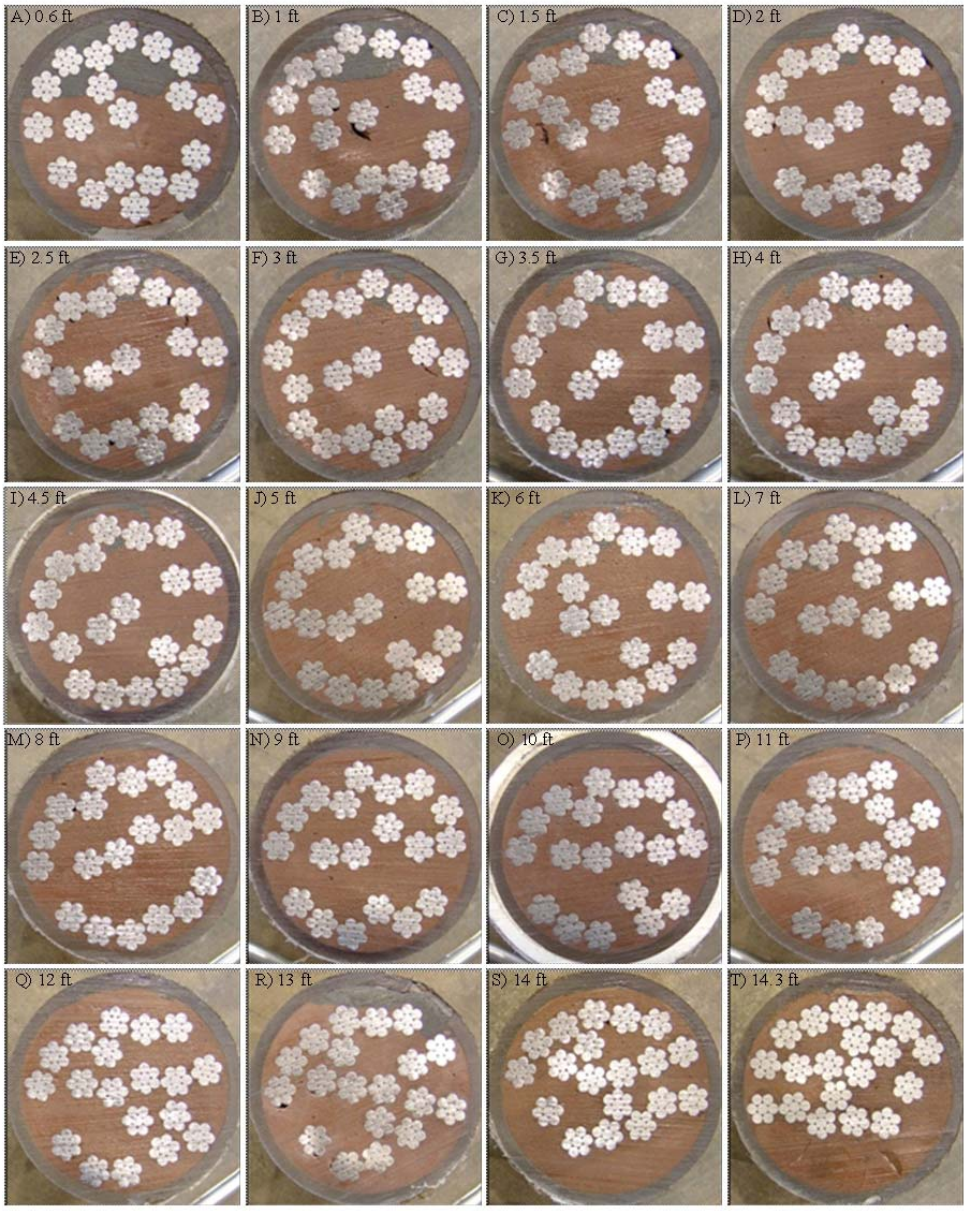

Figure A-23. Cut Sections of Specimen PG-C2-2 for the Filling Analysis of Repair Grout.

To compare the performance of repair grouts, the ratio of remaining void area after repair to the repaired area is estimated. The repaired area and area of voids after repair are calculated using AutoCAD® (Table A-19).

Table A-19. Void Area of Specimen PG-C2-2.

Cut Sections, ft (m)		Repaired Area, A_R, inch^2(10^{-4} m^2)	Void Area, A_V, inch^2(10^{-4} m^2)	Void Ratio, η (%)
A	0.6 (0.18)	2.033 (13.12)	0.0025 (0.016)	0.12
B	1 (0.30)	1.349 (8.71)	0.0174 (0.112)	1.29
C	1.5 (0.46)	0.673 (4.34)	0.0289 (0.186)	4.29
D	2 (0.61)	0.469 (3.03)	0.0023 (0.015)	0.49
E	2.5 (0.76)	0.281 (1.81)	0.0040 (0.026)	1.43
F	3 (0.91)	0.327 (2.11)	0.0021 (0.014)	0.64
G	3.5 (1.07)	0.371 (2.39)	0.0009 (0.006)	0.24
H	4 (1.22)	0.462 (2.98)	0.0025 (0.016)	0.54
I	4.5 (1.37)	0.302 (1.95)	0.0018 (0.012)	0.60
J	5 (1.52)	0.245 (1.58)	0.0010 (0.006)	0.41
K	6 (1.83)	0.272 (1.76)	0.0015 (0.010)	0.55
L	7 (2.13)	0.367 (2.37)	0.0026 (0.017)	0.71
M	8 (2.44)	0.284 (1.83)	0.0000 (0.000)	0.00
N	9 (2.74)	0.250 (1.61)	0.0014 (0.009)	0.56
O	10 (3.05)	0.235 (1.52)	0.0000 (0.000)	0.00
	11 (3.35)	0.221 (1.43)	0.0004 (0.003)	0.18
Q	12 (3.66)	0.215 (1.39)	0.0018 (0.012)	0.84
R	13 (3.96)	0.909 (5.87)	0.0042 (0.027)	0.46
S	14 (4.27)	0.120 (0.77)	0.0000 (0.000)	0.00
T	14.3 (4.37)	0.205 (1.32)	0.0000 (0.000)	0.00
Sum		**9.590 (61.87)**	**0.0753 (0.486)**	**0.79**

From the analysis of cut sections, the Specimen PG-C2-2 has the remaining void ratio, after repair, of 0.79% on average. The initial void area ranges over 0.1 inch^2 (0.65×10^{-4} m^2) or more about all the repaired sections. Therefore, the initial void condition for Specimen PG-C2-2 provides an easier condition for filling grouts when compared to others.

Table A-20 shows the time schedule for sealing ducts for Specimen PG-C2-2. Total sealing time for Specimen PG-C2-2 is 2 days and 0.88 hours before applying repair grout.

Table A-20. Sealing Time Schedule of Specimen PG-C2-2.

Sealing Procedure	Working Day	Working Time (min.)
Installing pipe saddle tap	Day 1	18
Connect grout hose and silicone sealing	Day 1	5
Mixing epoxy and sealing	Day 1	25
Wait	1 day	
Connect grout pump and reseal	Day 2	5
Sum	**2 days**	**53 (0.88 hours)**

A.9. SPECIMEN PG-C3-1

Figure A-24 depicts the initial void profiles of the sounding inspection and of the visual inspection before grouting for Specimen PG-C3-1.

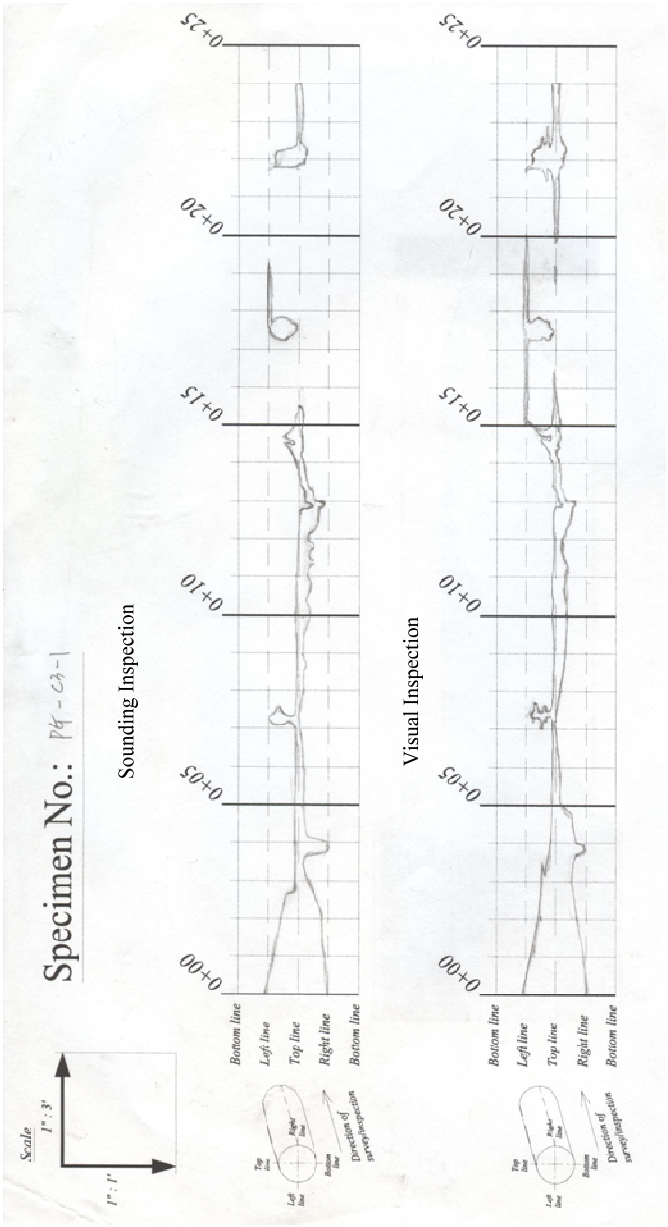

Figure A-24. Void Map of Specimen PG-C3-1.

The areas of both void profiles are estimated using AutoCAD® and provided in Table A-21.

Table A-21. Estimation of Void Profile in Specimen PG-C3-1.

Section, ft (m)	Sounding Inspection (SI), inch^2 (10^{-4} m^2)	Visual Inspection (VI), inch^2 (10^{-4} m^2)	SI - VI, inch^2 (10^{-4} m^2)
0~1 (0~0.3)	72.67 (468.9)	73.92(476.9)	-1.24 (-8.0)
1~2 (0.3~0.6)	56.95 (367.4)	57.77 (372.7)	-0.82 (-5.3)
2~3 (0.6~0.9)	35.90 (231.6)	43.46 (280.4)	-7.55 (-48.7)
3~4 (0.9~1.2)	20.97 (135.3)	38.20 (246.4)	-17.23 (-111.2)
4~5 (1.2~1.5)	15.01 (96.8)	26.25 (169.4)	-11.24 (-72.5)
5~6 (1.5~1.8)	10.47 (67.5)	10.96 (70.7)	-0.49 (-3.2)
6~7 (1.8~2.1)	7.48 (48.2)	6.41 (41.4)	1.07 (6.9)
7~8 (2.1~2.4)	14.92 (96.3)	14.63 (94.4)	0.29 (1.9)
8~9 (2.4~2.7)	8.55 (55.2)	11.47 (74.0)	-2.92 (-18.8)
9~10 (2.7~3.0)	11.45 (73.9)	15.98 (103.1)	-4.53 (-29.2)
10~11 (3.0~3.4)	15.68 (101.2)	16.74 (108.0)	-1.05 (-6.8)
11~12 (3.4~3.7)	15.79 (101.8)	13.33 (86.0)	2.46 (15.8)
12~13 (3.7~4.0)	20.46 (132.0)	18.57 (119.8)	1.90 (12.2)
13~14 (4.0~4.3)	9.44 (60.9)	9.05 (58.4)	0.39 (2.5)
14~15 (4.3~4.6)	14.42 (93.0)	17.59 (113.5)	-3.17 (-20.5)
15~16 (4.6~4.9)	3.62 (23.4)	12.38 (79.9)	-8.76 (-56.5)
16~17 (4.9~5.2)	0.00 (0.0)	6.15 (39.7)	-6.15 (-39.7)
17~18 (5.2~5.5)	16.81 (108.5)	20.46 (132.0)	-3.65 (-23.5)
18~19 (5.5~5.8)	6.40 (41.3)	6.49 (41.9)	-0.09 (-0.6)
19~20 (5.8~6.1)	1.01 (6.5)	4.14 (26.7)	-3.14 (-20.2)
20~21 (6.1~6.4)	0.00 (0.0)	6.17 (39.8)	-6.17 (-39.8)
21~22 (6.4~6.7)	6.52 (42.1)	17.16 (110.7)	-10.64 (-68.7)
22~23 (6.7~7.0)	14.11 (91.0)	23.99 (154.7)	-9.88 (-63.7)
23~24 (7.0~7.3)	7.27 (46.9)	7.83 (50.5)	-0.56 (-3.6)

The repair grout is filled from the top grout port and infiltrated to 7.3 ft (2.23 m) from the reference point (Figure A-25).

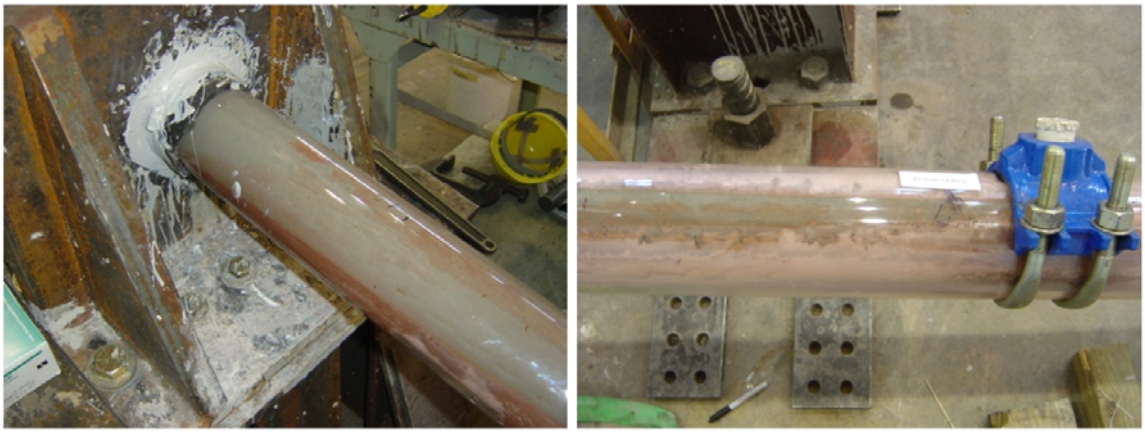

Figure A-25. Repair Grouted Ducts of Specimen PG-C3-1.

Figure A-26 shows the cross-sectional views of the cut sections obtained from Specimen PG-C3-1. From the cut sections, it is noted that the repair grout successfully replaces the main voids up to 6 ft (1.83 m) from the reference point, but after that voids were only partially repaired. The local large void #5 is filled completely by repair grout. The small voids still exist inside the initially grouted ducts, especially in-between strands. However, those voids cannot be repaired because the voids are isolated from the “bug holes” which is a route for repair grouts.

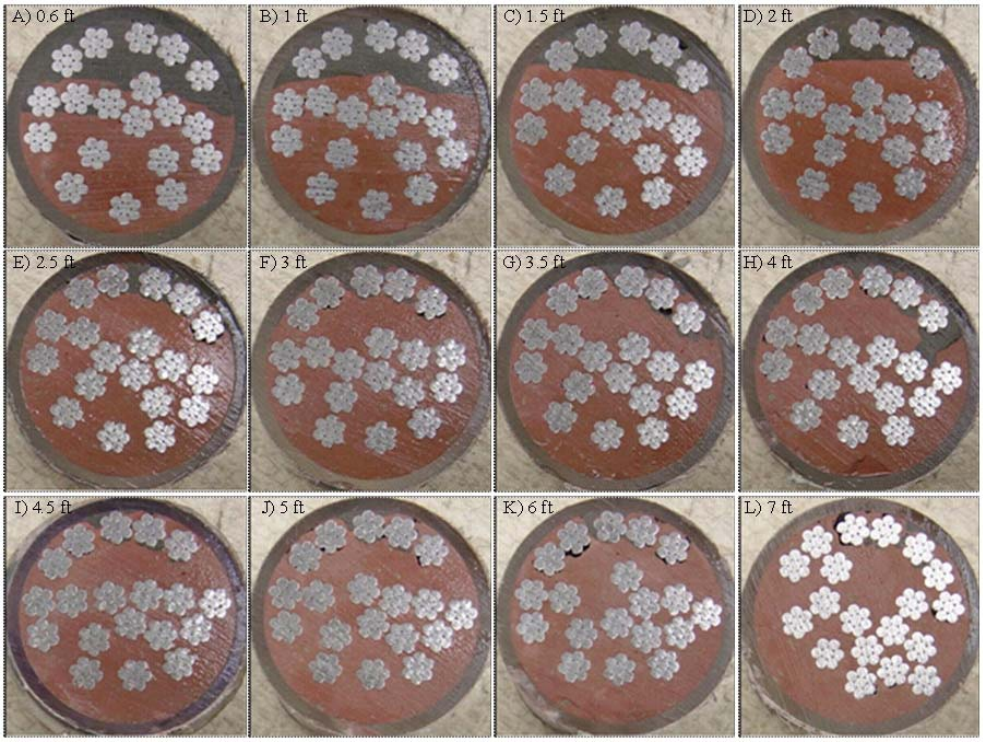

Figure A-26. Cut Sections of Specimen PG-C3-1 for the Filling Analysis of Repair Grout.

To compare the performance of repair grouts, the ratio of remaining void area after repair to the repaired area is estimated. The repaired area and area of voids after repair are calculated using AutoCAD® (Table A-22).

Table A-22. Void Area of Specimen PG-C3-1.

Cut Sections, ft (m)		Repaired Area, A_R, inch^2(10^{-4} m^2)	Void Area, A_V, inch^2(10^{-4} m^2)	Void Ratio, η (%)
A	0.6 (0.18)	2.395 (15.45)	0.0126 (0.081)	0.53
B	1 (0.30)	1.882 (12.14)	0.0089 (0.057)	0.47
C	1.5 (0.46)	1.407 (9.08)	0.0322 (0.208)	2.28
D	2 (0.61)	0.796 (5.13)	0.0032 (0.021)	0.40
E	2.5 (0.76)	0.487 (3.15)	0.0159 (0.103)	3.26
F	3 (0.91)	0.285 (1.84)	0.0080 (0.052)	2.81
G	3.5 (1.07)	0.440 (2.84)	0.0349 (0.225)	7.93
H	4 (1.22)	0.638 (4.12)	0.0120 (0.077)	1.88
I	4.5 (1.37)	0.239 (1.54)	0.0039 (0.025)	1.63
J	5 (1.52)	0.220 (1.42)	0.0094 (0.061)	4.27
K	6 (1.83)	0.188 (1.21)	0.0020 (0.013)	1.07
L	7 (2.13)	0.186 (1.20)	0.0000 (0.000)	0.00
Sum		**9.164 (59.12)**	**0.1430 (0.923)**	**1.56**

From the analysis of cut sections, the Specimen PG-C3-1 has the remaining void ratio, after repair, of 1.56% on average. The initial void area ranges over 0.1 inch^2 (0.65×10^{-4} m^2) or more about all the repaired sections. Therefore, the PG method with Class C-3 grout in Specimen PG-C3-1 has a lower FC than others.

Table A-23 shows the time schedule for sealing ducts for Specimen PG-C3-1. Total sealing time for Specimen PG-C3-1 is 3 days and 0.85 hours before applying repair grout.

Table A-23. Sealing Time Schedule of Specimen PG-C3-1.

Sealing Procedure	Working Day	Working Time (min.)
Mixing epoxy and sealing (one side)	Day 1	25
Wait	1 day	
Installing pipe saddle tap	Day 2	18
Connect pressure grout pump and reseal	Day 2	8
Sum	**2 days**	**51** **0.85 hours**

A.10. SPECIMEN PG-C3-2

Figure A-27 depicts the initial void profiles of the sounding inspection and of the visual inspection before grouting for Specimen PG-C3-2.

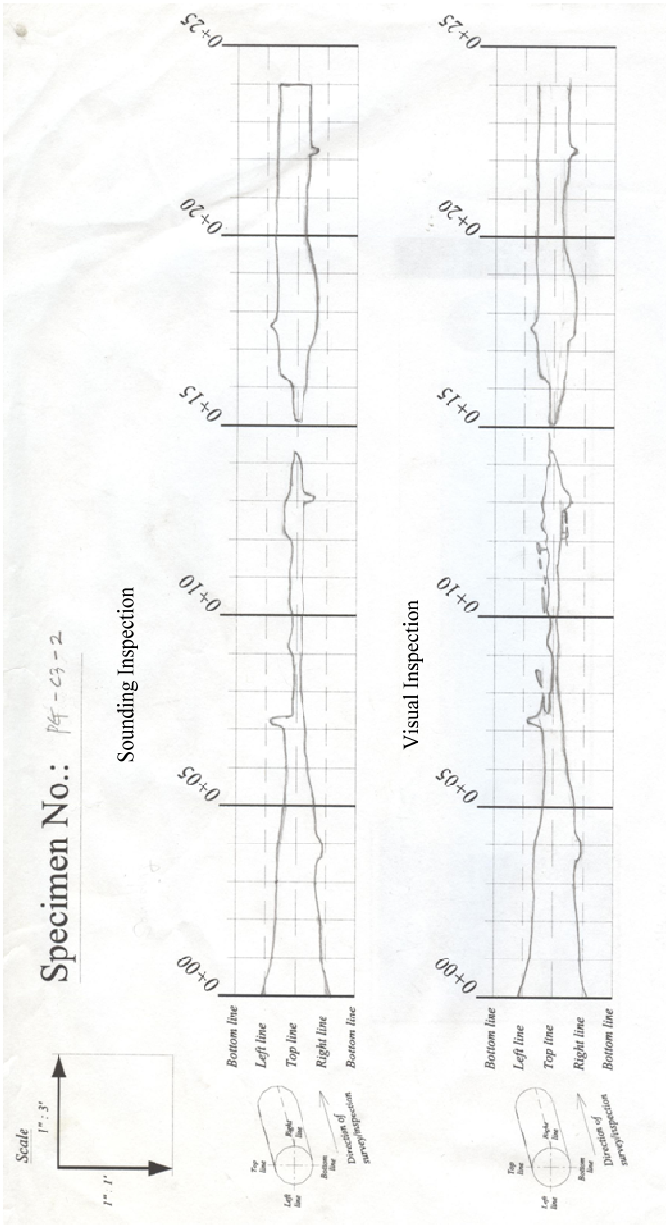

Figure A-27. Void Map of Specimen PG-C3-2.

The areas of both void profiles are estimated using AutoCAD® and provided in Table A-24.

Table A-24. Estimation of Void Profile in Specimen PG-C3-2.

Section, ft (m)	Sounding Inspection (SI), inch^2 (10^{-4} m^2)	Visual Inspection (VI), inch^2 (10^{-4} m^2)	SI - VI, inch^2 (10^{-4} m^2)
0~1 (0~0.3)	72.74 (469.3)	72.92 (470.5)	-0.18 (-1.2)
1~2 (0.3~0.6)	58.93 (380.2)	60.08 (387.6)	-1.15 (-7.4)
2~3 (0.6~0.9)	51.81 (334.2)	53.21 (343.3)	-1.40 (-9.0)
3~4 (0.9~1.2)	52.01 (335.6)	54.57 (352.0)	-2.56 (-16.5)
4~5 (1.2~1.5)	44.87 (289.5)	46.82 (302.1)	-1.96 (-12.6)
5~6 (1.5~1.8)	32.84 (211.9)	34.83 (224.7)	-1.98 (-12.8)
6~7 (1.8~2.1)	26.48 (170.9)	27.48 (117.3)	-0.99 (-6.4)
7~8 (2.1~2.4)	21.06 (135.9)	26.38 (170.2)	-5.32 (-34.3)
8~9 (2.4~2.7)	8.80 (56.8)	8.45 (54.5)	0.34 (2.2)
9~10 (2.7~3.0)	13.70 (88.4)	10.05 (64.9)	3.64 (23.5)
10~11 (3.0~3.4)	16.16 (104.3)	14.96 (96.5)	1.20 (7.8)
11~12 (3.4~3.7)	14.97 (96.6)	16.74 (108.0)	-1.77 (-11.4)
12~13 (3.7~4.0)	23.60 (152.3)	27.08 (174.7)	-3.48 (-22.4)
13~14 (4.0~4.3)	18.98 (122.5)	23.85 (153.9)	-4.86 (-31.4)
14~15 (4.3~4.6)	1.91 (12.3)	3.55 (22.9)	-1.64 (-10.6)
15~16 (4.6~4.9)	11.12 (71.8)	11.15 (71.9)	-0.02 (-0.1)
16~17 (4.9~5.2)	32.11 (207.1)	30.95 (199.6)	1.16 (7.5)
17~18 (5.2~5.5)	49.13 (316.9)	46.88 (302.5)	2.24 (14.5)
18~19 (5.5~5.8)	49.28 (317.9)	47.43 (306.0)	1.85 (11.9)
19~20 (5.8~6.1)	43.31 (279.4)	39.22 (253.0)	4.09 (26.4)
20~21 (6.1~6.4)	37.85 (244.2)	32.66 (210.7)	5.19 (33.5)
21~22 (6.4~6.7)	39.41 (254.3)	37.22 (240.1)	2.19 (14.1)
22~23 (6.7~7.0)	42.80 (276.1)	41.86 (270.1)	0.93 (6.0)
23~24 (7.0~7.3)	39.10 (252.3)	38.77 (250.1)	0.33 (2.1)

The repair grout is filled from the top grout port and infiltrated to 13.2 ft (4.02 m) from the reference point (Figure A-28).

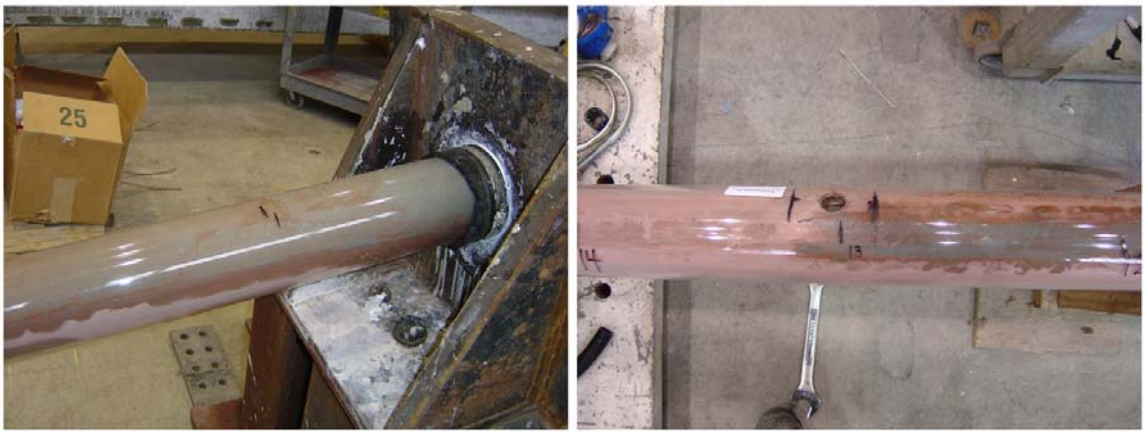

Figure A-28. Repair Grouted Ducts of Specimen PG-C3-2.

Figure A-29 shows the cross-sectional views of the cut sections obtained from Specimen PG-C3-2. From the cut sections, it is noted that the repair grouts successfully replaces the main voids up to 12 ft (3.66 m) from the reference point, but after that voids are only partially repaired. The local large void #4 and #5 are filled completely by repair grout.

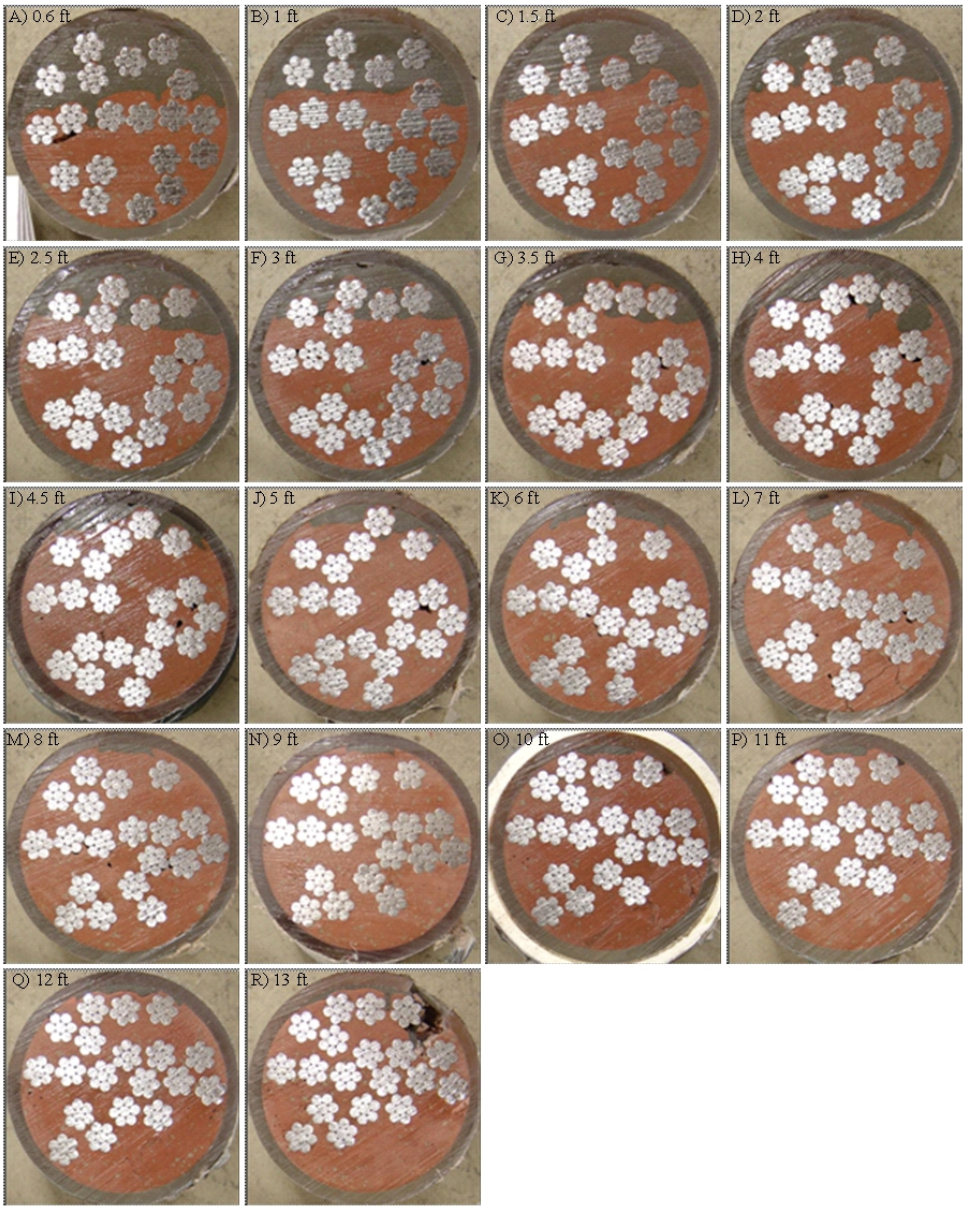

Figure A-29. Cut Sections of Specimen PG-C3-2 for the Filling Analysis of Repair Grout.

To compare the performance of repair grouts, the ratio of remaining void area after repair to the repaired area is estimated. The repaired area and area of voids after repair are calculated using AutoCAD® (Table A-25).

Table A-25. Void Area of Specimen PG-C3-2.

Cut Sections, ft (m)		Repaired Area, A_R, inch^2(10^{-4} m^2)	Void Area, A_V, inch^2(10^{-4} m^2)	Void Ratio, η (%)
A	0.6 (0.18)	2.927 (18.89)	0.0088 (0.057)	0.30
B	1 (0.30)	2.518 (16.24)	0.0400 (0.258)	1.59
C	1.5 (0.46)	2.164 (13.96)	0.0119 (0.077)	0.55
D	2 (0.61)	1.927 (12.43)	0.0027 (0.017)	0.14
E	2.5 (0.76)	1.771 (11.43)	0.0083 (0.054)	0.47
F	3 (0.91)	1.509 (9.74)	0.0324 (0.209)	2.15
G	3.5 (1.07)	1.319 (8.51)	0.0261 (0.168)	1.98
H	4 (1.22)	1.336 (8.62)	0.0046 (0.030)	0.34
I	4.5 (1.37)	0.764 (4.93)	0.0128 (0.083)	1.68
J	5 (1.52)	0.630 (4.06)	0.0106 (0.068)	1.68
K	6 (1.83)	0.374 (2.42)	0.0084 (0.054)	2.24
L	7 (2.13)	0.349 (2.25)	0.0031 (0.020)	0.89
M	8 (2.44)	0.188 (1.22^2)	0.0022 (0.014)	1.17
N	9 (2.74)	0.141 (0.91)	0.0000 (0.000)	0.00
O	10 (3.05)	0.180 (1.16)	0.0005 (0.003)	0.28
P	11 (3.35)	0.160 (1.04)	0.0016 (0.010)	1.00
Q	12 (3.66)	0.227 (1.46)	0.0061 (0.039)	2.69
R	13 (3.96)	0.297 (1.92)	0.0043 (0.028)	1.45
Sum		**18.781 (121.17)**	**0.1844 (1.190)**	**0.98**

From the analysis of cut sections, the Specimen PG-C3-2 has the remaining void ratio, after repair, of 0.98% on average. The initial void area ranges over 0.1 inch^2 (0.65×10^{-4} m^2) or more about all the repaired sections. Therefore, the PG method with Class C-3 grout in Specimen PG-C3-2 has a lower FC than others.

Table A-26 shows the time schedule of sealing ducts for Specimen PG-C3-2. Total sealing time for Specimen PG-C3-2 is 2 days and 0.97 hours before applying repair grout.

Table A-26. Sealing Time Schedule of Specimen PG-C3-2.

Sealing Procedure	Working Day	Working Time (min.)
Installing pipe saddle tap	Day 1	25
Connect hose and silicone sealing	Day 1	6
Mixing epoxy and sealing	Day 1	20
Wait	1 day	
Connect pressure grout pump and reseal	Day 2	7
Sum	**2 days**	**58 (0.97 hours)**

A.11. SPECIMEN PVG-C1-1

The initial void profiles produced by using both sounding inspection and visual inspection before repair grouting is shown in Figure A-30.

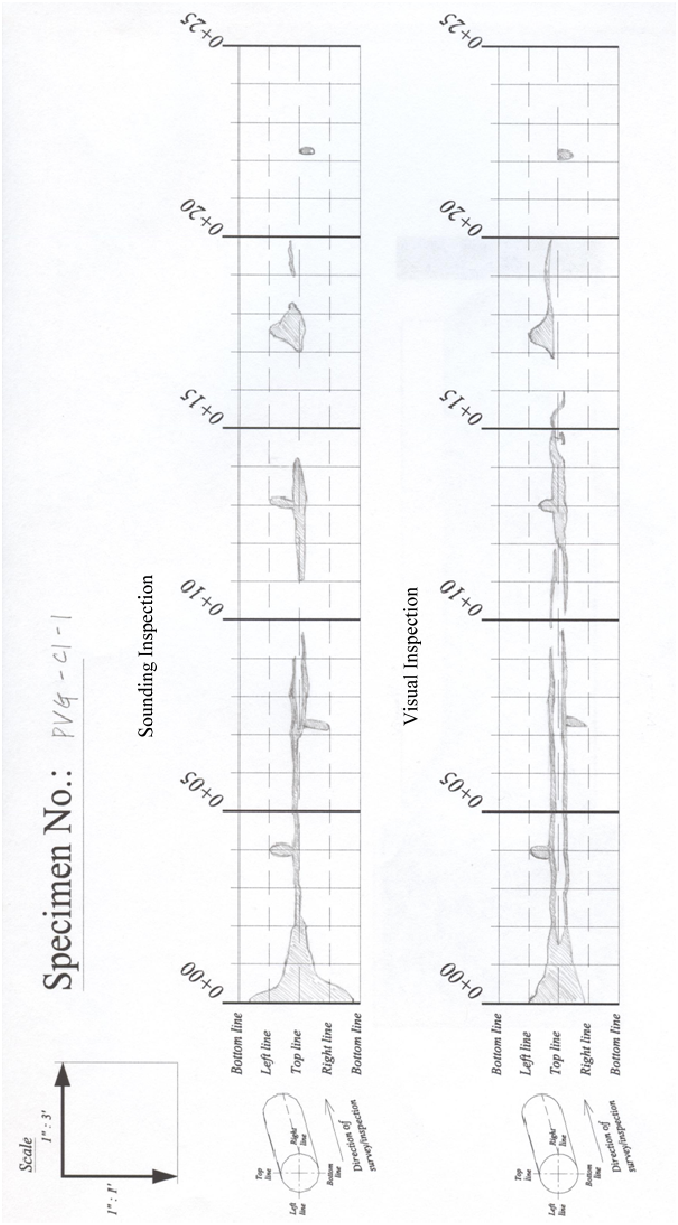

Figure A-30. Void Map of Specimen PVG-C1-1.

The areas of both void profiles are estimated using AutoCAD® and provided in Table A-27.

Table A-27. Estimation of Void Profile in Specimen PVG-C1-1.

Section, ft (m)	Sounding Inspection (SI), inch^2 (10^{-4} m^2)	Visual Inspection (VI), inch^2 (10^{-4} m^2)	SI - VI, inch^2 (10^{-4} m^2)
0~1 (0~0.3)	73.52 (474.3)	50.94 (328.7)	22.58 (145.6)
1~2 (0.3~0.6)	23.95 (154.5)	24.55 (158.4)	-0.61 (-3.9)
2~3 (0.6~0.9)	7.42 (47.8)	10.66 (68.8)	-3.24 (-20.9)
3~4 (0.9~1.2)	10.22 (65.9)	16.48 (106.3)	-6.26 (-40.4)
4~5 (1.2~1.5)	9.01 (58.1)	14.04 (90.6)	-5.03 (-32.4)
5~6 (1.5~1.8)	6.75 (43.5)	12.58 (81.1)	-5.83 (-37.6)
6~7 (1.8~2.1)	7.66 (49.4)	11.68 (75.3)	-4.02 (-25.9)
7~8 (2.1~2.4)	19.56 (126.2)	17.61 (113.6)	1.95 (12.6)
8~9 (2.4~2.7)	12.48 (80.5)	12.02 (77.5)	0.46 (3.0)
9~10 (2.7~3.0)	2.83 (18.2)	4.60 (29.7)	-1.77 (-11.4)
10~11 (3.0~3.4)	0.00 (0.0)	7.09 (45.7)	-7.08 (-45.7)
11~12 (3.4~3.7)	8.51 (54.9)	10.51 (67.8)	-1.99 (-12.9)
12~13 (3.7~4.0)	14.37 (92.7)	16.14 (104.1)	-1.77 (-11.4)
13~14 (4.0~4.3)	19.21 (124.0)	17.42 (112.4)	1.80 (11.6)
14~15 (4.3~4.6)	1.56 (10.1)	11.39 (73.5)	-9.84 (-63.5)
15~16 (4.6~4.9)	0.00 (0.0)	4.57 (29.5)	-4.57 (-29.5)
16~17 (4.9~5.2)	0.00 (0.0)	0.52 (3.4)	-0.52 (-3.4)
17~18 (5.2~5.5)	28.38 (183.1)	19.75 (127.4)	8.63 (55.7)
18~19 (5.5~5.8)	3.32 (21.4)	5.25 (33.8)	-1.93 (-12.4)
19~20 (5.8~6.1)	4.48 (28.9)	4.47 (28.8)	0.01 (0.1)
20~21 (6.1~6.4)	0.00 (0.0)	0.00 (0.0)	0.00 (0.0)
21~22 (6.4~6.7)	0.00 (0.0)	0.00 (0.0)	0.00 (0.0)
22~23 (6.7~7.0)	2.55 (16.4)	4.23 (27.3)	-1.68 (-10.8)
23~24 (7.0~7.3)	0.00 (0.0)	0.00 (0.0)	0.00 (0.0)

The repair grout is filled from the top grout port and infiltrated to 15.0 ft (4.57 m) from the reference point (Figure A-31).

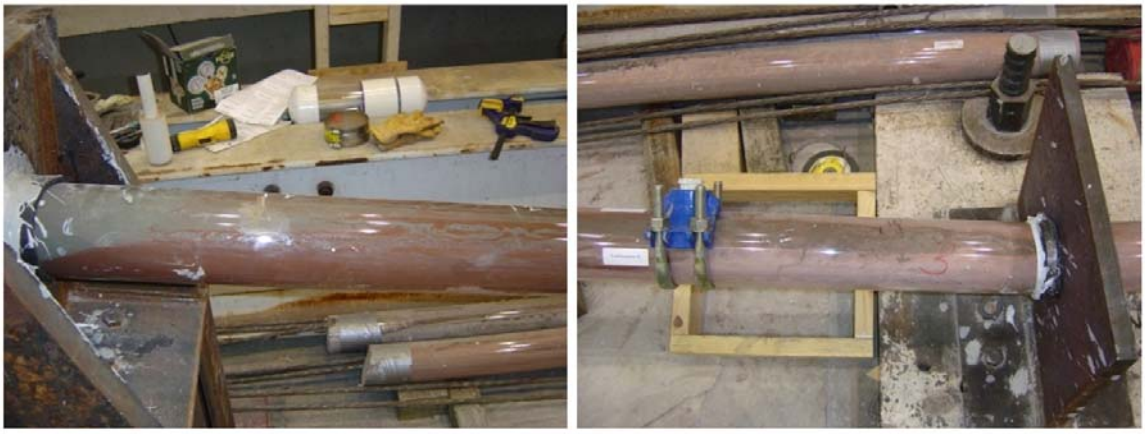

Figure A-31. Repair Grouted Ducts of Specimen PVG-C1-1.

Figure A-32 shows the cross-sectional views of the cut sections obtained from Specimen PVG-C1-1. From the cut sections, it is noted that the repair grout successfully replaces the main voids and repairs local large voids #3, #4, and #5. The small voids still exist inside the initially grouted ducts, especially in-between strands. However, those voids could not be repaired because the voids are isolated from the “bug holes” which is a route for repair grouts.

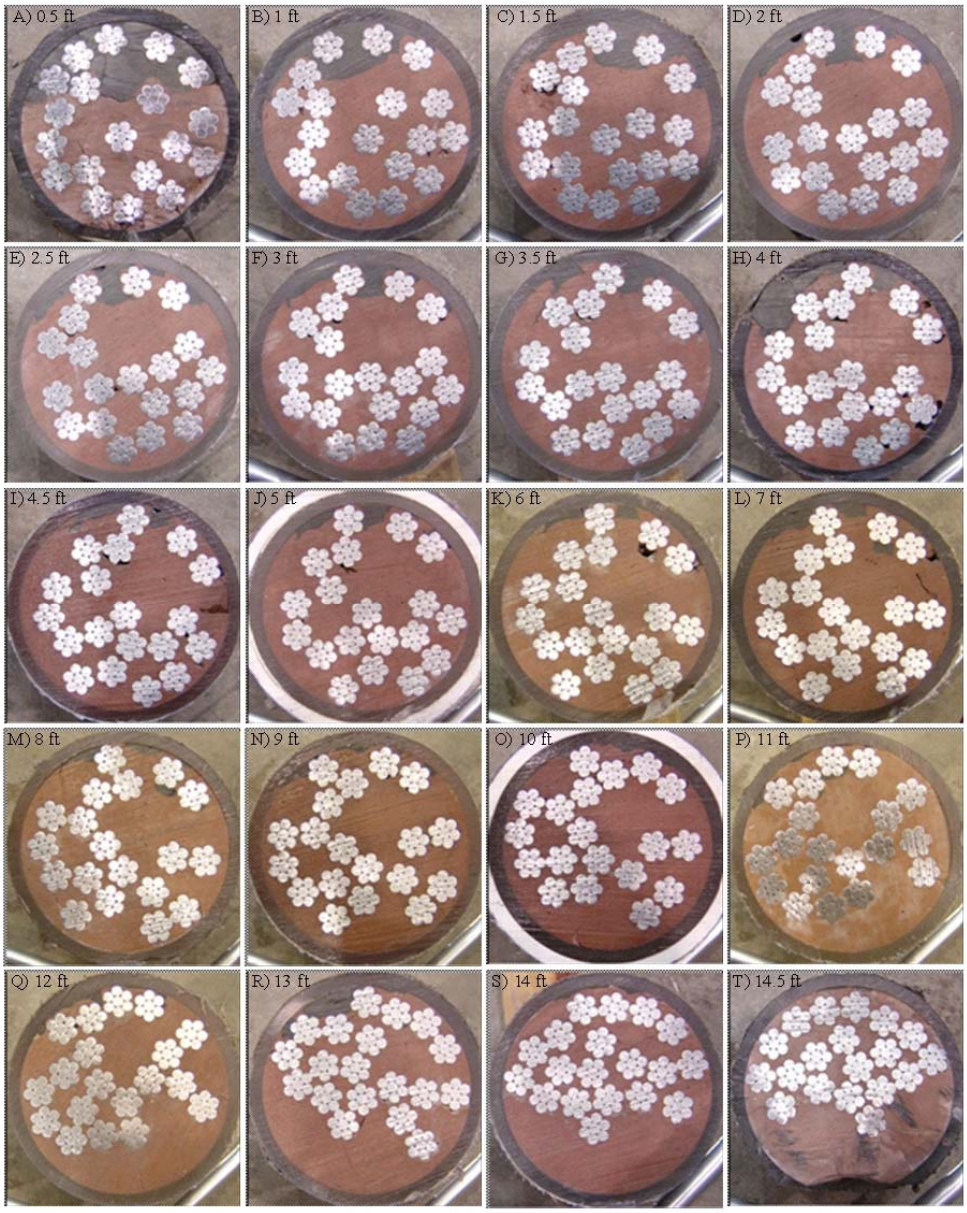

Figure A-32. Cut Sections of Specimen PVG-C1-1 for the Filling Analysis of Repair Grout.

To compare the performance of repair grouts, the ratio of remaining void area after repair to the repaired area is estimated. The repaired area and area of voids after repair are calculated using AutoCAD® (Table A-28).

Table A-28. Void Area of Specimen PVG-C1-1.

Cut Sections, ft (m)		Repaired Area, A_R, inch^2(10^{-4} m^2)	Void Area, A_V, inch^2(10^{-4} m^2)	Void Ratio, η (%)
A	0.5 (0.15)	2.280 (14.71)	0.0000 (0.000)	0.00
B	1 (0.30)	1.247 (8.05)	0.0000 (0.000)	0.00
C	1.5 (0.46)	0.871 (5.62)	0.0003 (0.002)	0.03
D	2 (0.61)	0.786 (5.07)	0.0264 (0.170)	3.36
E	2.5 (0.76)	0.714 (4.61)	0.0111 (0.072)	1.55
F	3 (0.91)	0.599 (3.87)	0.0000 (0.000)	0.00
G	3.5 (1.07)	0.491 (3.17)	0.0034 (0.022)	0.69
H	4 (1.22)	1.047 (6.75)	0.0039 (0.025)	0.37
I	4.5 (1.37)	0.408 (2.64)	0.0075 (0.048)	1.84
J	5 (1.52)	0.427 (2.75)	0.0044 (0.028)	1.03
K	6 (1.83)	0.284 (1.84)	0.0023 (0.015)	0.81
L	7 (2.13)	0.421 (2.72)	0.0012 (0.008)	0.29
M	8 (2.44)	0.327 (2.09)	0.0032 (0.021)	0.99
N	9 (2.74)	0.257 (1.66)	0.0047 (0.030)	1.83
O	10 (3.05)	0.156 (1.01)	0.0007 (0.005)	0.45
P	11 (3.35)	0.145 (0.94)	0.0000 (0.000)	0.00
Q	12 (3.66)	0.225 (1.45)	0.0000 (0.000)	0.00
R	13 (3.96)	0.552 (3.56)	0.0057 (0.037)	1.03
S	14 (4.27)	0.126 (0.81)	0.0004 (0.003)	0.32
T	14.5 (4.42)	0.051 (0.33)	0.0000 (0.000)	0.00
Sum		**11.413 (73.63)**	**0.0752 (0.485)**	**0.66**

From the analysis, remaining voids in the repair grout are estimated in each cut section; however, the void ratio in a section can be magnified when the remaining voids exist in a small repaired area. Thus, the filling performance for Specimen PVG-C1-1 is evaluated using the summation of estimated sections for Specimen PVG-C1-1. The remaining void ratio, after repair, obtained from the analysis comes out to be 0.66% for Specimen PVG-C1-1. The initial void area which is the repaired area as shown in Table

A-28 ranges over 0.1 inch^2 (0.65×10^{-4} m^2) or more by the Section S, however, the voids include small voids from the Section T.

Table A-29 shows the time schedule of sealing ducts and preparation of repair grouting for Specimen PVG-C1-1. Total sealing time for Specimen PVG-C1-1 is 5 days and 2.83 hours before applying repair grout.

Table A-29. Sealing Time Schedule of Specimen PVG-C1-1.

Sealing Procedure	Working Day	Working Time (min.)
Setting rubber end caps and sealing with silicone	Day 1	20
Installing pipe saddle tap with grease	Day 1	40
Mixing epoxy and sealing	Day 2	35
Wait	1 day	
Checking air-tight condition	Day 3	15
Searching leaking part and sealing	Day 3	20
Connect grout hose and checking air-tight condition	Day 4	20
Sealing with RTV silicone	Day 4	15
Checking air-tight condition and sealing	Day 4	5
Sum	**4 days**	**170 (2.83 hours)**

A.12. SPECIMEN PVG-C1-2

Figure A-33 shows depicts the initial void profiles of the sounding inspection and of the visual inspection before grouting for Specimen PVG-C1-2.

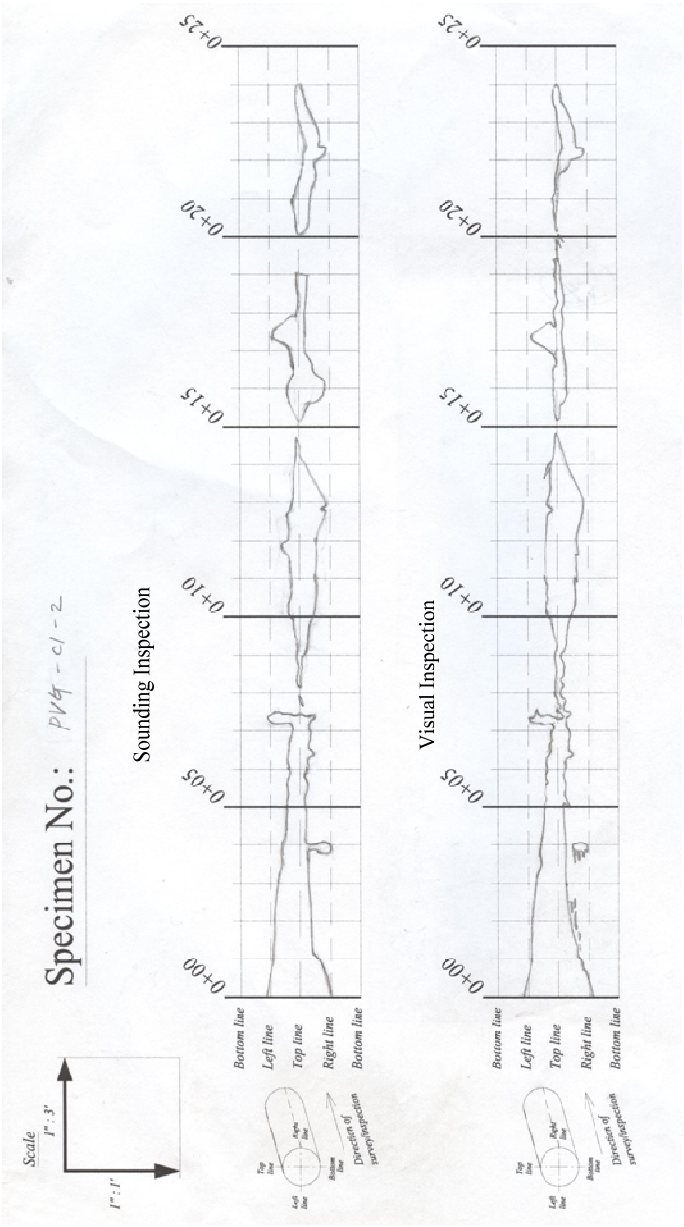

Figure A-33. Void Map of Specimen PVG-C1-2.

The areas of both void profiles are estimated using AutoCAD® and provided in Table A-27.

Table A-30. Estimation of Void Profile in Specimen PVG-C1-2.

Section, ft (m)	Sounding Inspection (SI), inch^2 (10^{-4} m^2)	Visual Inspection (VI), inch^2 (10^{-4} m^2)	SI - VI, inch^2 (10^{-4} m^2)
0~1 (0~0.3)	70.27 (453.4)	74.65 (481.6)	-4.38 (-28.3)
1~2 (0.3~0.6)	48.21 (311.0)	56.19 (362.5)	-7.97 (-51.4)
2~3 (0.6~0.9)	43.16 (278.5)	45.58 (294.1)	-2.42 (-15.6)
3~4 (0.9~1.2)	40.05 (258.4)	39.65 (255.8)	0.41 (2.6)
4~5 (1.2~1.5)	27.25 (175.8)	27.88 (179.9)	-0.63 (-4.1)
5~6 (1.5~1.8)	23.55 (152.0)	24.86 (160.4)	-1.31 (-8.5)
6~7 (1.8~2.1)	26.48 (170.9)	24.44 (157.7)	2.04 (13.2)
7~8 (2.1~2.4)	18.07 (116.5)	18.63 (120.2)	-0.56 (-3.6)
8~9 (2.4~2.7)	3.91 (25.2)	8.93 (57.6)	-5.02 (-32.4)
9~10 (2.7~3.0)	17.10 (110.3)	16.00 (103.2)	1.09 (7.1)
10~11 (3.0~3.4)	32.90 (212.3)	35.23 (227.3)	-2.33 (-15.0)
11~12 (3.4~3.7)	36.88 (237.9)	40.07 (258.5)	-3.19 (-20.6)
12~13 (3.7~4.0)	41.71 (269.1)	40.93 (264.1)	0.78 (5.0)
13~14 (4.0~4.3)	28.29 (182.5)	33.71 (217.5)	-5.42 (-35.0)
14~15 (4.3~4.6)	3.84 (24.8)	8.29 (53.5)	-4.45 (-28.7)
15~16 (4.6~4.9)	23.36 (150.7)	8.80 (56.7)	14.57 (94.0)
16~17 (4.9~5.2)	31.02 (200.1)	14.80 (95.5)	16.22 (104.6)
17~18 (5.2~5.5)	29.35 (189.4)	24.81 (160.1)	4.54 (29.3)
18~19 (5.5~5.8)	11.09 (71.5)	8.30 (53.6)	2.78 (18.0)
19~20 (5.8~6.1)	0.17 (1.1)	4.79 (30.9)	-4.62 (-29.8)
20~21 (6.1~6.4)	16.61 (107.2)	3.62 (23.3)	12.99 (83.8)
21~22 (6.4~6.7)	18.73 (120.8)	7.60 (49.0)	11.13 (71.8)
22~23 (6.7~7.0)	20.83 (134.4)	21.24 (137.0)	-0.41 (-2.7)
23~24 (7.0~7.3)	12.67 (81.8)	11.80 (76.1)	0.88 (5.7)

The repair grout is filled from the top grout port and infiltrated to 14.5 ft (4.42 m) from the reference point (Figure A-34).

Figure A-34. Repair Grouted Ducts of Specimen PVG-C1-2.

Figure A-35 shows the cross-sectional views of the cut sections obtained from Specimen PVG-C1-2. From the cut sections, it is noted that the repair grouts successfully replaces the main voids and repairs local large voids #3, #4, and #5. The small voids still exist inside the initially grouted ducts, especially in-between strands.

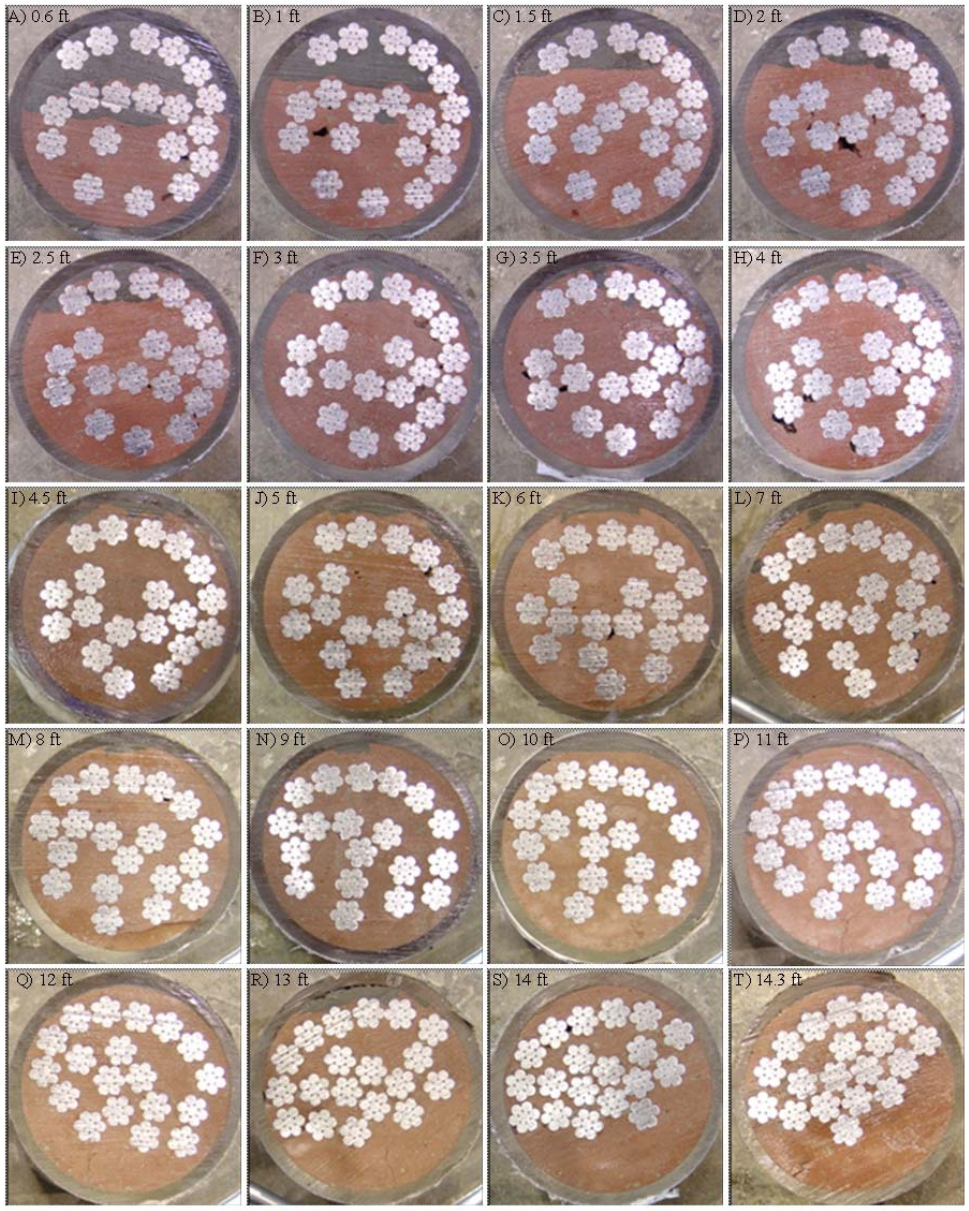

Figure A-35. Cut Sections of Specimen PVG-C1-2 for the Filling Analysis of Repair Grout.

To compare the performance of repair grouts, the ratio of remaining void area after repair to the repaired area is estimated. The repaired area and area of voids after repair are calculated using AutoCAD® (Table A-31).

Table A-31. Void Area of Specimen PVG-C1-2.

Cut Sections, ft (m)		Repaired Area, A_R, inch^2(10^{-4} m^2)	Void Area, A_V, inch^2(10^{-4} m^2)	Void Ratio, η (%)
A	0.6 (0.18)	2.981 (19.23)	0.0015 (0.010)	0.05
B	1 (0.30)	2.060 (13.29)	0.0010 (0.006)	0.05
C	1.5 (0.46)	1.110 (7.16)	0.0022 (0.014)	0.20
D	2 (0.61)	0.844 (5.44)	0.0008 (0.005)	0.09
E	2.5 (0.76)	0.716 (4.62)	0.0000 (0.000)	0.00
F	3 (0.91)	0.559 (3.61)	0.0000 (0.000)	0.00
G	3.5 (1.07)	0.419 (2.70)	0.0011 (0.007)	0.26
H	4 (1.22)	0.587 (3.79)	0.0028 (0.018)	0.48
I	4.5 (1.37)	0.299 (1.93)	0.0000 (0.000)	0.00
J	5 (1.52)	0.350 (2.26)	0.0028 (0.018)	0.80
K	6 (1.83)	0.253 (1.63)	0.0042 (0.027)	1.66
L	7 (2.13)	0.276 (1.78)	0.0058 (0.037)	2.10
M	8 (2.44)	0.125 (0.81)	0.0003 (0.002)	0.24
N	9 (2.74)	0.113 (0.73)	0.0000 (0.000)	0.00
O	10 (3.05)	0.273 (1.76)	0.0000 (0.000)	0.00
P	11 (3.35)	0.191 (1.23)	0.0003 (0.002)	0.16
Q	12 (3.66)	0.166 (1.07)	0.0000 (0.000)	0.00
R	13 (3.96)	0.615 (3.97)	0.0560 (0.361)	9.10
S	14 (4.27)	0.057 (0.37)	0.0016 (0.010)	2.81
T	14.3 (4.37)	0.021 (0.13)	0.0000 (0.000)	0.00
Sum		**12.013 (77.50)**	**0.0804 (0.519)**	**0.67**

The remaining void ratio, after repair, obtained from the analysis comes out to be 0.67% for Specimen PVG-C1-2. The initial void area ranges over 0.1 inch^2 (0.65×10^{-4} m^2) or more from the reference point to Section R, however, the voids include small contributions from Section S.

At first, the Specimen PVG-C1-2 was prepared for the VG method; however, it was replaced with the PVG method because it was not possible to create an air-tight condition. The Specimen took 9 days and 12.53 hours for preparation, but it was still leaking (See Table A-32). Although the preparation of VG method was failed, the sealing time schedule is considered at the analysis for economic feasibility because it shows the worst case for application of the VG method.

Table A-32. Fail to Prepare VG Methods in Specimen PVG-C1-2.

Sealing Procedure	Working Day	Working Time (min.)
Installing pipe saddle tap with grease	Day 1	35
Silicone and epoxy sealing	Day 1	40
Wait	1 day	
Setting rubber end caps and sealing with silicone	Day 2	15
Assemble T-connection and check air-tight condition	Day 3	40
Reassemble T-connection and change ball valve	Day 3	90
RTV silicone sealing and check air-tight condition	Day 3	40
Wait	1 day	
Check air-tight and silicone sealing	Day 4	45
Check air-tight and silicone sealing	Day 4	45
Epoxy mixing and sealing	Day 4	25
Wait	1 day	
Check air-tight and RTV silicone sealing	Day 5	36
Check air-tight, scrape epoxy, and seal with epoxy	Day 6	63
Retighten caps in pipe saddle tap using taflon tape	Day 6	19
Check air-tight and seal with epoxy and RTV silicone	Day 7	55
Check air-tight condition and seal with RTV silicone	Day 7	19
Epoxy mixing and sealing	Day 7	30
Check air-tight condition and reset end rubber caps	Day 8	30
Check air-tight and reinstall T-connection	Day 8	65
Checking air-tight condition and sealing	Day 8	18
Epoxy mixing and sealing	Day 8	32
Check air-tight condition	Day 9	10
FAIL to prepare VG method	**9 days**	**752 (12.53 hours)**

Table A-34 shows the time schedule of sealing ducts for Specimen PVG-C1-2. In the time schedule, the sealing procedures at day 2 are for replacing works with PVG method. The procedurs of epoxy sealing and setting end caps in Table A-32 are included in the sealing time schedule of Specimen PVG-C1-2. Total sealing time of PVG method for Specimen PVG-C1-2 is 2 days and 1.57 hours before applying repair grouts.

Table A-33. Sealing Time Schedule of Specimen PVG-C1-2.

Sealing Procedure	**Working Day**	**Working Time (min.)**
Setting rubber end caps and sealing with silicone	Day 1	15
Silicone and epoxy sealing	Day 1	40
Wait	1 day	
Connect hose and seal by silicone	Day 2	9
Connect vacuum safety device	Day 2	5
Reconnect pipe saddle tap with grease	Day 2	20
Check air-tight condition	Day 2	5
Sum	**2 days**	**94 (1.57 hours)**

A.13. SPECIMEN PVG-C2-1

Figure A-36 depicts the initial void profiles of the sounding inspection and of the visual inspection before grouting for Specimen PVG-C2-1.

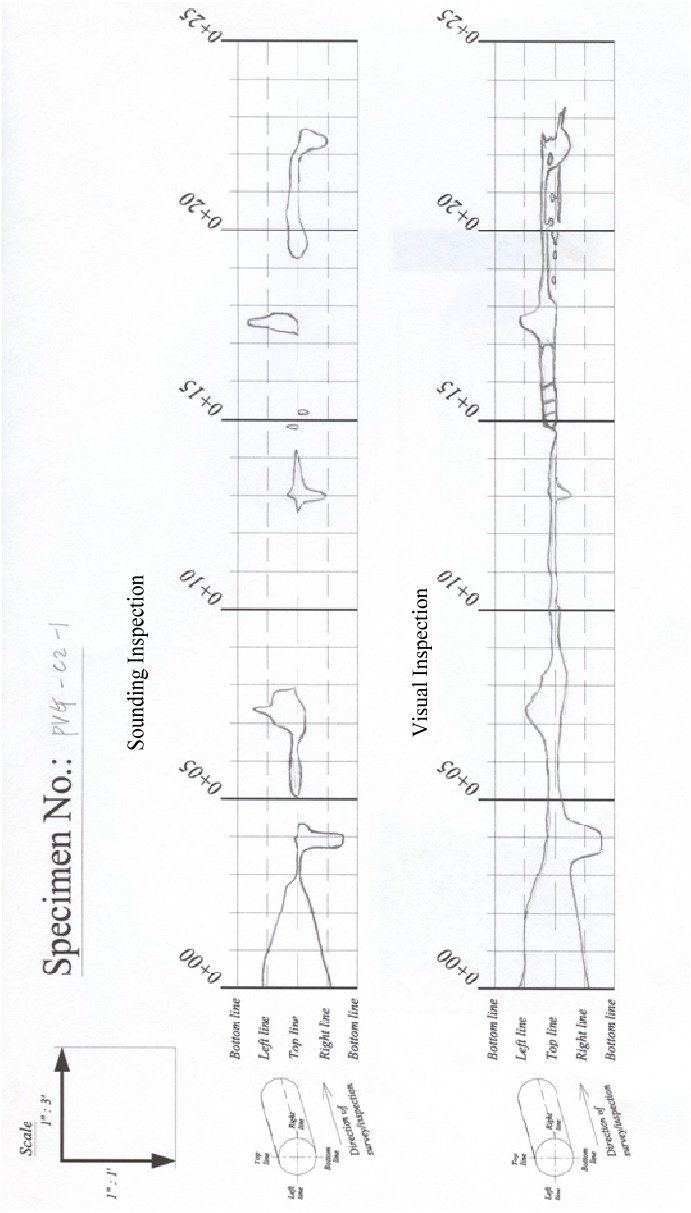

Figure A-36. Void Map of Specimen PVG-C2-1.

The areas of both void profiles are estimated using AutoCAD® and provided in Table A-34.

Table A-34. Estimation of Void Profile in Specimen PVG-C2-1.

Section, ft (m)	Sounding Inspection (SI), inch^2 (10^{-4} m^2)	Visual Inspection (VI), inch^2 (10^{-4} m^2)	SI - VI, inch^2 (10^{-4} m^2)
0~1 (0~0.3)	77.31 (498.8)	77.20 (498.1)	0.11 (0.7)
1~2 (0.3~0.6)	53.37 (344.3)	68.84 (444.1)	-15.48 (-99.8)
2~3 (0.6~0.9)	24.90 (160.6)	53.52 (345.3)	-28.62 (-184.7)
3~4 (0.9~1.2)	22.27 (143.7)	54.66 (352.7)	-32.39 (-209.0)
4~5 (1.2~1.5)	7.85 (50.7)	37.27 (240.5)	-29.42 (-189.8)
5~6 (1.5~1.8)	12.25 (79.0)	14.67 (94.6)	-2.42 (-15.6)
6~7 (1.8~2.1)	16.12 (104.0)	21.26 (137.2)	-5.14 (-33.2)
7~8 (2.1~2.4)	35.06 (226.2)	40.29 (259.9)	-5.23 (-33.8)
8~9 (2.4~2.7)	0.00 (0.0)	22.31 (144.0)	-22.31 (-144.0)
9~10 (2.7~3.0)	0.00 (0.0)	11.42 (73.7)	-11.42 (-73.7)
10~11 (3.0~3.4)	0.00 (0.0)	8.68 (56.0)	-8.68 (-56.0)
11~12 (3.4~3.7)	0.00 (0.0)	7.91 (51.1)	-7.91 (-51.1)
12~13 (3.7~4.0)	7.47 (48.2)	7.08 (45.7)	0.40 (2.6)
13~14 (4.0~4.3)	15.39 (99.3)	12.33 (79.6)	3.06 (19.8)
14~15 (4.3~4.6)	2.35 (15.2)	6.66 (43.0)	-4.31 (-27.8)
15~16 (4.6~4.9)	1.23 (8.0)	10.85 (70.0)	-9.62 (-62.0)
16~17 (4.9~5.2)	0.00 (0.0)	7.97 (51.4)	-7.97 (-51.4)
17~18 (5.2~5.5)	22.18 (143.1)	32.23 (207.9)	-10.05 (-64.8)
18~19 (5.5~5.8)	0.00 (0.0)	12.54 (80.9)	-12.54 (-80.9)
19~20 (5.8~6.1)	15.14 (97.7)	9.54 (61.5)	5.60 (36.1)
20~21 (6.1~6.4)	15.88 (102.5)	12.16 (78.5)	3.72 (24.0)
21~22 (6.4~6.7)	11.53 (74.4)	13.96 (90.1)	-2.43 (-15.7)
22~23 (6.7~7.0)	16.57 (106.9)	19.87 (128.2)	-3.30 (-21.3)
23~24 (7.0~7.3)	0.00 (0.0)	0.86 (5.5)	-0.86 (-5.5)

The repair grout is filled from the top grout port and infiltrated to 14.4 ft (4.39 m) from the reference point (Figure A-37).

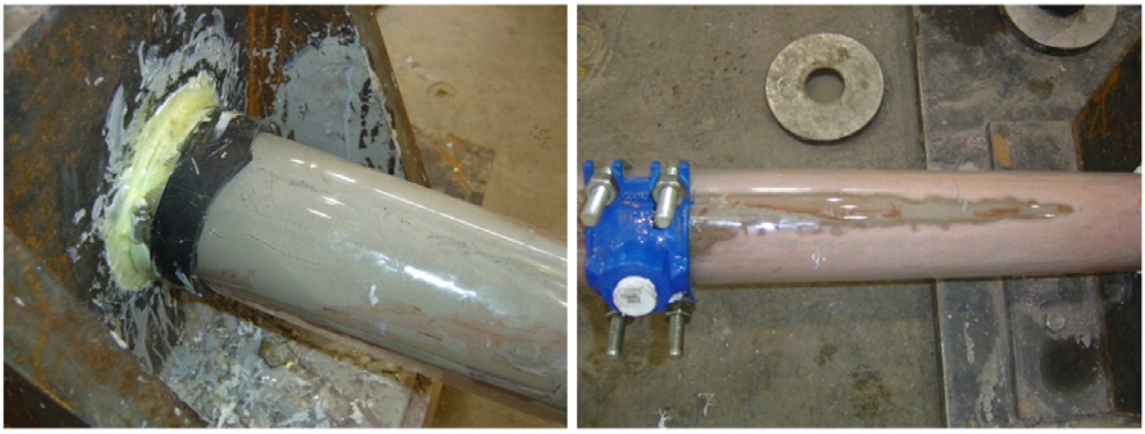

Figure A-37. Repair Grouted Ducts of Specimen PVG-C2-1.

Figure A-38 shows the cross-sectional views of the cut sections obtained from Specimen PVG-C2-1. From the cut sections, it is noted that the repair grout successfully replaces the main voids and repairs local large voids #3, #4, and #5.

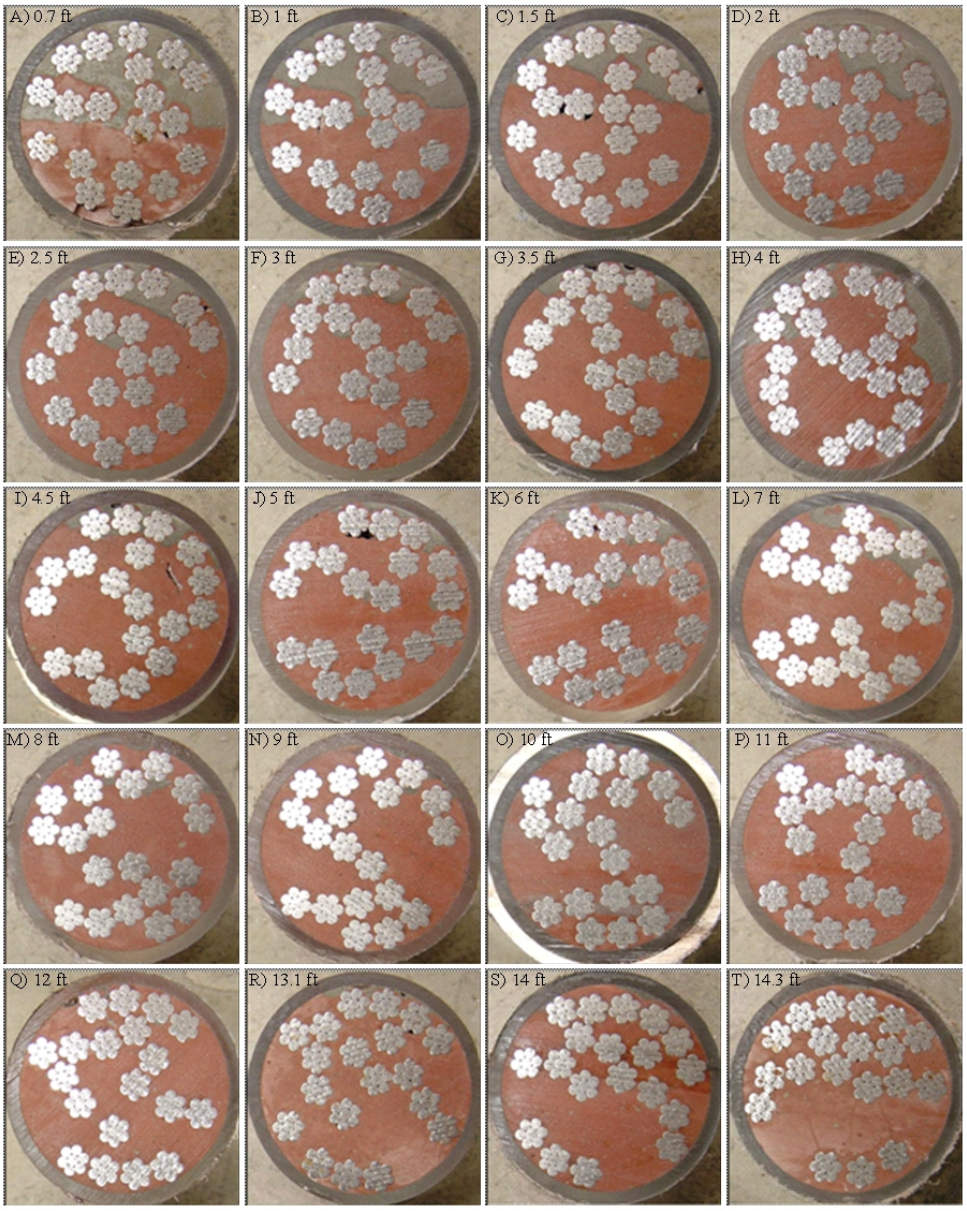

Figure A-38. Cut Sections of Specimen PVG-C2-1 for the Filling Analysis of Repair Grout.

To compare the performance of repair grouts, the ratio of remaining void area after repair to the repaired area is estimated. The repaired area and area of voids after repair are calculated using AutoCAD® (Table A-35).

Table A-35. A.5 Void Area of Specimen PVG-C2-1.

Cut Sections, ft (m)		Repaired Area, A_R, inch^2(10^{-4} m^2)	Void Area, A_V, inch^2(10^{-4} m^2)	Void Ratio, η (%)
A	0.7 (0.20)	2.980 (19.23)	0.0064 (0.041)	0.21
B	1 (0.30)	2.503 (16.15)	0.0073 (0.047)	0.29
C	1.5 (0.46)	1.613 (10.41)	0.0101 (0.065)	0.63
D	2 (0.61)	1.233 (7.95)	0.0028 (0.018)	0.23
E	2.5 (0.76)	0.943 (6.08)	0.0071 (0.046)	0.75
F	3 (0.91)	0.631 (4.07)	0.0015 (0.010)	0.24
G	3.5 (1.07)	0.557 (3.59)	0.0361 (0.233)	6.49
H	4 (1.22)	1.443 (9.31)	0.0062 (0.040)	0.43
I	4.5 (1.37)	0.521 (3.36)	0.0161 (0.104)	3.09
J	5 (1.52)	0.390 (2.52)	0.0013 (0.008)	0.33
K	6 (1.83)	0.593 (3.82)	0.0025 (0.016)	0.42
L	7 (2.13)	0.774 (4.99)	0.0000 (0.000)	0.00
M	8 (2.44)	0.314 (2.03)	0.0000 (0.000)	0.00
N	9 (2.74)	0.204 (1.31)	0.0000 (0.000)	0.00
O	10 (3.05)	0.162 (1.05)	0.0000 (0.000)	0.00
P	11 (3.35)	0.236 (1.52)	0.0023 (0.015)	0.98
Q	12 (3.66)	0.166 (1.07)	0.0281 (0.181)	16.98
R	13.1 (3.99)	0.253 (1.63)	0.0160 (0.103)	6.33
S	14 (4.27)	0.151 (0.98)	0.0005 (0.003)	0.33
T	14.3 (4.37)	0.053 (0.34)	0.0000 (0.000)	0.00
Sum		**15.717 (101.40)**	**0.1443 (0.931)**	**0.92**

From the analysis of cut sections, the Specimen PVG-C2-1 has the remaining void ratio, after repair, of 0.92% on average. The initial void area ranges over 0.1 inch^2 (0.65×10^{-4} m^2) or more from the reference point to Section S, however, the voids include small contributions from Section T.

Table A-36 shows the time schedule for sealing ducts and preparation of repair grouting for Specimen PVG-C2-1. Total sealing time for Specimen PVG-C2-1 is 1 day and 2.33 hours before applying repair grout.

Table A-36. Sealing Time Schedule of Specimen PVG-C2-1.

Sealing Procedure	Working Day	Working Time (min.)
Setting rubber end caps and sealing with silicone	Day 1	20
Installing pipe saddle tap with grease	Day 1	30
Checking air-tight condition	Day 1	20
Searching leaking part and sealing	Day 1	50
Connect grout hose and checking air-tight condition	Day 1	20
Sum	**1 day**	**140 (2.33 hours)**

A.14. SPECIMEN PVG-C2-2

Figure A-39 depicts the initial void profiles of the sounding inspection and of the visual inspection before grouting for Specimen PVG-C2-2.

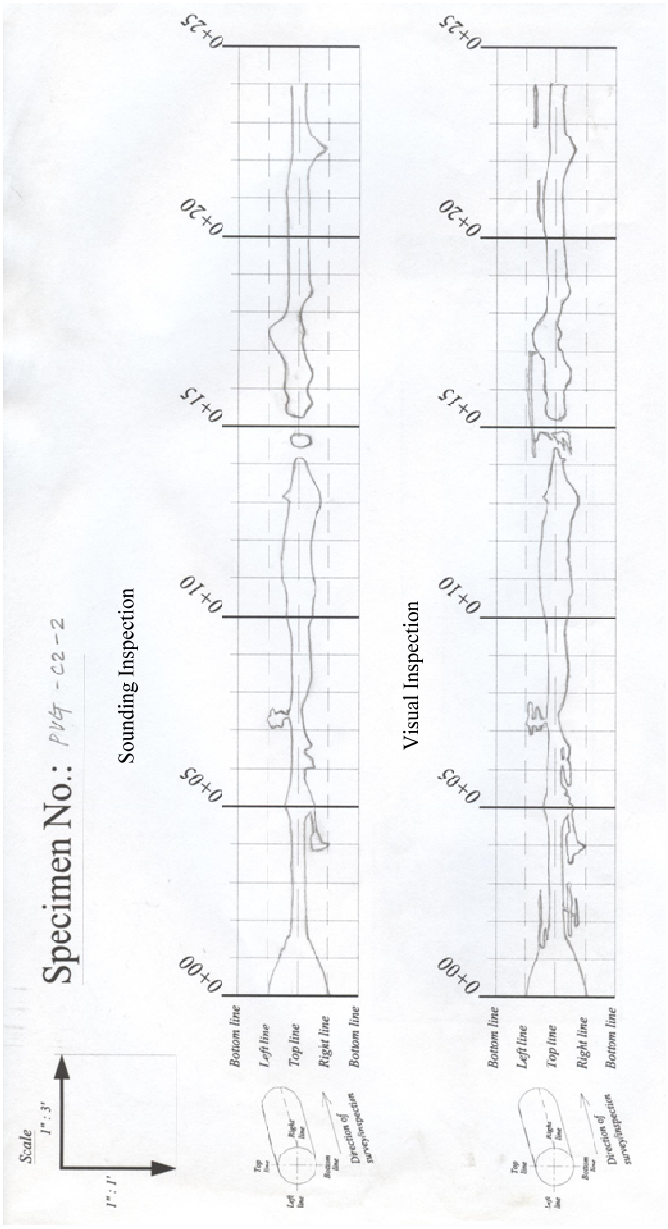

Figure A-39. Void Map of Specimen PVG-C2-2.

The areas of both void profiles are estimated using AutoCAD® and provided in Table A-37.

Table A-37. Estimation of Void Profile in Specimen PVG-C2-2.

Section, ft (m)	Sounding Inspection (SI), inch^2 (10^{-4} m^2)	Visual Inspection (VI), inch^2 (10^{-4} m^2)	SI - VI, inch^2 (10^{-4} m^2)
0~1 (0~0.3)	65.23 (420.9)	65.59 (423.155)	-0.35 (-2.3)
1~2 (0.3~0.6)	29.00 (187.1)	34.37 (221.743)	-5.37 (-34.6)
2~3 (0.6~0.9)	16.39 (105.8)	24.65 (159.061)	-8.26 (-53.3)
3~4 (0.9~1.2)	19.22 (124.0)	22.19 (143.140)	-2.97 (-19.2)
4~5 (1.2~1.5)	27.51 (177.5)	29.79 (192.186)	-2.28 (-14.7)
5~6 (1.5~1.8)	24.14 (155.7)	27.17 (175.314)	-3.04 (-19.6)
6~7 (1.8~2.1)	21.24 (137.0)	23.65 (152.604)	-2.41 (-15.6)
7~8 (2.1~2.4)	24.32 (156.9)	27.83 (179.536)	-3.51 (-22.7)
8~9 (2.4~2.7)	22.78 (147.0)	24.45 (157.771)	-1.68 (-10.8)
9~10 (2.7~3.0)	23.84 (153.8)	24.25 (156.462)	-0.41 (-2.7)
10~11 (3.0~3.4)	34.56 (223.0)	36.87 (237.852)	-2.31 (-14.9)
11~12 (3.4~3.7)	35.73 (230.5)	37.92 (244.676)	-2.19 (-14.1)
12~13 (3.7~4.0)	35.72 (230.5)	36.00 (232.241)	-0.28 (-1.8)
13~14 (4.0~4.3)	30.43 (196.3)	28.04 (180.889)	2.39 (15.4)
14~15 (4.3~4.6)	8.29 (53.5)	12.77 (82.364)	-4.48 (-28.9)
15~16 (4.6~4.9)	19.58 (126.3)	21.19 (136.723)	-1.61 (-10.4)
16~17 (4.9~5.2)	30.48 (196.7)	33.73 (217.607)	-3.25 (-21.0)
17~18 (5.2~5.5)	34.04 (219.6)	30.07 (194.024)	3.97 (25.6)
18~19 (5.5~5.8)	23.81 (153.6)	23.87 (154.002)	-0.06 (-0.4)
19~20 (5.8~6.1)	24.72 (159.5)	23.35 (150.651)	1.37 (8.8)
20~21 (6.1~6.4)	25.53 (164.7)	26.77 (172.694)	-1.23 (-8.0)
21~22 (6.4~6.7)	25.01 (161.3)	25.82 (166.611)	-0.82 (-5.3)
22~23 (6.7~7.0)	29.75 (191.9)	25.81 (166.534)	3.93 (25.4)
23~24 (7.0~7.3)	17.13 (110.5)	20.58 (132.756)	-3.45 (-22.2)

The repair grout is filled from the top grout port and infiltrated to 14.3 ft (4.36 m) from the reference point (Figure A-40).

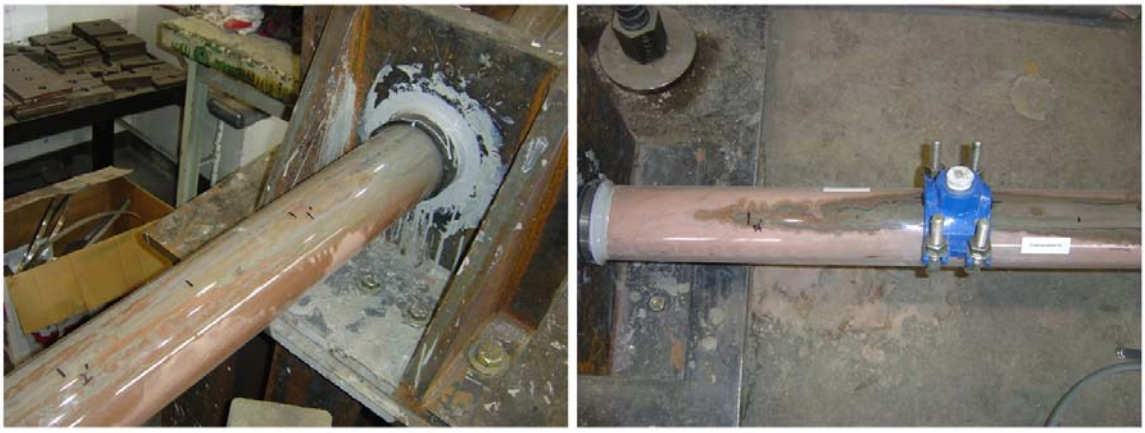

Figure A-40. Repair Grouted Ducts of Specimen PVG-C2-2.

Figure A-41 shows the cross-sectional views of the cut sections obtained from Specimen PVG-C2-2. From the cut sections, it is noted that the repair grouts successfully replaces the main voids and repairs local large voids #3, #4, and #5. The small voids still exist inside the initially grouted ducts, especially in-between strands. However, those voids cannot be repaired because the voids are isolated from the “bug holes” which is a route for repair grouts.

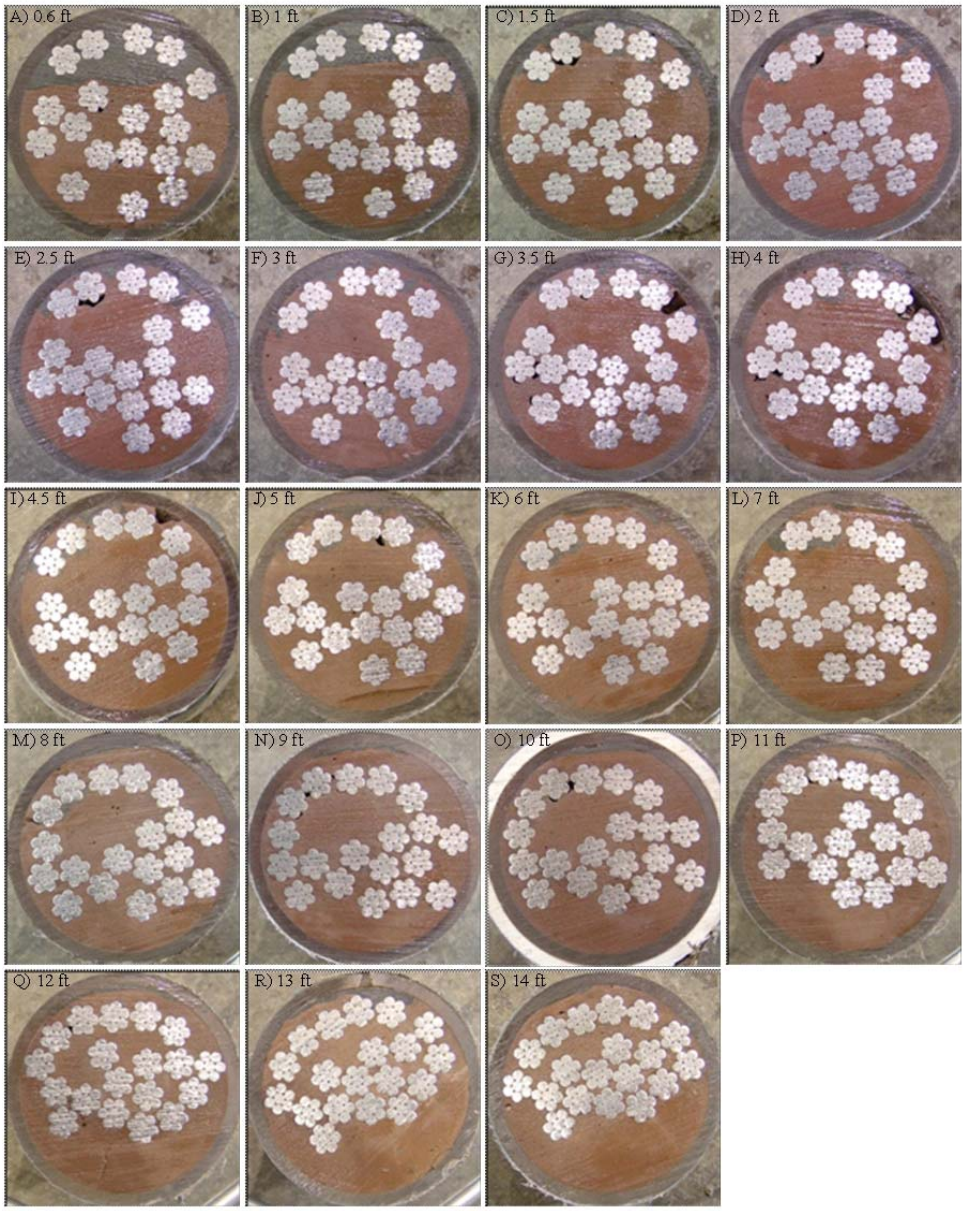

Figure A-41. Cut Sections of Specimen PVG-C2-2 for the Filling Analysis of Repair Grout.

To compare the performance of repair grouts, the ratio of remaining void area after repair to the repaired area is estimated. The repaired area and area of voids after repair are calculated using AutoCAD® (Table A-38).

Table A-38. Void Area of Specimen PVG-C2-2.

Cut Sections, ft (m)		Repaired Area, A_R, inch^2(10^{-4} m^2)	Void Area, A_V, inch^2(10^{-4} m^2)	Void Ratio, η (%)
A	0.6 (0.18)	2.274 (14.67)	0.0035 (0.023)	0.15
B	1 (0.30)	1.165 (7.52)	0.0022 (0.014)	0.19
C	1.5 (0.46)	0.490 (3.16)	0.0041 (0.026)	0.84
D	2 (0.61)	0.340 (2.19)	0.0095 (0.061)	2.80
E	2.5 (0.76)	0.351 (2.26)	0.0022 (0.014)	0.63
F	3 (0.91)	0.332 (2.14)	0.0017 (0.011)	0.51
G	3.5 (1.07)	0.257 (1.66)	0.0007 (0.005)	0.27
H	4 (1.22)	0.238 (1.53)	0.0006 (0.004)	0.25
I	4.5 (1.37)	0.291 (1.88)	0.0000 (0.000)	0.00
J	5 (1.52)	0.376 (2.42)	0.0000 (0.000)	0.00
K	6 (1.83)	0.352 (2.27)	0.0025 (0.016)	0.71
L	7 (2.13)	0.396 (2.56)	0.0021 (0.014)	0.53
M	8 (2.44)	0.214 (1.38)	0.0007 (0.005)	0.33
N	9 (2.74)	0.151 (0.97)	0.0005 (0.003)	0.33
O	10 (3.05)	0.194 (1.25)	0.0101 (0.065)	5.22
P	11 (3.35)	0.185 (1.19)	0.0017 (0.011)	0.92
Q	12 (3.66)	0.229 (1.48)	0.0000 (0.000)	0.00
R	13 (3.96)	0.405 (2.61)	0.0000 (0.000)	0.00
S	14 (4.27)	0.031 (0.20)	0.0000 (0.000)	0.00
Sum		**8.268 (53.34)**	**0.0421 (0.272)**	**0.51**

The remaining void ratio, after repair, obtained from the analysis comes out to be 0.51% for Specimen PVG-C2-2. The initial void area ranges over 0.1 inch^2 (0.65×10^{-4} m^2) or more from the reference point to Section R, but the voids include small contributions from Section S.

Table A-39 shows the time schedule of sealing ducts for Specimen PVG-C2-2. Total sealing time of Specimen PVG-C2-2 is 3 days and 1.53 hours before applying repair grout.

Table A-39. Sealing Time Schedule of Specimen PVG-C2-2.

Sealing Procedure	**Working Day**	**Working Time (min.)**
Installing pipe saddle tap with grease	Day 1	29
Setting end rubber cover and sealing	Day 1	4
Mixing epoxy and sealing	Day 1	27
Wait	1 day	
Checking air-tight condition	Day 2	17
Connecting grout hose and sealing	Day 2	8
Checking air-tight condition	Day 2	17
Connecting vacuum safety device and checking air-tight	Day 2	7
Sum	**2 days**	**90 (1.53 hours)**

A.15. SPECIMEN PVG-C3-1

Figure A-42 depicts the initial void profiles of the sounding inspection and of the visual inspection before grouting for Specimen PVG-C3-1.

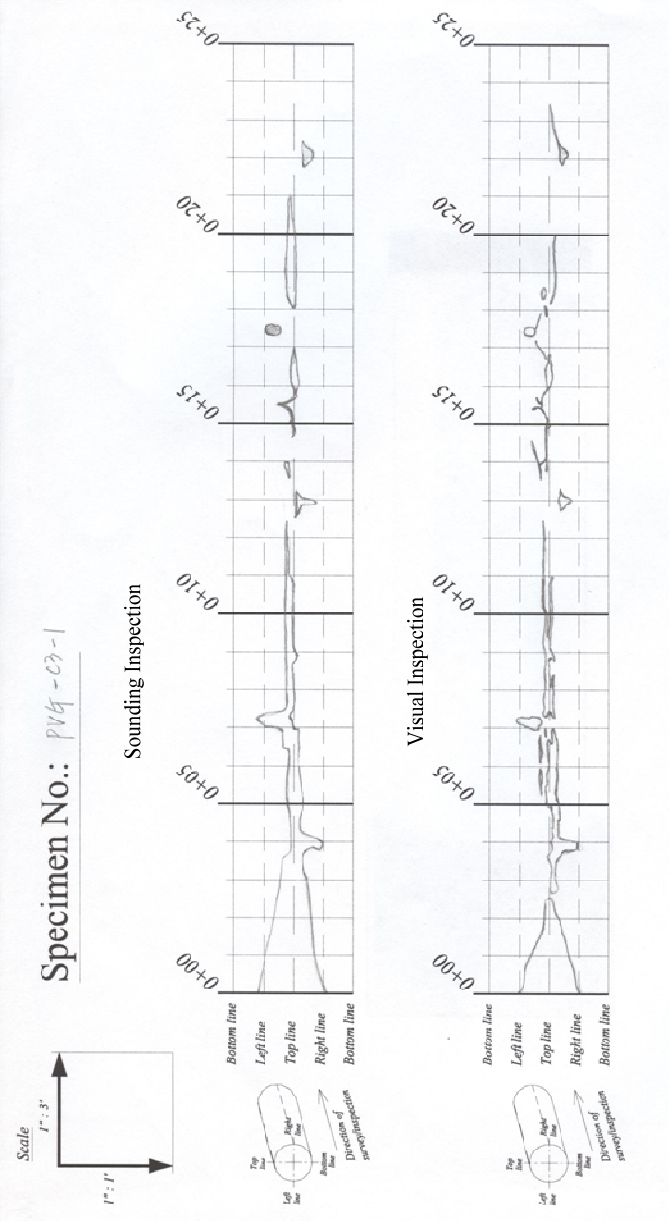

Figure A-42. Void Map of Specimen PVG-C3-1.

The areas of both void profiles are estimated using AutoCAD® and provided in Table A-37.

Table A-40. Estimation of Void Profile in Specimen PVG-C3-1.

Section, ft (m)	Sounding Inspection (SI), inch^2 (10^{-4} m^2)	Visual Inspection (VI), inch^2 (10^{-4} m^2)	SI - VI, inch^2 (10^{-4} m^2)
0~1 (0~0.3)	73.81 (476.2)	63.35 (408.7)	10.45 (67.4)
1~2 (0.3~0.6)	54.55 (351.9)	32.32 (208.5)	22.23 (143.4)
2~3 (0.6~0.9)	40.72 (262.7)	8.99 (58.0)	31.73 (204.7)
3~4 (0.9~1.2)	28.82 (185.9)	13.83 (89.3)	14.98 (96.7)
4~5 (1.2~1.5)	17.26 (111.3)	9.59 (61.9)	7.66 (49.4)
5~6 (1.5~1.8)	17.77 (114.6)	14.94 (96.4)	2.83 (18.2)
6~7 (1.8~2.1)	16.64 (107.3)	12.59 (81.2)	4.05 (26.1)
7~8 (2.1~2.4)	21.37 (137.9)	15.75 (101.6)	5.62 (36.3)
8~9 (2.4~2.7)	9.58 (61.8)	7.86 (50.7)	1.72 (11.1)
9~10 (2.7~3.0)	9.46 (61.1)	7.90 (51.0)	1.56 (10.1)
10~11 (3.0~3.4)	9.16 (59.1)	7.49 (48.3)	1.68 (10.8)
11~12 (3.4~3.7)	3.55 (22.9)	2.59 (16.7)	0.97 (6.2)
12~13 (3.7~4.0)	5.95 (38.4)	3.67 (23.7)	2.28 (14.7)
13~14 (4.0~4.3)	3.48 (22.4)	4.67 (30.1)	-1.19 (-7.7)
14~15 (4.3~4.6)	1.38 (8.9)	5.17 (33.4)	-3.79 (-24.5)
15~16 (4.6~4.9)	6.14 (39.6)	4.30 (27.7)	1.84 (11.9)
16~17 (4.9~5.2)	7.79 (50.3)	6.21 (40.0)	1.58 (10.2)
17~18 (5.2~5.5)	4.81 (31.0)	4.62 (29.8)	0.19 (1.2)
18~19 (5.5~5.8)	10.28 (66.3)	4.88 (31.5)	5.40 (34.8)
19~20 (5.8~6.1)	11.76 (75.9)	2.65 (17.1)	9.11 (58.8)
20~21 (6.1~6.4)	5.54 (35.8)	0.00 (0.0)	5.54 (35.8)
21~22 (6.4~6.7)	2.10 (13.5)	0.88 (5.7)	1.22 (7.9)
22~23 (6.7~7.0)	4.30 (27.7)	5.30 (34.2)	-1.00 (-6.5)
23~24 (7.0~7.3)	0.00 (0.0)	1.06 (6.8)	-1.06 (-6.8)

The repair grout is filled from the top grout port and infiltrated to 3.9 ft (1.19 m) from the reference point (Figure A-43).

Figure A-43. Repair Grouted Ducts of Specimen PVG-C3-1.

Figure A-44 shows the cross-sectional views of the cut sections obtained from Specimen PVG-C3-1. From the cut sections, it is noted that the repair grout successfully replaces the main voids up to 2.5 ft (0.76 m) from the reference point, but after that voids are only partially repaired. Also, it does not fill void #5 located in Section H. The small voids still exist inside the initially grouted ducts, especially in-between strands.

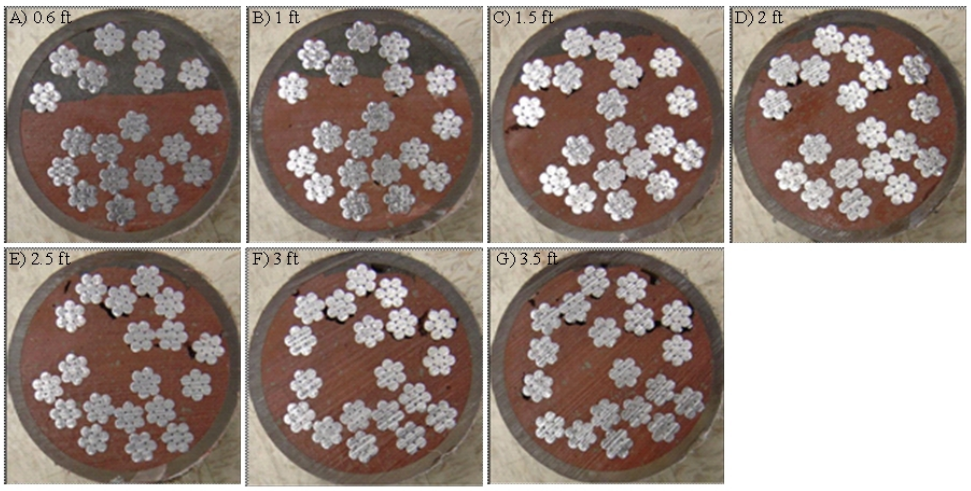

Figure A-44. Cut Sections of Specimen PVG-C3-1 for the Filling Analysis of Repair Grout.

To compare the performance of repair grouts, the ratio of remaining void area after repair to the repaired area is estimated. The repaired area and area of voids after repair are calculated using AutoCAD® (Table A-41).

Table A-41. Void Area of Specimen PVG-C3-1.

Cut Sections, ft (m)		Repaired Area, A_R, inch^2(10^{-4} m^2)	Void Area, A_V, inch^2(10^{-4} m^2)	Void Ratio, η (%)
A	0.6 (0.18)	2.182 (14.08)	0.0180 (0.116)	0.83
B	1 (0.30)	1.422 (9.17)	0.0054 (0.035)	0.38
C	1.5 (0.46)	0.551 (3.56)	0.0074 (0.048)	1.34
D	2 (0.61)	0.188 (1.21)	0.0018 (0.012)	0.96
E	2.5 (0.76)	0.163 (1.05)	0.0000 (0.000)	0.00
F	3 (0.91)	0.176 (1.14)	0.0526 (0.339)	29.84
G	3.5 (1.07)	0.074 (0.48)	0.0177 (0.114)	23.79
Sum		**4.756 (30.69)**	**0.1029 (0.664)**	**2.16**

From the analysis, remaining voids in repair grouts are estimated in each grout cut sections, however, a void ratio in a section can be magnified when the remaining voids exist only in a small repaired area. Thus, the filling performance for Specimen PVG-C3-1 is considered as using the summation of the estimated section. The remaining void ratio, after repair, obtained from the analysis comes out to be 2.16% for Specimen PVG-C3-1. The initial void area ranges over 0.1 $inch^2$ (0.65×10^{-4} m^2) or more from the reference point to Section F, however, the voids include contribution from Section G.

Table A-42 shows the time schedule of sealing ducts for Specimen PVG-C3-1. Total sealing time of Specimen PVG-C3-1 is 2 days and 2.25 hours before applying repair grout.

Table A-42. Sealing Time Schedule of Specimen PVG-C3-1.

Sealing Procedure	Working Day	Working Time (min.)
Setting rubber end caps and sealing with epoxy	Day 1	50
Wait	1 day	
Installing pipe saddle tap with grease	Day 2	45
Connect grout hose	Day 2	10
Checking air-tight condition	Day 2	30
Sum	2 days	135 (2.25 hours)

APPENDIX B

INSPECTION AND REPAIR MANUAL FOR EXTERNAL TENDONS IN SEGMENTAL, POST-TENSIONED BRIDGE SYSTEMS

TABLE OF CONTENTS

LIST OF FIGURES

1 INTRODUCTION

1.1 BACKGROUND INFORMATION

Post-tensioned (PT) bridges have the advantages of spanning longer distances, reducing the bridge's self-weight, and having shorter construction periods. Many PT bridges have been constructed over the last several decades. However, recent investigations of these bridges have identified voids in the ducts, and the exposed strands at these void locations can undergo corrosion. The rate of corrosion is very high when high humidity, water and/or chlorides are present inside the tendons. The corrosion of strands can lead to the failure of tendons. It is critical to be proactive in protecting tendons from corrosion because a tendon failure will adversely affect the bridge's performance, will be costly to replace, and will increase the probability of bridge failure. Therefore, an inspection program for the condition assessment of PT tendons should be developed to ensure public safety and extend the service life of PT bridges. The critical factors that should be identified in an inspection program include the identification of voids, moisture, and/or chlorides that have been or are present in the tendons at the time of inspection. This manual presents procedures for the inspection and minor repair of external tendon systems.

During the inspection, if moisture or chlorides are found infiltrating the tendons, a method is needed to prevent further infiltration of these substances. Common practice has been to repair with grout (i.e., fill the voids with repair grout) to prevent further ingress of the deleterious materials. Volume 2 of Report 0-4588-1 developed the pressure-vacuum grouting (PVG) method to perform repair grouting. However, a recent tendon failure in a bridge in Virginia indicates that repair grouting may lead to accelerated corrosion and early failure of the tendon. At the time of the development of this manual, repair grouting of tendons was not employed by TxDOT. Research is needed to determine if the corrosion activity is influenced by repair grouting. This manual will present the repair grouting procedures only in Appendix A. Should TxDOT decide to employ them in the future, it is recommended that this procedure be used only after the current moratorium or the wait-and-see approach on repair grouting is lifted. As such, the word "repair" in this manual refers to all repairs, such as repairing drain lines, ducts, grout ports, bridge joints, etc., with the exception of repair grouting.

1.2 Current Needs

Routine safety (visual) inspections of all bridges are performed every two years. It is expensive and time consuming to perform in-depth inspections, especially in-depth inspections of PT tendons inside segmental bridges. At the same time, the consequences of having a structural failure are severe—PT bridges in Texas carry significant traffic. Therefore, bridge owners should do everything economically feasible to prevent the exposure of strands to high relative humidity levels, water, and/or chloride conditions. These actions could include repairing drain lines, sealing ducts and grout holes, repairing bridge joints, or performing other repairs.

1.3 Inspection, Analysis, and Repair Strategy

This manual recommends an inspection, analysis, and repair strategy for external tendons found only in segmental, PT bridges. This manual is not intended to replace the existing inspection requirements for PT bridges but instead is a recommendation for the additional inspection and testing specifically for external tendons (not for internal tendons) in segmental, PT bridges. An inspection, analysis, and repair strategy that optimizes the resource requirements is developed by dividing the overall inspection, analysis, and repair program into three major steps. These are:

- special inspection and analysis program for PT systems,
- surveying of the selected tendons for in-depth inspection, and
- in-depth inspection, analysis, and repair program for PT systems.

Figure 1-1 shows a flowchart with the overall inspection, analysis, and repair program as described above. The following sections present further details on these three steps.

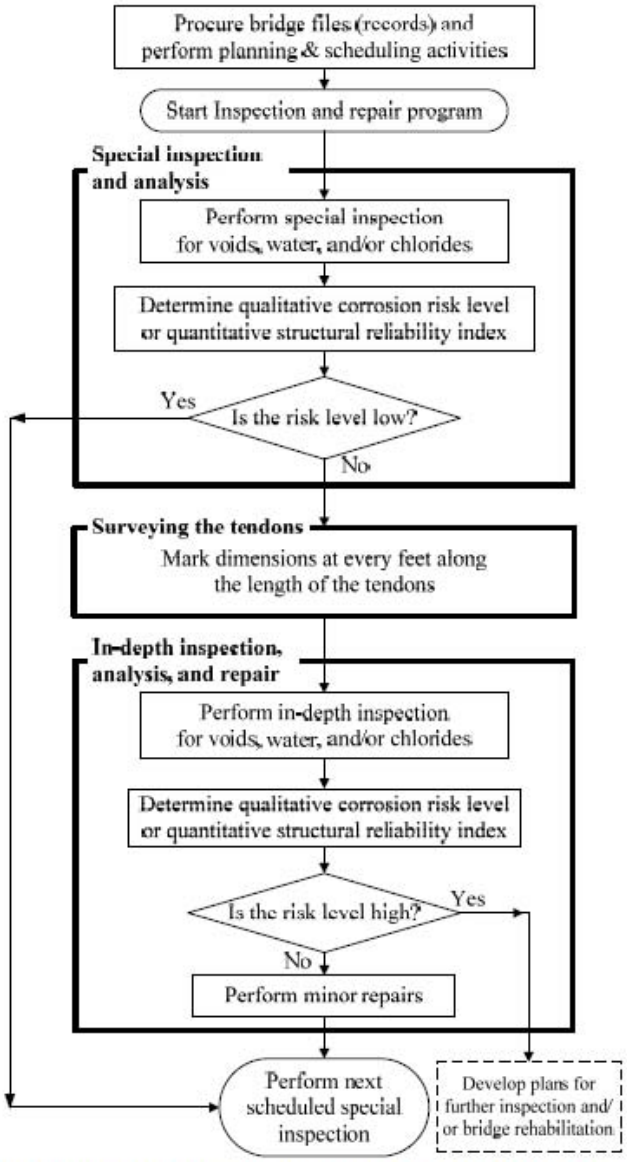

Figure 1-1. Overall Inspection, Analysis, and Repair Program for Post-Tensioned Bridges.

Special inspection and analysis program

This proposed program includes a "walk-through" inspection to identify the potential presence of voids in ducts and the presence of water and chlorides. It should be noted that the proposed special inspection procedures are not intended to replace but to augment the existing special inspection procedures for PT bridges. Based on the obtained information, the qualitative corrosion risk or quantitative structural reliability of the bridge system can then be assessed. The results from the risk or reliability analyses can be used to determine if in-depth inspections are needed.

Surveying of the tendons selected for in-depth inspection

The word "surveying" in this manual indicates the process of marking gridlines and/or markers on the tendons and inside the girder. This is done only for the in-depth inspection, analysis, and repair program.

In-depth inspection, analysis, and repair program

Past bridge inspections and Volume 1 of Report 0-4588-1 cite that the presence of voids along with moisture and chlorides can cause strand corrosion in PT bridges. Volume 1 of Report 0-4588-1 also identified that the rate of corrosion can be maximized at the interface between the void and the grouted region in the tendon. A completely exposed strand will also have very high corrosion rate when exposed to high relative humidity levels, water, and/or chloride conditions.

In-depth inspections should be performed on tendons that are identified as having medium or high risks of corrosion or capacity loss. These tendons are identified during special inspections and are typically tendons that have damage to the duct, have standing water in the tendon, have chlorides in the water, or exhibit more than surface corrosion of the strands. Random in-depth inspections can be performed if deemed necessary by the person in charge of the inspection. The following sections provide details of the in-depth bridge inspection program.

1.4 Personnel for the Inspection, Analysis, and Repair

This manual assumes that personnel associated with the inspection of PT systems have different responsibilities. This manual uses the following definitions.

- **Inspection program manager** – The person responsible for the overall management of the inspection, analysis, and repair program. He/she is also responsible for the testing of samples collected and the analysis of the inspection data.
- **Inspection team leader** – The person responsible for the field activities regarding the inspection program (including management of the inspection, surveying, and minor repair crews).

1.5 Tools for Risk Assessment and Decision Making

Based on the environmental conditions (i.e., relative humidity, moisture, and chloride conditions) inside the tendons, the qualitative corrosion risk level for the tendon and/or span can be determined. Qualitative corrosion risk levels are shown in Figure 1-2.

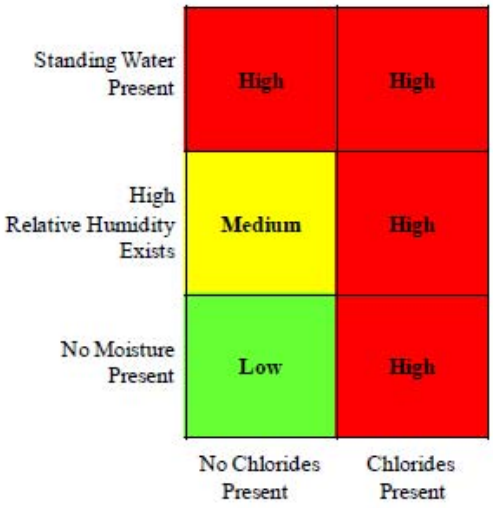

Figure 1-2. Qualitative Corrosion Risk Chart for PT Systems.

Appendix B provides examples of possible damage types that could be found on PT systems. These damage types with a particular corrosion risk level are shown in Table 1-1. Table 1-1 also summarizes the recommended actions for each damage type and/or corrosion risk level. In Table

1-1, some of the damage types are characterized by the level of corrosion on strands. Figure 1-3 provides a set of photographs of corroded strands that could assist in determining the corrosion level.

Table 1-1. Required Actions from Findings on Damage Type.

Corrosion Risk Level	Possible Damage Types*	Recommended Actions
Low (Green)	• No damage • Small void without other damage indicators • No strand corrosion*	• No repair • Continue regular inspections
Medium (Yellow)	• Cracked PT ducts, drainage pipe, spalled concrete with corrosion products (not from tendons), exposed grout cap, or opened grout port • Corrosion of anchor head plate or reinforcement at anchorage zone • Low levels of strand corrosion*	• Minor repairs required • Seal the PT system or repair/replace the leaking element to prevent water and/or chloride infiltration
High (Red)	• Water present in duct with or without chlorides • Moderate or high levels of strand corrosion* • Broken strands	• Develop and implement bridge rehabilitation program and replace the corroded tendon OR • Dry the tendon, fill the voids with repair grout, and prevent water and/or chloride infiltration (if TxDOT decides to perform repair grouting)

* Characteristics of strand corrosion are provided in Figure 1-3.

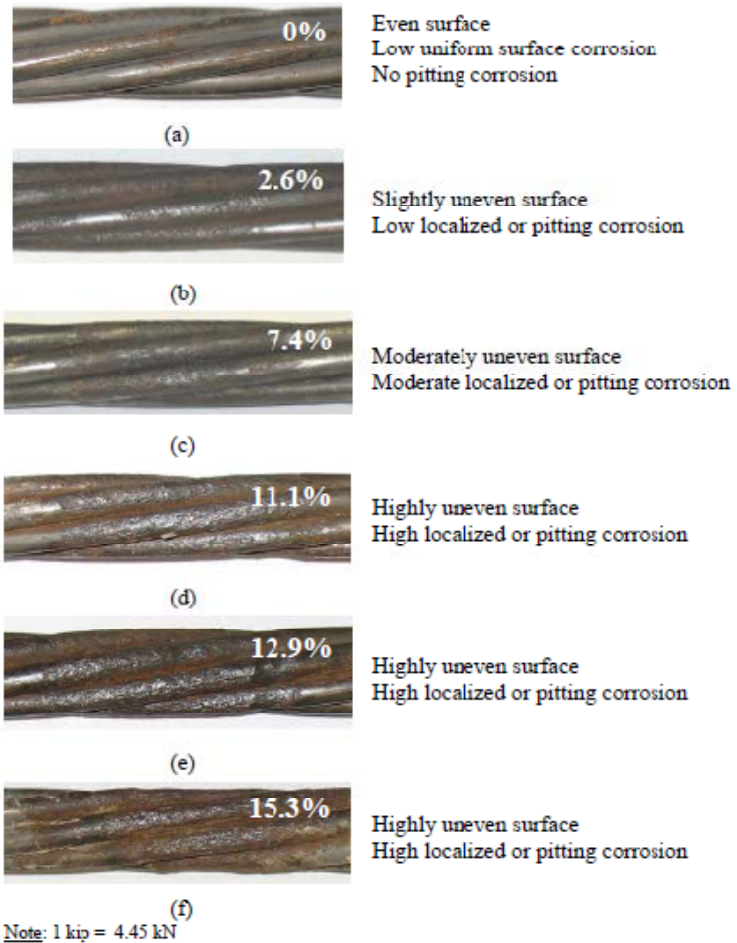

Note: 1 kip = 4.45 kN

Figure 1-3. Photographs Showing the Typical Tensile Strength, Corrosion Level, and Surface Characteristics of Strands (Note: These photographs were taken after cleaning the strand surface using a synthetic cleaning pad and/or a steel wire brush).

2 SPECIAL INSPECTION AND ANALYSIS PROGRAM

2.1 OBJECTIVES

The objectives of the special inspection program are to:

1. identify the type and location of damage in PT systems;
2. identify voids and their locations in PT systems;
3. identify the presence of moisture and/or chlorides (or the indicators that water has been present) in the PT system;
4. identify the causes and locations of water and/or chloride infiltration; and
5. collect the water samples, if present, and evaluate the chloride concentrations and pH.

The special inspection team leader will submit the findings to the special inspection program manager, who will then assess the "qualitative corrosion risk of the bridge span" and make further decisions for the in-depth inspection and testing program, if needed.

2.2 SAFETY

General safety precautions must be taken. Both personnel and public safety requirements must be met by following standard TxDOT requirements. Note that a segmental PT bridge may be considered a "confined space" and that inspectors may require appropriate training.

2.3 PLANNING, SCHEDULING, AND EQUIPMENT

Planning and scheduling

Based on bridge files, records, and other factors, the inspection program manager will develop the overall strategy for the special inspection program. It is recommended that special inspections be performed shortly after heavier rains or during the rainy season. This will allow the inspector to identify if water is present, before evaporation or drying. The inspection program manager will also identify the bridge spans for inspection and provide this information to the inspection team leader. The inspection team leader will be responsible for detailed planning and management of the field activities.

Tools and equipment for special inspection

Table 2-1 lists recommended tools and equipment required for special inspections. Note that this list may not be comprehensive.

Table 2-1. Recommended Tools and Equipment for Special Inspection.

Safety Tools	Special Inspection Tools
Hard hats	Special inspection form and pen
Head flashlights	Clipboard
Handheld flashlights	Steel tapping hammer (for inspecting voids in tendons)
Safety goggles	Mirrors (for inspecting damage underneath ducts)
Protective coveralls	Paint marker
Yellow safety vests	Spray paint that can be clearly seen (lighter colors)
Gloves	Plastic bottles (e.g., 80 ml) for collecting water samples
Respirators	Plastic pipette to collect water samples
Dust masks	Thermometer (for measuring temperature)
Ear plugs	Hygrometer (for measuring relative humidity)
First-aid kit	Tools for making holes (dremel with copper drill bit)
Extra batteries	HDPE pipe pieces and ABS cement to seal the ducts
Fire extinguisher	Digital camera
Air horn	Lift truck
Safety harness and rope	Binder with all papers (inspection manual, blue print, etc.)
Safety boots	Wet wipe to clean the duct surface
Hand-held radios (Walkie-talkie)	Wood and saw (for holding the door open) or chain and latch
Oxygen meter and CO meter	Keys and tools required to unlock and open the access door
Confined space training manual	
Drinking water	

2.4 Special Inspection Forms, Test Samples, and Reports

The data from the special inspection of each span should be recorded on the "special inspection form." Each span inspected will require at least one form. Figure 2-1 and Appendix C provide examples of the special inspection forms.

Note: This only applies to segmental PT bridges

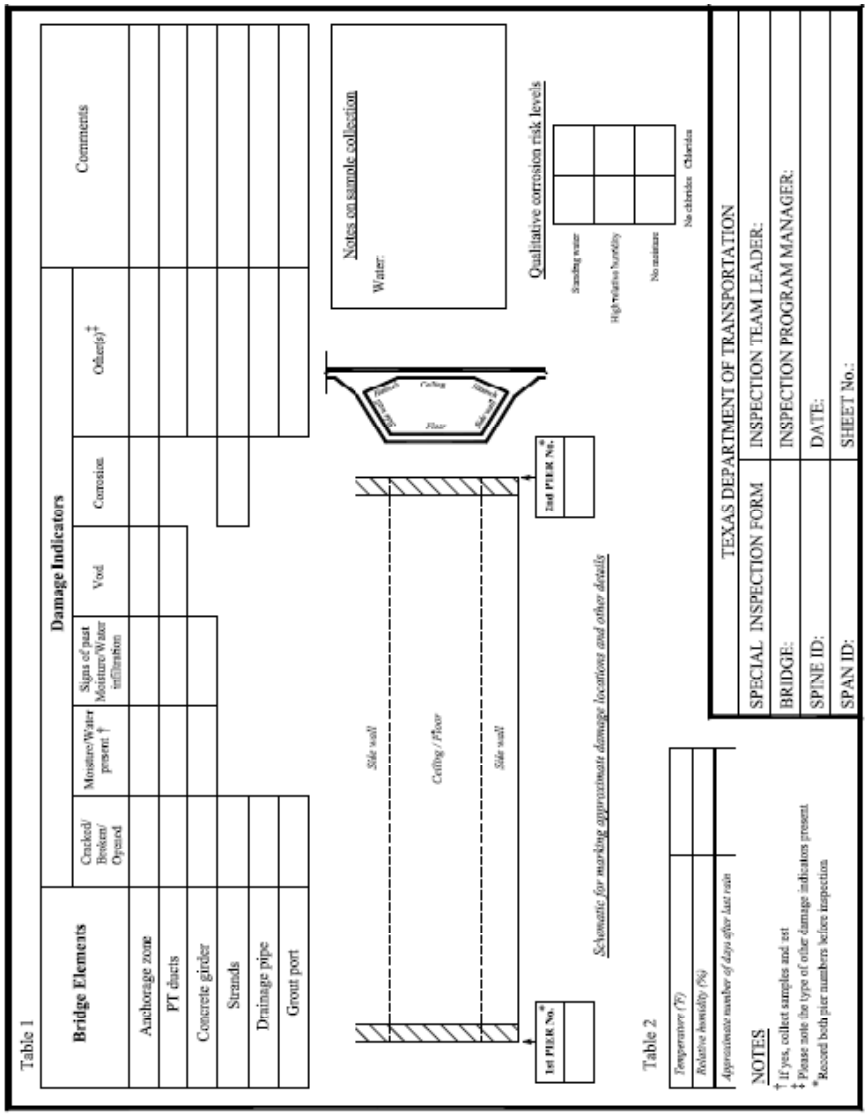

Figure 2-1. Special Inspection Form.

The special inspection team leader will also submit the test samples, if any, collected during the special inspection to the inspection program manager, who will then submit the test samples to the testing laboratory to obtain the test results. A "chain of command form" shall be maintained for all the samples collected.

2.5 General Procedures in Special Inspection and Analysis

This subsection provides the procedures to perform the special inspection program. Figure 2-2 shows the detailed flowchart for the special inspection and analysis. Note that the inspection program manager is responsible for the procurement of the bridge files and records and development of the special inspection and analysis strategy. The following steps provide the special inspection procedures. The bulleted steps in the following list start with a code (e.g., R-1) that represents the corresponding box in the flowchart. In the flowchart, the boxes inside the larger box with a thick border indicate the steps in the special inspection. The boxes outside the larger box indicate the procedures before and after the special inspection.

- **R-1**: Identify the starting and ending spans to be inspected.
- **R-2**: Select bridge files associated with the select bridge spans to be inspected and other relevant information. Collect files showing tendon profiles (indicating anchorage locations).
- **R-3**: Procure necessary tools and equipment before entering the starting span. Refer to Subsection 2.3 for the recommended list of tools and equipment.
- **R-4**: Take copy of the special inspection form for each span under inspection. Then record the following:
  - all information (except engineer's name) in the title box,
  - both pier numbers of the span in the appropriate boxes in the schematic shown, and
  - the environmental data (in Table 2).
- **R-5**: Table 1 on the special inspection form (Figure 2-1) shows different bridge elements and damage indicators or types. Typical photographs of these damage indicators are shown in Appendix B. Identify the presence of these damage indicators on the PT systems. If found, record the presence of these damage indicators in Table 1 of the special inspection form.
  - Damage types other than the types shown in Appendix B may also be observed. In such instances, photographs should be taken and information recorded as directed in the special inspection form.
  - If damage (such as cracked ducts, opened grout holes) is identified, then:

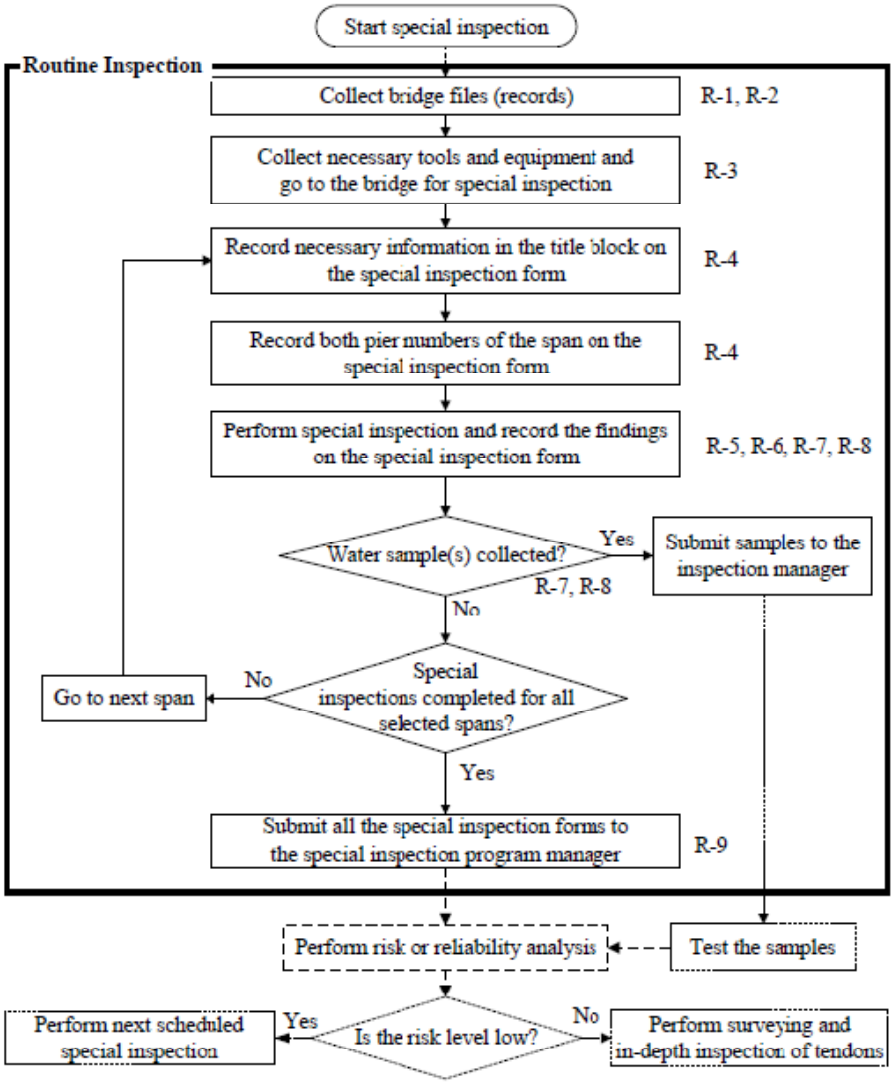

Figure 2-2. Flowchart of Special Inspection and Analysis.

  - mark the damage and its location and type in the special inspection form, and
  - mark the damaged area on the PT system, if any, with spray paint.
- If exposed strands are found, take photographs.

- **R-6**: Inspect for voids using sounding tests[1] at random locations along the sides of the tendons. If voids are found, then record the information in the table in the special inspection form.

- **R-7**: Inspect for the presence of water in the girder.
  - Check for the presence of standing water on the floor of the girder. If water is found, then mark the location on the drawing in the special inspection form. Also, look for possible sources of water ingress and mark them on the special inspection form.

- **R-8**: Inspect for the presence of water inside the tendons.
  - Identify the tendons that do not extend through the expansion joints (such as T1, T2, and T3 tendons shown in Figure 2-3 [a]). Select tendons and perform the following steps.
  - Identify a location to drill a 1/8-inch diameter hole on the horizontal portion of the duct between the deviator blocks (details are provided in Figure 2-3 [a] and [b]). Special drill bits made of copper are required to avoid strand damage.
  - Place a plastic container such that the draining water, if any, can be collected.
  - If water drains out of this hole, then:
    - collect the draining water into a small plastic bottle and fill out the chain of command form;
    - locate and check whether or not the grout hole at the anchorage of this tendon is opened or damaged; and
    - record all the information regarding the presence of water, possible sources and locations of water ingress, and sample collection on the special inspection form.
  - Seal the 1/8-inch diameter hole using an HDPE pipe piece and cement (see Figure 2-3 [c] for details).

- **R-9**: Submit all the completed special inspection forms and test samples, if any, to the inspection program manager.

[1] The sounding test is a procedure used to identify the presence of voids based on the noise produced by tapping of the duct surface using a metallic impact tool (typically a small hammer). A dull or low-pitch sound indicates the presence of voids. A high-pitch sound indicates a fully grouted tendon (i.e., no voids). This research found that the small void or "bleed line" along the top part of the tendon was not detrimental to the corrosion of strands, so this area, if small, does not need to be drawn on the special inspection form. It is recommended that sounding be performed along the sides of PT ducts to identify large voids.

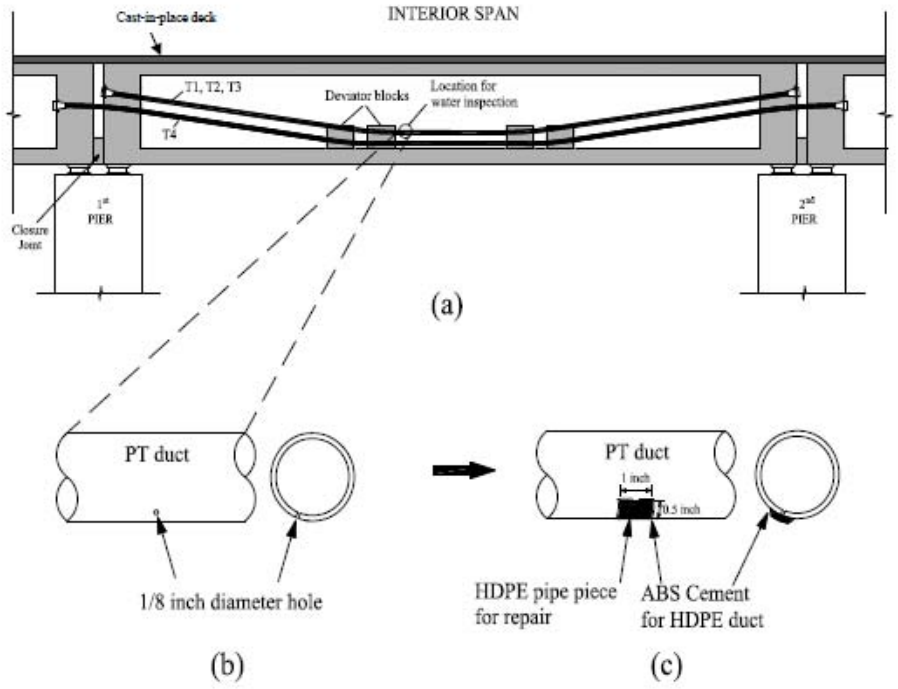

Note: 1 inch = 25.4 mm

Figure 2-3. Tendon System Showing (a) the Location for Water Inspection, (b) a Close-up of the Location for Water Inspection, and (c) the Sealed Duct after Water Inspection.

3 SURVEYING THE TENDONS

3.1 OBJECTIVES

The tendons selected for in-depth inspection need to be surveyed such that inspectors can quickly determine location of voids or other damaged areas. This section provides general procedures to survey the tendons.

3.2 GENERAL PROCEDURES IN TENDON SURVEY

The two main tasks for surveying include performing a survey along tendon profiles and documenting the location of anchorage zones (diaphragms) and deviator blocks on the in-depth inspection form. Figure 3-1 shows a flowchart of the tendon surveying process.

- S-1 to S-2: Prepare the information and equipment for surveying.
  - Check all tools and equipment required before entering the surveying span.
  - Go to the span.
  - Record all the information in the title block on the in-depth inspection sheet.
- S-3 to S-4: Record the starting point.
  - The start point in each span is designated by the order of numbering spans. Thus, the diaphragm located toward the lower numbered span is the start point in spans. (See Figure 3-2—Section A-A is the starting point on this span.)
  - Record the pier number under the starting point.
- S-5 to S-9: Mark the dimensions along the length of the tendons.
  - Mark segment numbers using marking spray and stencil (if needed) (see Subsection 3.3).
  - Mark tendon numbers using marking spray and stencil (see Subsection 3.3).
  - Measure the thickness of both diaphragms. This is to estimate the length of the portion of the tendon embedded inside the concrete diaphragm (see Figure 3-4).
  - Mark survey stations at every foot from the inside diaphragm at the start point (as shown in Figure 3-4 and Figure 3-5) until a deviator block is reached.
  - See Figure 3-4 and Figure 3-5 to see an example showing how the deviator blocks are marked on the in-depth inspection form. Document locations of deviator block on the in-depth inspection form. Continue marking the dimensions until entire tendon length is marked.
  - Perform marking with a paint marking pen.
- S-10 to S-12: After completing the survey, submit all the in-depth inspection forms to the inspection program manager.

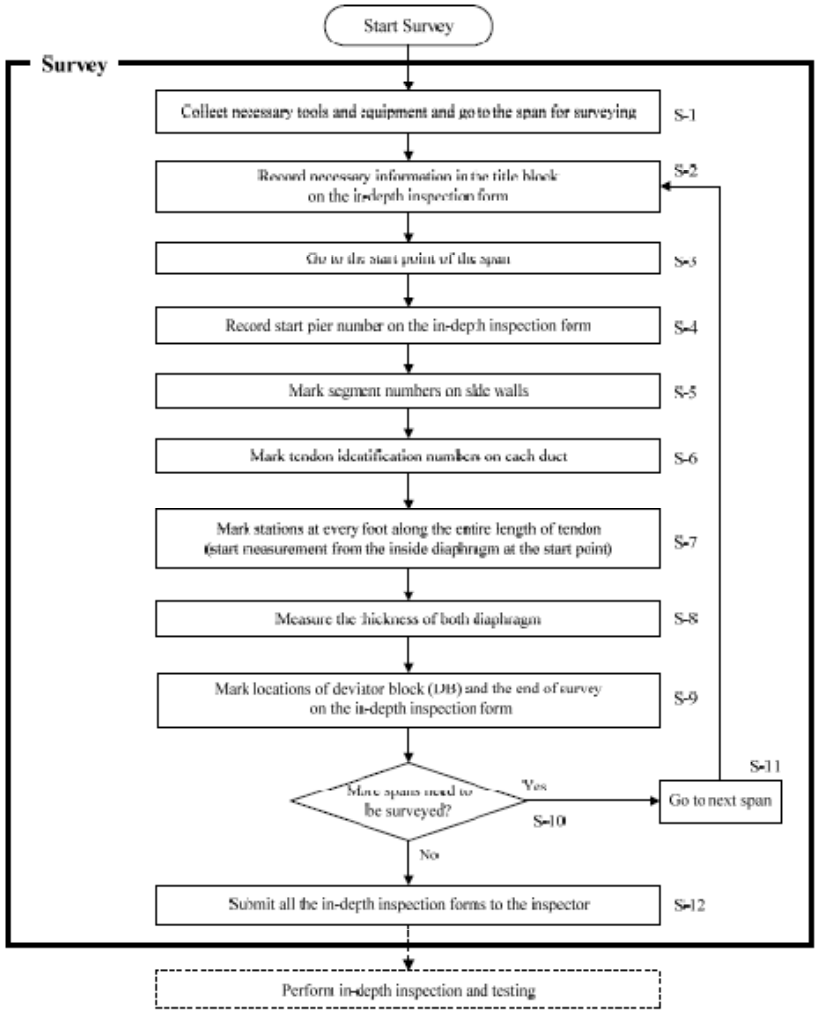

Figure 3-1. Flowchart for Surveying the Tendons and Segments.

3.3 Numbering the Tendons and Segments

Standardization of numbering the tendons and segments is critical in the management of bridge tendon conditions. Inspectors must mark the PT ducts and segments in a clear and readable manner.

Figure 3-2 provides a general idea on the numbering of spans and piers on a typical PT bridge. Figure 3-3 shows the schematic of a typical tendon identification system. The two sectional views shown correspond to the first and second piers in Figure 3-2. The cross-section of a girder is divided into left (L) and right (R) sides. However, the left side and right side can be reversed if the surveying direction is reversed. Figure 3-2 and Figure 3-3 show that the survey and inspection are in the same direction as the increasing span numbers. Hence, "Left" means the left side when looking down the span into the direction of increasing span numbers (the direction of inspection).

The numbering of segments begins at the start point of the surveying and inspection in each span. Thus, the numbering of segments increases in the same direction as the span number increases and follows standard procedures. Numbering segments can be performed using permanent markers or paint and stencil. This should be done for every segment in a girder.

3.4 Marking the Concrete diaphragms and Deviator Blocks

First, inspectors measure the thickness of both diaphragms. The portion of the tendon outside the diaphragm is then surveyed. The "start point" in the in-depth inspection form is defined as the point at which the tendon comes out of the diaphragm. Then location of the deviator blocks from this "start point" is measured. The deviator blocks are marked on the in-depth inspection form. The total length of the tendon will be estimated by the inspection manager. The "end of survey" point is defined as the point which the far tendon enters into the concrete diaphragm. This is also marked in the in-depth inspection form. These are shown in Figure 3-4 and Figure 3-5. Considering the smooth duct surface and the lack of daylight, a yellow paint marker is recommended as the marking tool. Figure 3-6 shows the interior view of a span after surveying.

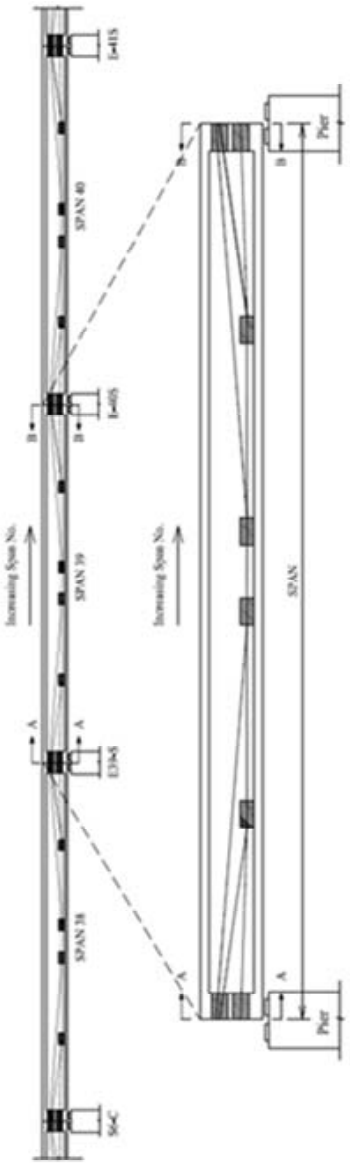

Figure 3-2. Typical View of an External Tendon System Showing the Span and Pier Identification Systems.

Figure 3-3. Typical Numbering System for Tendons of a PT Girder.

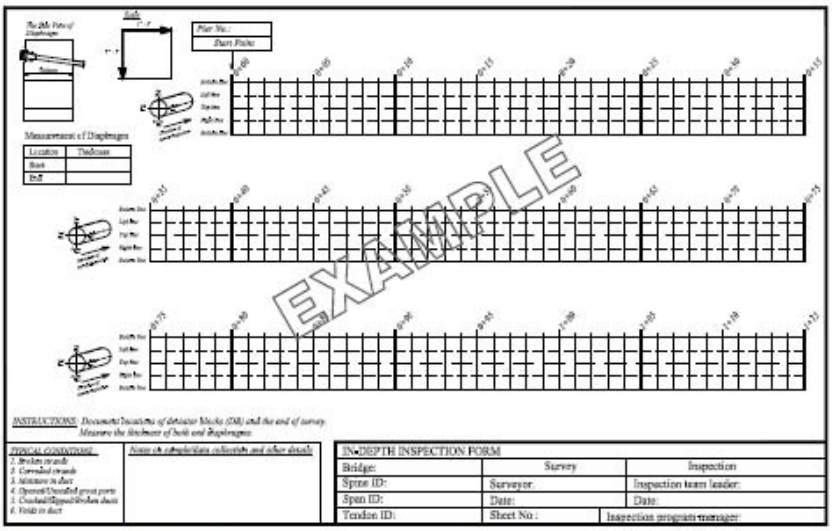

Figure 3-4. In-Depth Inspection Sheet before Marking Location of Deviator Block.

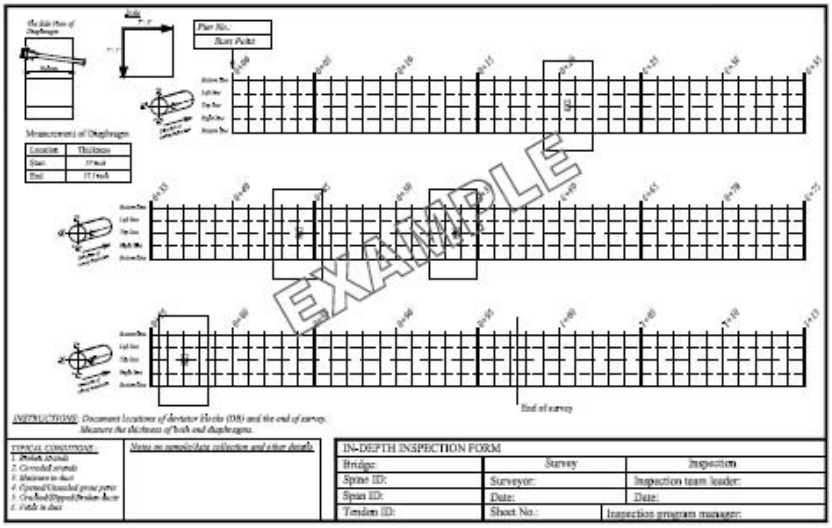

Figure 3-5. In-Depth Inspection Sheet after Marking Location of Deviator Block

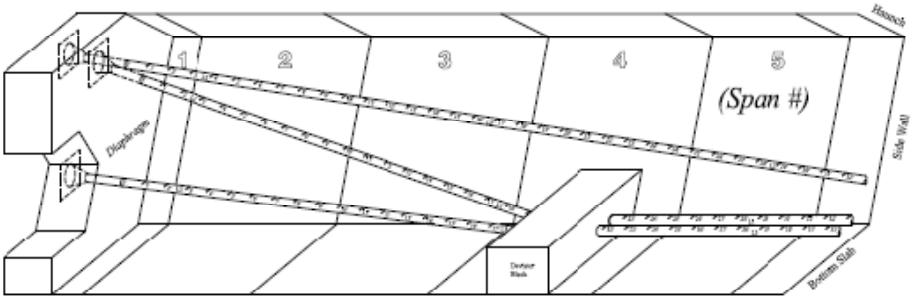

Figure 3-6. An Isometric Interior View of a Bridge Girder (after Surveying).

4 IN-DEPTH INSPECTION, ANALYSIS, AND REPAIR PROGRAM

4.1 Introduction and Objectives

This in-depth inspection is intended to be performed if the special inspection program has indicated that further inspections are needed. The in-depth inspection will require more time, will be more costly, and will require larger opening holes in the ducts of PT tendons. However, this inspection will also provide qualitative information on the condition of the strands, providing relevant information on the condition of the bridge.

The objectives of the in-depth inspection program are to:

1. identify the type and location of damage in PT systems;
2. identify the size and location of voids in PT systems;
3. identify the presence of moisture and/or chlorides (or the indicators that water has been present) in the PT system, especially at the interface between the void and grout;
4. identify and confirm the causes and locations of water and/or chloride infiltration;
5. collect the water samples, if present, and evaluate the chloride concentrations; and
6. collect photographs of strands and identify the level of corrosion of strands.

The in-depth inspection team leader will submit the findings to the in-depth inspection program manager, who will then assess the "qualitative corrosion risk of the bridge span" and make further decisions for the in-depth inspection and testing program, if needed.

4.2 Safety

General safety precautions must be taken. Both personnel and public safety requirements must be met by following standard TxDOT requirements. Note that a PT bridge may be considered a "confined space" and that inspectors require appropriate training.

4.3 Planning, Scheduling, and Equipment

Planning and scheduling

Based on the data from special inspections, bridge files, records, and other factors, the in-depth inspection program manager will develop the overall strategy for the in-depth inspection

program. The in-depth inspection program manager will also identify the bridge spans for inspection and provide this information to the inspection team leader. The inspection team leader will be responsible for detailed planning and management of the field activities.

It is recommended that in-depth inspections, if needed, be performed by the same inspection crew. It is also recommended that in-depth inspections be performed immediately after the special inspections (during the same season) to prevent further deterioration.

Tools and equipment for in-depth inspection

Table 4-1 provides a list of recommended tools and equipment required for in-depth inspections. Note that this list may not be comprehensive.

Table 4-1. Tools and Equipment for In-Depth Inspection.

Safety Tools	In-depth Inspection Tools
Hard hats	Inspection form, clipboard, and pen
Head flashlights	Steel tapping hammer (for identifying voids in ducts)
Handheld flashlights	Mirror (for inspecting damages underneath ducts)
Safety goggles	Borescope
Protective coveralls	Generator (with gas and oil) for borescope
Yellow safety vests	Extension cord
Gloves	Tools for making holes (dremel with copper drill bit)
Respirators	Sealing tools (e.g., HDPE pipe piece, ABS cement, etc.)
Dust masks	Paint marker
Ear plugs	Spray paint (light color)
First-aid kit	Plastic vials for water samples
Extra batteries	Plastic pipette to collect water samples
Fire extinguisher	Plastic bags for grout samples
Air horn	Tweezers (for picking grouts in ducts)
Safety harness and rope	Digital camera
Safety boots	Binder with all papers (inspection manual, blue print, etc.)
Hand-held radios (Walkie-talkie)	Lift truck
Oxygen meter and CO meter	Keys and tools required to unlock and open the access door
Confined space training manual	Wet wipe to clean the duct surface
Drinking water	Wood and saw (for holding the door open) or chain and latch
Oxygen meter and CO meter	

4.4 In-Depth Inspection Forms, Test Samples, and Reports

The data from the in-depth inspection of each span should be recorded on the "in-depth inspection form." Each span inspected will require at least one form. Figure 4-1 shows a sample copy of the in-depth inspection form.

The in-depth inspection team leader will submit test samples, if any, collected during the in-depth inspection to the in-depth inspection program manager, who will then submit the test samples to the testing laboratory to obtain test results. A chain of command form shall be maintained for all the samples collected.

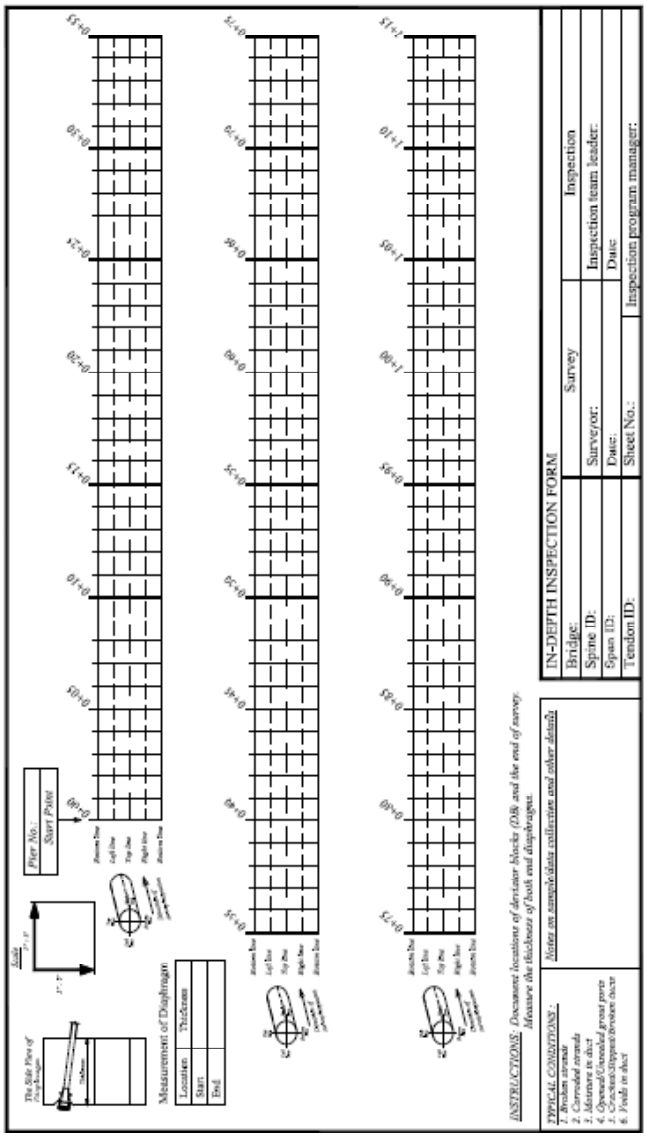

Figure 4-1. In-Depth Inspection Form.

4.5 General Procedures in In-Depth Inspection

The in-depth inspection consists of more detailed evaluation techniques than the special inspections. These evaluation techniques include more detailed visual inspections, some with a borescope. Note that the inspection program manager is responsible for the procurement of the bridge files and records and development of the in-depth inspection strategy. It is also required that the tendons for inspection be surveyed before beginning the in-depth inspection program. The following steps provide the in-depth inspection procedures. The bulleted steps in the following discussion start with a code (e.g., I-1) that represents the corresponding box in the flowchart. The procedures for performing such an in-depth inspection follow. Figure 4-2 shows the flowchart of the process. In the flowchart, the activities inside the larger box with a thick border indicate the steps in the in-depth inspection. The activities shown outside the larger box are procedures required before and after the in-depth inspection.

- **I-1 to I-3**: Perform initial preparation.
  - Identify the spans to be inspected.
  - Select the bridge drawings associated with the select bridge span.
  - Procure necessary tools and equipment before entering the bridge (refer to Table 4-1).
  - Record the inspector name and inspection date on the in-depth inspection form. (This form should have the information from the tendon survey.)
  - Go to the starting span.
  - Identify tendons that need further assessment.
- **I-4**: Perform in-depth inspection at the anchorage zone.
  - If access through the grout hole is possible, then inspect for potential voids and strand corrosion using a borescope. If possible, take photographs of the exposed strand showing the level of corrosion.
  - Record the strand condition in the bottom left box on the in-depth inspection form. Figure 1-3 shows the photographs of strands with different levels of corrosion.
  - If the presence of water is found, then collect the water into a small plastic bottle (using a hand-held vacuum and tubing) and record the information on the in-depth inspection form.

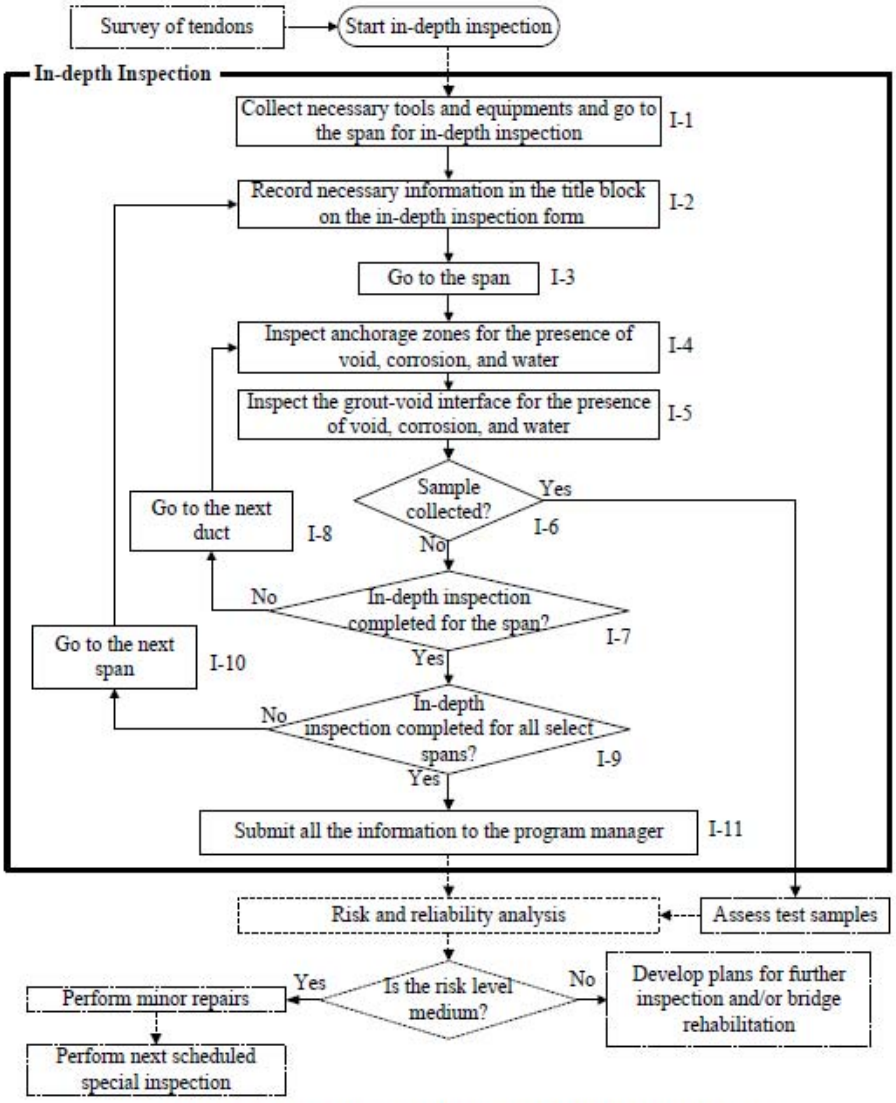

Figure 4-2. Flowchart of the In-Depth Inspection and Analysis.

- **I-5**: Perform detailed inspection inside the tendons, especially at the grout-void interface.
  - Using the sounding procedures given in Section 4.6, draw the void profile on the in-depth inspection form.
  - Identify a location to drill a 1/2-inch diameter hole[2] at the grout-void interface, as shown in Figure 4-3 (a), (b), and (c).
  - Place a plastic container such that the draining water, if any, can be collected.
  - If water drains out of this hole, then:
    - Collect the draining water into a small plastic bottle.
    - Record all the information regarding the presence of water onto the in-depth inspection form.
    - Insert the insertion tube of the borescope through the 1/2-inch diameter hole and inspect the level of corrosion of strands at the grout-void interface. Take photographs of the strands.
  - After the inspection using the borescope is completed, seal the 1/2-inch diameter hole as shown in Figure 4-3 (d) such that strands are protected from the outside environment.

- **I-6**: Perform sample collection and testing.
  - Collect test samples (solution or grout samples), if deemed necessary. Water samples can be collected from standing water in the box girder or from inside tendons. Samples must be identified with the location of collection (i.e., from girder or from a tendon).
  - Label the samples and record additional information, such as sample ID, sample location, etc. Use "notes on sample/data collection and other details" on the in-depth inspection form for recording this information, and also document this information on the chain of command form.
  - Submit the collected samples to the inspection program manager, who will then transport samples to the laboratory for assessment.
  - The laboratory will test the chloride concentration and pH in the samples.
  - The laboratory will then return results to the in-depth inspection program manager for assessment or to provide better information for the reliability analysis.

- **I-7 to I-10**: Perform in-depth inspections on all tendons identified as having potential voids or durability issues. After completing the in-depth inspection on the span, transfer the tools and materials to the next span.

- **I-11**: After completing the in-depth inspection, inspectors should submit in-depth inspection forms to the program manager for further analysis and decision making regarding performing minor repairs or developing rehabilitation programs.

[2] The 1/8-inch copper drill bit (used in the special inspection) can be used for this purpose. First, draw a 1/2-inch diameter circle on the duct surface. Then, drill several 1/8-inch diameter holes along the circumference of the marked circle until a 1/2-inch diameter hole is formed.

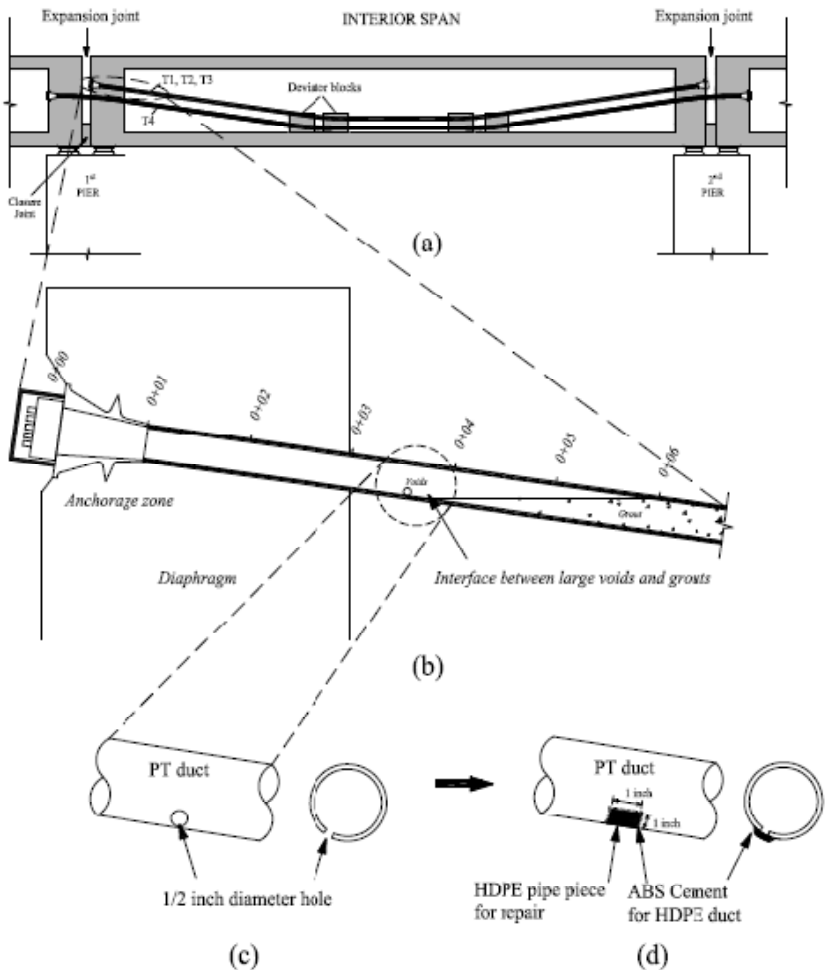

Note: 1 inch = 25.4 mm

Figure 4-3. Tendon System Showing (a) the Location of Water Inspection for In-Depth Inspection, (b) a Close-up View of Area for the Water Inspection, (c) a Close-up of Location for Water Inspection, and (d) the Sealed Duct after Water Inspection.

4.6 Void Profiling of Tendons using Sounding Tests

The objective of the in-depth sounding technique is to detect voids to identify grout-void interface locations. This information should be recorded on the in-depth inspection form (Figure 4-1). Note that the grids on the in-depth inspection form indicate the unrolled duct surface by cutting the bottom line of ducts, as shown in Figure 4-4. Inspectors should tap all around the PT ducts with a tapping hammer and perform this inspection for each PT duct separately. Figure 4-5 shows the marking for the voids in PT ducts. This void profile assists in identifying the grout-void interface in tendons.

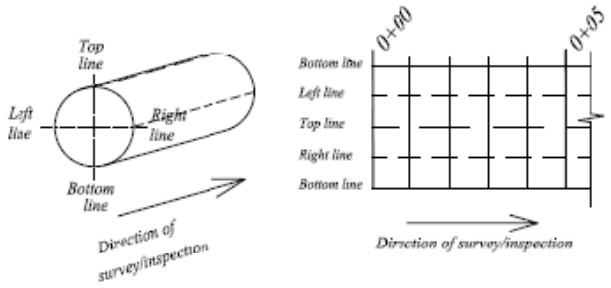

Figure 4-4. Unrolled Duct Surface in the Grids on In-Depth Inspection Form.

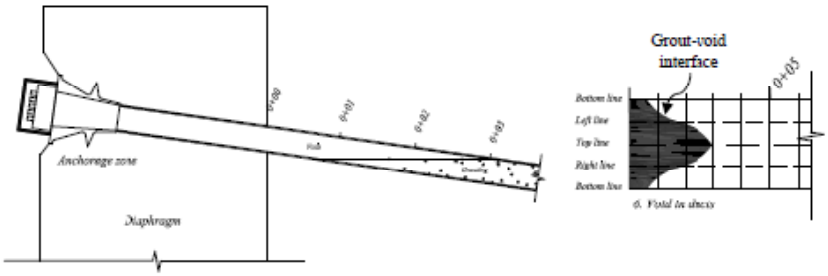

Figure 4-5. Marking Voids on the In-Depth Inspection Form.

APPENDIX A. REPAIR GROUTING PROCEDURE

INTRODUCTION

Repair grouting is defined as the process of filling the voids in a tendon with a repair grout. Currently, the vacuum grouting (VG) method is the recommended repair grouting method. This method is capable of adequately filling voids in ducts but is very expensive and time-consuming. This is because the VG method requires an air-tight tendon, which is hard to achieve in the field. By taking these difficulties into account, Research Project 0-4588 developed and recommended a feasible repair grouting method, the pressure-vacuum grouting (PVG) method. Further details of the methodology and evaluation of this method are given in Volume 2 of Research Report 0-4588-1.

The PVG method utilizes the beneficial characteristics of both pressure grouting (PG) and VG methods. The PVG method has the same filling capability and filling performance as the VG method and better economic feasibility than the VG method. This manual provides general procedures for the PVG method. Based on the recommendations from the in-depth inspection program manager, the repair program manager identifies the tendons to be repair grouted.

SAFETY

General safety precautions must be taken. Both personnel and public safety requirements must be met by following standard TxDOT requirements. Note that a PT bridge may be considered a "confined space" and that inspectors may require appropriate training.

PLANNING, SCHEDULING, EQUIPMENT, AND FORMS

Planning and scheduling

Based on the data from in-depth inspections, bridge files, records, and other factors, the repair program manager will develop the overall strategy for the repair program. The repair program manager will also identify the bridge tendons and/or spans for repair and provide this information to the repair team leader. The repair team leader will be responsible for detailed planning and management of the field activities. It is recommended that repair, if needed, be

performed immediately after the special inspections (during the same season) to prevent further deterioration of the PT systems.

Tools and equipment for repair grouting

A list of recommended tools and equipment required for repair grouting is provided below. Note that this list may not be comprehensive.

- electrical power source,
- grout materials,
- mixing water,
- water for cleaning tools,
- measuring scale (to weigh water and grout materials),
- hand grout pump,
- vacuum pump,
- grout hose and connections,
- 10-gallon buckets (3 pieces),
- Nalgene drop-dispensing bottle (for protecting vacuum pump from grout in-flow),
- pipe saddle tap with ball valve (for connecting to air outlet),
- 2500 rpm drill with paddle (2 pieces),
- material testing devices (flow cone, cube [3 sets], 1000 ml cylinder with strand [3]), and
- provision to dump or pour extra grout.

Repair grouting report form

A repair grouting report form has been developed to record all the data associated with the repair grouting and is shown in Figure A-1.

REPAIR GROUTING REPORT

BRIDGE:	SPINE ID:
SPAN ID:	SHEET No.:

1. Measurement of void volume and determination of the amount of repair grouts

- Person in charge: _____

Tendon ID	Void volume by volumeter (A)	Required volume (B)	w/p of repair grouts (C)	Wet density of repair grouts (D)	Weight of repair grouts (E)	Weight of water (F)

Note: document C and D from manufacture's specification; B = 1.1 * A + 3.6 ft^3 (0.017 m^3); E = B / D; F = C * E

2. Material testing

Person in charge		Date	
Temperature (°F)		Humidity (%)	
Mixing time (min.)		Grout temperature (°F)	
Start time of mixing		End time of mixing	

- Flow cone test (Tex-437-A Method 2)

Fresh Test	30 Min Flow Cone
Test start time:	Test start time:
Efflux time (s):	Efflux time (s):

Note: wet cone 1 min before each test; re-mix grout for 30 s before 30 min test

- Compression test (Tex-442-A)

Cube	7 days (date:)	28 days (date:)
1	ksi	ksi
2	ksi	ksi
3	ksi	ksi

- Wick-induced bleed test (Tex-441-A) Note: $V_b = V_w - V_g$

Time	Interval	Cylinder A (ml)			Cylinder B (ml)			Cylinder A (ml)		
		V_w	V_g	V_b	V_w	V_g	V_b	V_w	V_g	V_b
	0 min									
	15 min									
	30 min									
	45 min									
	1 hr									
	2 hr									
	3 hr									
Final Measure										

3. Repair grouting

Repair Grouting Actions				Examination		
Date	Tendon ID	Person in charge	Note	Date	Repaired condition	Person in charge

Figure A-1. Repair Grouting Report Form.

GENERAL PROCEDURES FOR PVG METHOD

- **R-1 to R-2**: Perform general preparation.
  - Identify the span and tendon for repair.
  - Collect necessary tools and equipment and go to the span for repair.
  - Record all the information in the title block and Item 1 on the repair grouting report form.
- **R-3**: Perform preparation for repair grouting.
  - Document the tendon ID for repair grouting on the repair grouting report form (see Figure A-1).
  - If possible, determine (or approximate) the void volume and record on the repair grouting report form.
  - Compute the required volume of repair grouts (B) using the equation provided in the repair grouting report form. Compute the weight of the repair grout and water (E, F) required for mixing.
- **R-4:** Based on the completed in-depth inspection forms, mark the end of voids, as shown in Figure A-2.
  - If the voids on the in-depth inspection forms are continuously connected all along the PT ducts, mark the location at the middle of the PT ducts (in between deviator blocks).
  - If cracked/broken PT ducts are shown on the in-depth inspection forms, seal the damaged part with a 5-minute epoxy or cover with a neoprene sheet (the neoprene sheets should be secured with hose clamps).
  - Drill a 1-inch diameter air outlet hole using a copper drill bit at the marked locations and connect the vacuum safety device with the vacuum pump (see Figures A-3 and A-4).
  - Connect the hand grout pump to the grout port at the top of the anchorage.
  - Apply the vacuum pump until the pressure inside the tendon reduces by approximately 80 percent of atmospheric pressure (23.9 inHg). If the vacuum pump cannot reduce the pressure by 80 percent of atmospheric pressure, try to inspect the entire tendon again and seal the damaged parts with 5-minute epoxy.
- **R-5:** Prepare the repair grout mixture per manufacturer's recommendations. Perform the required material testing per specifications.
- **R-6:** Perform repair grouting by the PVG method and finishing.
  - Apply the vacuum pump to reduce pressure by 80 percent of atmospheric pressure (23.9 inHg).
  - Open the grout inlet at the top anchorage and inject repair grout using a hand grout pump.

- Close the valve of the vacuum safety device until the hand grout pump cannot pump more grout. If the repair grout flows out of the air outlet, close the ball valve at the pipe saddle tap and apply the hand grout pump until it cannot pump more grout.
- Turn off the vacuum pump.
- Close the valve of the grout inlet.

- **R-7:** Disconnect the vacuum safety device and pipe saddle tap, and seal the air outlet.
- **R-8 to R-11:** Evaluate the repair grouting.
  - On the following day after repair grouting, perform sounding tests on the repaired tendons to identify voids, if remaining. Record the observed void conditions in the repaired tendon on the repair grouting report form.
  - Submit the report to the repair program manager.

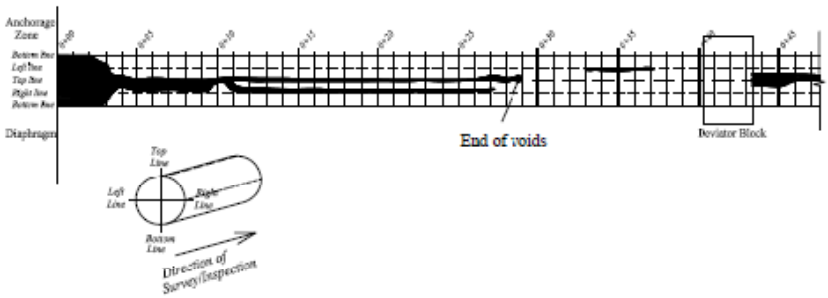

Figure A-2. Location of the End of Voids on the Detailed Inspection Sheets.

(a) (b)

Figure A-3. (a) Air Outlet Hole for PVG Method, and (b) Pipe Saddle Tap and Ball Valve for Connecting Vacuum Safety Device and Vacuum Pump.

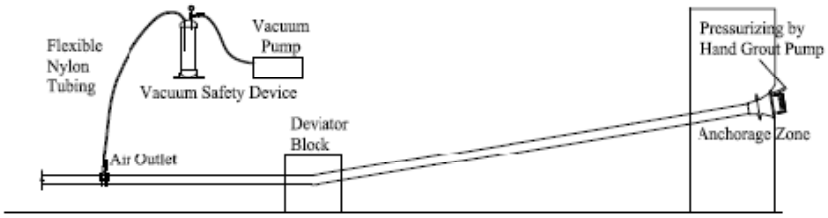

Figure A-4. Typical View for the Application of PVG Method in the Field.

APPENDIX B. DAMAGES IN POST-TENSIONED SYSTEMS

A. Broken strands and broken ducts.

B. Corroded and broken strands and broken ducts.

C. Cracked ducts.

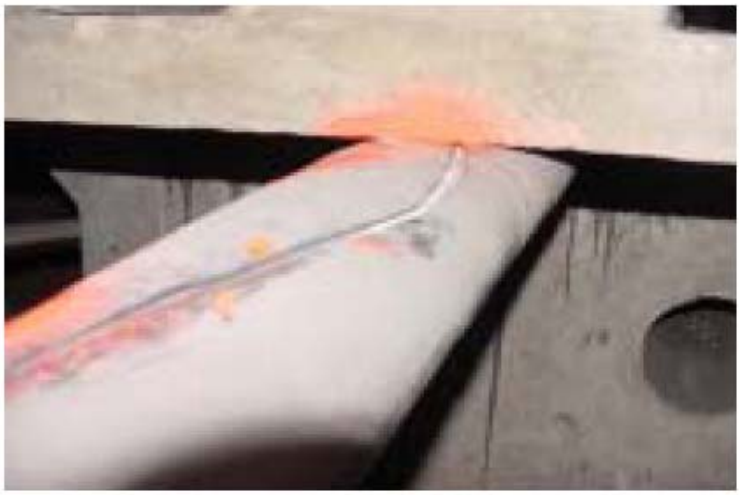

D. Cracked ducts.

E. Broken ducts and exposed strands.

F. Broken ducts and exposed strands.

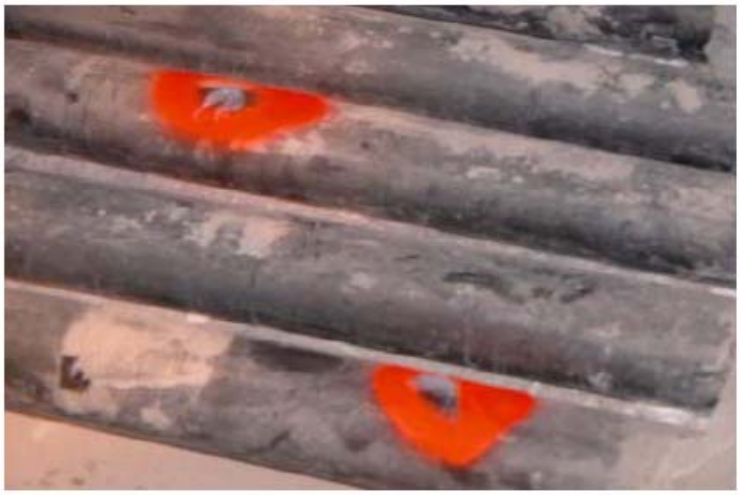

G. Ducts with holes.

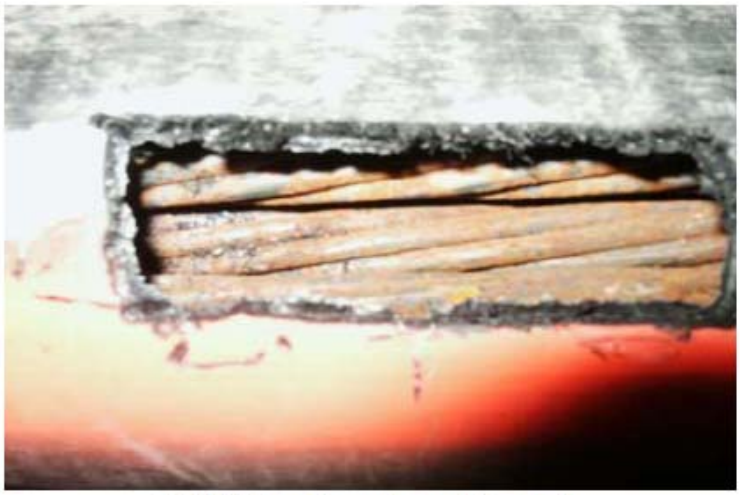

H. Voids in tendons and corroded strands.

I. Missing anchorage cap, exposed anchor head, and corroded strands.

J. Loose anchorage (indicating broken strands).

K. Opened grout port.

L. Opened grout port, broken anchorage cap, and exposed anchorage zone.

M. Standing water in the concrete box girder.

N. Standing water in the concrete box girder.

O. Sign of past moisture infiltration in the concrete girder, broken drainage pipe.

P. Sign of past moisture infiltration in the concrete girder, broken drainage pipe.

APPENDIX C. INSPECTION FORMS

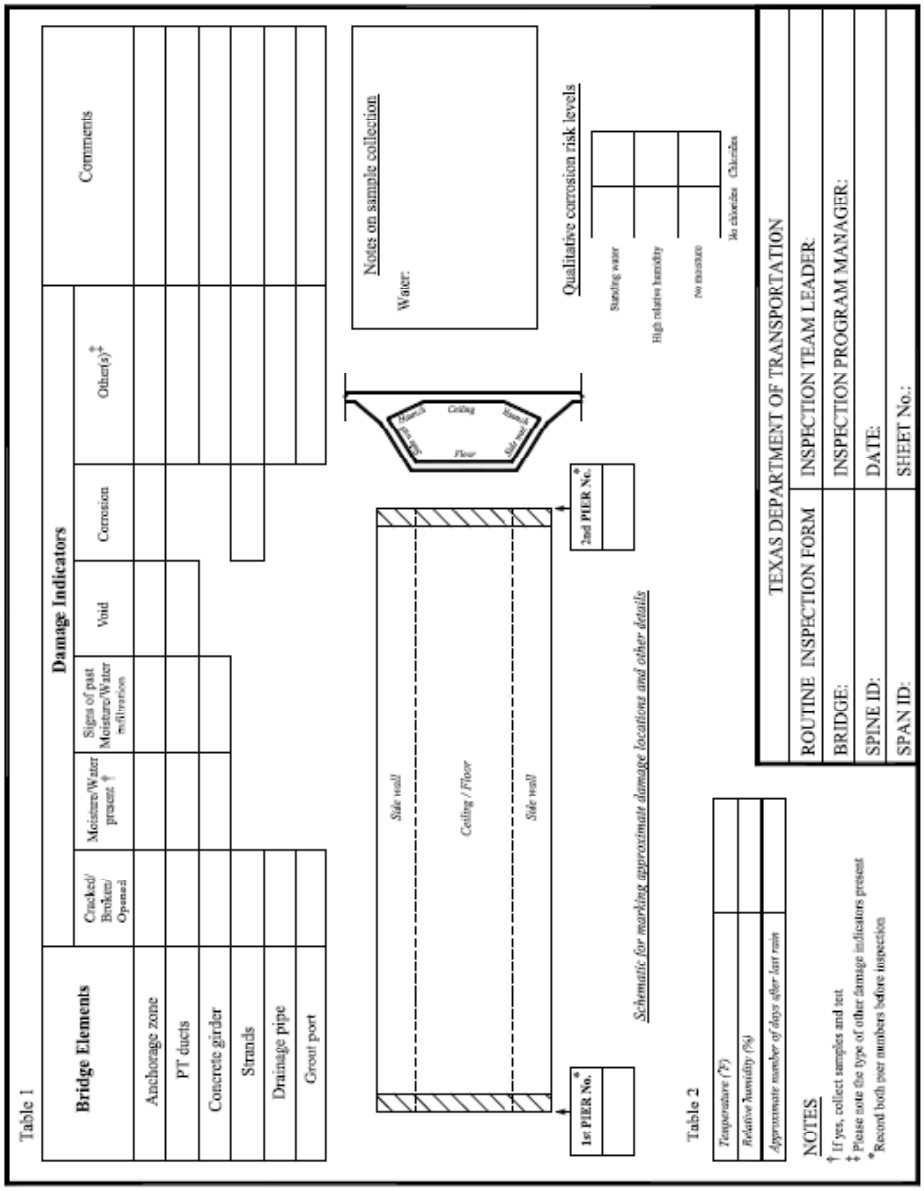
Table 1
Bridge Elements
Damage Indicators
Cracked/ Broken/ Opened
Moisture/Water present †
Signs of past Moisture/Water infiltration
Void
Corrosion
Other(s)‡
Comments
Anchorage zone
PT ducts
Concrete girder
Strands
Drainage pipe
Grout port
Notes on sample collection
Water:
Qualitative corrosion risk levels
Standing water
High relative humidity
no moisture
No chlorides
Chlorides
Floor
Ceiling
Floor
Side wall
Ceiling / Floor
Side wall
1st PIER No.*
2nd PIER No.*
Schematic for marking approximate damage locations and other details
Table 2
Temperature (°F)
Relative humidity (%)
Approximate number of days after last rain
TEXAS DEPARTMENT OF TRANSPORTATION
ROUTINE INSPECTION FORM
INSPECTION TEAM LEADER:
BRIDGE:
INSPECTION PROGRAM MANAGER:
SPINE ID:
DATE:
SPAN ID:
SHEET No.:
NOTES
† If yes, collect samples and test
‡ Please note the type of other damage indicators present
*Record both pier numbers before inspection

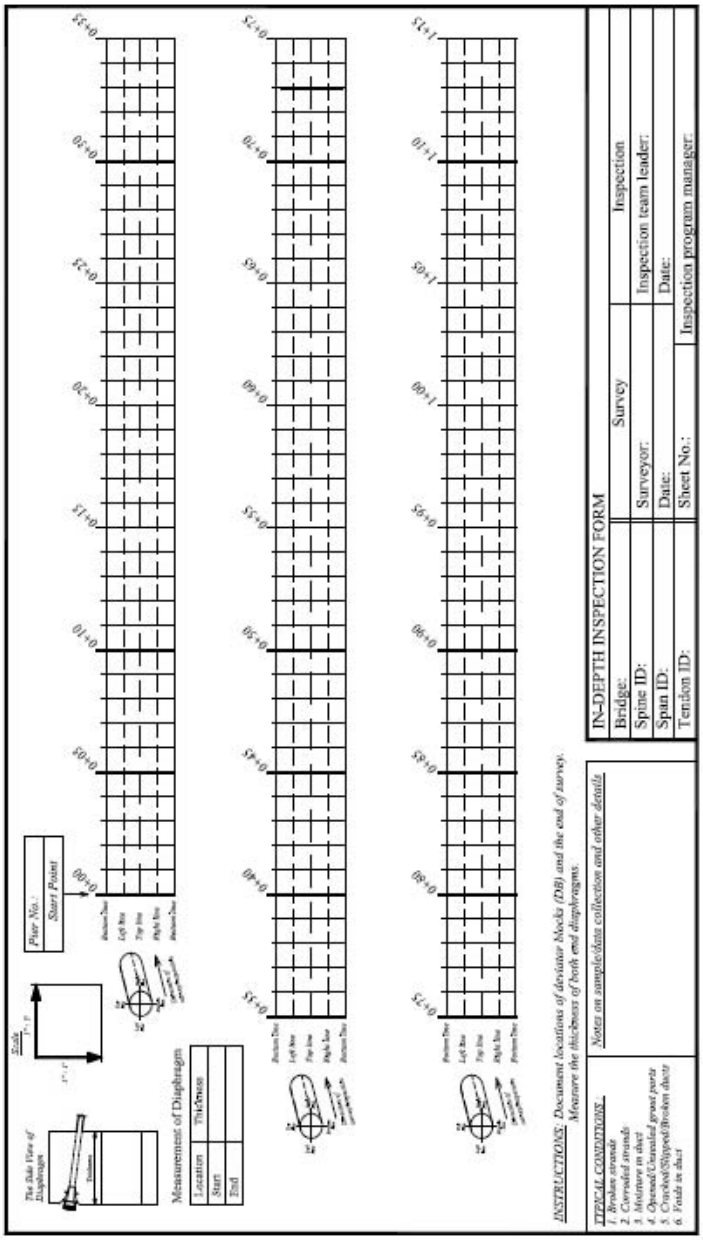
IN-DEPTH INSPECTION FORM
Survey
Inspection
Bridge:
Spine ID:
Span ID:
Tendon ID:
Surveyor:
Date:
Sheet No.:
Inspection team leader:
Date:
Inspection program manager:
INSTRUCTIONS: Document locations of deviator blocks (DB) and the end of survey.
Measure the thickness of both end diaphragms.
TYPICAL CONDITIONS:
1. Broken strands
2. Corroded strands
3. Moisture in duct
4. Opened/Unsealed grout joints
5. Cracked/Slipped/Broken ducts
6. Voids in duct
Notes on sample/data collection and other details
Measurement of Diaphragm
Location
Thickness
Start
End
Pier No.:
Start Point
Bottom Duct
Left Box
Top Box
Right Box
Bottom Duct

APPENDIX C

STRENGTH TEST RESULTS OF GROUT

The compressive strength test of cubic molds is carried out to ensure the performance of hardened grouts, and it is executed by following Tex-442-A (TxDOT 2006). The test strength of initial grout and repair grout is provided in Table C-1.

Table C-1. Cube Strength of Grouts.

Specimen	Average Compressive Strength, ksi (10^4 kPa)			
	Initial Grout		Repair Grout	
	7 days	28 days	7 days	28 days
VG-C1-1	5.871 (4.048)	6.641 (4.579)	7.916 (5.458)	9.517 (6.562)
VG-C1-2	6.079 (4.191)	7.157 (4.935)	8.304 (5.726)	11.576 (7.982)
VG-C2-1	4.497 (3.101)	5.823 (4.015)	8.508 (5.866)	11.636 (8.023)
VG-C2-2	6.731 (4.641)	7.907 (5.452)	10.439 (7.198)	13.610 (9.384)
VG-C3-1	5.577 (3.845)	6.253 (4.311)	5.936 (4.093)	6.992 (4.821)
PG-C1-1	5.574 (3.843)	6.616 (4.562)	8.495 (5.857)	10.834 (7.470)
PG-C1-2	5.870 (4.047)	7.814 (5.388)	8.604 (5.932)	11.991 (8.268)
PG-C2-1	4.823 (3.325)	6.889 (4.750)	9.173 (6.325)	10.669 (7.356)
PG-C2-2	7.597 (5.238)	8.867 (6.114)	10.881 (7.502)	12.528 (8.638)
PG-C3-1	5.296 (3.652)	8.080 (5.571)	6.302 (4.345)	11.292 (7.786)
PG-C3-2	5.876 (4.052)	6.880 (4.744)	7.295 (5.030)	8.425 (5.809)
PVG-C1-1	5.840 (4.027)	7.525 (5.188)	7.518 (5.184)	9.640 (6.647)
PVG-C1-2	5.003 (3.450)	6.290 (4.337)	8.768 (6.046)	10.964 (7.560)
PVG-C2-1	5.523 (3.808)	6.698 (4.618)	7.695 (5.306)	11.352 (7.827)
PVG-C2-2	8.080 (5.571)	9.362 (6.455)	10.724 (7.394)	11.686 (8.057)
PVG-C3-1	5.405 (3.727)	5.916 (4.079)	5.720 (3.944)	8.056 (5.555)

VITA

Seok Been Im was born in Seoul, South Korea in 1975 and grew up in Seoul, South Korea. He entered the Department of Civil & Environmental Engineering at Korea University, Seoul, in 1995 and received his B.E. degree in 1999. After graduation, he worked in VSL Korea as a field engineer, and he gained his experience for post-tensioning system and maintenance of bridge systems. In 2002, he entered the graduate degree program in Korea University, and pursued his Master of Science degree for structural engineering in the Department of Civil & Environmental Engineering. In 2004, he received his M.S degree and continued to work at Korea University as a researcher. In 2005, he began his Ph.D degree for structural engineering at Texas A&M University, and received his Doctor of Philosophy degree in Civil Engineering in December 2009.

Zachry Department of Civil Engineering

3136 TAMU

Texas A&M University

College Station, TX 77843-3136

e-mail: sbeeni75@gmail.com